BEHAVIOUR OF CONE PENETRATION TESTS IN SATURATED SANDS

A Thesis submitted to the
University of London
(Imperial College of Science and Technology)
for the degree of
Doctor of Philosophy in the Faculty of Engineering

by

Pedricto Rocha Filho
B.Sc. (Civil Eng.), M.Sc. (Civil Eng.), M.Sc. (Soil Mech.), D.I.C.

May 1979

ABSTRACT

An experimental study is carried out in the laboratory to examine the influence of the excess pore pressure on the cone penetration test measurements and its implications on the correlations between cone resistance and soil properties. This work was intended to provide a basis for interpreting in situ cone penetration tests in the North Sea. For this reason, the used sand was prepared to a grading curve which falls inside the range corresponding to North Sea sands. The study included performing and evaluating cone penetration and plate loading tests in saturated sand samples. The penetration tests were carried out using a standard FUGRO cone with a porous pressure device added at the conical point.

The results of this study show that the excess pore pressure can strongly influence the cone measurements. They also demonstrate that correlations established for dry sand cannot be extrapolated to saturated conditions.

For normally consolidated conditions a relationship between cone resistance and compressibility was obtained which depends upon the relative density. For overconsolidated conditions the corresponding relationship was obtained as a function of relative density and overconsolidation ratio. An equation is proposed which considers the effect of overconsolidation upon the cone resistance, based on both a theoretical approach and experimental results. From a comparative analysis it was found that for a compact material the cone resistance would indicate almost the same settlement irrespective of the stress history of the deposit.

It was concluded that the geometrical configuration of the penetrometer used is inadequate for testing deposits which have relatively high pore pressure values compared to cone resistances.

ACKNOWLEDGEMENTS

The work described in this thesis was carried out in the Geotechnics Division of the Building Research Station as a mutual co-operation between this Department and the Soil Mechanics Division of the Imperial College of Science and Technology. The Conselho Nacional de Pesquisa (Brazilian National Research Council) provided the financial support during the period in which the research leading to this thesis was undertaken. I am grateful to these organizations for making this research possible.

I wish especially to express my gratidue to Dr. A. D. M. Penman, who, in addition to his constant guidance, has rendered valuable assistance in various other ways in the preparation of this volume.

I would like to acknowledge my indebtedness to Dr. J. B. Burland, Head of Geotechnics Division, for providing access to the Building Research Station facilities and making useful contributions throughout the course of this research.

I am indebted to Dr. P. R. Vaugham who supervised this work.

I would like to thank Dr. J. A. Charles who read and commented on the manuscript, making valuable contributions.

I also owe much to my friends in the Geotechnics Division at the Building Research Station, whose kindness and help have been far more than words can ever express, in particular to: Mr. C. P. Abbis, Mr. D. Burford, Mr. R. Driscoll, Mr. B. J. Eason, Mr. K. A. Gallagher, Mr. M. Ivey, Mr. G. Price, Dr. H. D. St. John, Mr. K. W. Tarr and Mr. K. Watts. Mr. K. W. Tarr gave valuable assistance on the computer analysis involved in this thesis. I would like to thank Miss E. Gentzsch for her help in many ways.

I would like to thank Mr. A. Hussain and Mr. R. Quarterman who gave efficient and valuable assistance on the development of the mechanical and electronical equipment.

Thanks are due to my colleagues in the Soil Mechanics group at the Imperial College, in particular to Mr. T. M. P. Campos, Mr. L. M. Costa-Filho and his wife Hermusia, Mr. I. Egeli, Mr. A. Gens, Mr. F. R. Lopes, Mr. F. Lupini, Mr. M. Martins, Mr. M. Takahashi and members of the staff Mr. D. W. Hight and Dr. A. E. Skinner, for their constant interest throughout the course of this research. The personal concern and cheerfulness of Mrs. B. Price is also appreciated.

I am grateful to Miss J. A. Moir for draughting the drawings and to Mrs. B. A. Barnes for the accurate typing of this thesis.

I wish to express my deepest gratitude to my wife Marta for her continuing encouragement and support.

ERRATA

Page	Line*	Word	Corrected
ii	16	Vaugham	Vaughan
ii	23	K W Tarr	K J Tarr
viii	10	TEST	TESTS
30	2	EXPERIMETAL	EXPERIMENTAL
33	17	Vesic (1973)	Vesic (1972)
87	13	sleeve(*) resistance	(*) load cell is lton, giving a maximum working friction sleeve
55		FIGURE 3.3 plus title	FIGURE 3.4 plus title
56		FIGURE 3.4 plus title	FIGURE 3.3 plus title
86	2	voltimeters	voltmeters
231	10	simetric	symmetric

*Line counted from top of page including titles and subtitles

LIST OF CONTENTS

ABSTRACT i

ACKNOWLEDGEMENTS ii

LIST OF CONTENTS iv

NOTATION ix

CHAPTER 1 INTRODUCTION 1

CHAPTER 2 SETTLEMENT ANALYSIS BASED ON STATIC CONE PENETRATION TESTS

2.1 Introduction 4

2.2 Linear Correlations for Normally Consolidated Dry Sands 5

2.3 Non-Linear Correlations for Normally Consolidated Dry Sands

2.3.1 General 8

2.3.2 Theoretical Approach 9

2.3.3 Experimental Results 12

2.4 Correlations for Overconsolidated Dry Sands 14

2.5 Correlations for Saturated Sands 18

2.6 Summary and Concluding Remarks 20

CHAPTER 3 GENERATION OF EXCESS PORE PRESSURE DURING PENETRATION TESTS

3.1 General 32

3.2 Theoretical Background 33

3.3 Observed Values of Excess Pore Pressure Induced During a Penetration Process 40

3.4 Influence of the Probe Form on the Induced Excess Pore Pressure Value 42

3.5 Influence of Filter Position on the Measured Excess Pore Pressure Value 43

3.6 Effects of the Excess Pore Pressure on Penetration Resistance Values 47

3.7 Summary and Concluding Remarks 52

CHAPTER 4	OBJECTIVE OF THIS WORK		78
CHAPTER 5	DESCRIPTION OF APPARATUS		
	5.1	General	81
	5.2	Testing Chamber	82
	5.3	Driving System	83
	5.4	Pressure Unit	84
	5.5	Electrical Penetrometer	
		5.5.1 Description	85
		5.5.2 Recording System	85
		5.5.3 Calibration of the Penetrometer Load Cells	86
		5.5.4 Saturation and Calibration of the Pore Pressure Device	88
CHAPTER 6	DESCRIPTION OF THE SAND		
	6.1	Grading Curve	103
	6.2	Specific Gravity	104
	6.3	Maximum and Minimum Void Ratios	105
	6.4	Triaxial Test Results	106
CHAPTER 7	PREPARATION OF SAMPLE AND TESTING TECHNIQUE		
	7.1	Preparation of the Sample	117
	7.2	Testing Procedure	
		7.2.1 General	118
		7.2.2 Consolidation of the Sample	119
		7.2.3 Plate Loading Test	120
		7.2.4 Continuous Cone Penetration Test	120
		7.2.5 Static Penetrometer Load Test	121
		7.2.6 "Aside" Continuous Cone Penetration Test	121
		7.2.7 Determination of the Sample Compactness	122
	7.3	Summary and Indexing of Tests	124

CHAPTER 8 ANALYSIS I - INTERPRETATION OF CONE PENETRATION RESULTS

8.1 General 128

8.2 Results from Continuous Cone Penetration Tests 128

8.2.1 Analysis of Point Resistance 129

8.2.2 Analysis of Friction Sleeve Resistance 131

8.2.3 Analysis of the Excess Pore Pressure 132

8.3 Static Penetrometer Load Test Results

8.3.1 General 134

8.3.2 Analysis of the Results

8.4 Influence of the Excess Pore Pressure on Measured Values

8.4.1 General 136

8.4.2 Influence of Excess Pore Pressure on Cone End Resistance 137

8.4.3 Influence of Excess Pore Pressure on Friction Sleeve Resistance 138

8.5 Relative Density as Indicated by the Cone End Resistance

8.5.1 General 138

8.5.2 Analysis of the Results 139

8.6 Friction Ratio as an Indication of Soil Classification

8.6.1 General 141

8.6.2 Analysis of the Results 142

8.7 Dissipation of the Excess Pore Pressure

8.7.1 General 143

8.7.2 Consideration on the Geometrical Factor Value 143

8.7.3 Consideration on the Permeability and Compressibility Effects upon the dissipation time 145

8.7.4 Analysis of the Results 148

8.8 Summary and Concluding Remarks 150

CHAPTER 9 ANALYSIS II - RELATIONSHIP BETWEEN COMPRESSIBILITY AND CONE END RESISTANCE

9.1 General 189

9.2 Interpretation of One Dimensional Consolidation Test 189

9.3 Interpretation of Plate Loading Test

9.3.1 General 190

9.3.2 Influence of the Central Hole 191

9.3.3 Influence of the Wall Confinement 192

9.3.4 Evaluation of the Deformation Modulus 193

9.4 Comparison between Deformation Modulus from One Dimensional Consolidation and Plate Load Tests 196

9.5 Correlation between Compressibility and Cone End Resistance

9.5.1 General 197

9.5.2 The Determination of Representative Value of Compressibility 197

9.5.3 The Determination of Representative Value of Cone Resistance 198

9.5.4 Correlation for Normally Consolidated Conditions 198

9.5.5 Correlation for Overconsolidated Conditions 199

9.6 Errors Involved in the Compressibility Evaluation if the Stress History of the Deposit is not known 202

9.7 Summary and Concluding Remarks 205

CHAPTER 10 CONCLUSIONS AND SUGGESTIONS FOR FURTHER RESEARCH

10.1 General 225

10.2 Cone Penetrometer 225

10.3 Rate Effect 225

10.4 Cone Resistance as an Indicator of Compressibility 226

APPENDIX A NUMERICAL ANALYSIS

A.1 Routine for Solution of the Non-linear Equation 227

A.2 Applications of the Finite Elements Method

A.2.1 Description of the Finite Elements Program 231

A.2.2 Wall Friction Effect on the Consolidation Process 231

A.2.3 Wall Confinement Effect on Plate Loading Results 232

A.3 Deflection of the Top of the Sample 234

APPENDIX B PRELIMINARY TEST 239

LIST OF REFERENCES 249

NOTATION

a	=	attraction, cohesion intercept divided by the tangent of the friction angle
A	=	Skempton's pore pressure parameter, A_f value at failure
C	=	constant of compressibility
C_c	=	compression index
C_s	=	swelling index
c_h	=	horizontal coefficient of consolidation
D_R	=	relative density
D_s	=	effective particle diameter
D_{60}	=	soil particle at which 60% of the soil weight is finer, D_{10} is the corresponding value at 10%
E	=	Young's Modulus of Elasticity
E_s	=	constrained modulus
E_p	=	plate loading deformation modulus
E_t	=	triaxial tangent deformation modulus for initial loading
$E_s(\frac{1}{3})$	=	triaxial secant deformation modulus for one third of failure load
$E_s(\frac{1}{2})$	=	triaxial secant deformation modulus for half of failure load
F_q	=	dimensionless cavity expansion factor
FR	=	friction ratio, ratio between friction sleeve and cone end resistance
f_s	=	friction sleeve resistance
H	=	thickness of particular layer considered
I	=	plate load influence factor
I_r	=	rigidity index, ratio between the shear modulus and the initial shear strength
K	=	coefficient of permeability
K_o	=	at-rest coefficient of earth pressure
K_L	=	coefficient of soil viscosity
m	=	modulus number
m_v	=	coefficient of volume change

NC = normally consolidated condition

N_q = dimensionless bearing capacity factor

OC = overconsolidated condition

OCR = overconsolidation ratio

p' = consolidation pressure

p_u = ultimate cavity pressure

q = initial isotropic state of stress

q_c = cone end resistance, often referred as point resistance

q_o = ultimate point resistance during pile testing

q_p = net cone resistance

r = radial distance from cavity centre

R_p = radius of plastic zone (cavity expansion)

R_u = ultimate cavity radius

$R_{(p')}$ = effective depth of consolidation reduction factor

t = time

T = time factor

U = pore pressure

z = depth

α = number expressing the relationship between cone resistance and compressibility for normally consolidated conditions; Henkel's pore pressure parameter

β = number expressing the relationship between cone resistance and compressibility for overconsolidated conditions; Henkel's pore pressure parameter

γ = unit weight

δ = plate settlement

Δ = average volumetric strain occurring in the plastic zone during a cavity expansion

Δe = change in void ratio

ΔU = excess pore pressure

$\Delta\sigma$ = vertical increment of pressure; average normal stress change

$\Delta\tau$ = average shear stress change

η = number expressing the relationship between compressibility and confining stress

ν = Poisson's ratio

ξ_v = volume change factor

$\sigma_1, \sigma_2, \sigma_3$ = major, intermediate, minor principal stress

$\sigma_R, \sigma_t, \sigma_z$ = radial, tangential, axial stress in polar coordinates

τ = shear stress

τ_o = initial shear strength

τ_u = ultimate shear strength

ϕ = angle of shearing resistance

ϕ_o = constant angle defining the curved failure envelope

Other symbols are defined where introduced in the text.

CHAPTER 1

INTRODUCTION

One of the earliest technical publications describing the use of static sounding tools dated from 1922 (Fellenius et al 1922). This reference describes a static sounding method developed in about 1917, by the Swedish State Railways. It consisted of a sounding rod which was forced into the soil, in part by a static load and in part by rotation of the rod. From this simple sounding method, a series of mechanical improvements were introduced (Barentsen (1936), Terzaghi (1930), Huizinga (1942), De Beer (1945), Ostenfeld (1942), Vermeiden (1948), Begemann (1953)), culminating in the present-day mechanical cone penetration test with local friction sleeve. Even with the improvements, the basic principle of cone penetration tests still remains the same, i.e. to push a rod into the ground, to measure the force required and to interpret this force in terms of soil properties.

The development of electrical transducers has increased the potential of many in situ techniques, transforming limited and unreliable tools into powerful instruments at the disposal of the civil engineer. The static sounding method can be considered one of the in situ testing techniques that has most improved with the advent of transducer technology. As a result, the electrical cone penetrometer with internal load cells has been developed, which permits a continuous and direct recording of the resistances (point and sleeve). A very important reason to justify the development of the electrical penetrometer is that the refinements eliminate: a) separate advance of the conical point and the sleeve; b) point and sleeve load transmissions through the inner rods to the surface. These points can impose serious limitations on the mechanical systems. Rocha-Filho (1976) comments on the mechanical and electrical cone penetrometer tests, their advantages and disadvantages, and potential sources of errors in the performance of these tests.

Terzaghi and Peck (1967) have pointed out that: "If the sounding method is to be used to full advantage, the technique must be adapted to the

subsoil conditions". For this reason a great variety of cone penetration equipment and methods have been developed, in response to the variety of problems and soil conditions found in practice.

In the European Symposium on Penetration Testing, held in Stockholm, 1974, there were indicated some extra possibilities of measurements which can be adapted to the electrical penetrometer. In addition to the point and sleeve resistances, alternatives to or combinations of the following measurements, were mentioned:

1) Pore pressure
2) Permeability
3) Fricative sound on penetrometer tip or seismic measuremements (by phonic devices)
4) Density and moisture content (by nuclear devices)
5) Resistivity

Obviously, the most favourable combination will be adopted according to the necessity imposed by the different design requirements. However, the measurement of the induced pore pressure during a penetration process should be considered one of the most important requirements. An understanding of the phenomenon controlling the excess pore pressure development should make it possible to interpret the results in terms of fundamental soil properties. Consequently, this knowledge may provide a theoretical basis, so that extrapolation of results to real problem need not be mostly empirical.

The theoretical developments with respect to the determination of the fundamental soil parameters from the penetration results, continues along two separate paths: the bearing capacity and the cavity expansion approaches.

Most of the existing theories on bearing capacity are based on the work of Prandtl (1921). His solution was later empirically modified in order to include the effects of different parameters, (Reissner (1924), Terzaghi (1943), Meyerhof (1951, 1955), Skempton (1951)). Empirical and semi-empirical

formulas, as well as numerical solutions covering a variety of important practical problems, are now available.

The cavity expansion approach consists basically of obtaining the ultimate pressure required to expand a cavity in the soil mass, (Bishop, Hill and Mott (1945), Gibson (1950), Chadwick (1959), Skempton et al (1953), Gibson and Anderson (1961), Ladanyi (1961, 1963), Vesic (1972)). Its increasing use is due to the absence of a more realistic analytical model of the penetration process that is based on a reliable theoretical basis.

This thesis will be concerned with the measurements of excess pore pressure and their effects during the penetration process. The structure of this thesis falls naturally into three main topics: instrumentation, settlement analysis and rate effect. Chapter 2 is concerned exclusively with cone penetration resistance as an indication of soil compressibility. In this chapter, the methods used for predicting the settlement of foundations on sands based on cone penetration resistance are discussed. An attempt is made to analyse the main parameters affecting the relationship between cone resistance and compressibility for normally-and over-consolidated sands. Chapter 3 deals with the measurements and effects of excess pore pressure during the penetration process reported in the literature. In chapter 4 the objective of this work is discussed. Chapters 5, 6 and 7 are concerned respectively with: details and performance of the apparatus, description of the soil, sample preparation and testing procedure. In chapter 8 the results obtained from cone penetration tests are analysed. An attempt is made to indicate qualitatively the rate effect on penetration resistances. Chapter 9 presents results from plate loading tests. Relationships between cone resistance and compressibility for normally-and over-consolidated conditions have been established. An approach is outlined for considering the effect of stress history upon the relationship between cone resistance and compressibility. Finally, Chapter 10 summarises the important conclusions emerging from this research.

It is hoped that these findings will lead to an improved understanding of the penetration process in saturated sands.

CHAPTER 2

SETTLEMENT ANALYSIS BASED ON STATIC CONE PENETRATION TESTS

2.1 INTRODUCTION

The cone penetration test has been used extensively as an indirect method for predicting the settlement of foundations on sands. This method consists of establishing an empirical correlation between compressibility and cone resistance values. Theoretically the number expressing this relationship can be influenced by a variety of factors. In practice, this number is presented as a linear correlation or as a non linear correlation considering it as a function of the relative density.

Sutherland (1974) comments on the historical development of this method presenting some of the main relationships applied for granular material. De Beer (1974a) table IV, summarises the use of static cone resistance as an indicator of compressibility around the world. Sanglerat (1972) describes some of the current methods. Mitchell and Gardner (1975) present in their very comprehensive state-of-the-art report many of the correlations indicating compressibility as functions of the static cone resistance. Their list covers normally consolidated, overconsolidated, dry and wet soils.

Judging from the attention devoted to the use of static cone resistance for determining compressibility, one can say that this method, either for its practicality or due to the absence of a better one, is presently the best empirical method for such a purpose.

The empirical nature of the penetration resistance tests and the extrapolation of the measured failure condition to the deformation properties are the main sources of criticism directed at such a method when applied to settlement analysis. However, as pointed out by Schmertmann (1970), the

method can provide a measure of the shear strength and for granular soil the compressibility is greatly dependent on its shear strength.

Surely the first use of the cone test in sand was to measure strength. Compressibility was then derived from strength as a secondary correlation.

2.2 LINEAR CORRELATIONS FOR NORMALLY CONSOLIDATED DRY SAND

Most of the relationships between cone resistance and compressibility are based on the semi-empirical correlation obtained by Buisman (1940) working with Terzaghi's one-dimensional compression formula for settlement analysis.

From the one-dimensional approach, the settlement of a footing will be given by:

$$\delta = \frac{1}{C} \text{Ln} \left(1 + \frac{\Delta\sigma}{\sigma_o} \right) H \qquad 2.1$$

where C = constant of compressibility

σ_o = is the effective overburden pressure at the considered depth

$\Delta\sigma$ = is the vertical increment of pressure at the depth due to the foundation loading

H = is the thickness of the particular layer considered.

Buisman (1940) assumed in his analysis: 1) a penetrometer having an idealized hemispherical base; 2) the occurrence of only vertical elastic compression below the penetrometer. Employing Boussinesq's stress distribution theory, he developed a relationship between cone resistance and the constant of compressibility as:

$$C \leqslant \frac{3}{2} \frac{q_c}{\sigma_o} \qquad 2.2$$

$$C\sigma_o = \frac{3}{2} q_c = \frac{1}{m_v} = E_s \qquad 2.3$$

giving a lower limit of the constrained (oedometer) modulus.

De Beer (1945) extended this approach and based on the following simplification:

$$\delta = \frac{1}{C} \text{Ln} \left(1 + \frac{\Delta\sigma}{\sigma_o}\right) H \simeq \frac{1}{C} \frac{\Delta\sigma}{\sigma_o} H \qquad 2.4$$

proposed a linear increase of Buisman's E_s (constrained modulus) with effective overburden pressure.

Dahlberg (1974) pointed out that this simplification is only possible if $\Delta\sigma$ is small compared with σ_o. He further comments that the use of eq. 2.4 for settlement calculation is in theory limited to very loose compressible soils, in which lateral contact or transmission of the stresses among grains would not exist, i.e. the case of vertical elastic compression with Poisson's ratio equal to zero.

In general, the relationship between cone resistance and compressibility defined by one-dimensional approach is obtained as follows:

$$\Delta e = C_c \text{Log} \left(1 + \frac{\Delta\sigma}{\sigma_o}\right) \qquad 2.5$$

C_c is the compression index

Δe is the change in void ratio

From eq. 2.1 and eq. 2.5 it follows:

$$C = 2.3 \frac{(1 + e)}{C_c} \qquad 2.6$$

defining a parameter α relating C and C_c to q_c

$$\alpha q_c = C\sigma_o = \frac{2.3\,(1 + e)}{C_c}\,\sigma_o \qquad 2.7$$

The coefficient of volume change, m_v, can be expressed as:

$$m_v = \frac{C_c}{2.3\,\sigma_o\,(1 + e)} \qquad 2.8$$

so, it follows that

$$E_s = \frac{1}{m_v} = \alpha q_c \qquad 2.9$$

Meyerhof (1965), observing settlements of 17 structures, noted that the actual settlements were overestimated by a factor of two when compared with those predicted by Buisman's method. He suggested a correction leading to an arbitrary modification in Buisman's α factor from 1.5 to 1.9.

Trofimenkov (1964) from in situ cone penetration and plate load tests found that;

$$E_s = 5q_c + 100 \text{ (in Kg/cm}^2\text{)} \quad \text{- average value} \qquad 2.10$$

$$E_s = 2.5q_c \quad \text{- lower limit} \qquad 2.11$$

Bachelier and Parez (1965) investigated the relationship between cone resistance and the oedometer constrained modulus. They found for fine sand that

$$E_s = 1.3q_c \qquad 2.12$$

Thomas (1968) from laboratory investigation concluded that, the relationship between cone resistance and compressibility characteristics of three sands was independent of the sand grading, particle size and overburden pressure. He found that:

$$E = \alpha q_c \text{ where } 3 < \alpha < 12 \qquad 2.13$$

Schmertmann (1970) proposed a new method for computation of the static settlement of isolated, rigid, concentrically shallow foundations over sand. The method employs elastic half-space theory in a simplified form and uses the static cone bearing capacity as a practical means for determining in-situ compressibility E_s. He adopts a simplified distribution of vertical strain under a foundation expressed as a strain influence factor and considers the significant vertical strain to extend to a depth of two times the least width of the foundation. From in situ screw-plate load test, he obtained the following relationship:

$$E_s = 2q_c \qquad 2.14$$

Bogdanovic (1973) based on analysis of silo settlements over a period of

10 years, found that:

$$E_s = 1.5q \qquad 2.15$$

Schmertmann, Hartman and Brown (1978) improved the Schmertmann (1970) strain factor method for the prediction of settlement over sand and suggested that:

$$E_s = 2.5q_c \text{ for axisymmetric (square, circular footings)} \qquad 2.16$$

$$E_s = 3.5q_c \text{ for plane strain (long footings)} \qquad 2.17$$

Figure 2.1 summarises all these relationships.

2.3 NON-LINEAR CORRELATIONS FOR NORMALLY CONSOLIDATED DRY SANDS

2.3.1 GENERAL

De Beer (1974b) presents a dimensional analysis on the problem of using results from static sounding tests. He concluded that the cone resistance is dependent on a very large number of independent parameters, therefore, it is not possible to establish an absolute relationship between the cone resistance and one of the parameters separately. He further comments that it does not preclude the possibility of establishing approximate relationships, which have a practical meaning, provided precautions are taken to define the limits of application. He also classifies parameters of varying degrees of influence.

In general, the penetration resistance of a soil is a complex function of its deformation, strength and compressibility characteristics.

In some conditions, grain crushing may have a strong influence on the value of the cone resistance. Due to very high localized stresses, grain crushing might occur during tests presenting high values of cone resistance. Thomas (1968) found that grain crushing in sand is likely for values of cone resistance greater than 100 Kg/cm^2. Veismanis (1974) concluded from

laboratory investigations that for a sand having the same initial density, the cone resistance is a linear function of overburden stress up to a cone resistance that produces extensive grain crushing. He observed grain crushing in a specific sand for cone resistance of about 100 Kg/cm^2. Figure 2.2 shows the influence of grain crushing on cone resistance value.

After reaching the so called "critical depth" the cone resistance remains constant, no longer increasing with depth of penetration. However, the compressibility decreases, increasing the value of E, with confining stresses. Therefore, a relationship indicating compressibility as a unique function of cone resistance should be applied only above the critical depth.

Folque (1974), presents a method of indirect correlations for obtaining compressibility below the critical depth. He considers the results obtained above the critical depth and extrapolates them using the approach by Ko and Scott (1967) relating the variation of bulk modulus of elasticity with hydrostatic pressure.

2.3.2 THEORETICAL APPROACH

Using expansion cavity theory, (Vesic (1972)), for cohesionless material we have:

$$p_u = \sigma F_q \qquad 2.18$$

where p_u is the ultimate cavity pressure

σ is the initial state of stress, it can be expressed as a function of the initial vertical stress (σ_i) and the at-rest coefficient of earth pressure (k_o) and F_q is the dimensionless cavity expansion factor given as:

$$F_q = f_1(\phi) \left[I_r \xi_v\right]^{f_2(\phi)} \qquad 2.19$$

f_n denotes function of the parameter in the brackets

I_r is the rigidity index, defined as the ratio between shear modulus and initial shear strength or $I_r = f_3(E, \nu, \sigma, \phi)$

ξ_v is the volume change factor, dependent on the volumetric strain in the plastic region. This factor can be expressed as a function of the friction angle, state of stress and stress-strain curve indicated by a compressibility factor,

$\xi_v = f_4 (\phi, \sigma, E,)$

Replacing these values in eq. 2.18 and expressing ν and K_o in terms of ϕ, we have:

$$p_u = f_5 (\sigma_i) f_6 (\phi) [E]^{f_7(\phi)} \quad \text{or}$$

rearranging $E = F_1 (\phi) \times F_2 (\sigma_i) \times (p_u)^{F_3(\phi)}$ 2.20

From eq. 2.20, one can conclude that, for a given sand, the relationship between compressibility and cone resistance is not linear and depends at least on the relative density and confining pressure.

The effect of grain crushing can be taken into account by considering curved envelopes on the theory of expansion cavity. Baligh (1976) presents solutions for cavity expansion in sands with curved envelopes.

The expansion pressure, p_{uc}, in the case of a curved failure envelope can be written as:

$$p_{uc} = \beta p_u \qquad 2.21$$

β is the modification factor, and has been solved as a function of ϕ_o, I_r, Δ,σ / σ_o and α,

where ϕ_o and α are constant angles defining the curved envelope.

σ_o is an arbitrary reference stress.

Δ is the average volumetric strain in the plastic region.

For given values of ϕ_o, I_r, and α, the β values decreases with increasing confining pressure, and it follows:

$$p_{uc} < p_u \qquad 2.22$$

leading to $E_c < E$ 2.23

Consequently, correction should be made in the value of the compressibility if grain crushing does not occur under the proposed foundation loading.

Janbu (1974a) outlined the main steps of a proposed method for determining compressibility from cone resistance values. From his previous work, (Janbu (1963)), the tangent modulus of compressibility, M, determined by triaxial or oedometer tests is equal to:

$$M = m \sqrt{(p' + a)\, \sigma_r} \qquad 2.24$$

where m is the modulus number, varying from 100 to 500 (depends on the relative density).

p' is the consolidation pressure (effective overburden pressure for field condition)

a is the attraction, defined as the cohesion intercept divided by the tangent of the friction angle. In granular soils this value could be due to particles cementation.

σ_r is the reference stress equal to 100 K_N/m^2.

Janbu and Senneset (1974) have showed that the net cone resistance is given by:

$$q_p = (N_q - 1)(p' + a) \qquad 2.25$$

where q_p is the net cone resistance, equal to q_c minus the overburden pressure.

N_q is the bearing capacity factor depending on the friction angle

So, it follows that:

$$M = m_p \sqrt{q_p \times \sigma_r} \qquad 2.26$$

$$\text{where } m_p = \frac{m}{\sqrt{N_q - 1}} \qquad 2.27$$

He indicates that the largest value of m_p will be for dry cemented sands.

2.3.3 EXPERIMENTAL RESULTS

Schultze and Meltzer (1965) concluded from laboratory and field tests that the correlation between cone resistance and compressibility is dependent on the overburden pressure. They used the method proposed by Schultze and Moussa (1961) for evaluating the modulus of compressibility based on the maximum, minimum and the natural values of the void ratio. The expression for the modulus of compressibility was determined as:

$$E_s = \eta \times \sigma^{0.522} \quad (\text{in Kg/cm}^2) \qquad 2.28$$

and,

$$\eta = 301.1 \text{ Log } q_c - 382.3\gamma z = 60.3 \pm 50.3 \qquad 2.29$$

The expression for the coefficient η was established from a result of statistical analysis applied over a number of 90 tests. It is valid for values of γz (overburden pressure) varying from 0 Kg/cm^2 to 0.8 Kg/cm^2.

As noted by Thomas (1968), the true influence of overburden pressure at great pressure was not measurable. This was due to limitation in the apparatus used for this investigation with no independent means of applying a vertical pressure.

By comparing the relationship 2.28 and 2.24, one could note the similarity between the proposed and Janbu methods.

It is interesting to note that they also proposed a relationship for determining the relative density as:

$$D_R = 0.351 \text{ Log } q_c - 0.421 \gamma z + 0.071 \pm 0.067 \qquad 2.30$$

By comparing this expression with equation 2.29, we have:

$$\eta = K_1 D_R \simeq 857.8 \ D_R \qquad 2.31$$

Where K_1 is a constant

and, assuming σ = 1Kg/cm^2 in the equation 2.28, it leads to:

$$E_s = \eta \simeq 857.8 D_R \ (D_R = 0 \text{ to } 1 \text{ and } E_s \text{ in Kg/cm}^2) \qquad 2.32$$

Vesic (1970) from insitu tests on instrumented piles, established a simple empirical relationship relating compressibility and ultimate point resistance, q_o, of the pile as:

$$\frac{E_s}{q_o} = 5.5\ (1 + D_R^2) \qquad 2.33$$

The above equation was established by considering Boussinesq's solution for the distribution of the state of stress.

By assuming Midlin's solution for the state of stress under the penetrometer point, he suggested the following relationship:

$$E_s = 2\ (1 + D_R^2)\ q_c \qquad 2.34$$

Consequently, the Buisman's α value would range from 2 to 4 for the loosest and densest states respectively.

Figure 2.3, presents results obtained by Veismanis (1974) from an extensive series of tests, using a flexible-wall testing chamber, where the soil properties, the stresses (vertical and horizontal) and the deformation could be accurately controlled and measured.

His most important observation is that the modulus of deformation is not a unique function of cone resistance and this relationship depends on the initial relative density.

He also observed that for sands following a parabolic stress-strain curve for oedometric compression, a parabolic relationship between compressibility and cone resistance in the pre-crushing region would be expected. This same parabolic tendency was observed by Thomas (1968) in the relationship between compressibility and cone resistance.

Trofimenkov (1974) presented some results obtained from in situ testing on fine alluvial medium and dense sands. The compressibility characteristics of the material have been obtained using plate loading tests. Figure 2.4 shows values of compressibility plotted against cone resistance.

Even considering that these results were obtained for in situ conditions with many uncontrolled variables, it can be noticed that the correlation between compressibility and cone resistance cannot be satisfactorily represented by a single relationship.

Results obtained by Thomas (1968) can also be considered as indicative of the non-linear relationship between compressibility and cone resistance. He found that the number expressing the relationship between compressibility and cone resistance decreases as the cone resistance value increases, See Fig. 2.5.

Dahlberg (1974) investigated from in situ tests in a preloaded natural sand deposit the relationship between compressibility and cone resistance. The compressibility characteristics of the deposit have been estimated using screw plate load test. He found that the relationship between compressibility corresponding to the virgin compression range and cone resistance increases as the cone resistance increases, See Fig. 2.6.

Comparing the results obtained by Thomas and Dahlberg, it can be argued that the tendency of the curve expressing this relationship can be strongly influenced by the method used to determine the compressibility, e.g., oedometer or plate load test.

2.4 CORRELATIONS FOR OVERCONSOLIDATED DRY SANDS

De Beer (1967) proposed a method for evaluating compressibility from cone resistance values for preloaded sands. He uses the constant of compressibility, C, calculated from the cone resistance given by equation 2.2. From oedometer tests carried out on samples having the same density as in the field, two parameters C_{oed} and A_{oed} are defined for loading and unloading conditions respectively as:

$$C_{oed} = 2.3 \frac{(1 + e)}{C_c} \qquad 2.35$$

$$A_{oed} = 2.3 \frac{(1 + e)}{C_s} \qquad 2.36$$

where C_c is the compressibility index

C_s is the swelling index

So, the relationship between compressibility and cone resistance will be given as:

$$E_s = \frac{3}{2} \times \frac{A_{oed}}{C_{oed}} \times q_c \qquad 2.37$$

Due to the necessity of sampling and laboratory testing, one can argue about the practical application of this method.

Compared with the number of correlations proposed for normally consolidated sands, it can be said that the effect of overconsolidation on the relationship between compressibility and cone resistance has been less extensively studied.

From the theoretical point of view, any proposed correlation will suffer the influence from all factors affecting the relationship for normally consolidated plus the effect of overconsolidation.

Veismanis (1974) using a calibration testing chamber investigated the influence of overconsolidation in different sands.

His main conclusions can be summarized as:

a. for a given sand, overburden pressure and initial relative density, the cone resistance will be higher in an overconsolidated sample than in a normally consolidated one.

b. for a given sand and initial relative density, the cone resistance is virtually controlled by the horizontal stress.

Figure 2.7 presents his results, indicating the significance of the overconsolidation ratio. From Fig. 2.7, it can be observed that a relationship between the normalised cone resistance and the lateral stress ratio can be expressed as:

$$\frac{q_{coc}}{q_{cnc}} = \frac{K_{ooc}}{K_{onc}} \qquad 2.39$$

where q_{cnc} is the cone resistance value for normally consolidated conditions.

q_{coc} is the cone resistance value for overconsolidated conditions.

K_{onc} is the coefficient of earth pressure for normally consolidated conditions.

K_{ooc} is the coefficient of earth pressure for overconsolidated conditions.

He argues that this finding only applies to cylindrical-shape electrical penetrometers and proposes a correlation applied to mechanical penetrometers, see Fig. 2.7.

Fig. 2.7 also presents the relationship proposed by Schmertmann (1975) expressed as:

$$\frac{q_{coc}}{q_{cnc}} = 1 + 0.75 \left[\frac{K_{ooc}}{K_{onc}} - 1 \right] \qquad 2.40$$

Assumed values for the lateral stress ratio can be analysed by using the approach proposed by Wroth (1975).

He suggested for lightly overconsolidated soils that:

$$K_{ooc} = OCR \times K_{onc} - \frac{\nu}{1 - \nu} (OCR - 1) \qquad 2.41$$

and for heavily consolidated soils that:

$$m \left[\frac{3 (1 - K_{onc})}{1 + 2K_{onc}} - \frac{3 (1 - K_{ooc})}{1 + 2K_{ooc}} \right] = Ln \left[\frac{OCR (1 + K_{onc})}{1 + 2K'_{ooc}} \right] \qquad 2.42$$

where OCR denotes overconsolidation ratio.

ν is the Poisson's ratio.

m is the inverse of the gradient for unloading conditions in a plot

$$\left[(\sigma_1' + \sigma_3') / \frac{1}{3} (\sigma_1' + \sigma_2' + \sigma_3') \right] \text{ vs Log } \left(\frac{\sigma_1' + \sigma_2' + \sigma_3'}{3} \right)$$

He argues that m can be related to the plasticity index (L_p) and that for sands $m \geq 1.5$.

He also defines lightly overconsolidated soils as the range for which the unloading path is linear ($K_{onc} \leq K_{ooc} \leq 1$ or $1 \leq OCR \leq 5$ say).

Equation 2.41 and 2.42 have been solved using results obtained by Daramola (1978) from an extensive series of laboratory tests on Ham River Sand, classified as a medium-fine sand. The solution of equation 2.42 is presented in Appendix A.1.

From Figure 2.8, we have:

$$K_{onc} = 0.7 - 0.4\ D_R \qquad 2.43$$

And from Figure 2.9:

$$\frac{\nu}{1-\nu} = \frac{0.88 - 0.6\ D_R}{1.12 - 0.6\ D_R} \qquad 2.44$$

Figure 2.10 presents the values of the lateral stress ratio plotted against overconsolidated ratio for different values of the initial relative density. Experimental values obtained by Veismanis (1974) are shown as well.

Some conclusions may be drawn from figure 2.10 as:

a. There is a good agreement between experimental and theoretical values.

b. The range of validity of equation 2.41 increases with increasing relative density, i.e., for a relative density of about 80% and overconsolidation ratio value of 8 the unload path may still be linear.

c. For lightly overconsolidated soils the relationship between lateral stress ratio and overconsolidated ratio is strongly influenced by the initial relative density, and it can be expressed as:

$$\frac{K_{ooc}}{K_{onc}} = (1.9\ D_R + 0.15) \times OCR^{\frac{0.44\ (1 - D_R)}{Ln\ D_R + 1.61}} \qquad 2.45$$

d. for heavily overconsolidated soils this relationship is independent of the initial relative density and can be expressed by a single correlation as:

$$\frac{K_{ooc}}{K_{onc}} = 0.88 \times OCR^{0.38} \qquad 2.46$$

Figure 2.11 presents values obtained by using equations 2.45 and 2.46. This fugure also indicates the correlation proposed by Schmertmann (1975), indicating the lateral stress ratio as a unique function of the overconsolidation ratio and independent of relative density. His correlation can be expressed as:

$$\frac{K_{ooc}}{K_{onc}} = OCR^{0.42} \qquad 2.47$$

Following the present analysis, it can be said that:

$$\frac{q_{coc}}{q_{cnc}} = f\left(\frac{K_{ooc}}{K_{onc}}\right) \qquad 2.48$$

and for lightly overconsolidated soils the lateral stress ratio depends on relative density and overconsolidation ratio while for heavily overconsolidation soils it depends on overconsolidation ratio only.

Hence, any proposed relationship indicating compressibility as a function of cone resistance for overconsolidated soils, in the form:

$$E_{oc} = \beta\, q_{coc} \qquad 2.49$$

where, $q_{coc} = f(D_r, OCR)\, q_{cnc}$ (lightly overconsolidated)

$q_{coc} = f(OCR)\, q_{cnc}$ (heavily overconsolidated)

must consider at least the influence of overconsolidation ratio, relative density and factors affecting the relationship for normally consolidated soils.

2.5 CORRELATIONS FOR SATURATED SANDS

The relationship between compressibility and cone resistance for saturated soils will be strongly influenced by the permeability or generation-dissipation of the excess pore water pressure during the measurement of these values.

Because of the relatively high permeability of sands, the compressibility of the materials are almost the same for saturated and dry conditions. However, during a penetration test in sands generation of excess pore water pressure is likely to happen and may affect the cone resistance value. Therefore, compared with dry sands, the relationship proposed for saturated sands at a given initial relative density and overburden pressure will be:

a. expressed by a higher number, in the case of generating positive excess pore water pressure;

if, $E_{s(d)} = \alpha_{(d)}\, q_{c(d)}$ and $E_{s(s)} = \alpha_{(s)}\, q_{c(s)}$,

for, $E_{s(d)} = E_{s(s)}$ and $q_{c(d)} > q_{c(s)}$,

it follows that: $\alpha_{(d)} < \alpha_{(s)}$

b. expressed by a smaller number, in the case of generating negative excess pore water pressure;

for, $E_{s(d)} = E_{s(s)}$ and $q_{c(d)} < q_{c(s)}$),

if follows that: $\alpha_{(d)} > \alpha_{(s)}$

c. expressed by the same number, in the case of no generation of excess pore water pressure;

for, $E_{s(d)} = E_{s(s)}$ and $q_{c(d)} = q_{c(s)}$,

if follows that: $\alpha_{(d)} = \alpha_{(s)}$

The symbols (d) and (s) denote dry and saturated conditions.

Webb (1970) from in situ screw plate and cone penetration tests established the following relationship for a sand below the water table,

$$E' = \frac{5}{2}(q_c + 30) \text{ in tsf} \qquad 2.50$$

where E' is the equivalent modulus of compressibility equal to $E/(1 - \nu^2)$

Bogdanović (1973) based on analysis of silo settlements over a period of 10 years, found for silty saturated sands that:

$$E_s = \alpha\, q_c \text{ (in Kg/cm}^2\text{)} \qquad 2.51$$

with α ranging from 1.5 to 1.8 for $20 < q_c < 40$.

2.6 SUMMARY AND CONCLUDING REMARKS

The discussions presented in these sections have shown that the use of the static penetration test as an indirect method for evaluating the settlement on granular materials has a historical and practical background supporting its applications. The main aspects of this method are:

1) There are many correlations relating compressibility and cone resistance as a linear function. For normally consolidated conditions the number expressing this linear function varies from 1.3 to 12.

2) The relationship between compressibility and cone resistance for normally consolidated sands is not linear and depends at least on the relative density and confining pressure.

3) This non linear correlation is not a unique function and may increase or decrease with an increase in the cone resistance value. The tendency of the curve will be determined by the stress-strain curve of the sand and by the method used to obtain the compressibility, e.g., oedometer or plate load test.

4) For preloaded sand this relationship is strongly affected by the overconsolidation ratio plus factors influencing the normally consolidated condition.

5) For saturated sands, this relationship will be strongly influenced by the permeability or generation-dissipation of the excess pore water pressure during the measurement of these values. In granular material the compressibility is not significantly affected by saturation. However, the cone resistance value can be higher or lower than the drained condition in case of positive or negative excess pore water pressure occurring during the penetration test.

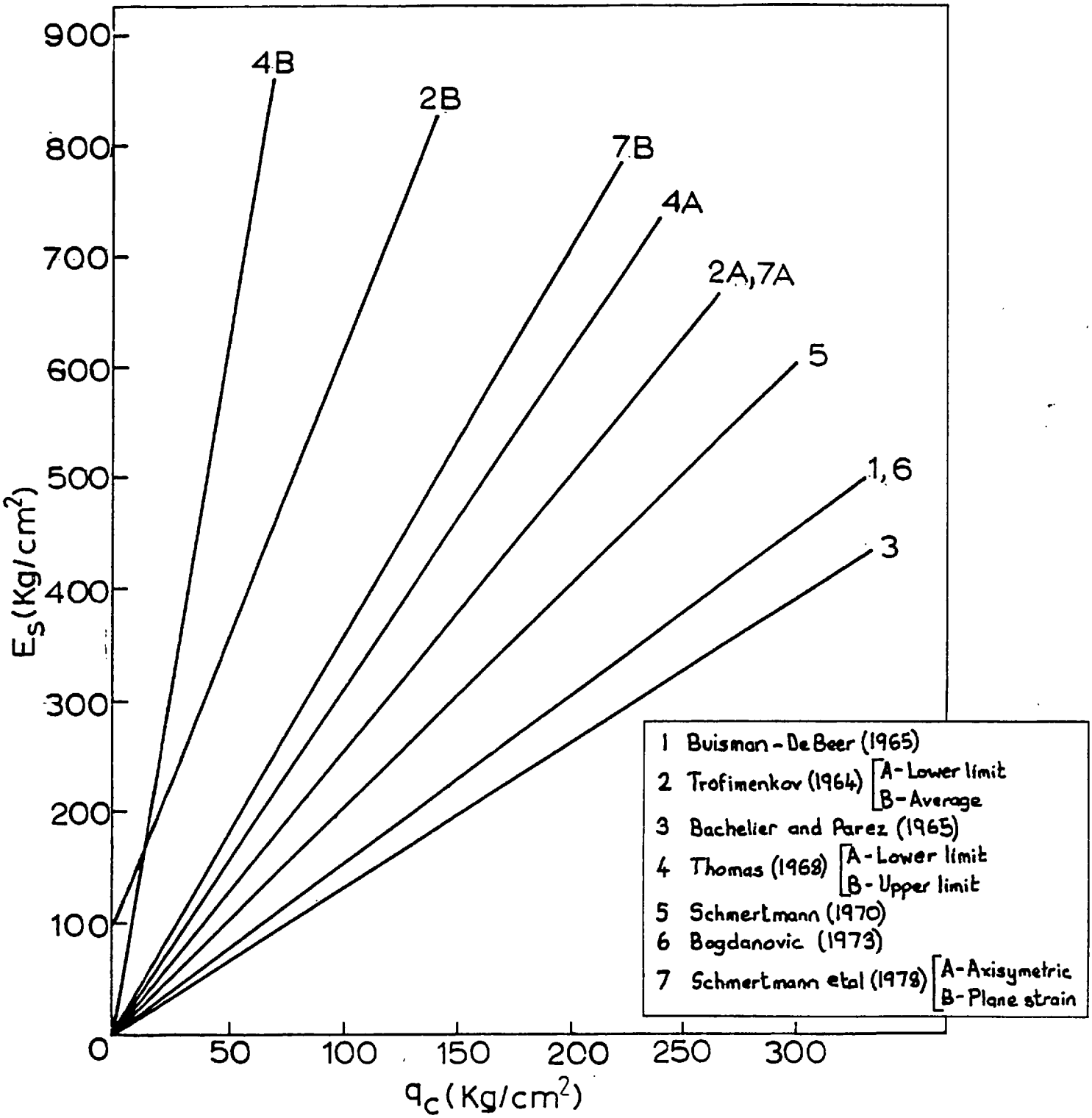


FIGURE 2.1 - LINEAR CORRELATIONS BETWEEN COMPRESSIBILITY AND CONE END RESISTANCE.

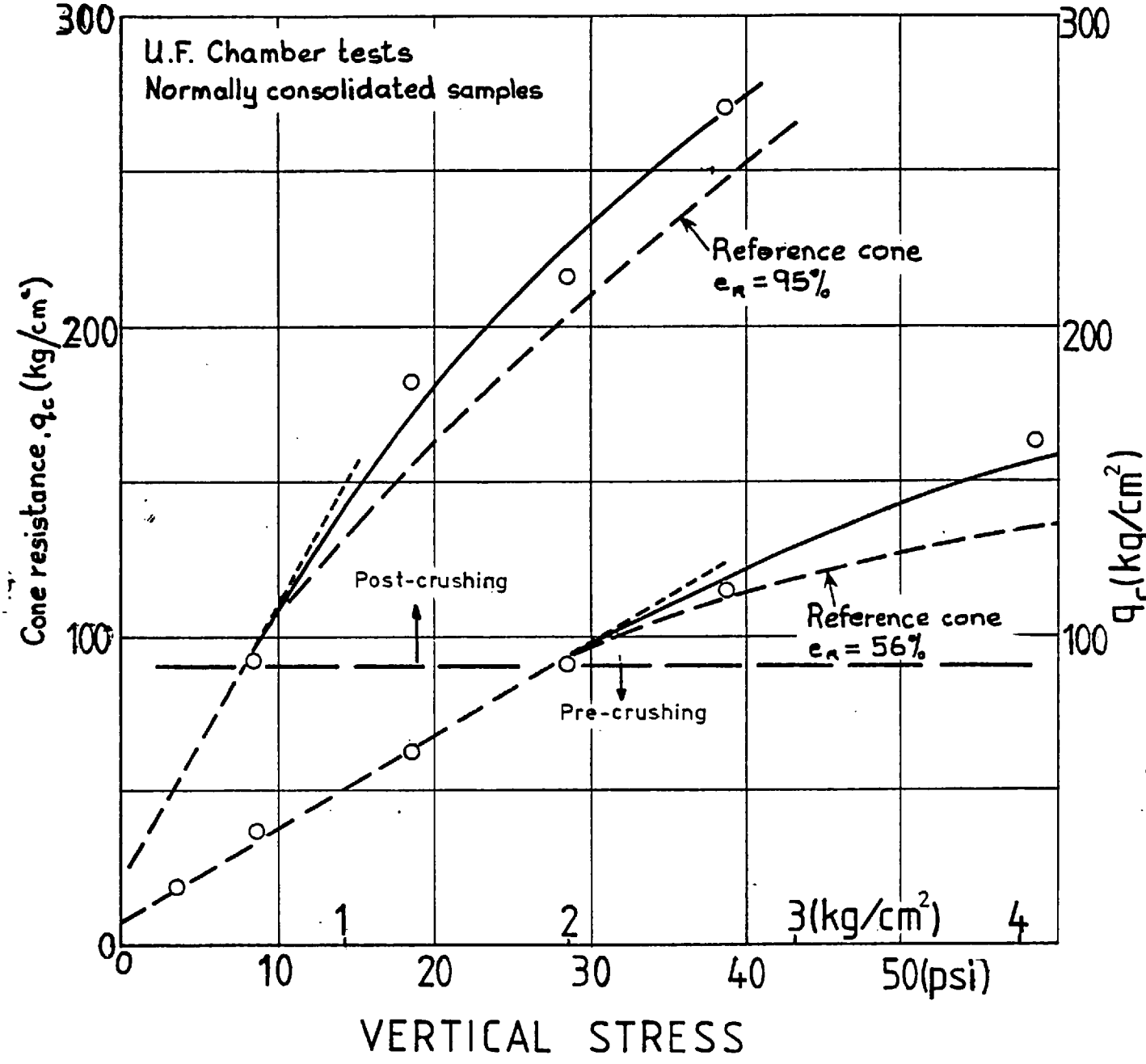


FIGURE 2.2 - EFFECT OF GRAIN CRUSHING ON CONE RESISTANCE(FROM VEISMANIS,1974)

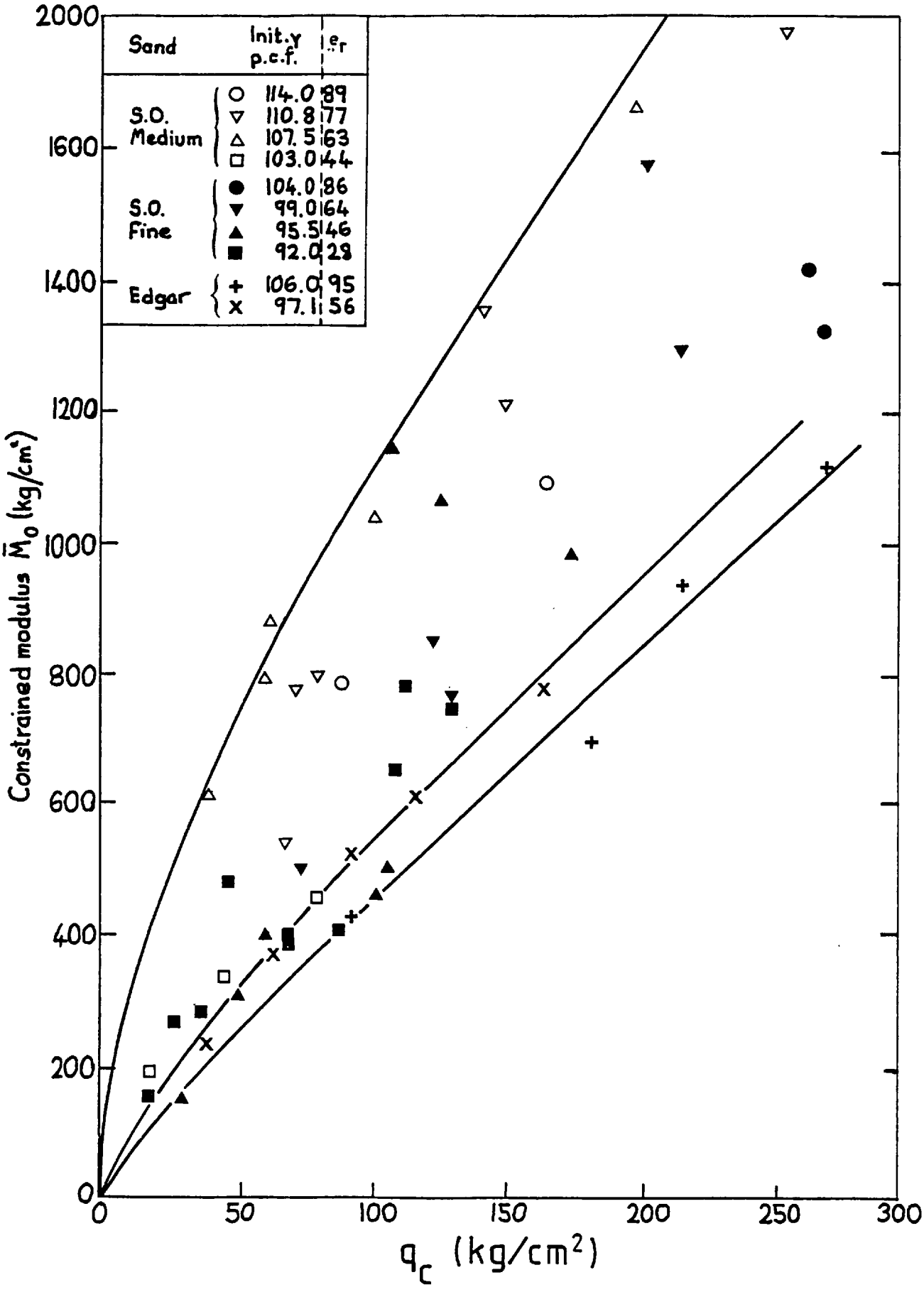


FIGURE 2.3 - CONSTRAINED MODULUS VS CONE RESISTANCE. NC DRY SANDS.
(FROM VEISMANIS ,1974)

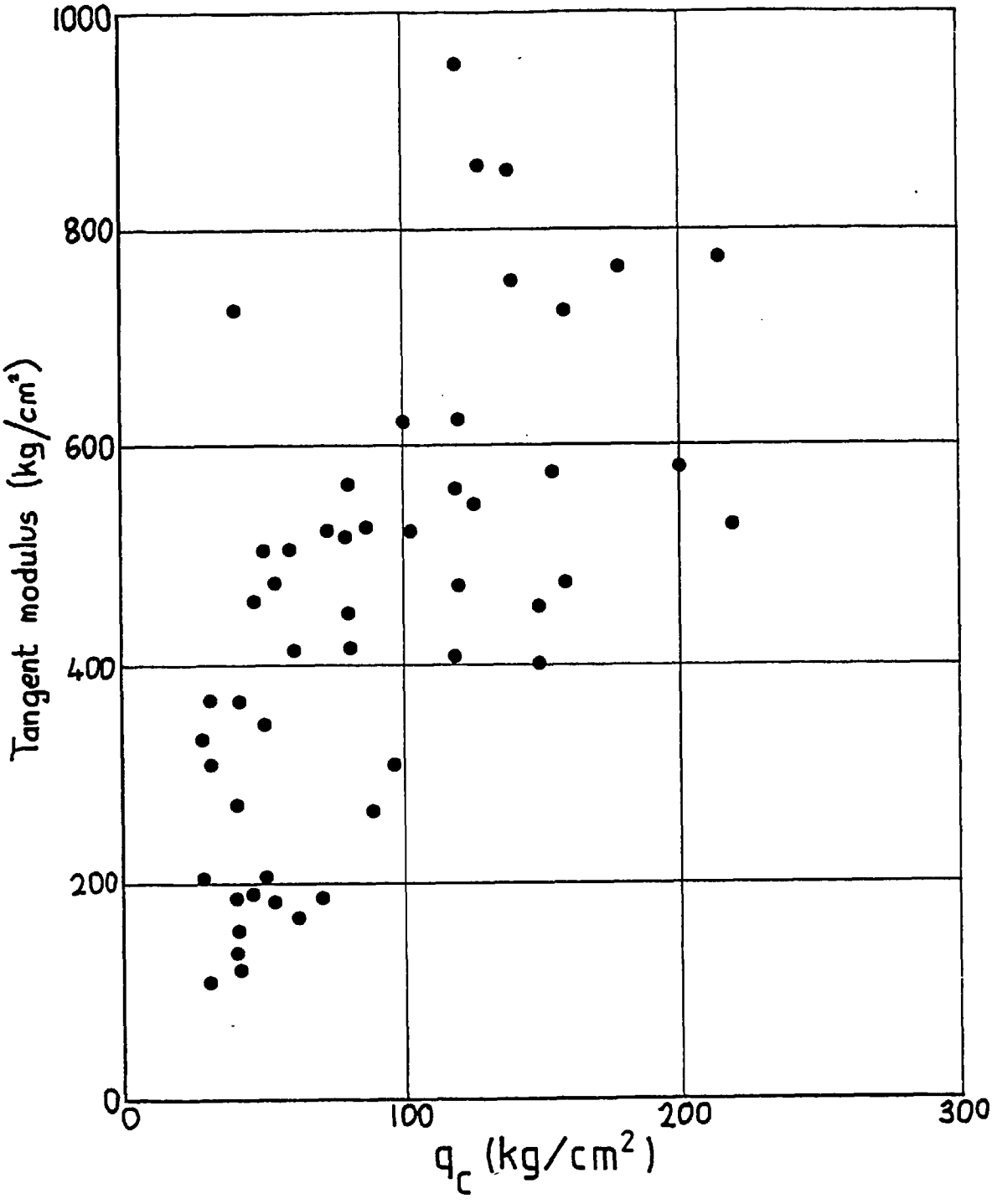
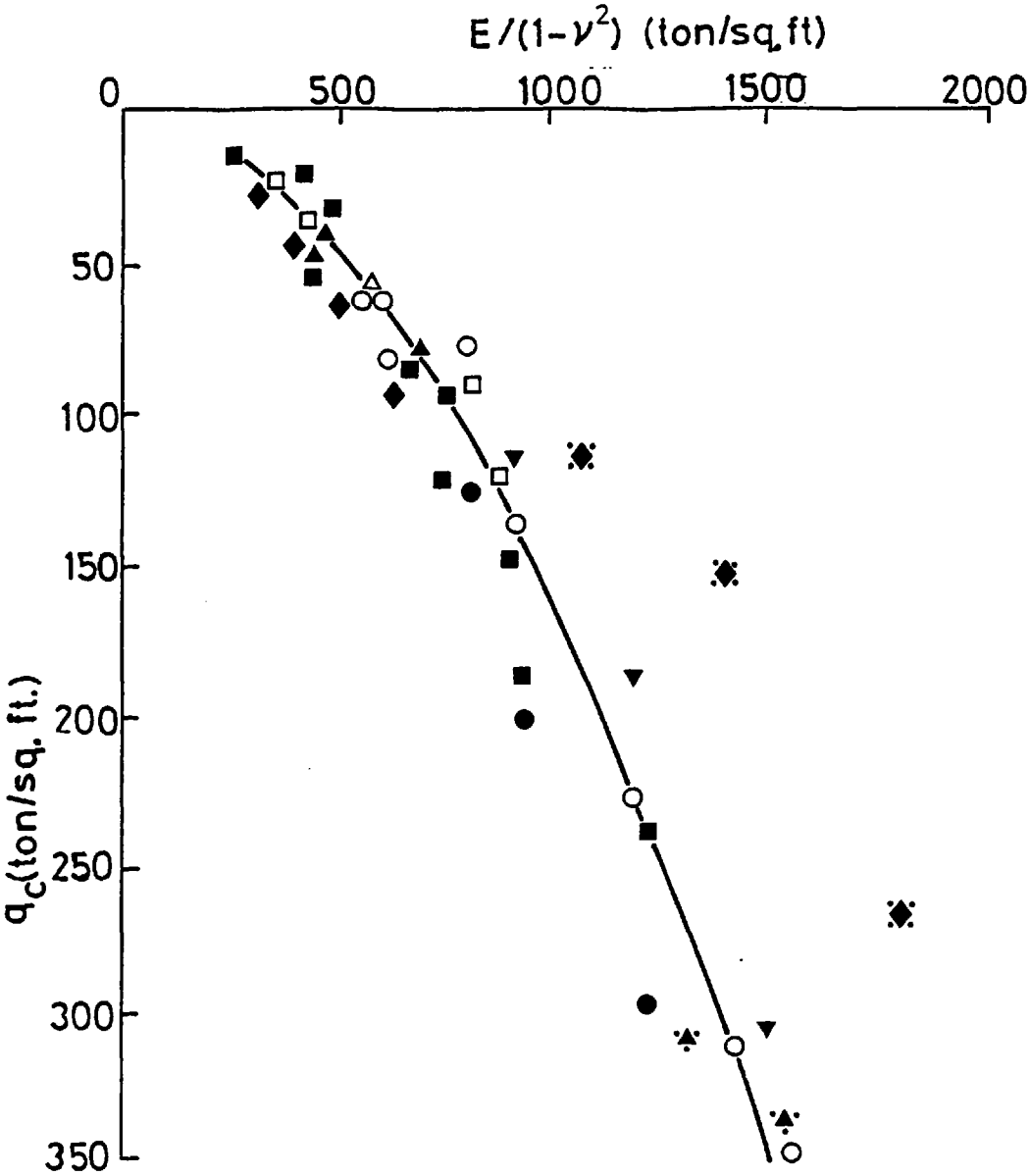


FIGURE 2.4 - PLATE TANGENT MODULUS VS CONE RESISTANCE(FROM TROFIMENKOV,1974)



SAND	SYMBOL	INITIAL POROSITY
1	▲	0.45
	□	0.43
	○	0.38
	▼	0.36
2	▲	0.47
	■	0.46
	●	0.40
3	◆	0,43
	⁘	0,37
	⁂	0,33

FIGURE 2.5 - VARIATION IN CONE RESISTANCE WITH COMPRESSION MODULUS FOR THREE SANDS (FROM THOMAS, 1968).

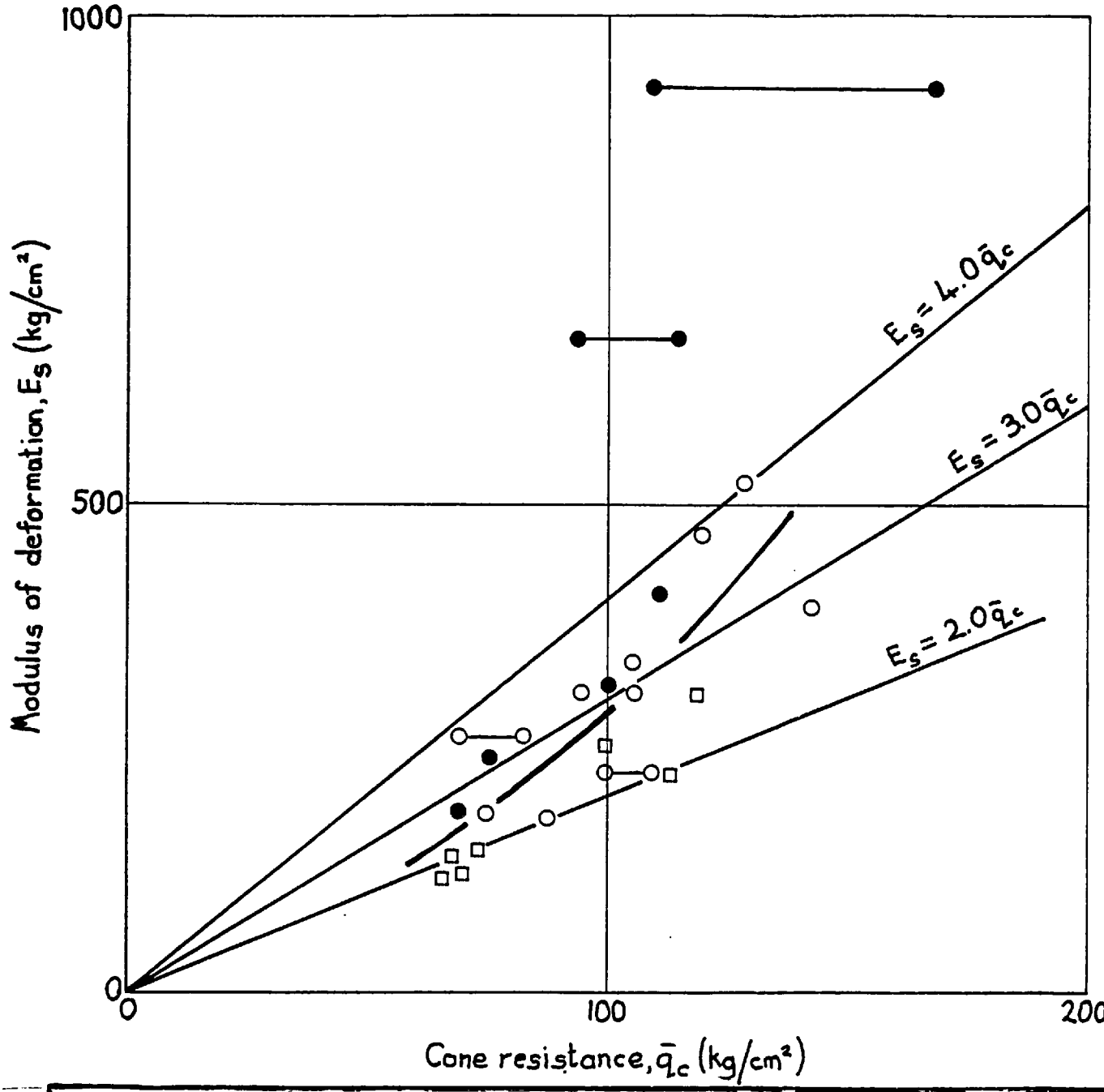


FIGURE 2.6 - RELATIONSHIP BETWEEN SCREW PLATE DEFORMATION MODULUS FOR A SLIGHTLY OVERCONSOLIDATED SAND AND CONE RESISTANCE. MODULUS CORRESPONDING TO THE VIRGIN COMPRESSION RANGE. (FROM DAHLBERG, 1974).

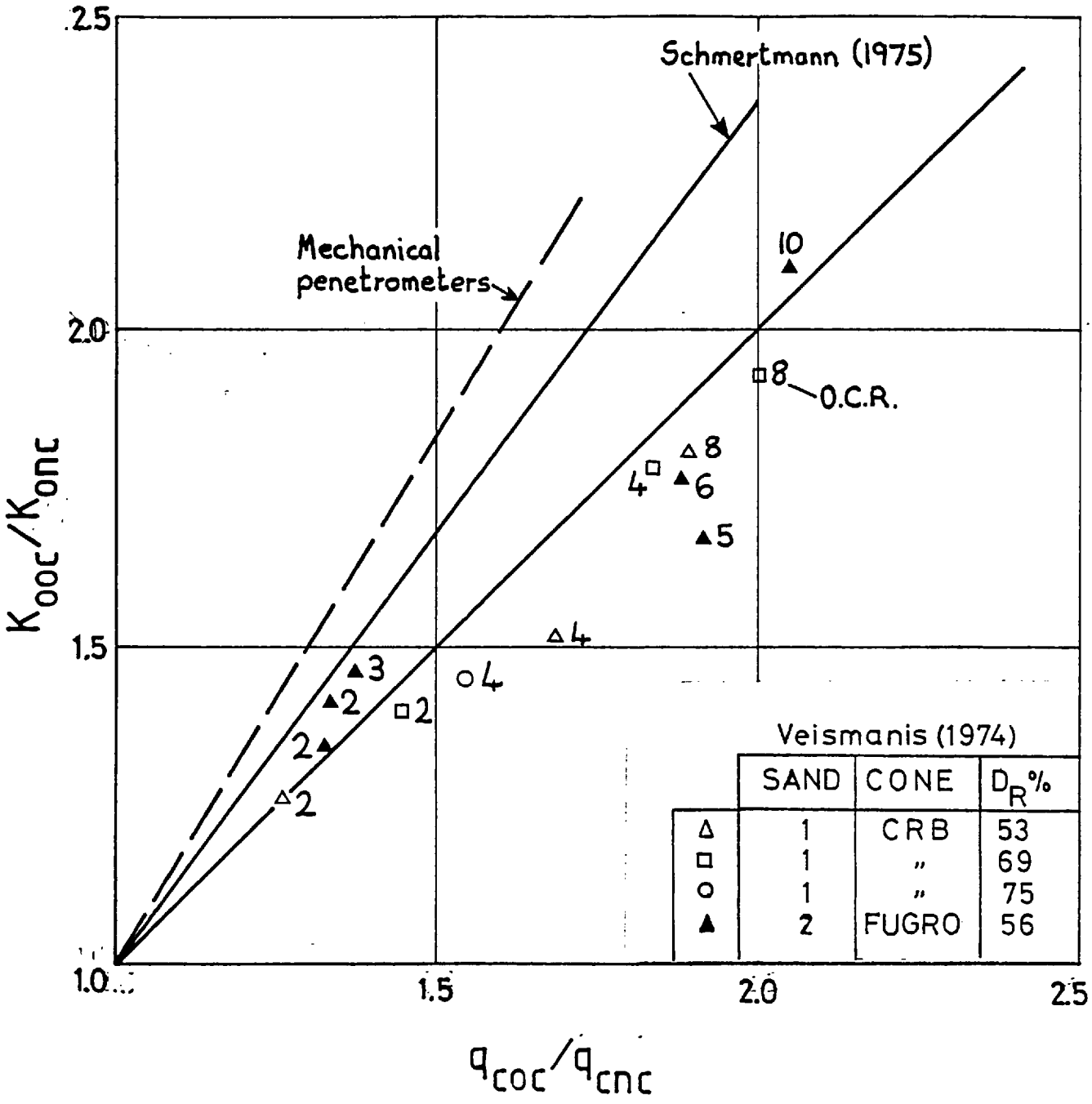


FIGURE 2.7 - CONE RESISTANCE VS LATERAL STRESS RATIO: NORMALISED PLOT

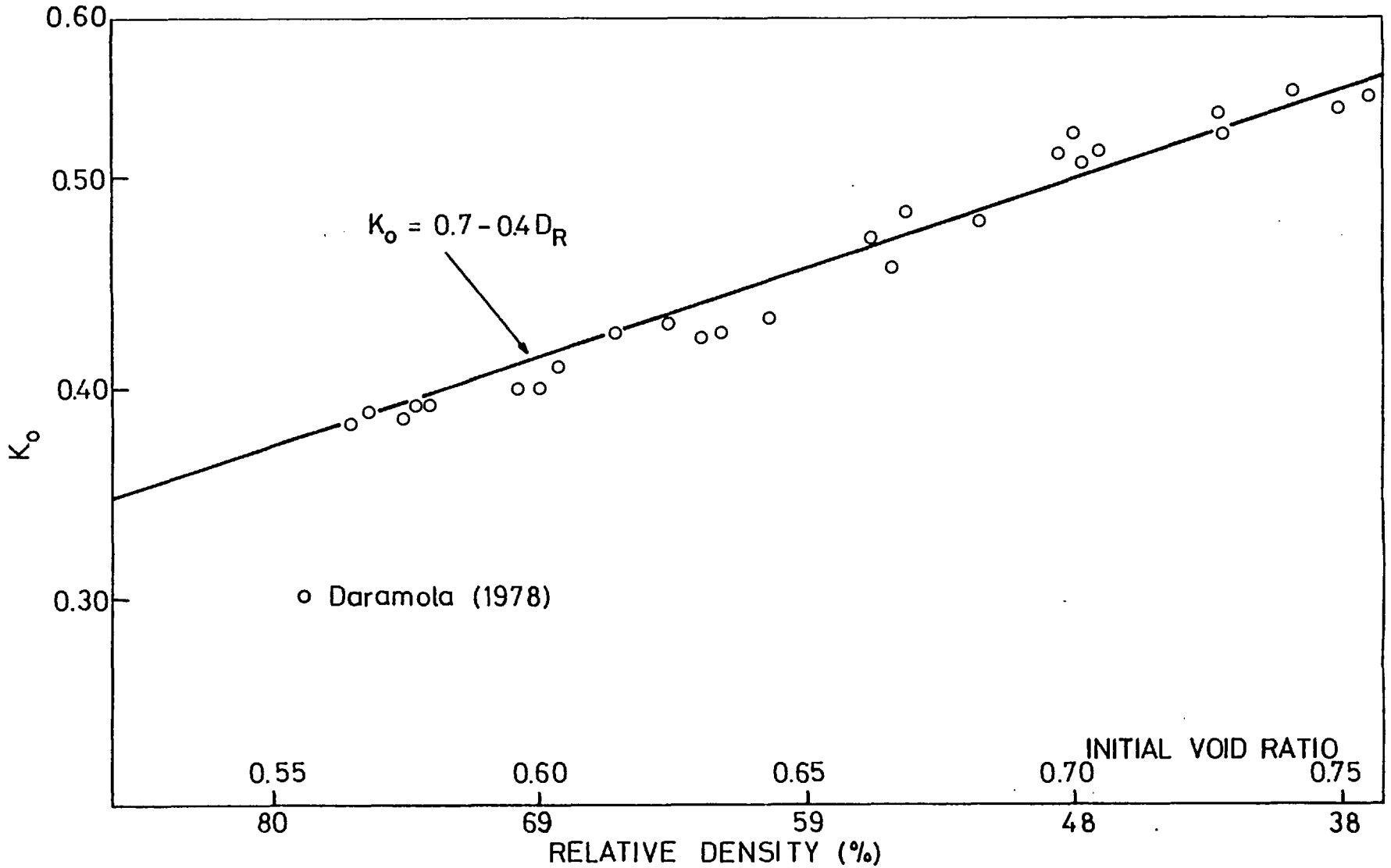


FIGURE 2.8 - VARIATION OF K_o WITH INITIAL VOIDS RATIO

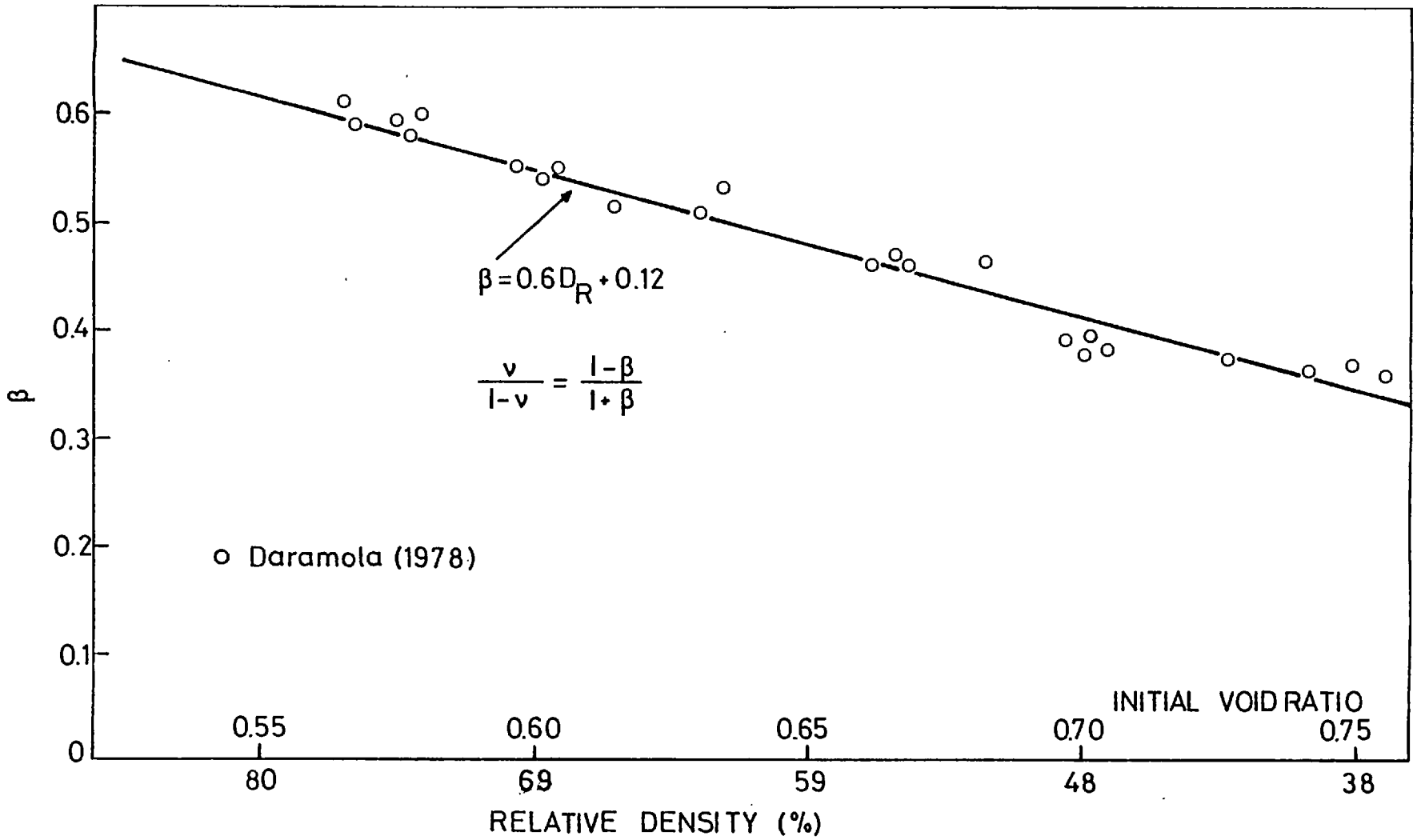


FIGURE 2.9 - VARIATION OF SLOPE OF UNLOADING PATH WITH INITIAL VOIDS RATIO

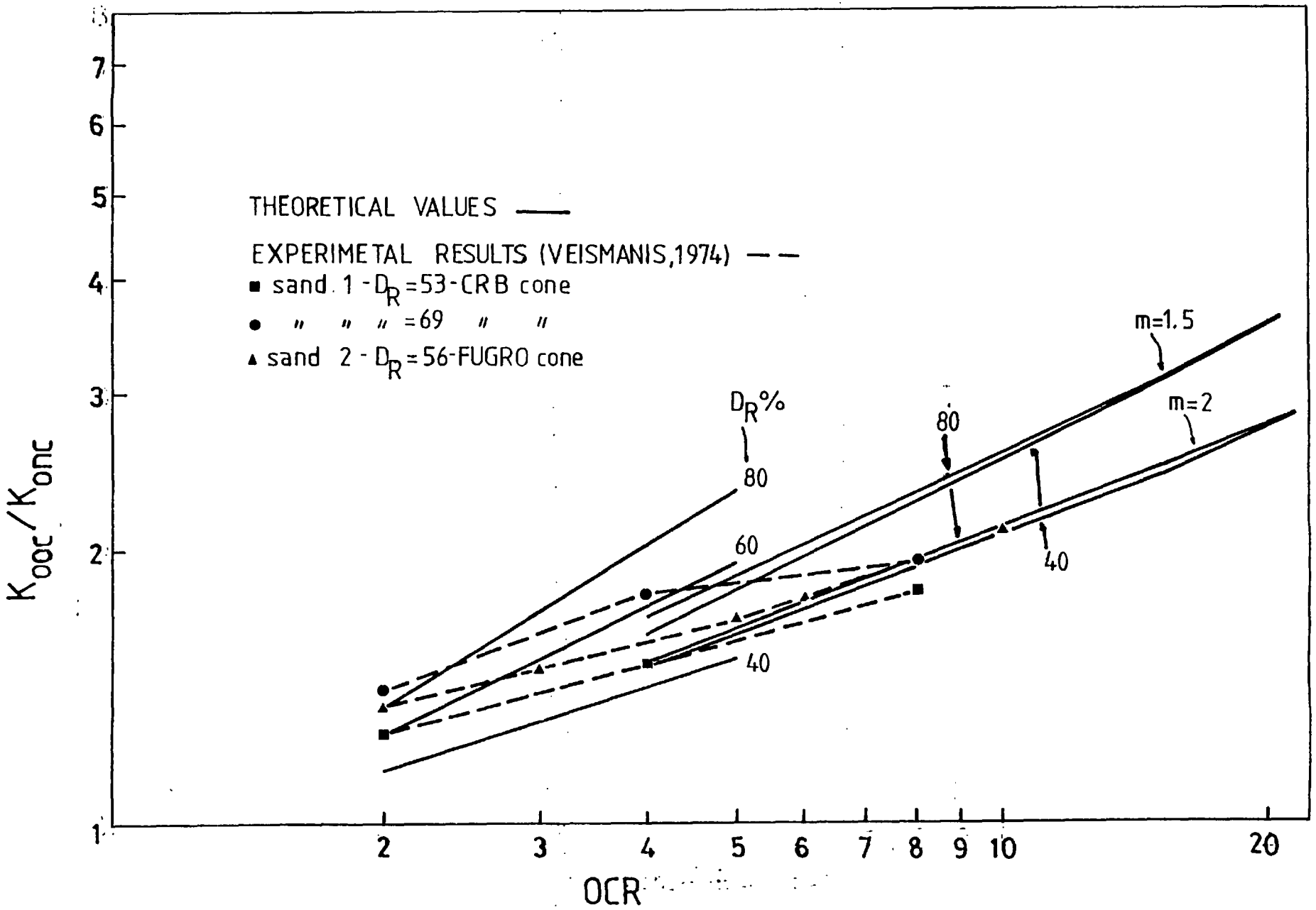


FIGURE 2.10 - LATERAL STRESS RATIO VS OVERCONSOLIDATION RATIO.

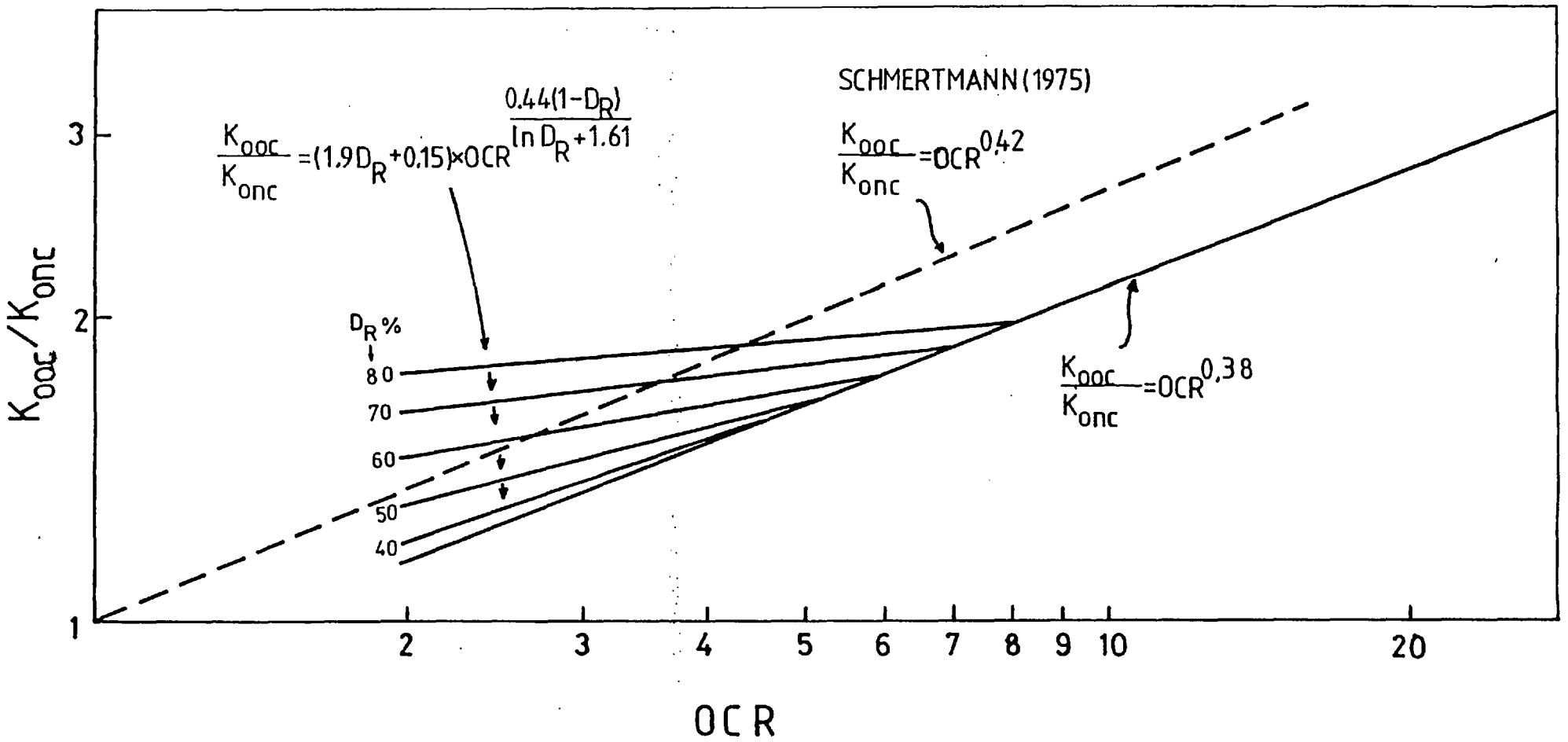


FIGURE 2.11 - VARIATION OF LATERAL STRESS RATIO WITH STRESS HISTORY.

CHAPTER 3
GENERATION OF EXCESS PORE PRESSURE DURING PENETRATION TESTS

3.1 GENERAL

The accuracy of extrapolating results from any field test to the actual problems depends on the understanding of this correlation in terms of fundamental soil properties. Therefore, the interpretation of this relationship requires a knowledge of the effective stress and pore pressure effects during the test and the real problem. This knowledge may provide a theoretical basis for this extrapolation, the absence of it may lead to correlation of an empirical nature.

From the practical viewpoint, the problem associated with the predetermination of the actual working conditions from field test results, is not only related to the generation of the excess of the pore water pressure but also a dissipation problem. Therefore, the coefficient of permeability is the fundamental soil parameter controlling this phenomenon. For soils having relatively high value of the coefficient of permeability, any localized generation of excess pore pressure will quickly equalise to the ambient pressure and this effect may quantitatively be insignificant. On the other hand, for relatively low value of the coefficient of permeability any localized generation of excess pore pressure may strongly influence the magnitude of the measured parameter.

For the specific case of excess pore pressure generated-dissipated during the cone penetration test, the information from the technical literature is rather scanty. The technical literature offers a little more information on the excess pore pressure built up during pile driving, even so, this information is not abundant. Due to the geometrical similarity between cone penetration tests and actual driven piles, information from one can be used to understand the phenomena involved in the other. However problems associated with scale, form and rate of penetration, should be noted.

3.2 THEORETICAL BACKGROUND

The excess pore pressure accompanying changes in total stress may be expressed as functions of the average normal stress change and of the average shear stress change as follows:

$$\Delta U = \beta \Delta\sigma + \alpha \Delta\tau \qquad 3.1$$

where; $\Delta\sigma = (\Delta\sigma_1 + \Delta\sigma_2 + \Delta\sigma_3)/3$ is the average normal stress change.

$\Delta\tau = \left[(\Delta\sigma_1 - \Delta\sigma_2)^2 + (\Delta\sigma_2 - \Delta\sigma_3)^2 + (\Delta\sigma_3 - \Delta\sigma_1)^2\right]^{\frac{1}{2}} / 3$, is the average shear stress change.

α and β are the pore-pressure parameters defined by Henkel (1959).

$$\Delta\sigma_N = \sigma_{N\,(final)} - \sigma_{N\,(initial)}$$

For field conditions, difficulties in using this approach arise with the definition of the final state of stress. For the specific case of a penetration process (penetrometer, pile, etc.), problems associated with rotations of the principal stresses as well as definition of the plastic zone will, obviously, make the analysis more complex.

Vesic (1973), using the theory of cavity expansion in an infinite soil mass, and assuming that initially the soil mass was subjected to an isotropic compressive state of stress, found that: (see Fig. 3.1).

a) the pore pressure induced by an expansion of a spherical cavity as:

$$\frac{\Delta U}{\tau_f} = 0.943\,\alpha_f + 4\,\mathrm{Ln}\left(\frac{R_p}{r}\right) \qquad 3.2$$

for a variation of the total stresses within the plastic zone expressed as:

$$\frac{\Delta\sigma_R}{\tau_f} = 4\,\mathrm{Ln}\left(\frac{R_p}{r}\right) + \frac{4}{3} \qquad 3.3$$

$$\frac{\Delta\sigma_t}{\tau_f} = 4\,\mathrm{Ln}\left(\frac{R_p}{r}\right) - \frac{2}{3} \qquad 3.4$$

$$\frac{\Delta\sigma_z}{\tau_f} = 4 \text{ Ln} \left(\frac{R_p}{r}\right) - \frac{2}{3} \qquad 3.5$$

where σ_R, σ_t and σ_z are the mean principal stresses in polar coordinates ($\Delta\sigma_R = \Delta\sigma_1, \Delta\sigma_z = \Delta\sigma_t = \Delta\sigma_2 = \Delta\sigma_3$),

α_f is the value of α at failure,

R_p is the radius of the plastic zone,

r is the radial distance from cavity centre,

τ_f is the ultimate shear strength,

b) The pore water pressure induced by an expansion of a cylindrical cavity as:

$$\frac{\Delta U}{\tau_f} = 0.817\alpha_f + 2 \text{ Ln} \left(\frac{R_p}{r}\right) \qquad 3.6$$

for a variation of the total stresses within the plastic zone expressed as:

$$\frac{\Delta\sigma_R}{\tau_f} = 2 \text{ Ln} \left(\frac{R_p}{r}\right) + 1 \qquad 3.7$$

$$\frac{\Delta\sigma_t}{\tau_f} = 2 \text{ Ln} \left(\frac{R_p}{r}\right) - 1 \qquad 3.8$$

$$\frac{\Delta\sigma_z}{\tau_f} = 2 \text{ Ln} \left(\frac{R_p}{r}\right) \qquad 3.9$$

where, $\Delta\sigma_R = \Delta\sigma_1$, $\Delta\sigma_t = \Delta\sigma_3$, $\Delta\sigma_z = \Delta\sigma_2 = (\Delta\sigma_R + \Delta\sigma_t)/2$.

It should be noted, however, that in this approach, the actual geometry of the failure surface accompanying the penetration process has been simplified in order to include realistic soil properties in the analysis. The spherical and cylindrical cavities expansion is a one-dimensional problem, thus rigorous solutions are relatively easy to obtain even when complex material properties are considered (Baligh (1975)).

Following this approach, the pore water pressure developed at the point end of a penetration process (penetrometer, pile), can be determined by considering the geometrical process as a spherical cavity expansion

phenomenon. Thus, the pore pressure recorded at the tip of the penetrometer or instrumented pile, will be obtained by considering Eq. 3.2 and taking r equal to R_u (see Fig. 3.1).

Hence, for $r = R_u$

$$\frac{R_p}{R_u} = \left(\frac{E_u}{3\tau_o}\right)^{1/3} \qquad 3.10$$

where R_u is the ultimate cavity radius

E_u is the undrained deformation modulus of the soil

τ_o is the initial shear strength

The equations 3.2, 3.3, 3.4 and 3.5 become respectively:

$$\frac{\Delta U}{\tau_{fu}} = 0.943\,\alpha_f + \frac{4}{3}\,\mathrm{Ln}\left(\frac{E_u}{3\tau_o}\right) \qquad 3.2a$$

$$\frac{\Delta\sigma_R}{\tau_{fu}} = \frac{4}{3}\left[\mathrm{Ln}\left(\frac{E_u}{3\tau_o}\right) + 1\right] \qquad 3.3a$$

$$\frac{\Delta\sigma_t}{\tau_{fu}} = \frac{4}{3}\left[\mathrm{Ln}\left(\frac{E_u}{3\tau_o}\right) - \tfrac{1}{2}\right] \qquad 3.4a$$

$$\frac{\Delta\sigma_z}{\tau_{fu}} = \frac{4}{3}\left[\mathrm{Ln}\left(\frac{E_u}{3\tau_o}\right) - \tfrac{1}{2}\right] \qquad 3.5a$$

where, τ_{fu} is the undrained shear strength.

Following the same reasoning, the pore water pressure developed along the shaft during a penetration process (penetrometer, pile) can be determined assuming a cylindrical cavity expansion as representative of the phenomenon. Thus, for $r = R_u$:

$$\frac{R_p}{R_u} = \left(\frac{E_u}{3\tau_o}\right)^{\frac{1}{2}} \qquad 3.11$$

and the equations 3.6, 3.7, 3.8 and 3.9 become respectively:

$$\frac{\Delta U}{\tau_{fu}} = 0.817\,\alpha_f + \mathrm{Ln}\frac{E_u}{3\tau_o} \qquad 3.6a$$

$$\frac{\Delta\sigma_R}{\tau_{fu}} = \mathrm{Ln}\left(\frac{E_u}{3\tau_o}\right) + 1 \qquad 3.7a$$

$$\frac{\Delta\sigma_t}{\tau_{fu}} = \mathrm{Ln}\left(\frac{E_u}{3\tau_o}\right) - 1 \qquad 3.8a$$

$$\frac{\Delta\sigma_z}{\tau_{fu}} = \mathrm{Ln}\left(\frac{E_u}{3\tau_o}\right) \qquad 3.9a$$

Comparing Eq. 3.2a with Eq. 3.6a it can be observed that the pore water pressure developed during a penetration process will be bigger at the point than along the shaft. Consequently, there will be a flow from the point end towards the shaft. The implication of this fact will be discussed on the chapter concerning problems associated with measurements of pore water pressure during a penetration process, see Section 5.5.4.

Lo and Stermac (1965) present a very simplified theory for estimating the maximum pore water pressures induced by pile driving. According with their theory, the maximum pore water pressure along the shaft will be composed of two parts, one resulting from change in total ambient pressure and the other from shearing, as follows:

$$\Delta U_a = (1 - K_o)\sigma'_{1i} \quad \text{(ambient pressure)} \qquad 3.12$$

$$\Delta U_s = (\Delta U/_p)_m \sigma'_{1i} \quad \text{(shearing)} \qquad 3.13$$

and we have: $$\Delta U = \left[(1 - K_o) + (\Delta U/_p)_m\right]\sigma'_{1i} \qquad 3.14$$

where, σ'_{1i} is the initial vertical effective stress

K_o is the at-rest coefficient of earth pressure

$(\Delta U/_p)_m$ is the maximum pore pressure ratio measured in a conventional consolidated-undrained test.

p is the consolidation pressure.

The same assumptions can be considered in the case of negative excess pore pressure, as illustrated in Fig. 3.2a. Fig. 3.2b, indicates quantitatively the influence of dissipation on the $\Delta U/\tau_f$ ratio. Clearly, during a penetration test in which rate of penetration varies between 0.5 cm/sec to 2 cm/sec, the maximum value of $\Delta U/\tau_f$ ratio would be associated with clay deposits and minimum values would be expected in clean sand and gravel deposits.

Let us consider the pore water pressure generating at the tip of a penetrometer being driven into a cohesionless soil subjected to an isotropic state of stress. Using a spherical cavity expansion to represent the phenomenon we have:

$$\Delta\sigma_1 = \Delta\sigma_R;\ \Delta\sigma_2 = \Delta\sigma_z = \Delta\sigma_3 = \Delta\sigma_t,$$

and the general expression relating pore water pressure and changes in total stress becomes:

$$\Delta U = \Delta\sigma_t + \frac{1}{3}(1 + \alpha\sqrt{2})(\Delta\sigma_R - \Delta\sigma_t) \qquad 3.15$$

or

$$\Delta U = \Delta\sigma_t + A(\Delta\sigma_R - \Delta\sigma_t) \qquad 3.16$$

$$\Delta U = \sigma_{tf} - \sigma_i + A(\sigma_{Rf} - \sigma_{tf}) \qquad 3.17$$

where σ_i is the initial isotropic stress.

A is the pore water pressure parameter defined by Skempton (1954).

However, from expansion cavity theory, for $r = R_u$ (see Fig. 3.1);

$$\frac{\sigma_R}{\sigma_i} = \frac{3(1 + \sin\phi)}{3 - \sin\phi}\left[I_{rr}\right]^{4\sin\phi/3(1+\sin\phi)} \qquad 3.18$$

where,

$$I_{rr} = \frac{I_r}{1 + I_r\Delta}$$

and I_r is the rigidity index representing the ratio of the shear modulus of the soil to its initial shear strength.

Δ is the volumetric strain occuring in the plastic zone.

and from Mohr - Coulomb's failure criterium:

$$\sigma_{tf} = \sigma_{Rf} \tan^2 (45^o - \phi/2) \qquad 3.19$$

$$\sigma_{Rf} - \sigma_{tf} = 2\tau_f \qquad 3.20$$

Equation 3.17 becomes:

$$\Delta U = \left[\tan^2(45^o - \phi/2) \frac{3(1 + \sin\phi)}{3 - \sin\phi} (I_{rr})^{4 \sin\phi/(3 + 3 \sin\phi)} - 1 \right] \sigma_i + 2A\tau_f \qquad 3.21$$

The values of ϕ, I_{rr} and A depend on the factors controlling the dissipation during the penetration process or in other words they will depend on the volumetric strain occuring in the plastic zone. Obviously, any theoretical attempt to correlate these interdependent variables would be extremely complex. Eq. 3.21 can be written in the form:

$$\Delta U = f_1(\Delta)\tau_f + f_2(\Delta)\sigma_i \qquad 3.22$$

Assuming the cone resistance value as a measure of the ultimate shear strength we have:

$$\Delta U = F_1(\Delta) q_c + F_2(\Delta)\sigma_i \qquad 3.23$$

This equation indicates the influence of the initial confining stress level upon the excess pore water pressure. ΔU increases with an increase in the confining pressure. However the first term, $F_1(\Delta)\, q_c$, is the principal factor governing Eq. 3.21. Results obtained from tests carried out in this research will be used in an attempt to solve Eq. 3.21 semi-empirically.

It should be noted that:

For $q_c = q_{cu}$ (cone resistance value obtained for no dissipation during the penetration process, Δ and $\phi = 0$)

$$\frac{\Delta U}{\tau_{fu}} = 0.943\,\alpha_f + \frac{4}{3} \operatorname{Ln} \frac{E_u}{3\tau_o} \qquad (3.2)$$

and $q_c = q_{cd}$ (cone resistance value obtained for full dissipation during the penetration process)

$\Delta U = 0$

These approaches can only be applied for the fully undrained condition occurring during the penetration process. This requires the assumption of no volume change and the $\phi_u = 0$ concept in respect to the application of external load. Consequently, the undrained shear strength will only be dependent on the consolidation pressure. Undrained shear occurs in practical problems whenever external loads change at a rate much faster than the rate at which the induced pore pressures can dissipate. This is the case of soils having relative low value of the coefficient of permeability in relation to the rate of penetration. Therefore, for these assumptions, the maximum pore water pressure induced by the penetration process can be estimated. However, deviations in these assumptions, will introduce a frictional component on the shear strength transforming it to a total stress path dependent problem. This could be the case of soils having relatively high value of coefficient of permeability in relation to the rate of penetration. During the penetration process, drainage can occur and the pore water pressure set up will be strongly dependent on the factors controlling the generation - dissipation phenomenon.

Fig. 3.2a, illustrates the pore water pressure generation-dissipation phenomenon influencing the ultimate shear resistance, for a cohesionless soil consolidated at p'_c. For positive excess pore pressure, three distinct values of the shear resistance can be considered:

a) τ_{fu} - lower limit, corresponding to the maximum pore pressure value. $\Delta U_{(max)}$ can be reasonably predicted by expansion cavity theory.

b) τ_{fD} - upper limit, corresponding to no excess pore pressure, $\Delta U = 0$

c) τ_{fp} - intermediate value, its value tends to τ_{fu} as ΔU approaches $\Delta U_{(max)}$ and tends to τ_{fD} as ΔU equals to zero. ΔU depends on the factors controlling the generation-dissipation phenomenon, theoretical approach would be extremely complex.

Domaschuk (1968) has made an attempt to estimate the excess pore pressure considering drainage occurring during the penetration process. His theoretical expression can be written for the case of unrestricted drainage as:

$$\Delta U = (\beta \Delta\sigma + \alpha \Delta\tau) L \qquad 3.24$$

where $L = f(r, c_h, t)$

r is the radial distance from pile centre

c_h is the horizontal coefficient of consolidation

t is the time.

The value of L lies between zero and 1, being zero when c_h or t is infinitely large. It approaches 1 as c_h decreases and t approaches zero. Thus L will always be less than 1. It will be equal to zero in case of highly permeable soils, and equal to 1 in case of relative impermeable soils.

Clark and Meyerhof (1972) from measured pore water pressure set up during pile driving into an instrumented clay bed and using Domaschuk's method, calculated the value of L for different depths. They concluded that, because of the several factors which influence L, many of which are interdependent, any attempt at a theoretical derivation would be extremely complex. It can only be said that it varies from zero to 1, depending upon the soil type, pile size and material, and driving time.

3.3 OBSERVED VALUES OF EXCESS PORE PRESSURE INDUCED DURING A PENETRATION PROCESS

As discussed in the previous sections, there is a need to understand the pore water pressure generation-dissipation phenomenon induced during a penetration process. For the fully undrained condition this problem can be solved theoretically in a reasonable way by using expansion cavity theory. However, for the partially drained condition this problem presents a very complex theoretical solution and a semi-empirical approach may provide the

answers. Hence, for the second case, one must rely on measured pore water pressure values during a penetration process. At the present, information from the technical literature on this subject is rather scanty. Perhaps, this scarcity is associated with the difficulties in obtaining such values. The difficulties associated with measurement of excess pore pressure during a penetration process will be discussed in later sections.

Senneset (1974) shows measured values of the excess pore pressure induced during a penetration of an electric piezometer. This piezometer is of NGI - type with the porous filter placed ca. 1 cm above the cone point. There is a water saturated chamber in contact with a vibrating wire device for the measurement of the pore water pressure. Fig. 3.3 and Fig. 3.4 indicate results obtained during the probe penetration and the cone resistance value obtained with a penetrometer. The probe and the penetrometer have the same dimensions. The rate of penetration for the probe and penetrometer is 2 cm/sec for both cases.

Fig. 3.3 indicates value of the ratio between the excess pore water pressure and cone resistance, $(\Delta U/q_c)$, up to 0.27 in a moraine clay while Fig. 3.4 shows a maximum value for the same ratio around 0.01 for sand.

Torstensson (1975) reports measured values of the excess pore water pressure induced during a penetration of a cylindrical piezometer probe. The porous filter with 15 mm diameter and 5 mm height is placed above the conical point. The pore pressure is measured by an eletrical transducer. The rate of penetration is 1 m/min. Fig. 3.5 indicates results obtained with this probe. This result also indicates higher values of the induced excess pore water pressure in clay than in sand layers.

Wissa et al (1975) measured the excess pore water pressure during the penetration process. Using a piezometer probe consisting of a high air entry, stainless steel, porous tip, hydraulically connected to a flush diaphragm pressure transducer and placed at the conical point. The probe is pushed into

the ground at about 0.5 cm/sec penetration rate. Typical results measured during the probe penetration are:

SOIL TYPE	U (Kg/cm^2)
Very loose clayey sand	0.08
Soft highly plastic clay	0.04
Loose silty sand	0.015
Dense silty sand	- 0.015
Stiff clayey sand	- 0.02
Stiff highly plastic clay	- 0.016

These results indicate almost the same value of the excess pore pressure for all types of soils penetrated. Howeves, the most important fact related with these observations is the indication of positive values for soft clay and loose sand deposits and negative values for stiff clay and dense sand deposits.

3.4 INFLUENCE OF THE PROBE FORM ON THE INDUCED EXCESS PORE PRESSURE VALUE

In this section, the probe form will be defined as the geometrical configuration of the penetrometer, e.g., cylindrical or necked shape, cone point angle etc. Holden (1974) has made a very interesting contribution to the general discussion on the form of penetrometer tip. He comments on the very complex nature of the stress field produced around a penetrometer tip during a penetration process. Obviously different form of the penetrometer will produce different stress fields. Consequently, the form of the penetrometer can greatly influence the excess pore water pressure induced during the penetration process.

Fig. 3.6 and 3.7 indicate values obtained by Baligh et al (1977) using two probes with the same geometrical configuration and with different cone point

angle. Results indicated on Fig. 3.6 have been obtained at a site consisting mainly of Boston Blue Clay while the results indicated on Fig. 3.7 correspond to a varved clay deposit. It can be observed from both cases that there is a consistent indication of a higher pore water pressure for the 60^{o} cone angle probe than for the 18^{o} cone angle probe.

3.5 INFLUENCE OF THE FILTER POSITION ON THE MEASURED EXCESS PORE PRESSURE

The expansion cavity approach has indicated that the pore pressure value induced by a spherical cavity expansion will be bigger than the value produced during a cylindrical cavity expansion. Therefore, a gradient from the point towards the shaft of the penetrometer is likely to exist. Hence, any filter located along the shaft must be placed at some distance from the point end in order to reduce the influence of the end effect. Clearly this distance will be function of the factors affecting the stress field or the geometry of the failure surface during the penetration process.

Torstensson (1975) has reported very interesting results obtained with three different pore pressure unit positioning arrangements, see Fig. 3.8. These results have been carried out on a normally consolidated clay deposit with a rate of penetration of 1 m/min. It can be observed that the registered excess pore pressure value decreases as the filter moves away from the point end.

Massarch et al (1975) measured the excess pore pressure at different levels during the penetration of a multiple piezometer in a normally consolidated clay deposit. The multiple piezometer has a diameter of 33 mm and is provided with a number of pore pressure units spaced 1.0 m apart, see Fig. 3.9a. They reported that high excess pore pressure have been observed immediately after the installation. After the excess pore water pressure due to installation having been completely dissipated, the multiple piezometer has

been subjected to loading, unloading and further penetration. Fig. 3.9b indicates the excess pore water pressure at different levels during these operations. It can be observed that a large increase of pressure has been recorded at the tip. Along the shaft, these values are very small, having almost the same magnitude at different levels.

Konrad (1977) reports results obtained during the penetration of an instrumented pile into an instrumented clay deposit. The pile with a diameter of 219 mm was instrumented using Gloetzl pore pressure cells, placed at different levels along the shaft, see Fig. 3.10. The clay deposit was instrumented using Geonor piezometers driven in at different depths. Fig. 3.10 indicates the positioning of these piezometers and also the final position of the pile after installation. Fig. 3.11, shows results of the excess pore pressure indicated by the pore pressure cells during the penetration process. It can be observed that cells 1 and 7, located nearer the point end, indicate bigger values. All the other pore pressure cells recorded values of the same magnitude. These measurements indicate that, for a ratio of 6.85 between the distance from the point end and the pile diameter, there was no influence of end effects on the value of the excess pore pressure. Fig. 3.12 presents the measured excess pore pressure values registered by the piezometers 4, 5, 6 and 7 while Fig. 3.13 indicates the values obtained by the piezometers 1, 2 and 3. All these piezometers indicated the same pattern of excess pore pressure set up during advancing of the pile. The pattern observed with the piezometer is identical to that indicated by the pore pressure cells after the pile tip has passed the piezometer. Comparing the measured excess hydrostatic pressure values indicated by the piezometers and correspondent pressure cells when they are at the same level, i.e. piezometer 7 and pressure cells 2 and 8 at 3.05 m depth etc., they indicate that this value decreases as the radial distance from the pile increases.

For this specific case, a fixed point within the soil mass indicated a negative excess pore pressure value at the moment it sensed the stress field

produced by the advancing pile. As the pile advances this value becomes positive and reaches a maximum when the fixed point and the pile tip are almost at the same level. With further pile advance, there is a reduction on the magnitude of the pore water pressure and this value becomes constant when the pile tip is at some distance below the fixed point. This well documented behaviour may suggest that the stress field produced by the advancing pile controls the magnitude of the excess pore pressure set up.

The nature of the stress field produced during the advancing penetrometer (or pile), can be analysed using Mindlin's solution for a vertical point load (P) acting beneath the surface of a semi-infinite mass, see Fig. 3.14. Fig. 3.15 presents values of the "compressive" ($\sigma_z + \sigma_x$) and shear ($\sigma_z - \sigma_x$) stresses, at a given point (P6), induced during the penetration process. Both values are plotted as a percentage of the point load P. This figure also indicates the ratio between shear and "compressive" stresses ($\sigma_z - \sigma_x$) / ($\sigma_z + \sigma_x$) obtained for different penetrometer positions in relation to the considered point.

The fixed point P6 represents the position of the piezometer 6, see Fig. 3.10. The excess pore pressure values indicated by this piezometer, during advancing of the pile (see Fig. 3.12), is also presented in Fig. 3.15.

The result indicate that at the moment the mass first senses the penetrometer stresses, the shear and "compressive" stresses values are almost of the same magnitude. The ratio between these two values is close to unity and keeps in the same order with further penetration until a relatively sudden decrease as the penetrometer approaches the fixed point, see Fig. 3.15.

For the penetration depth corresponding to a stress ratio close to the unity, the shear stress component can be considered relatively significant compared to the "compressive" stress component. However, as the penetrometer advances, the produced stress field becomes predominantely of "compressive" nature.

Under the relatively significant shear stress field, the piezometer indicated an increasingly negative excess pore pressure value. This pore pressure value reaches a maximum negative value and becomes gradually positive following increases in the "compressive" stress component. Relatively high positive pore pressure value was observed as the stress field became predominantely of "compressive" nature. The piezometer indicated a maximum positive pore pressure value for a pile position corresponding to a maximum value in the "compressive" stress component, see Fig. 3.15.

Roy (1979), commenting on the same results, suggested that measurements of negative pore pressure values could be due to the piezometer pull out resulting from lateral deflection of its connection tube caused by the advancing pile. This can be considered a more reasonable explanation as the stress path produced is unlikely to generate negative values of the excess pore pressure in sensitive clays.

As the penetrometer (or pile) approximates the fixed point, the stress field produced by the push rods (or pile shaft) becomes significant. Therefore the penetration process can not be represented by the Midlin's solution. In this case, the penetrometer (or pile) dimensions should be considered in the analysis.

As a conclusion, it can be said that the stress field produced at a given point within the soil mass, resulting from a penetration process, has two distinct natures: a) relatively significant shear stress component; b) predominantely "compressive" stress component.

Obviously, the magnitude of the excess pore pressure will result from the soil response to the individual or combined effect of the stress field produced. Under the same stress field, a collapsible soil (loose sand, soft clay) would response differently than a dilating one (dense sand, stiff clay).

Schmertmann (1974a) reports results obtained during penetration into sandy clay indicating development of negative pore pressure above the base of the cone, despite the probable significant positive pore pressure below this base.

During the penetration, fracturing of the soil may occur and can affect the excess pore pressure generation-dissipation process. Massarch and Broms (1977) have presented a study of this phenomenon caused by pile driving in clay deposits. Clearly, the problem associated with the distribution of the excess pore pressure surrounding an advancing penetrometer is very complex. As pointed out by Schmertmann (1974b), even assuming homogeneous soil, the excess of hydrostatic pressure would depend, at least, on the rate of penetration, the soil permeability, the undrained stress-strain and the drained compressibility-strain behaviour of the soil, plus the form of the tip.

3.6 EFFECTS OF THE EXCESS PORE PRESSURE ON PENETRATION RESISTANCE VALUES

Plantema (1957) reports one of the first laboratory attempts to observe the influence of the water during a penetration process on a sand sample. He carried out tests on five sands with different grading curves in dry, moist and saturated conditions. The samples have been prepared in a flexible wall cell-apparatus with 0.95 m diameter and 0.75 m height and different densities had been achieved by compaction. Fig. 3.16 shows details of the penetrometer device while Fig. 3.17 indicates typical values measured during the penetration tests. Fig. 3.18 presents results of a series of tests obtained for different densities and degrees of saturation in three specific sands. It can be observed that for these three sands the penetration resistance, at a given density, increases substantially with an initial increasing in the degree of saturation up to a point where there is a drop in the penetration value with further increase in the saturation condition. For sand I the penetration values for fully saturated conditions is smaller than for the dry conditions, while for sands III and IV results indicate penetration resistance for fully saturated conditions bigger than for dry conditions. Thus, these results have shown that for fully saturated conditions, the penetration resistance value in sands can be either

smaller or bigger compared to dry conditions. Although these results indicated the influence of the degree of saturation on the penetration resistance, they should however be treated as indicative values only. Information referring to the relative density of the sand should be given in order to help the understanding of the collapsing or dilating behaviour influencing the magnitude of the penetration value.

Drozd (1974) presents results obtained from model tests indicating the influence of the degree of saturation on the penetration resistance value. Laboratory model tests were carried out on seven sands of different grading curves, grain size ranging from 0.05 mm to 5 mm. Dry samples were prepared in a box and different densities achieved by vibration. Saturated samples were prepared by slowly raising the water level inside the box after the sample densification or by sedimentation of the sand under water and then densification by vibration. The penetration resistance has been indicated by the number of blows necessary to drive into the sample a one third scale sampler. The actual size sampler and test procedure have been described by Drozd and Svasta (1974). Fig. 3.19 indicates variation in penetration resistance values with relative density for dry and saturated conditions. For the same sand, the influence of the degree of saturation on the penetration resistance value, at a given density, is shown in Fig. 3.20.

Drozd (1965) reported that for very compacted sand there is a further increase in the penetration resistance value with additional increase in the degree of saturation.

Fig. 3.21 summarises results obtained from these seven different sands, for dry and saturated conditions. Thus, it can be observed that for loose conditions, the penetration resistance values decrease with saturation. However, the opposite effect is observed in very dense samples, when the penetration resistance is bigger for saturated conditions than for dry samples. Clearly, the collapsing and dilating behaviour of loose and dense sample respectively, can be invoked to explain the influence of the excess pore

pressure generated during the penetration process is indicated in Fig. 3.22. Several standpipe piezometers were installed in the saturated sample and the variation of the water level inside the piezometer caused by the sampler penetration was recorded.

Information was not given concerning the piezometers and penetrometer positioning, thus, the value indicated should be considered qualitatively. These results indicate that the generated excess pore water pressure decreases with an increase in the relative density. For loose samples there is an indication of a relatively high excess pore pressure. For very compacted samples there is a tendency to produce negative excess pore pressures.

Shultze and Melzer (1965) also report different penetration resistance values obtained during penetration tests for dry and saturated samples at a given density.

All the information presented so far has indicated a qualitative influence of the excess pore pressure on the magnitude of the penetration resistance. However, for practical purposes, this influence needs to be specified quantitatively.

Due to the complexity of the theoretical approach, it appears that varying the rate of penetration and observing changes in penetration resistance is a simpler method of quantifying this influence.

Dayal and Allen (1975) have performed constant rate of penetration tests with various velocities in remoulded clay and sand samples of several strengths and moisture contents. The rate of penetration ranged from 0.13 cm/sec to 81.14 cm/sec, giving a maximum velocity ratio of 624. They found that for sand samples there is no appreciable difference in either cone resistance or friction sleeve resistance for a rate of penetration ranging within the indicated interval. However, for clay samples, an increase in the cone and friction resistances was caused by an increase in penetration velocity. Fig. 3.23 indicates the values of the cone resistance ratio plotted against

velocity ratio. As a result, they established the following relationship relating the increase in cone resistance and in friction sleeve resistance to the logarithm of the velocity ratio respectively as:

$$\frac{q_{cd} - q_c}{q_c} = K_L \text{ Log } (\frac{V}{V_s}) \qquad 3.25$$

$$\frac{f_{cd} - f_c}{f_c} = K_L \text{ Log } (\frac{V}{V_s}) \qquad 3.26$$

where K_L is the slope of the line, determined from Fig. 3.23 and 3.24 respectively, and, excepting the very soft clay sample, this value represents the soil viscosity coefficient, (see table 3.1).

TABLE 3.1 - SOIL VISCOSITY COEFFICIENT (K_L)

UNDRAINED SHEAR STRENGTH (Kg/cm^2)	K_L		
	FROM CONE RESISTANCE	FROM FRICTION SLEEVE	
		LOW VELOCITY (<15 cm/sec)	HIGH VELOCITY (>30 cm/sec)
0.03	1.5	0.38	0.93
0.09	0.25		
0.47	0.21	0.31	0.75
0.52	0.155	0.24	0.66
0.66	0.12		
0.81	0.03	0.17	0.38

When considering these results as indicative of excess pore pressure influencing the penetration resistance, it should be noted that the values obtained for the minimum rate of penetration, i.e. 0.13 cm/sec, are still in the undrained condition. For clays, the drained conditions will be achieved for much lower speed of penetration. This has been confirmed by the results obtained by Bemben and Myers (1974). Fig. 3.25 indicates the influence of the rate of penetration on cone resistance value obtained from in situ investigation

in a fairly uniform deposit of varved clay. Each point on the figure represents the cone resistance at a common depth in adjacent sounding spaced of 1.25 m. It can be observed that the drained condition for this particular deposit, has been achieved for a maximum rate of penetration around 0.05 cm/sec. Additional increase of the rate of penetration provoked a reduction on the penetration resistance indicating the excess pore pressure influencing the ultimate shear strength, see Fig. 3.25. Thus, for this particular deposit the undrained condition has been achieved for a penetration speed around 0.2 cm/sec. There is a reduction of 30% in the cone resistance value for the undrained conditions compared to drained conditions. Further increase in the rate of penetration indicated an increasing on the penetration resistance value, showing the influence of the viscous resistance on the penetration process. For the rate of penetration ranging from 0.2 cm/sec to higher values these results confirm the influence of soil viscosity on the penetration process observed by Dayal and Allen (1975).

Kok (1974) reports results obtained during in situ penetration tests in medium fine to medium coarse sand below the water table for 0.5 cm/sec and 2.0 cm/sec rate of penetration. He concluded that there was no significant statistical difference in the cone measurements obtained from the two penetration speeds.

Schmertmann (1974a) presents results indicating variation in cone penetration resistance for different rate of penetration. These tests have been carried out in slightly clayey dense sand and sensitive organic clayey sand. Results obtained in the first deposit indicated an increase of 25% in cone resistance value as the sounding method changed from discontinuous (drained) to continuous penetration (excess pore pressure). He argues that this was due to excess negative pore pressure, likely to occur in dense sand with probable positive dilatancy. For the second deposit, there was an increase of about 48% in cone resistance value as the rate of penetration decreased from 2 cm/sec to 0.01 cm/sec. An increase of 18% was observed when the penetration speed reduced from 2 cm/sec to 0.13 cm/sec for the same deposit.

3.7 SUMMARY AND CONCLUDING REMARKS

In this chapter, discussions on the problem associated with the generation-dissipation of the excess pore water pressure surrounding an advancing penetrometer have been presented. The main points observed are:

1) The excess pore pressure generated during the penetration process may strongly influence the magnitude of the ultimate shear strength indicated by the resistance value.

2) A knowledge of the generation-dissipation phenomenon may provide a theoretical basis for extrapolating results from cone penetration tests to actual working conditions.

3) For clay deposits, a very slow rate of penetration is required to achieve drained condition. For practical purposes, it can be assumed that in such deposits penetration will occur in undrained conditions. For the undrained condition the excess pore pressure surrounding the tip and along the shaft can be closely estimated using spherical and cylindrical cavity expansion approach respectively.

4) For clean sand, or deposits presenting high permeability, the influence of the excess pore pressure can be neglected. Hence, for practical purposes, penetration resistance in such deposits will occur in fully drained conditions.

5) Intermediate conditions will occur in deposits containing silty fine sands, clayey sands, etc. For such deposits, a small variation in the rate of penetration will cause different penetration resistance values. A theoretical approach to quantify the influence of the excess of pore pressure on penetration resistance for this condition is very complex. Observing the change in penetration resistance value with variation in the rate of penetration seems to be the simpler method to quantify this effect.

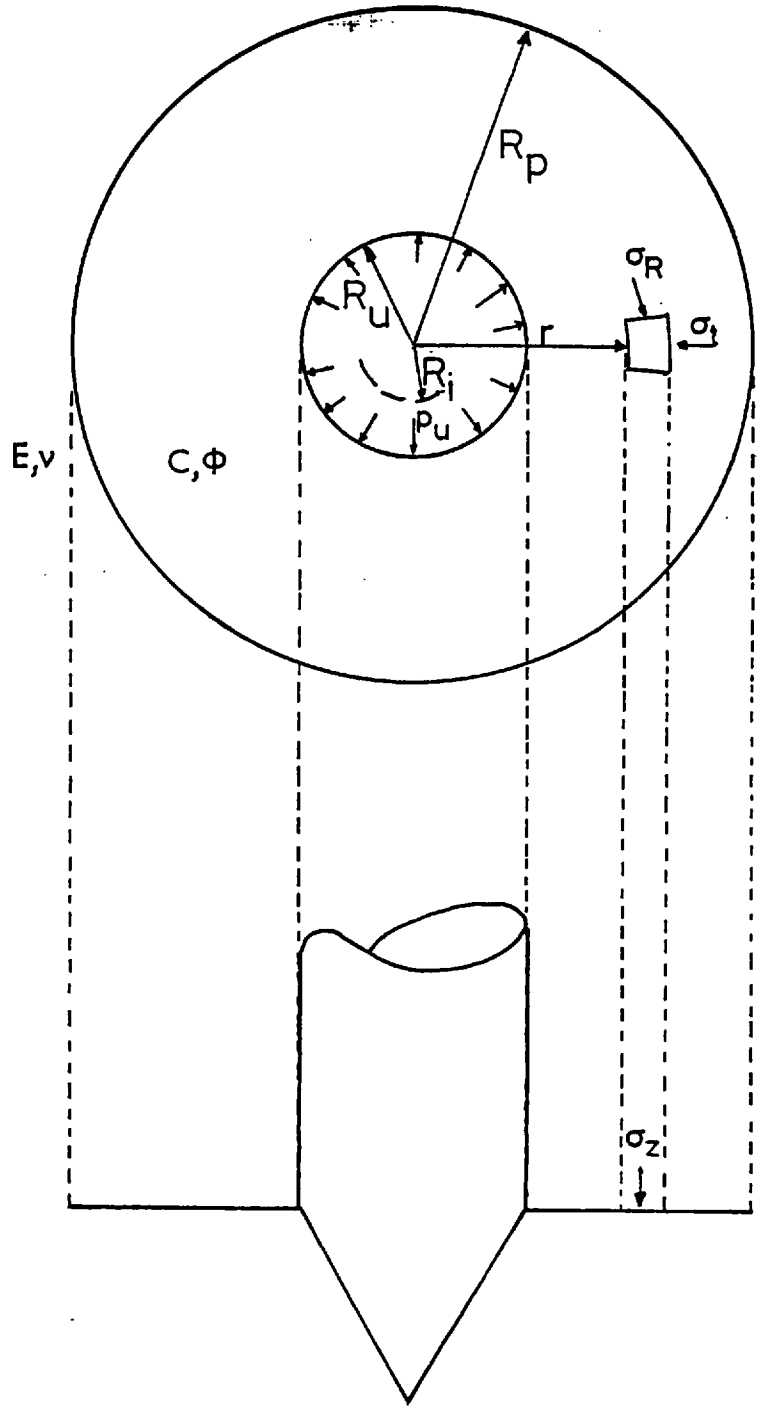


FIGURE 3.1 - EXPANSION OF CAVITY.

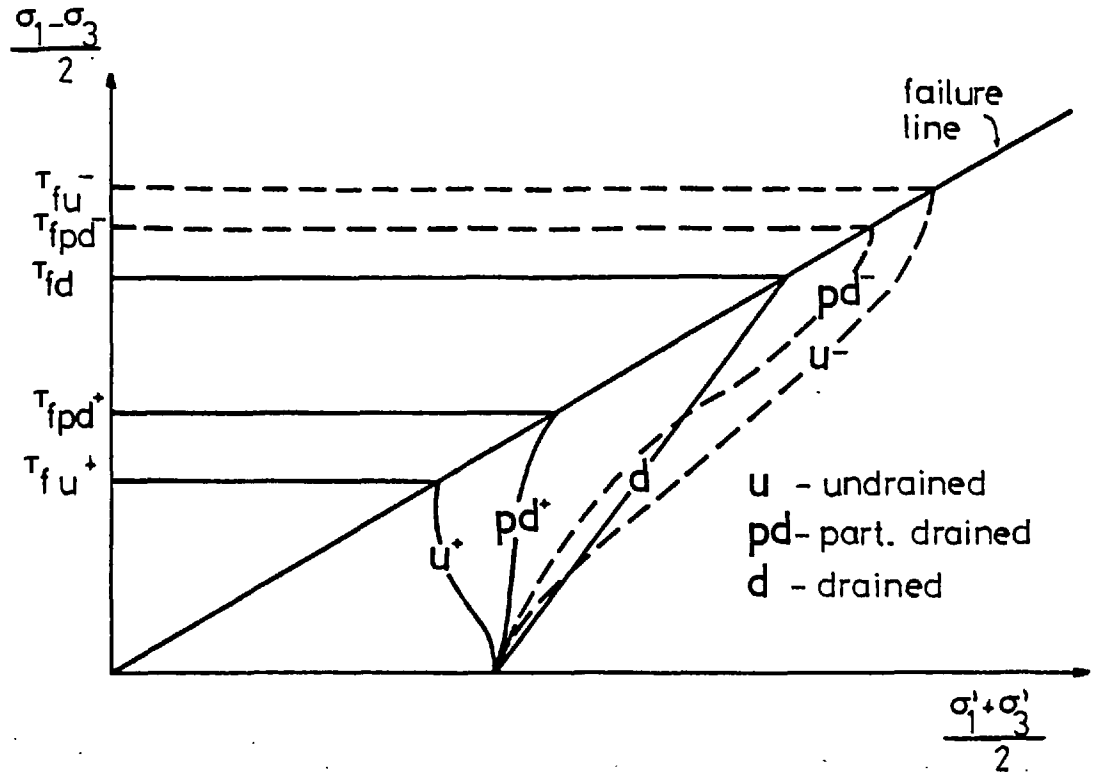


FIGURE 3.2a - EXCESS PORE PRESSURE INFLUENCING SHEAR STRENGTH.

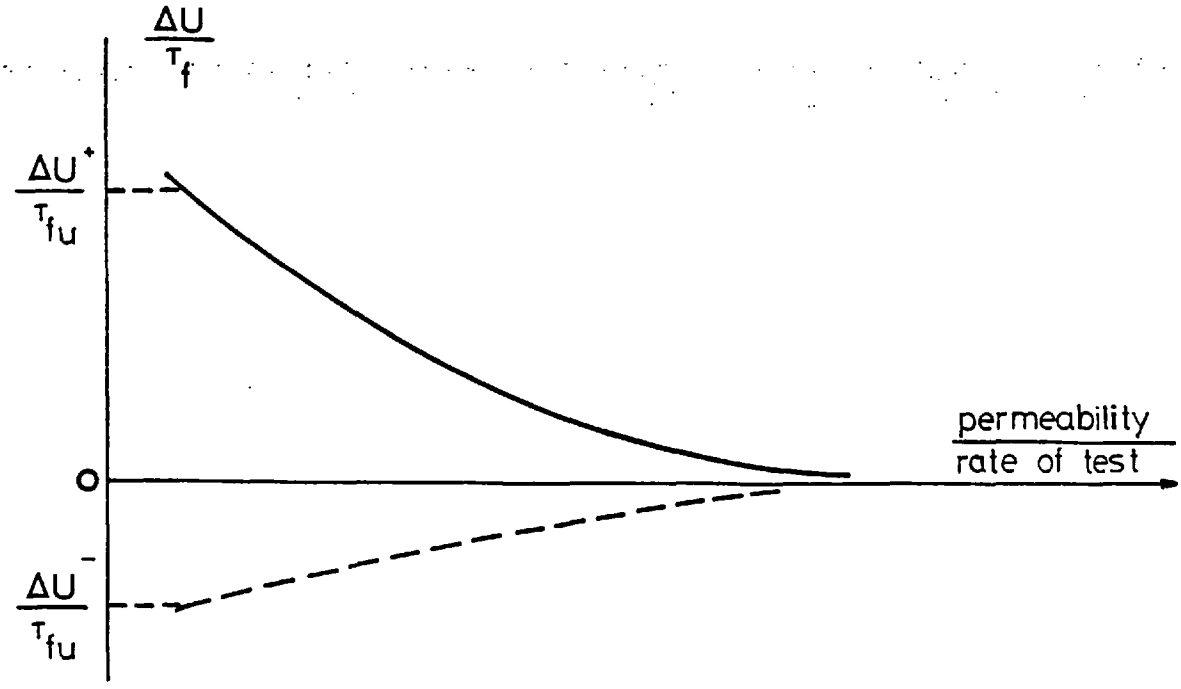


FIGURE 3.2b - EXCESS PORE PRESSURE AS A FUNCTION OF PERMEABILITY-RATE OF TEST RATIO.

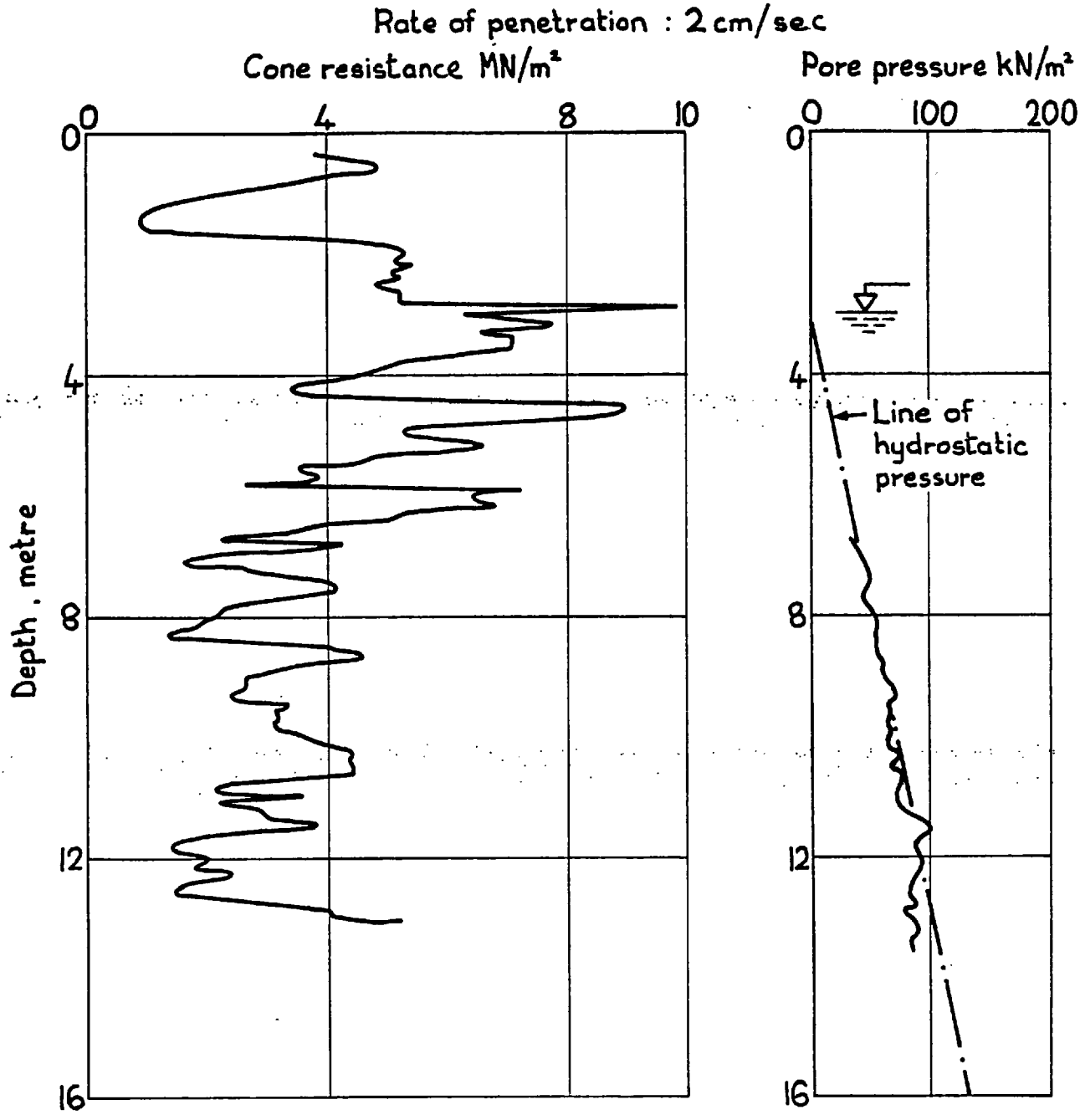


FIGURE 3.3 - CONE RESISTANCE AND PORE PRESSURE OBSERVATIONS IN MORAINE CLAY (FROM SENNESET, 1974).

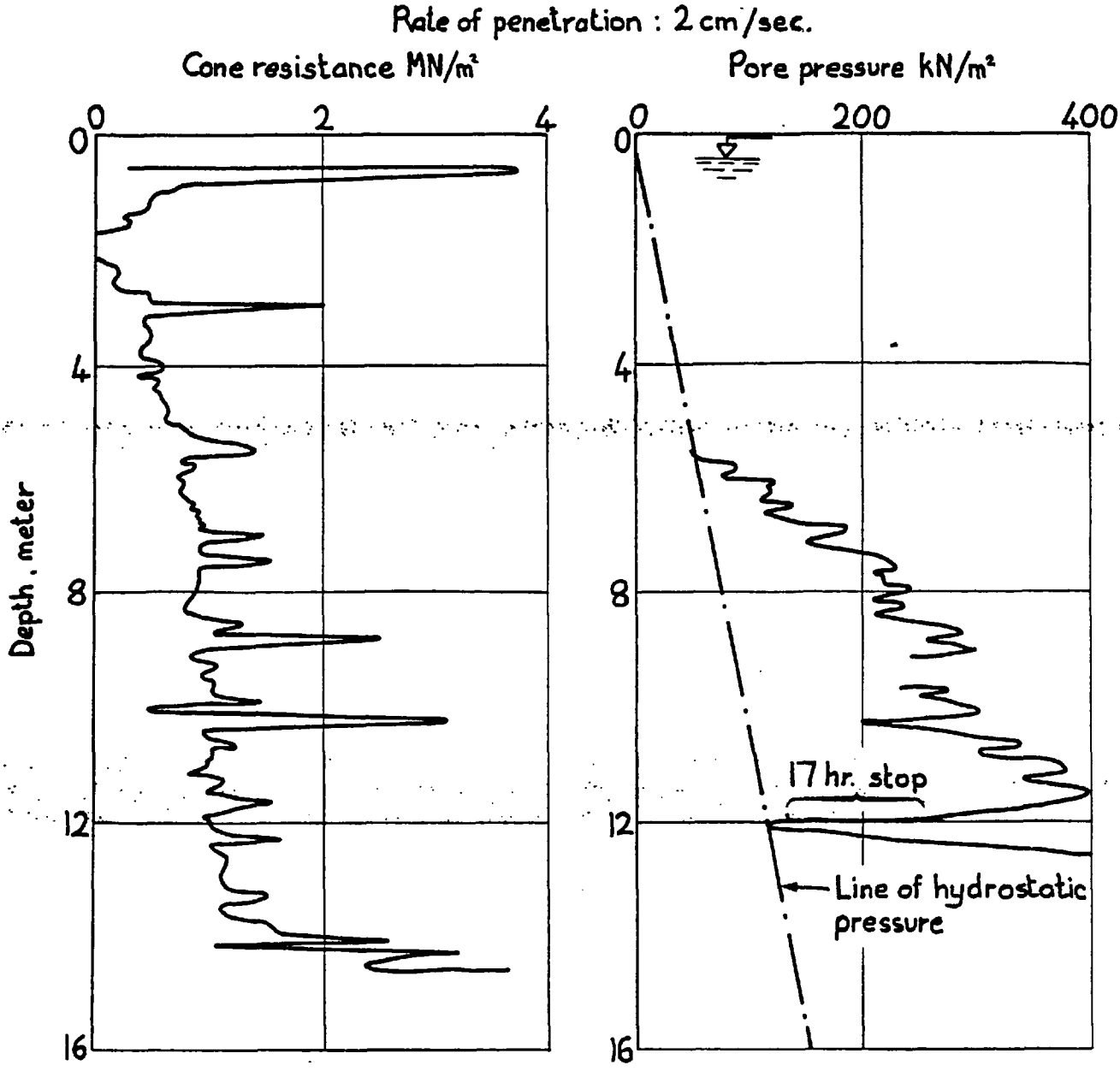


FIGURE 3.4 - CONE RESISTANCE AND PORE PRESSURE OBSERVATIONS IN SAND (FROM SENNESET, 1974).

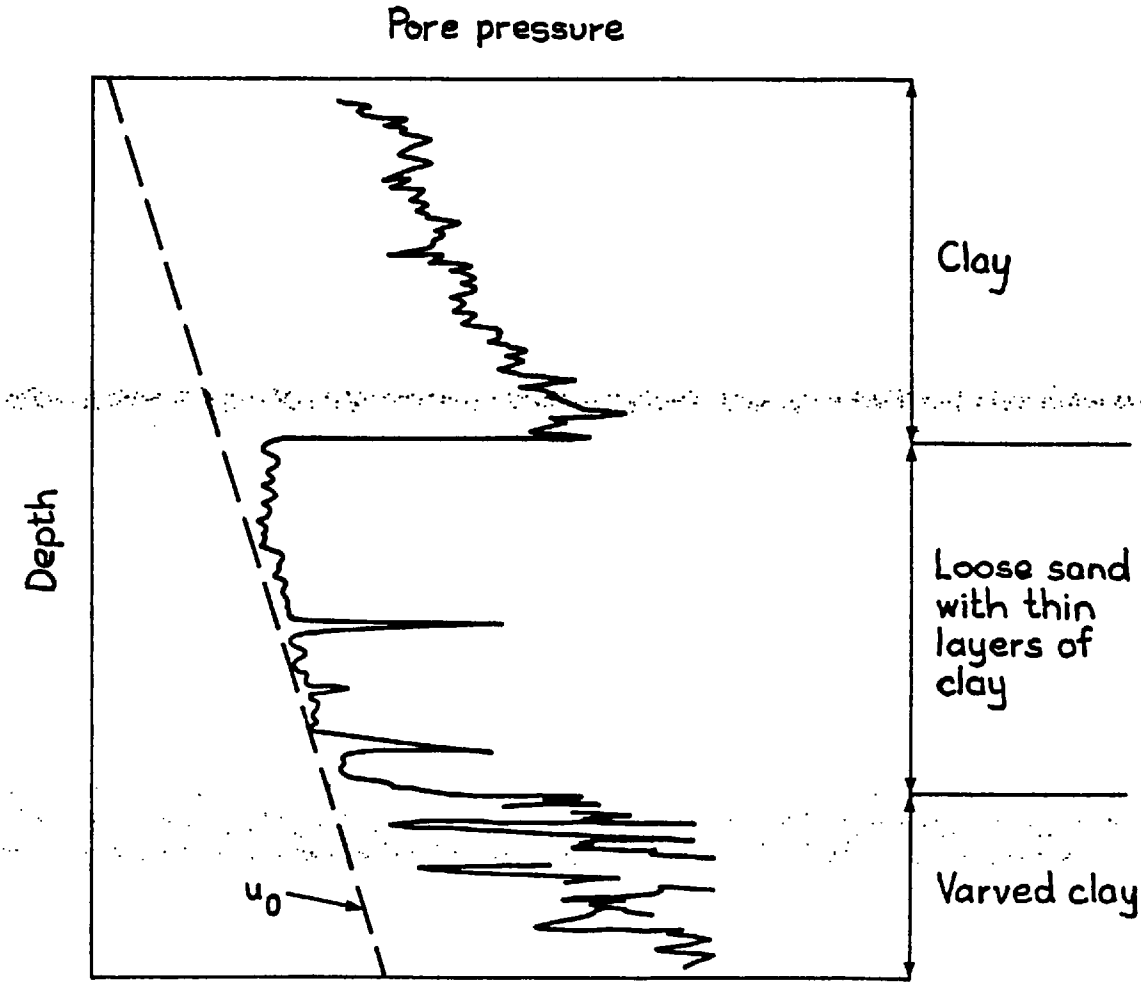


FIGURE 3.5 - TYPICAL PORE PRESSURE VS. DEPTH DIAGRAM REPRESENTING A LAYERED SOIL (U_o = EQUILIBRIUM PORE PRESSURE) (FROM TORSTENSON, 1975).

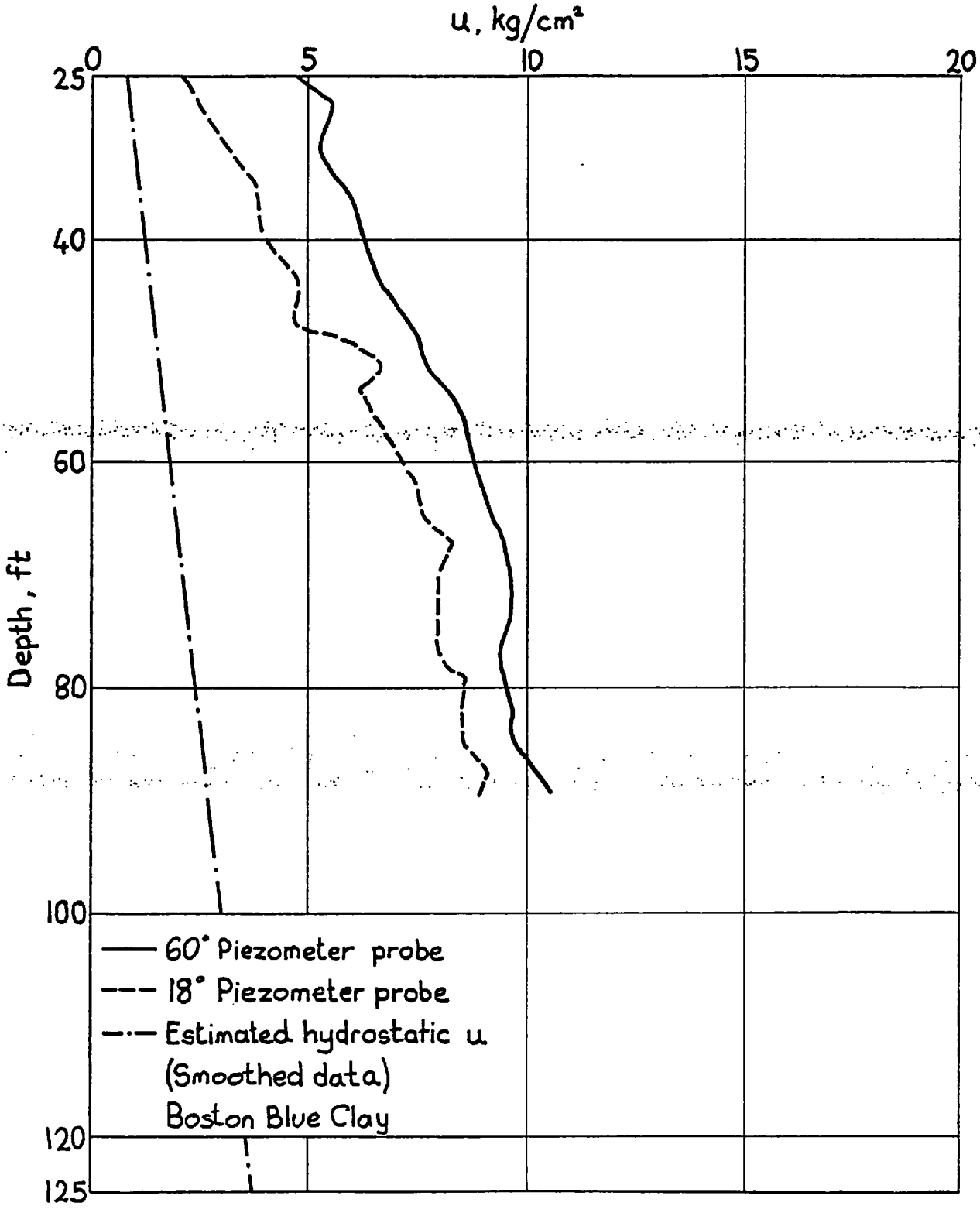


FIGURE 3.6 - STEADY STATE PORE PRESSURE DURING PENETRATION OF THE PIEZOMETER PROBE. SAUGUS, Ma. (FROM BALIGH et al, 1977).

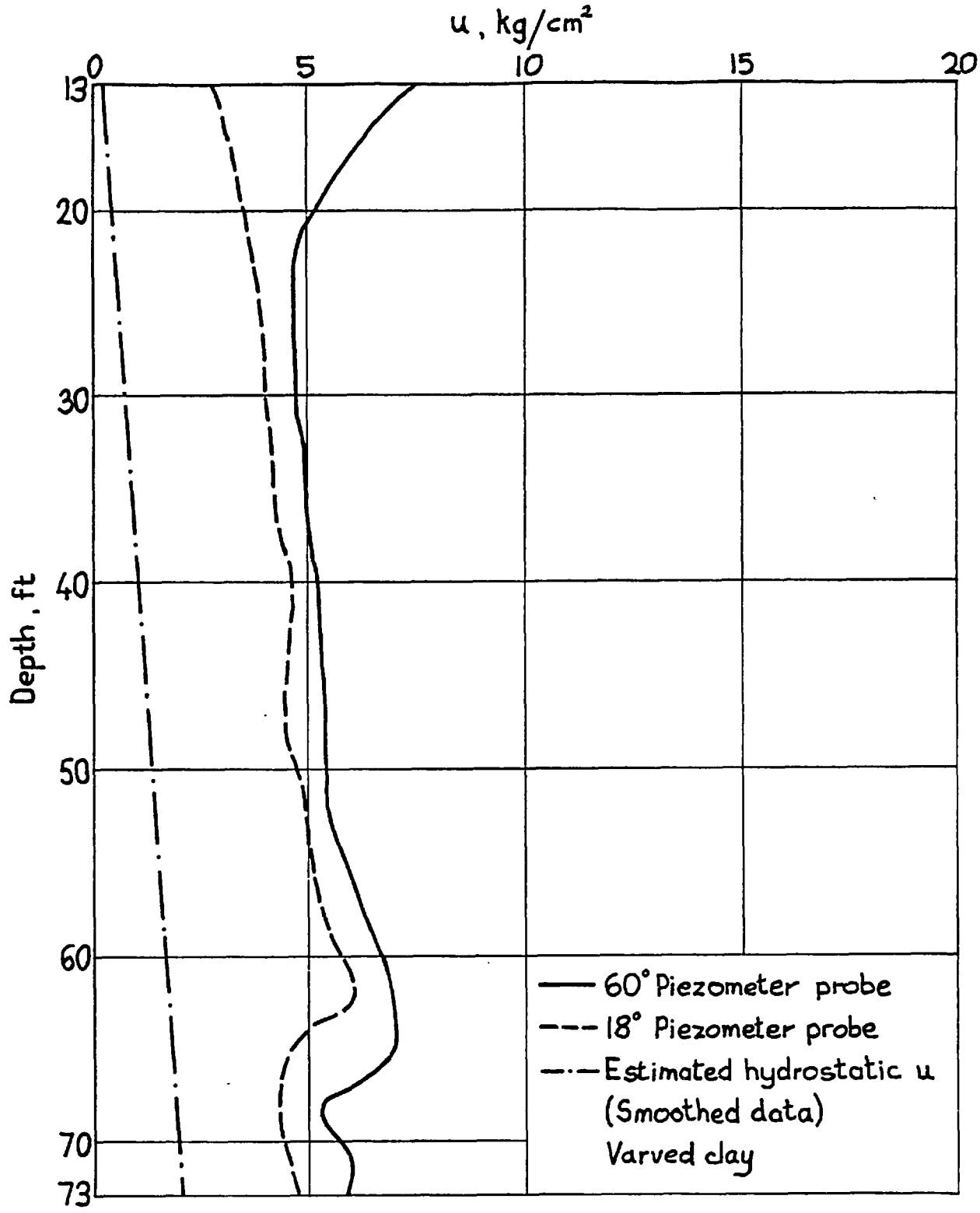


FIGURE 3.7 - STEADY STATE PORE PRESSURE DURING PENETRATION OF THE PIEZOMETER PROBE. AMHERST, Ma. (FROM BALIGH et al, 1977).

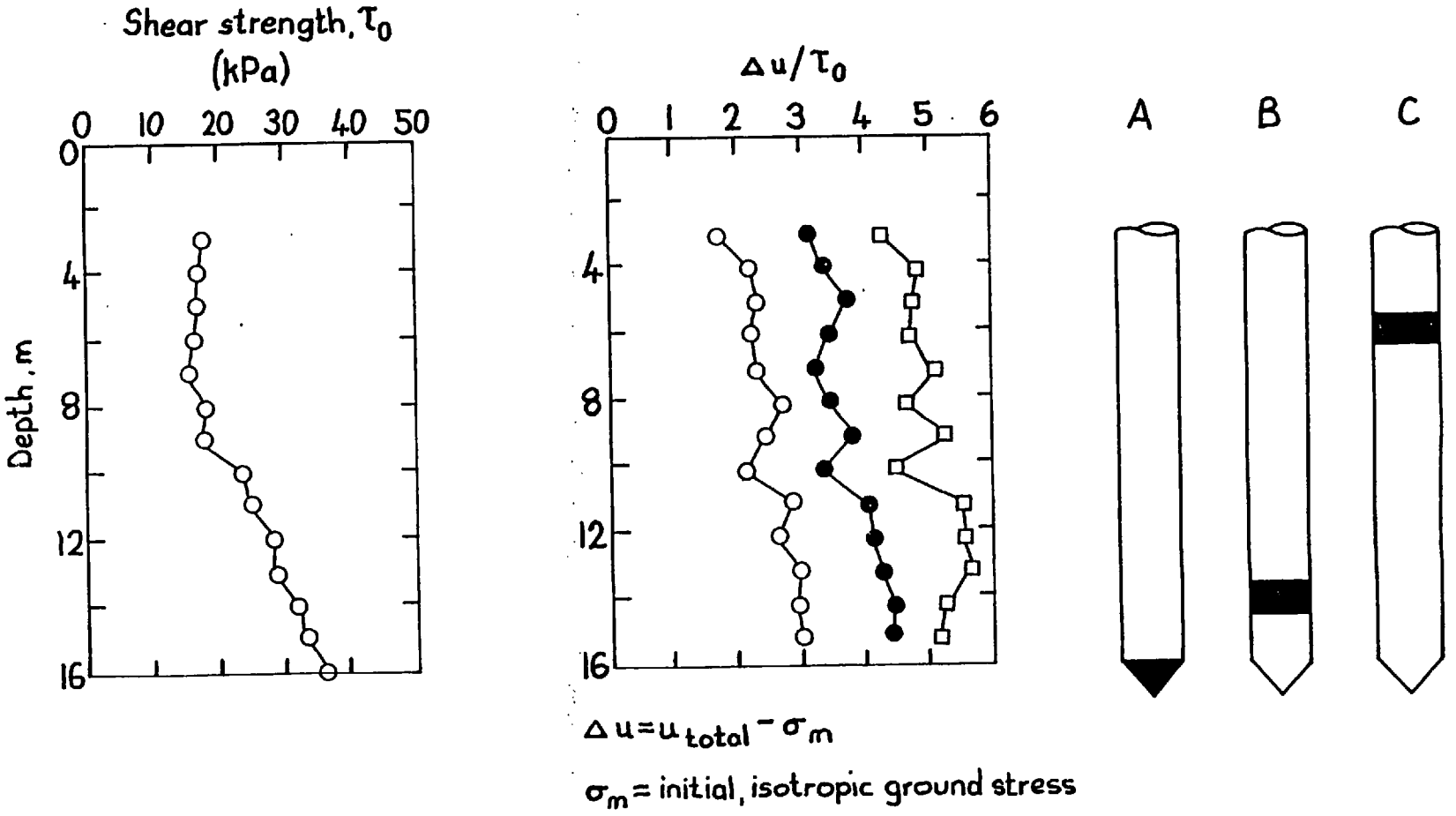


FIGURE 3.8 - RESULTS FROM PORE PRESSURE SOUNDINGS MADE IN A NORMALLY CONSOLIDATED CLAY. VARIATION WITH DEPTH OF THE RATIO $\Delta U/\tau_o$, WHERE ΔU = EXCESS PORE PRESSURE AND τ_o = UNDRAINED SHEAR STRENGTH OBTAINED FROM FIELD-VANE TESTS. (FROM TORSTENSON, 1975).

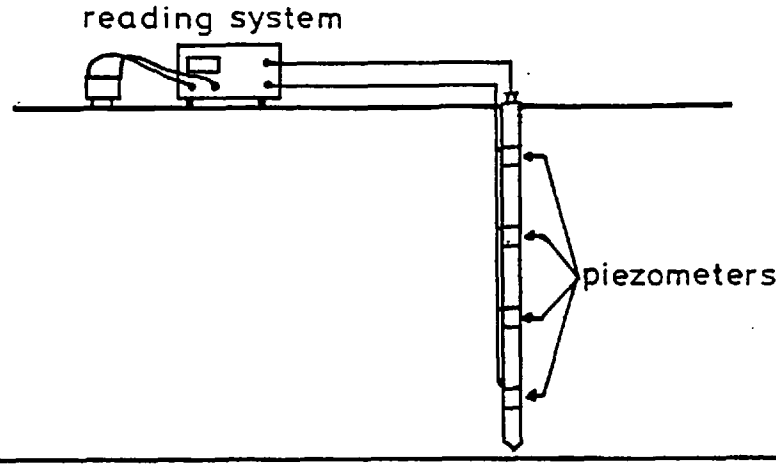


FIGURE 3.9a - MULTIPLE PIEZOMETER DEVICE (FROM MASSARCH et al, 1975).

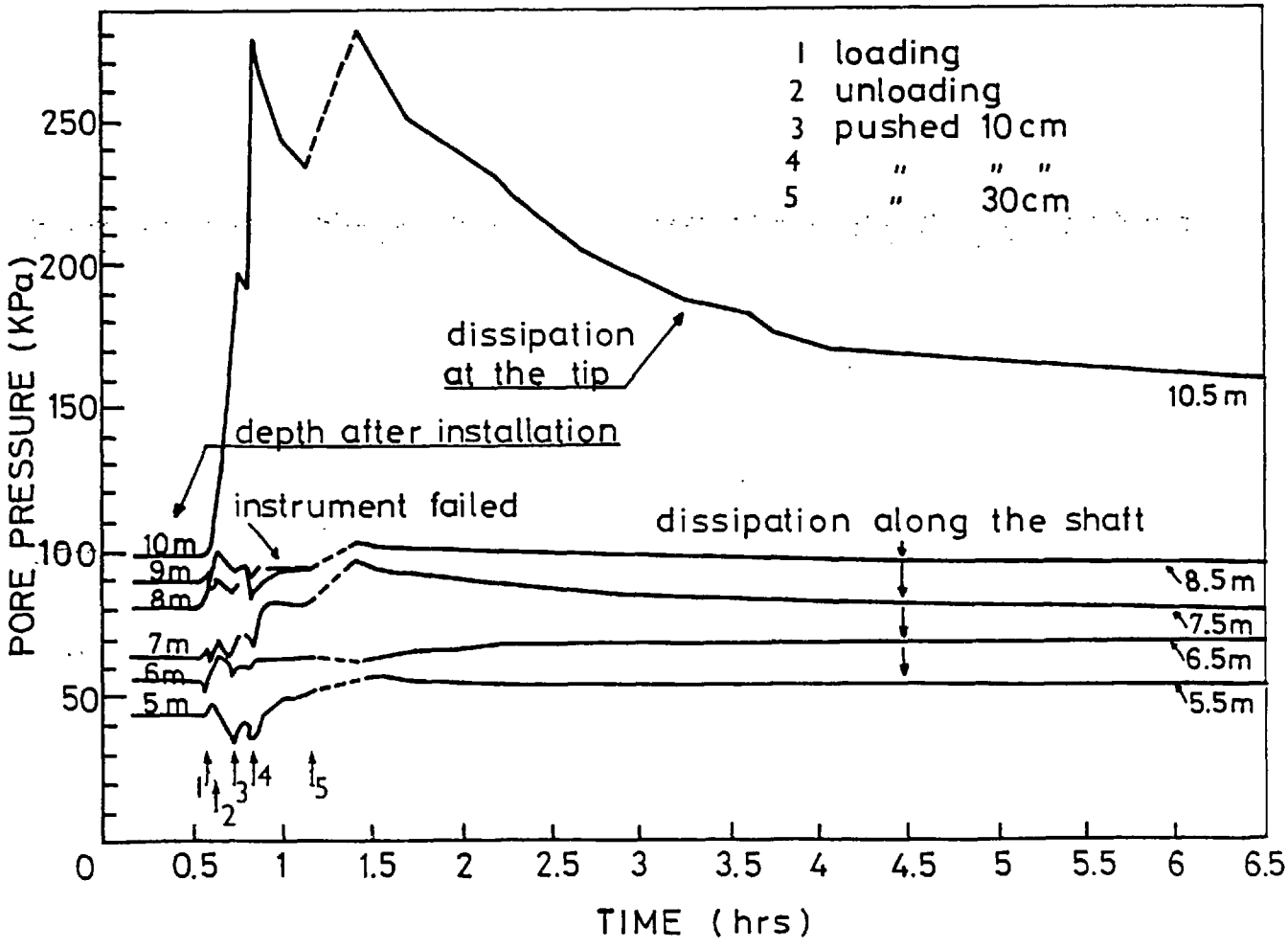


FIGURE 3.9b - PORE PRESSURE DISSIPATION AROUND PIEZOMETER ASSEMBLY (FROM MASSARCH et al, 1975).

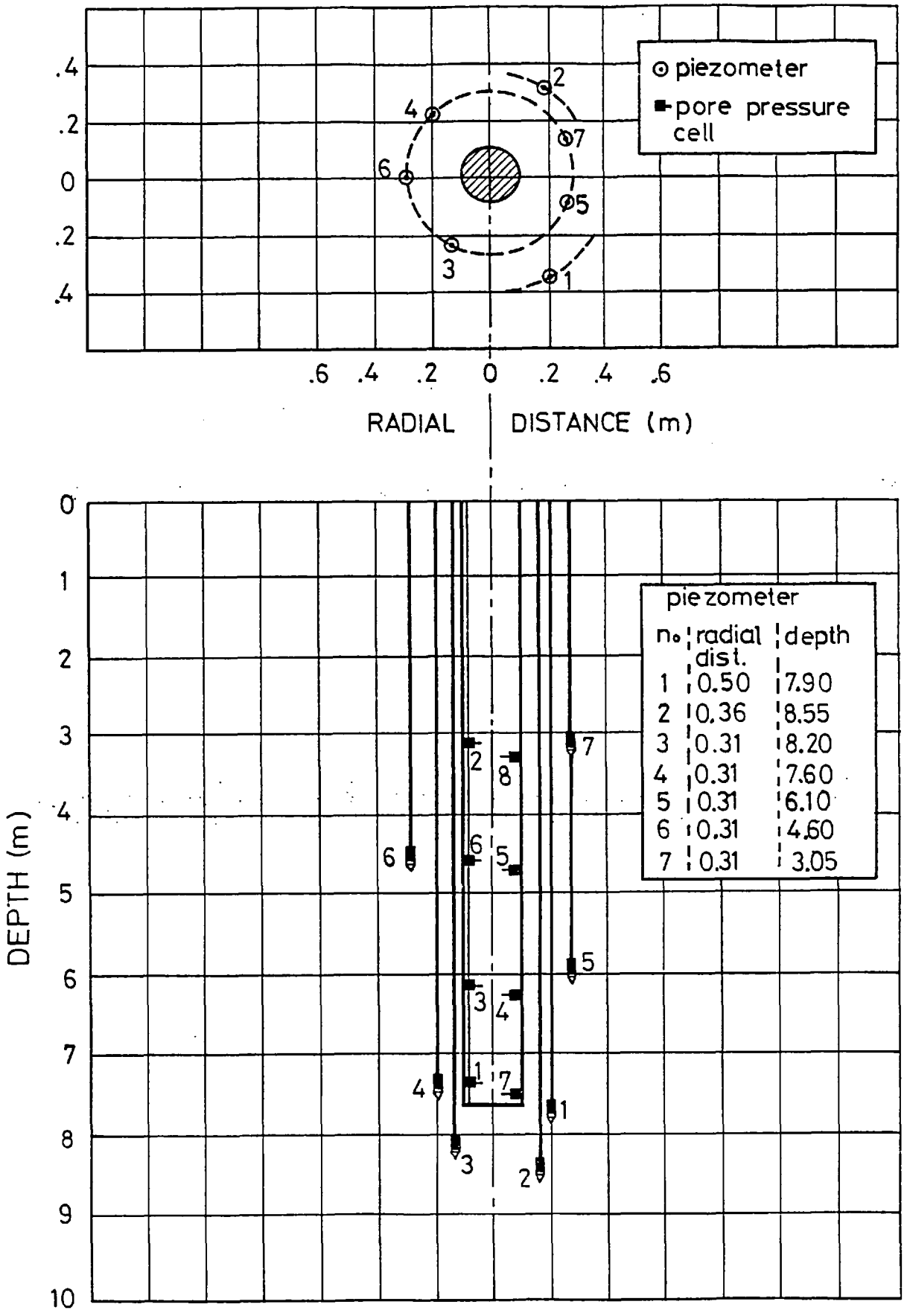


FIGURE 3.10 - DISPOSITION OF THE DRIVEN PIEZOMETERS AROUND THE INSTRUMENTED PILE (AFTER KONRAD, 1977).

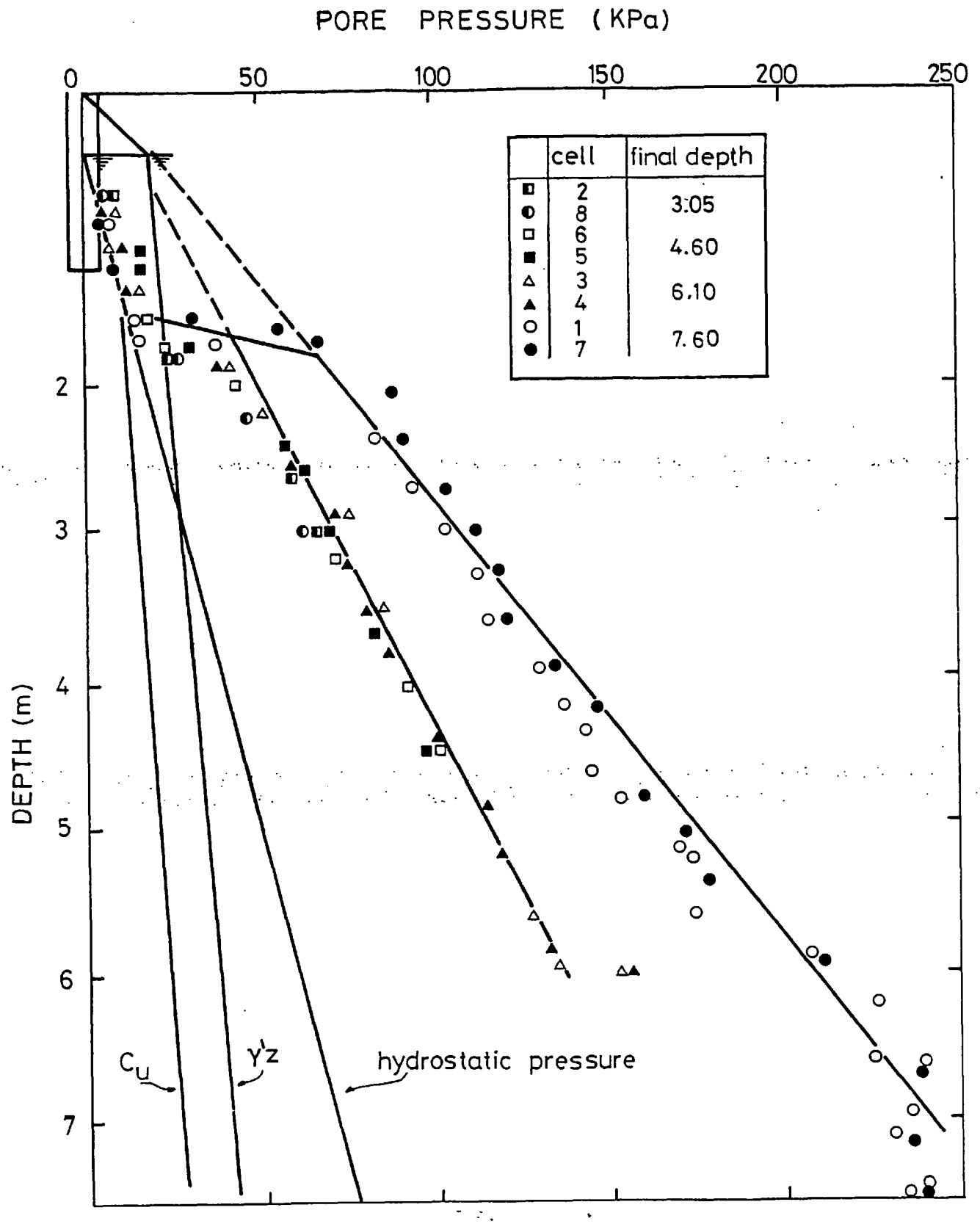


FIGURE 3.11 - EXCESS PORE PRESSURE ALONG THE PILE SHAFT DURING PENETRATION (AFTER KONRAD, 1977).

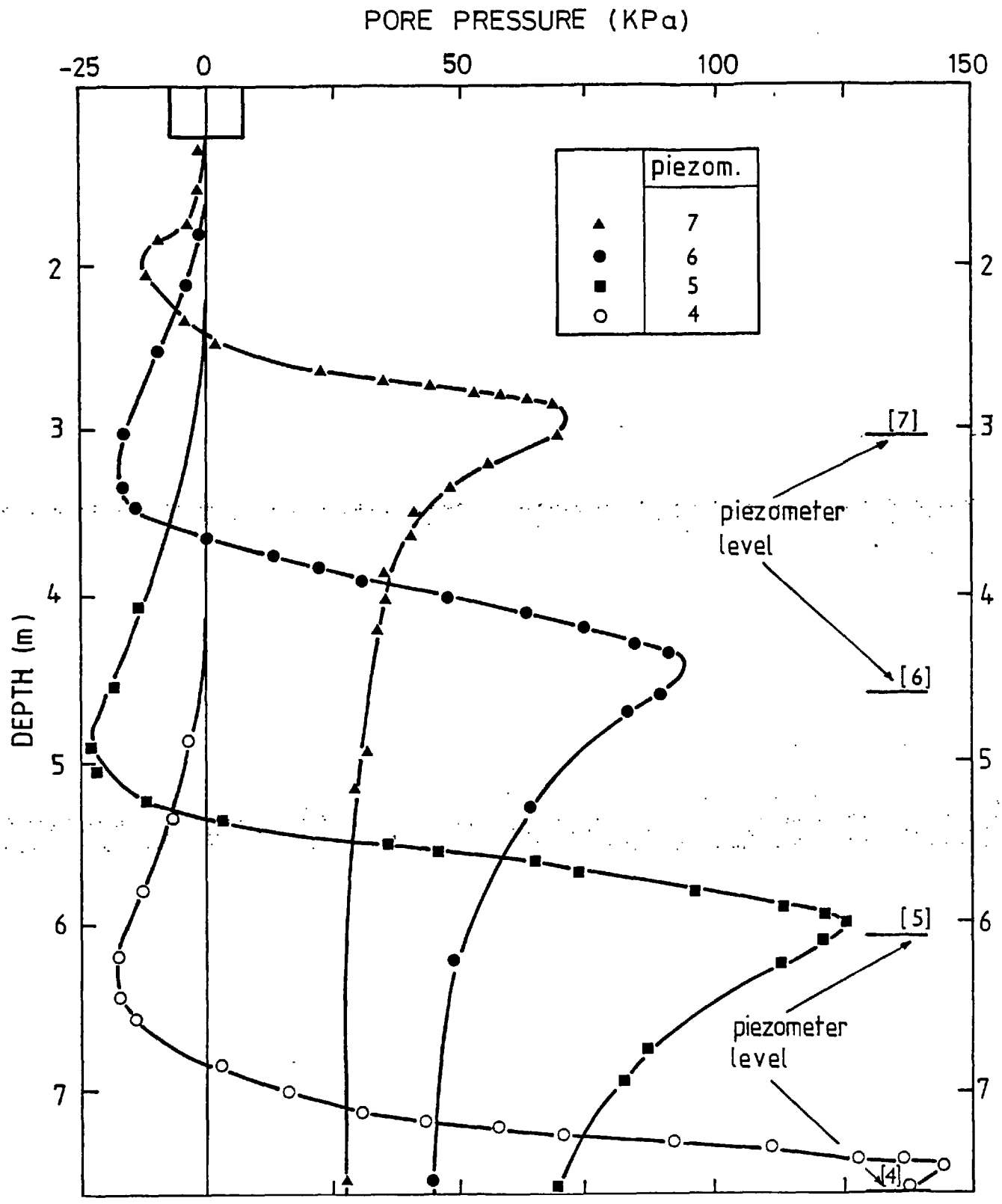


FIGURE 3.12 - EXCESS PORE PRESSURE INDICATED BY THE INSTALLED PIEZOMETERS DURING PILE DRIVING (AFTER KONRAD 1977).

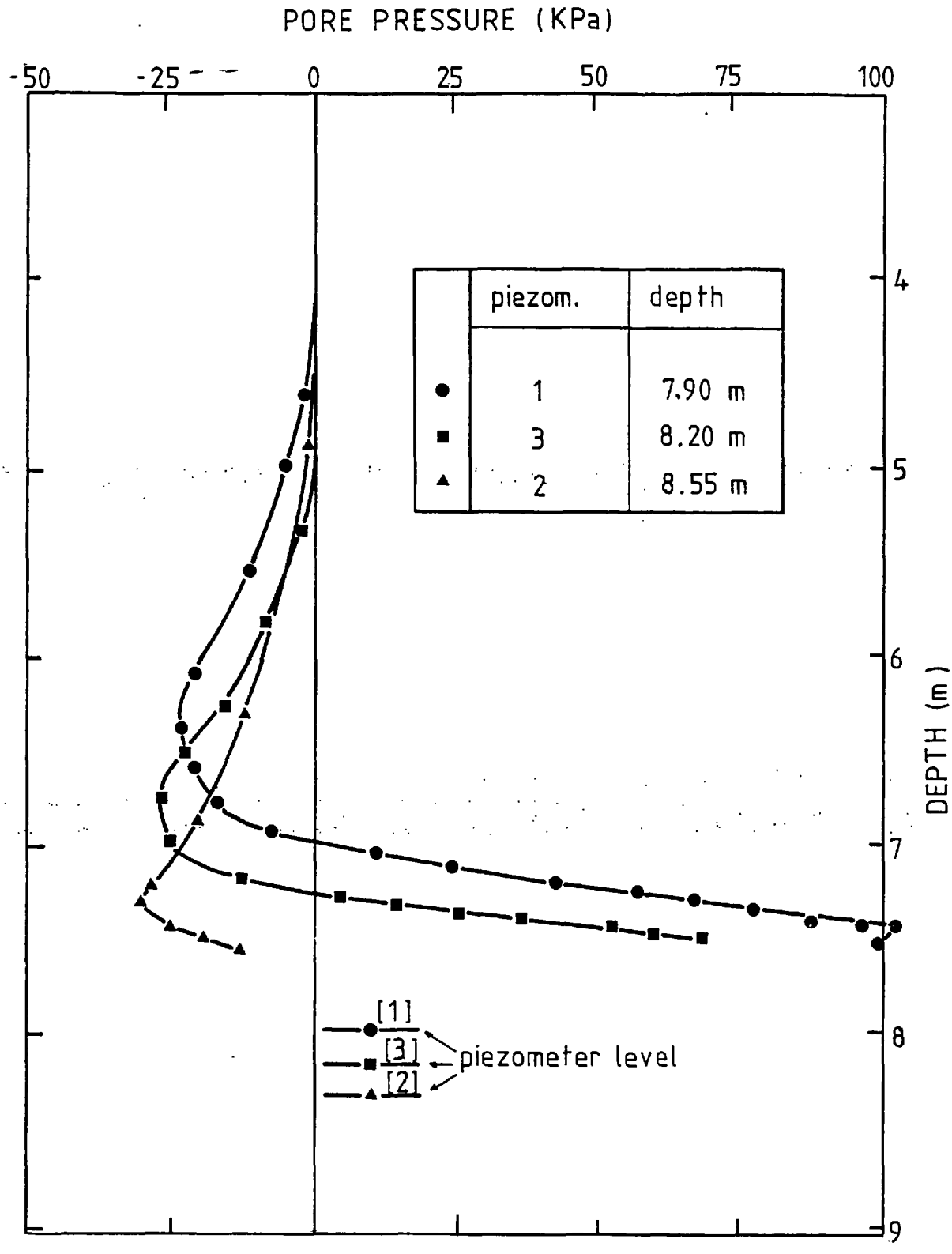
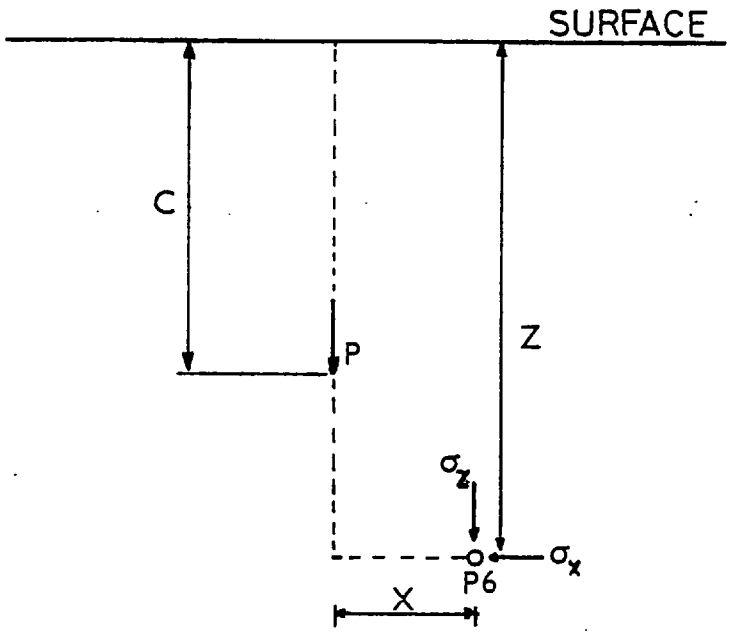


FIGURE 3.13 - EXCESS PORE PRESSURE INDICATED BY INSTALLED PIEZOMETERS DURING PILE DRIVING (AFTER KONRAD, 1977).



P =POINT LOAD

C =POINT LOAD POSITION

P6=POINT CONSIDERED (PIEZOMETER 6–SEE FIG.3.12)

Z =VERTICAL DISTANCE EQUAL TO 4.1m

X =HORIZONTAL DISTANCE EQUAL TO 0.31m

σ_z=INDUCED VERTICAL STRESS

σ_x=INDUCED HORIZONTAL STRESS

FIGURE 3.14 - VERTICAL POINT LOAD ACTING BENEATH THE SURFACE OF A SEMI-INFINITE MASS.

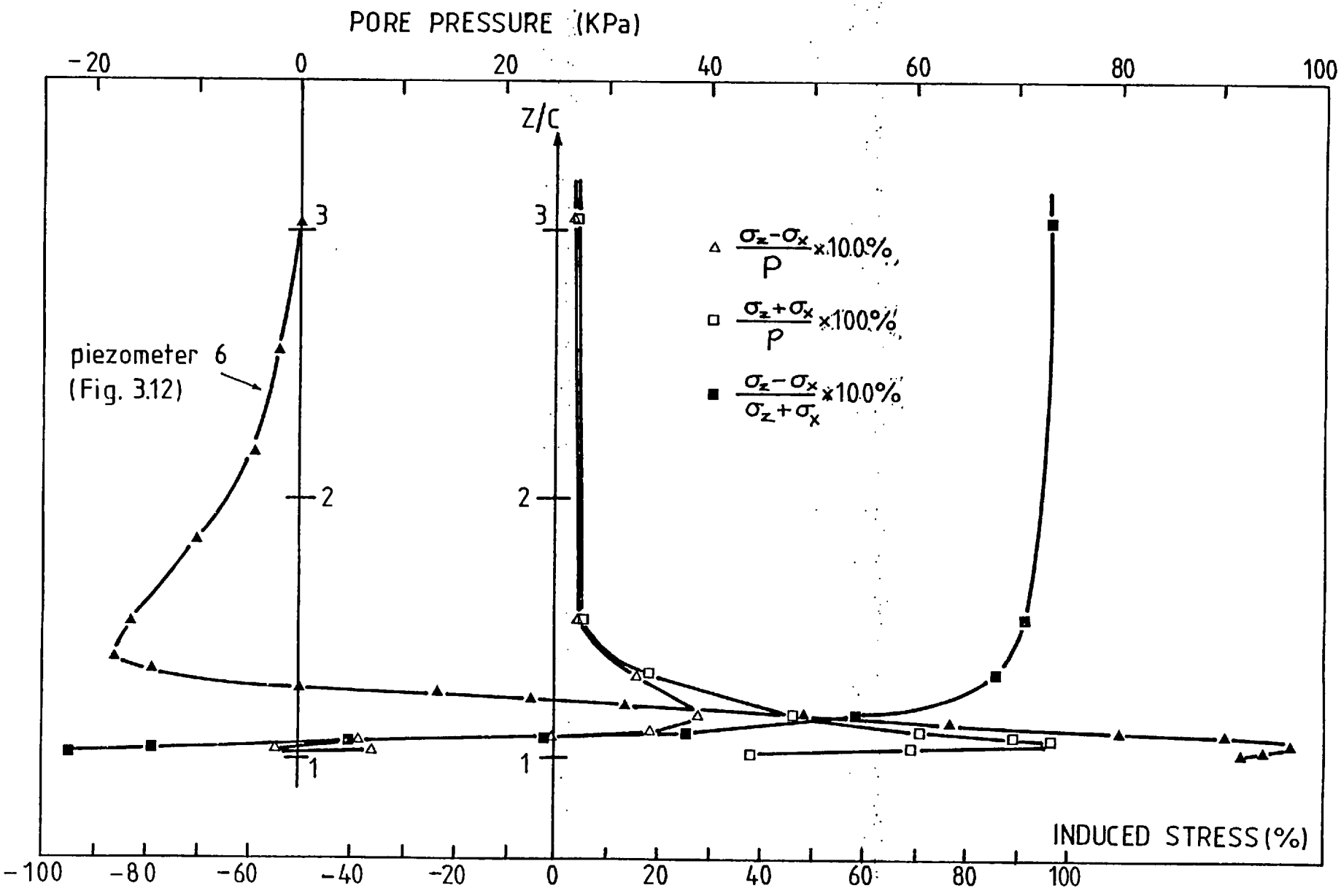


FIGURE 3.15 - STRESS FIELD INDUCED AT A FIXED POINT DURING A PENETRATION PROCESS.

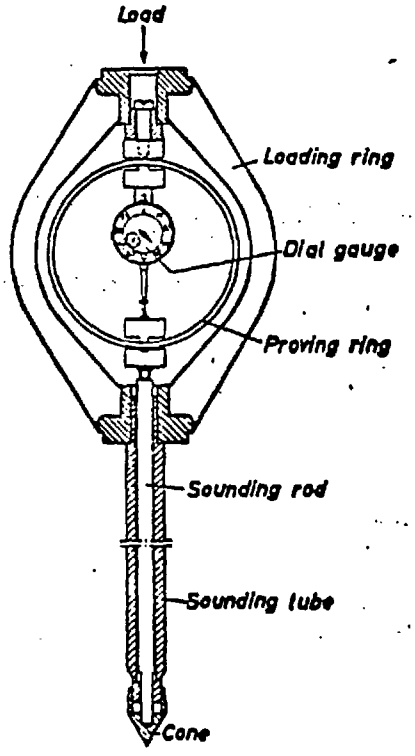


FIGURE 3.16 - PENETROMETER DEVICE (FROM PLANTEMA, 1957).

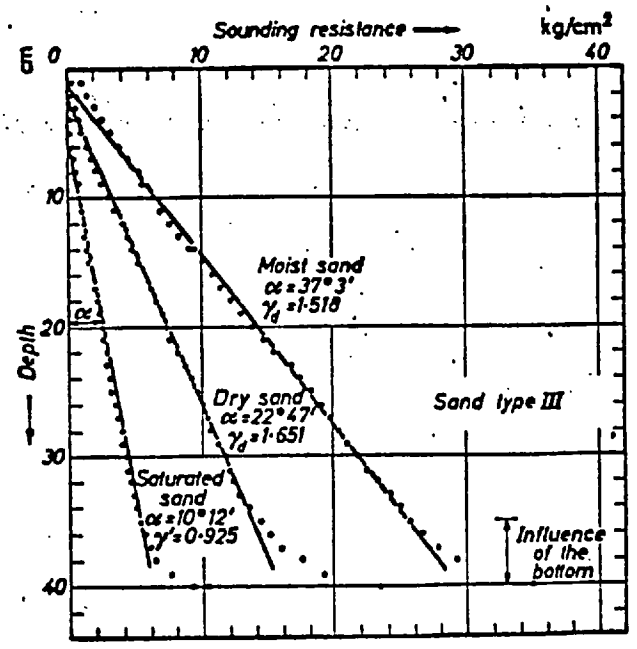


FIGURE 3.17 - TYPICAL VALUES MEASURED DURING THE PENETRATION TESTS (FROM PLANTEMA, 1957).

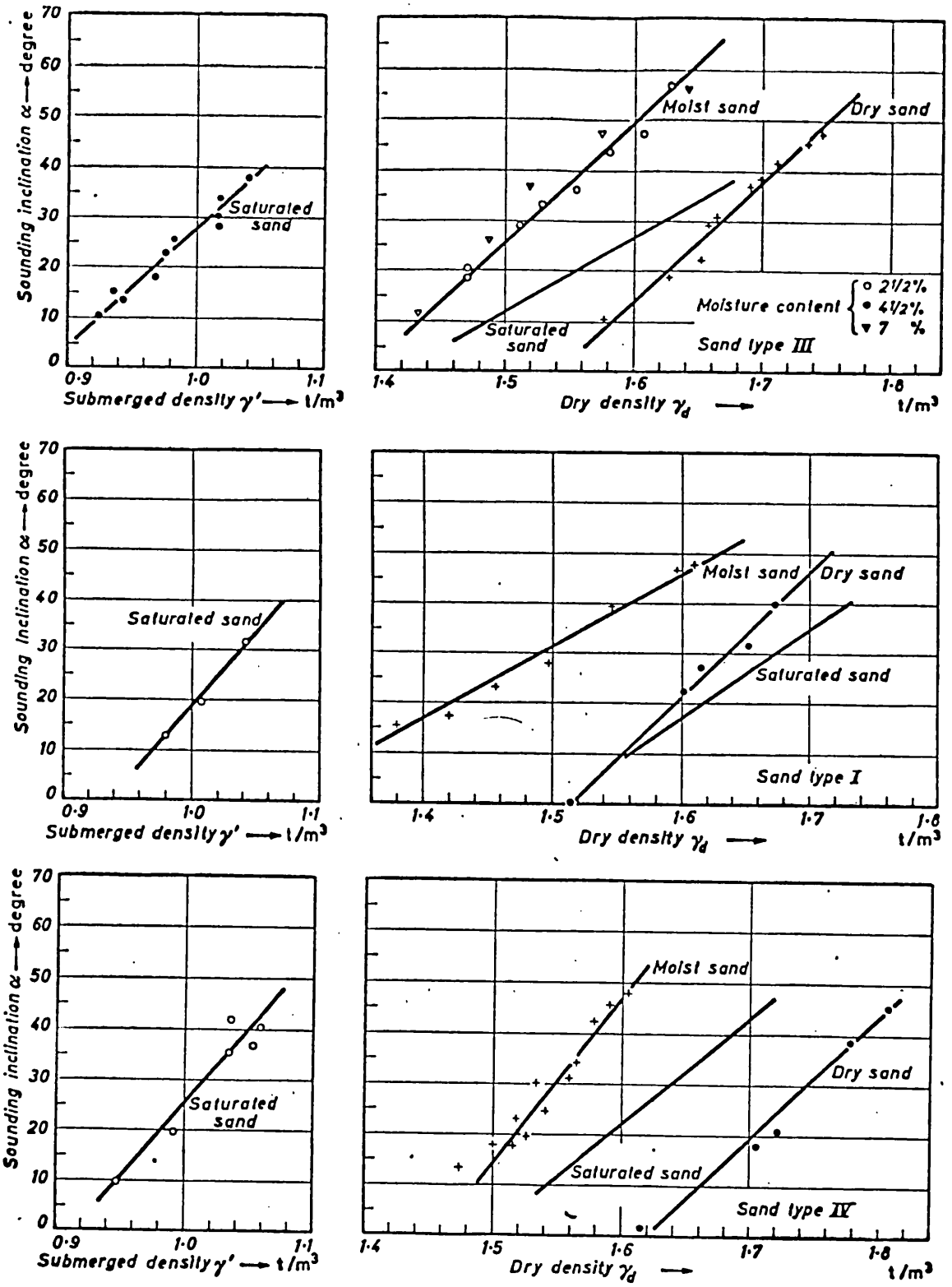


FIGURE 3.18 - PENETRATION TEST ON DRY, MOIST AND SATURATED SAND SAMPLES (FROM PLANTEMA, 1957).

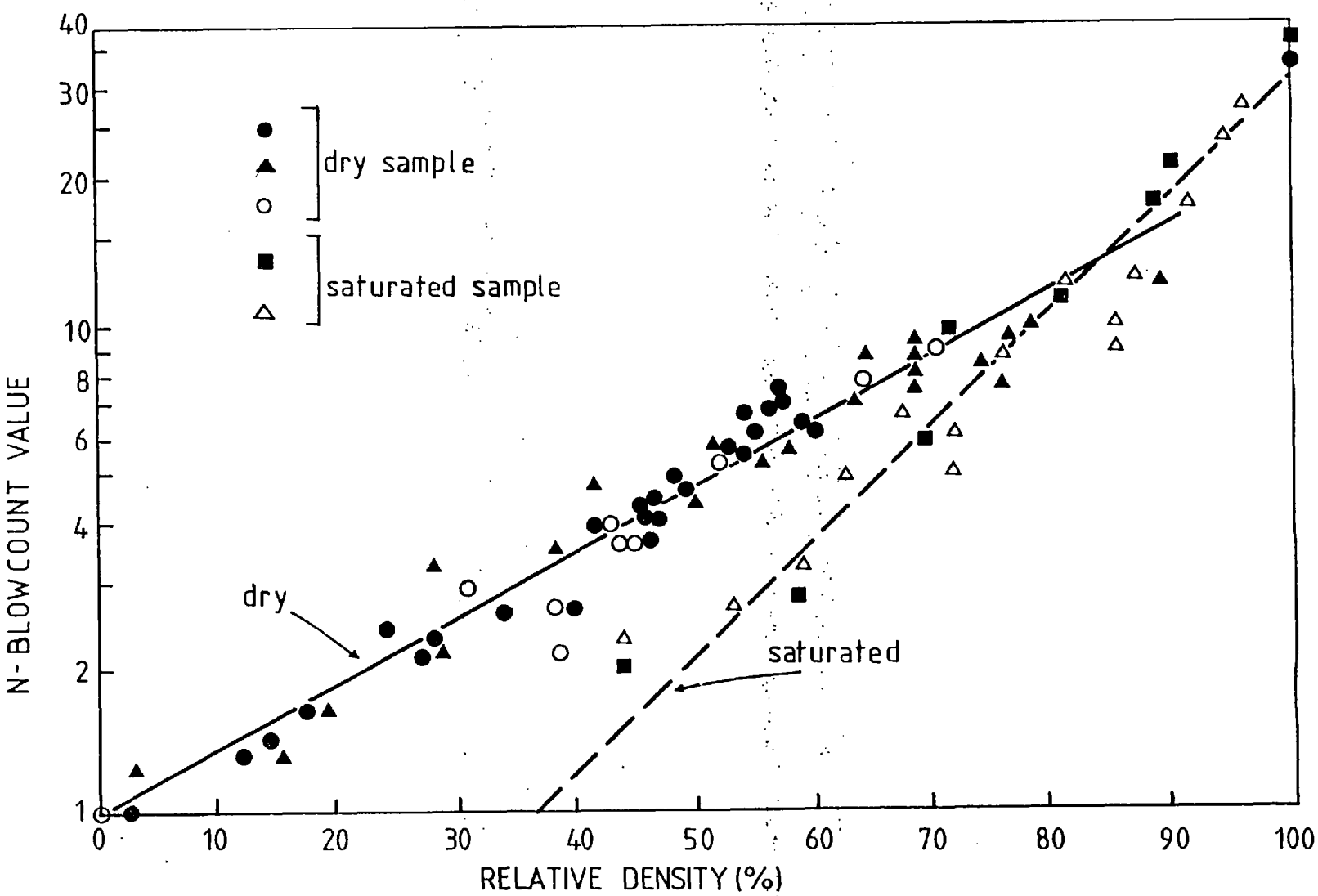


FIGURE 3.19 - PENETRATION TEST ON DRY AND SATURATED SAMPLES (FROM DROZD, 1974).

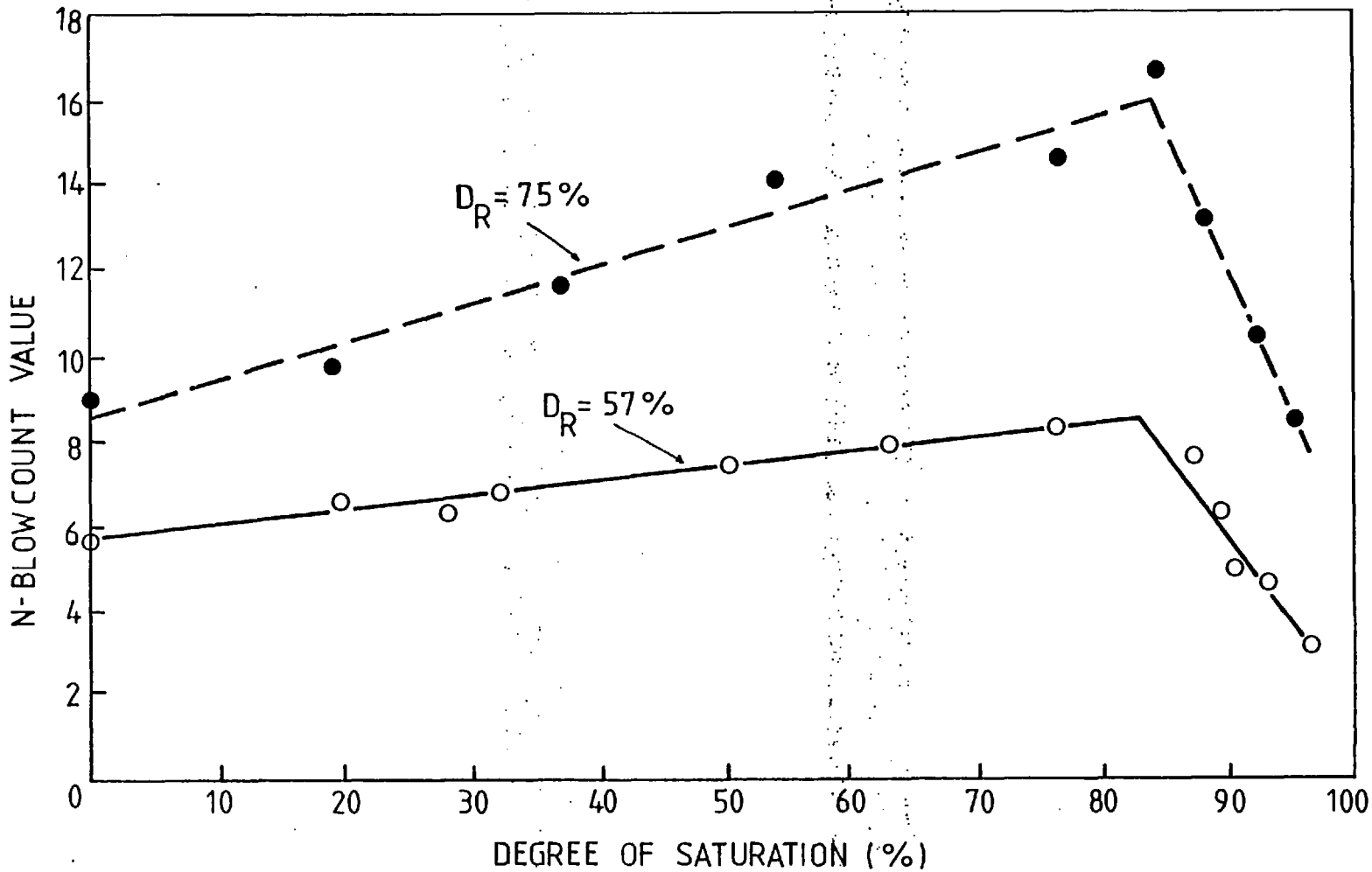


FIGURE 3.20 - INFLUENCE OF THE DEGREE OF SATURATION ON RESISTANCE VALUE (FROM DROZD, 1974).

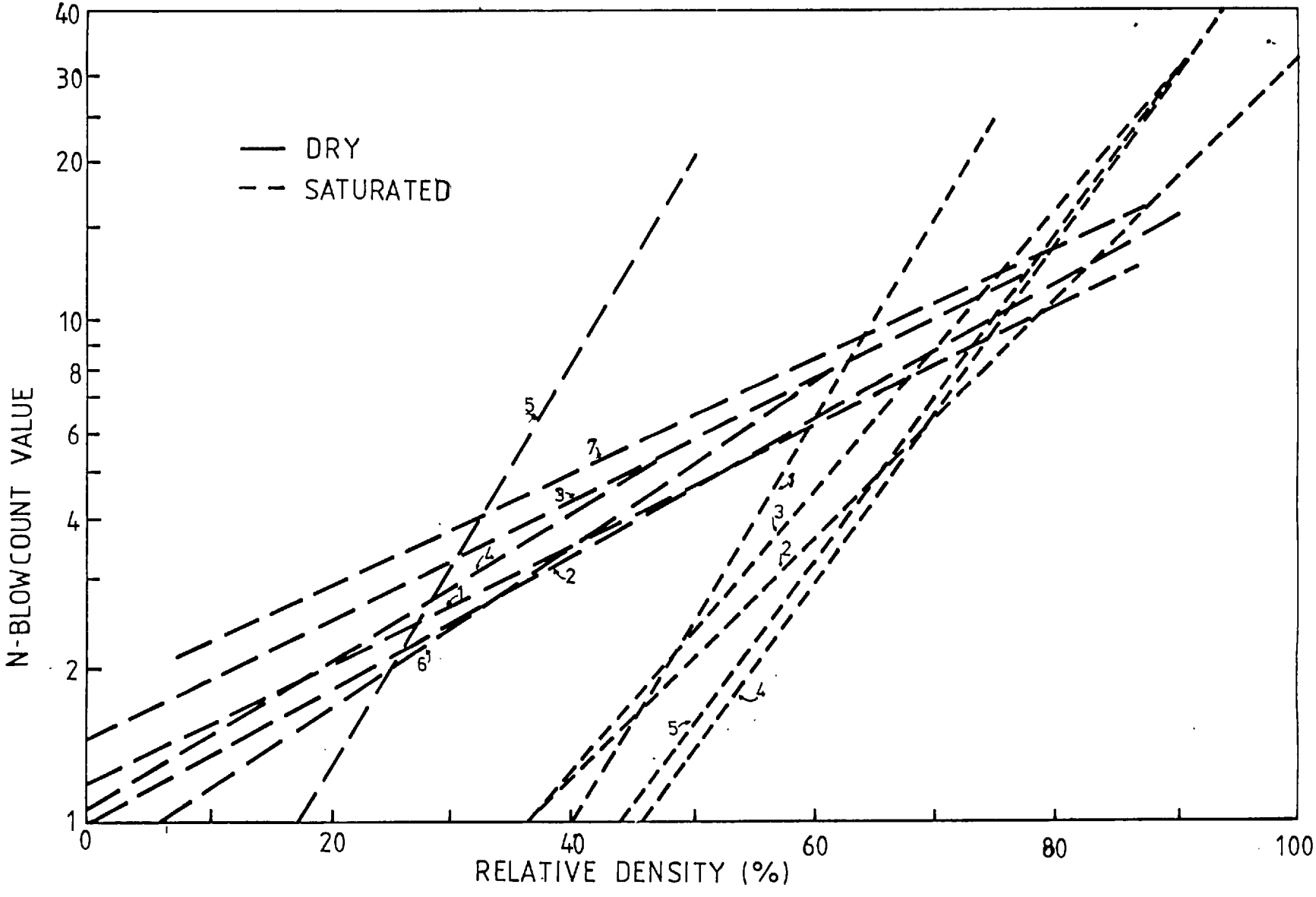


FIGURE 3.21 - PENETRATION RESISTANCE FOR DRY AND SATURATED CONDITIONS FOR SEVERAL SANDS (FROM DROZD, 1974).

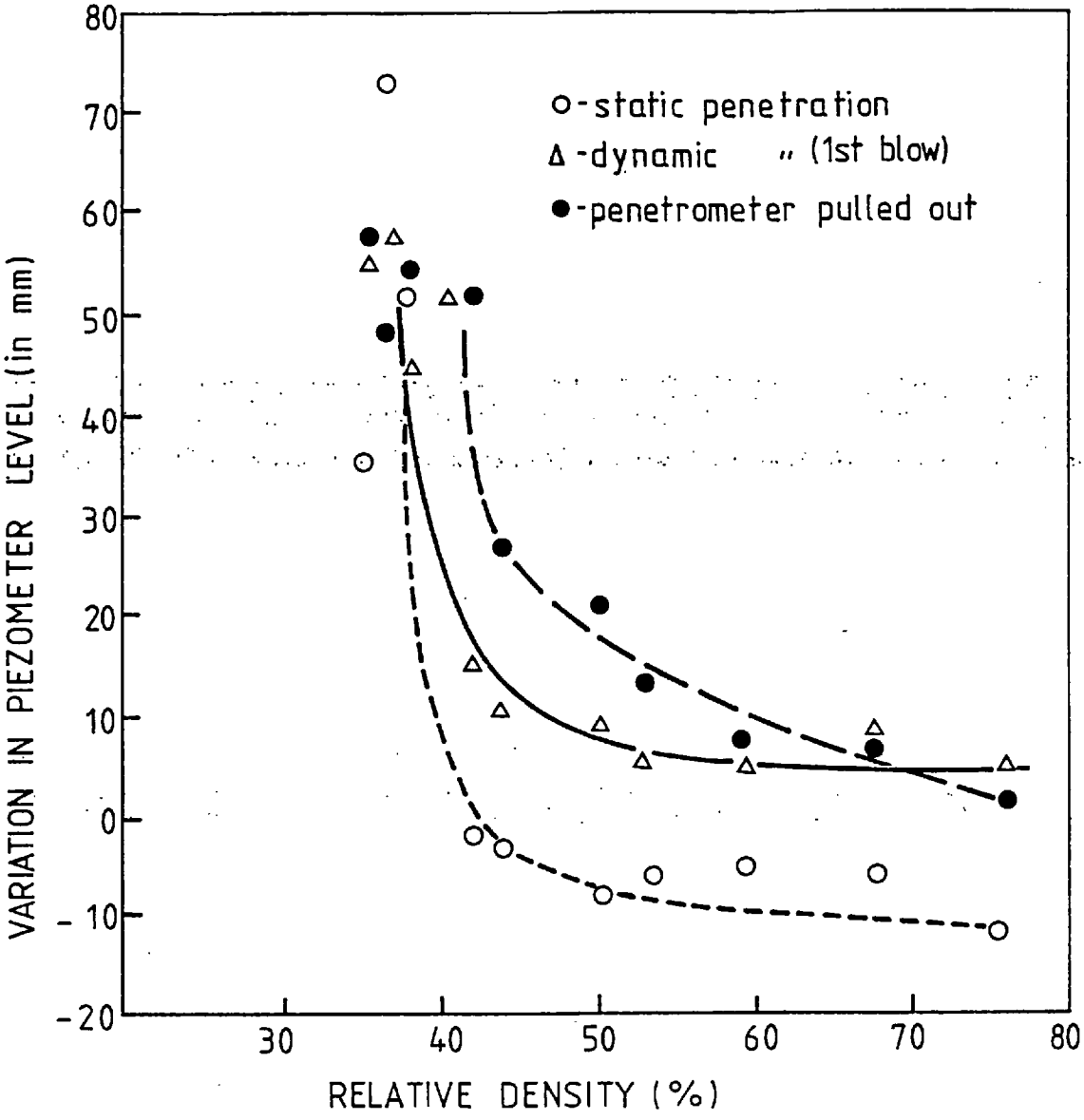


FIGURE 3.22 - EXCESS PORE PRESSURE DURING PENETRATION PROCESS (FROM DROZD, 1974).

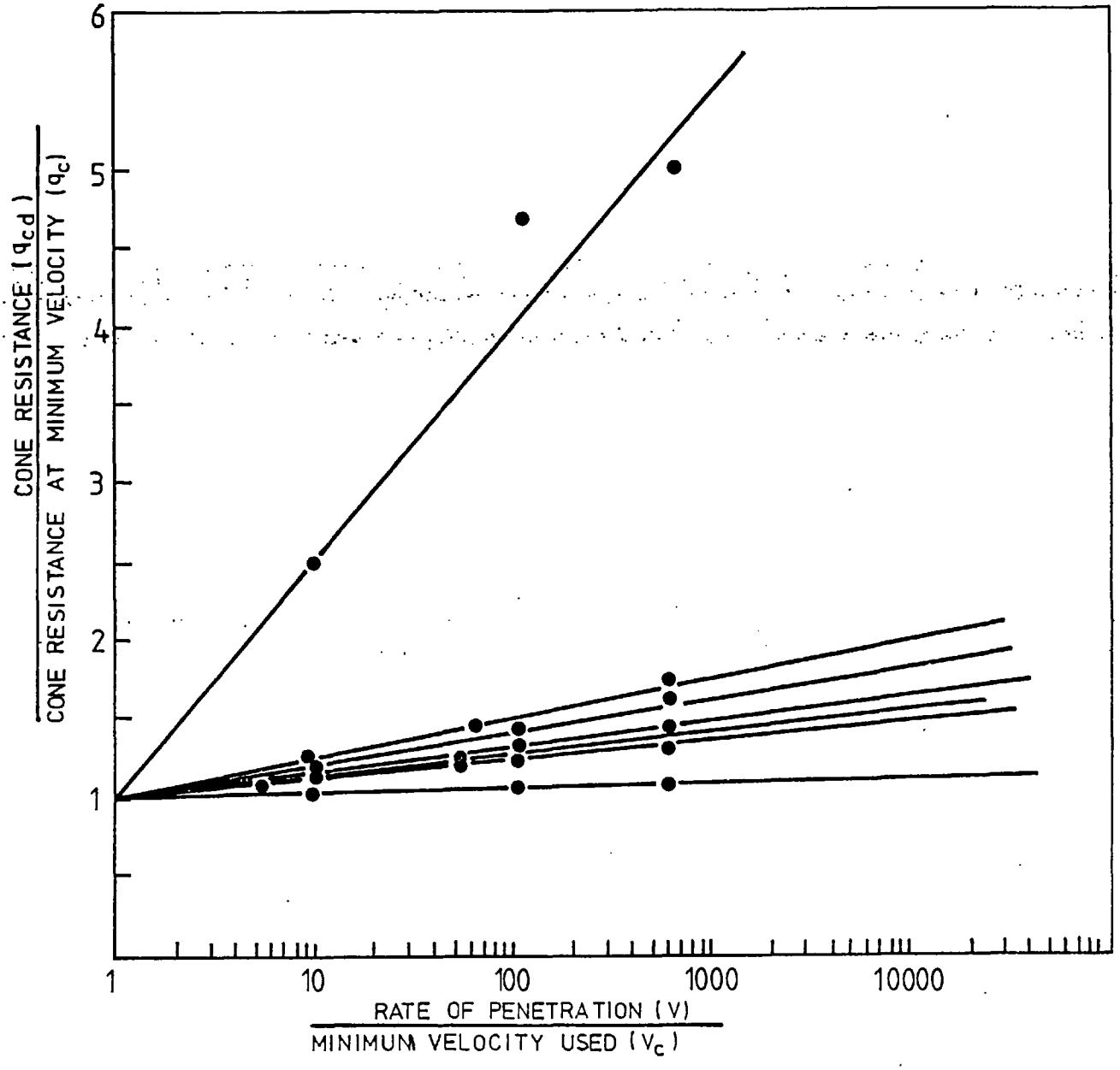


FIGURE 3.23 - PLOTS OF THE q_{cd}/q_c VERSUS $\log_{10}(V/V_c)$ RELATIONSHIP (FROM DAYAL AND ALLEN, 1975).

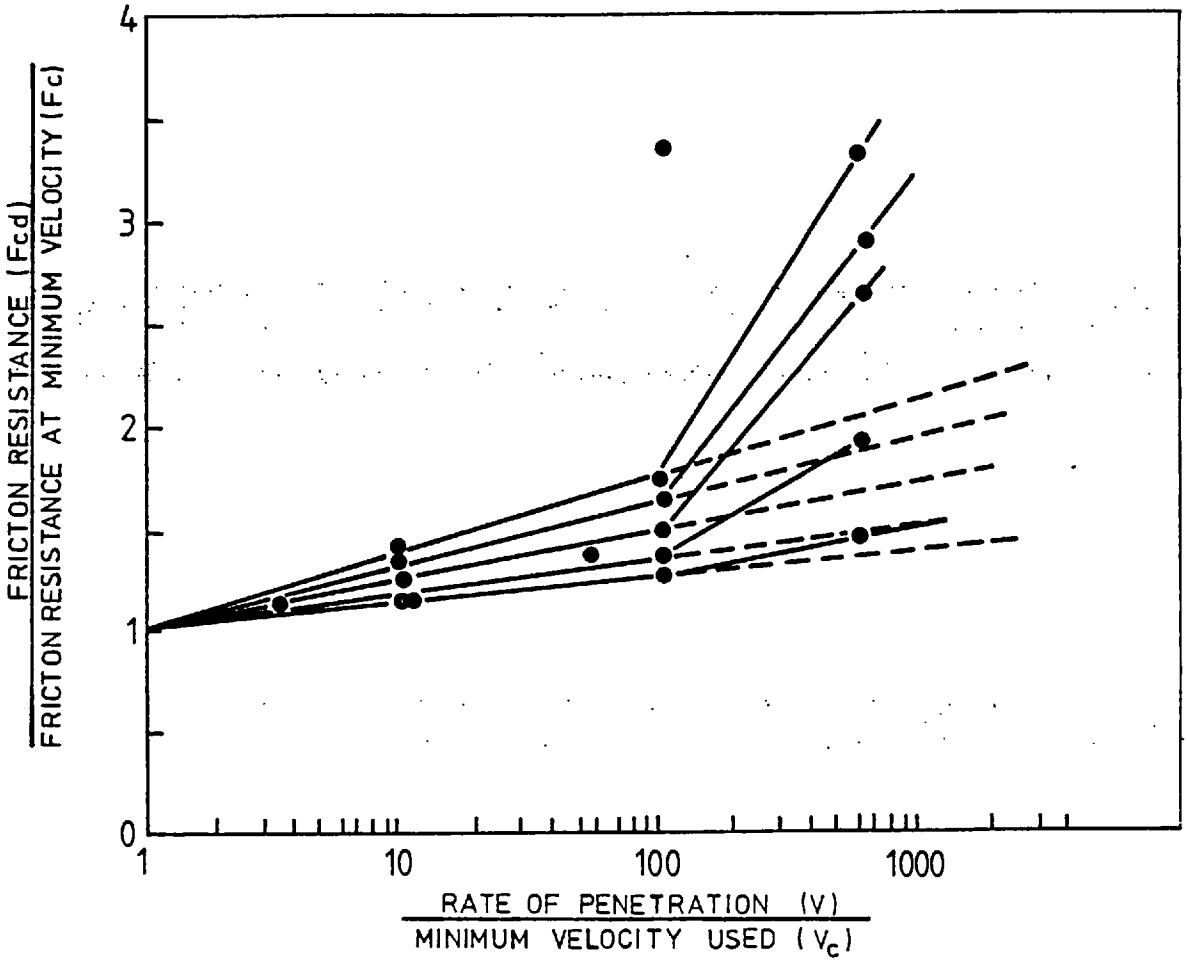


FIGURE 3.24 - PLOTS OF THE F_{cd}/F_c VERSUS $\log(V/V_c)$ RELATIONSHIP (FROM DAYAL AND ALLEN, 1975).

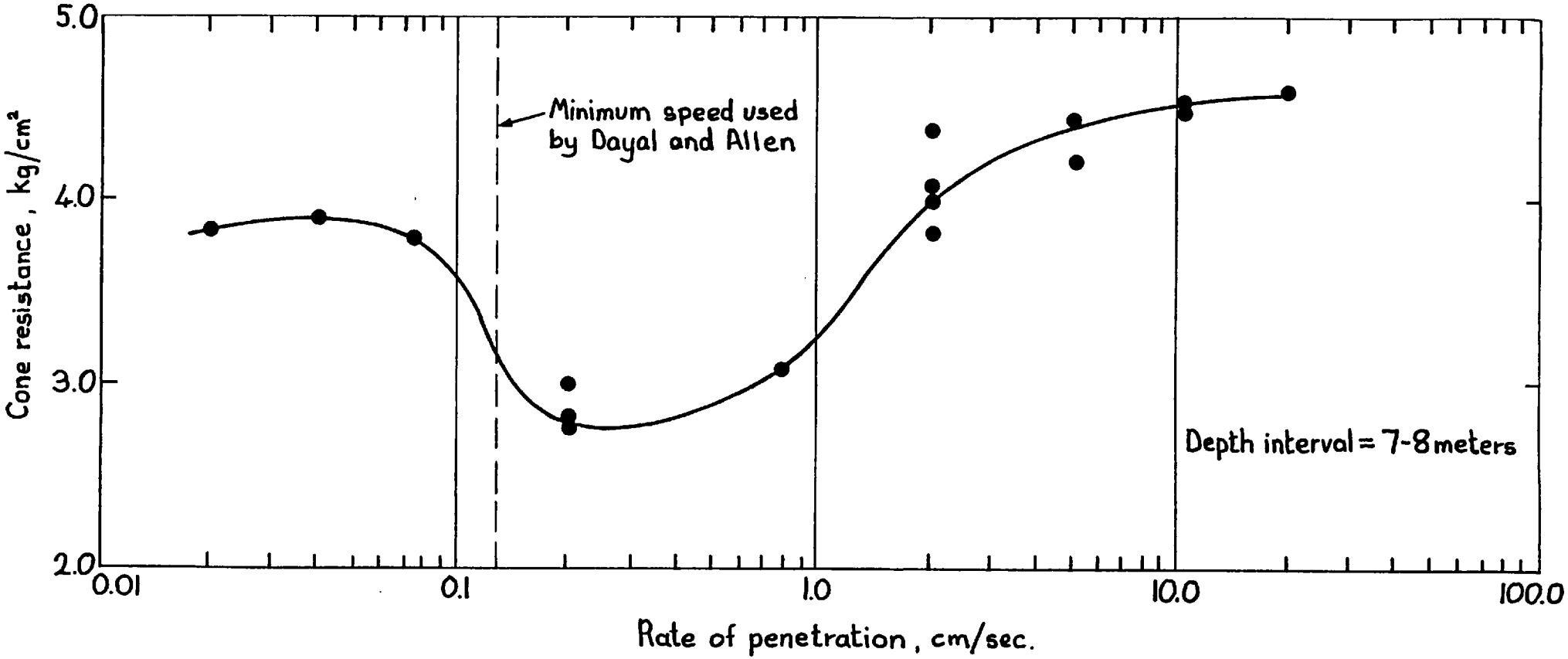


FIGURE 3.25 - THE INFLUENCE OF RATE OF PENETRATION ON STATIC CONE RESISTANCE VALUES (FROM BEMBEN AND MYERS, 1974).

CHAPTER 4

OBJECTIVE OF THIS WORK

Bjerrum (1973) reports that in situ cone tests carried out in the upper fine sand at the North Sea, indicated a point resistance of the order of 70-500 Kg/cm^2. Calibration tests carried out at the Norwegian Geotechnical Institute laboratory in the same sand, indicated that these values correspond to a relative density exceeding 100%. Eide (1974) suspects that these relatively high values, could be due to negative excess pore pressure effects. Mitchell and Lunne (1978), also commenting on results from North Sea sites, suggest that the very high cone resistances might also have been caused by dilation of the dense sands causing negative pore pressures.

In the European Symposium on Penetrating Testing, Stockholm 1974, the importance of the excess pore pressure, both positive and negative, surrounding an advancing penetrometer was pointed out by several contributions (Senneset, Janbu and Senneset, Schmertmann, Hansbo, Bemben and Myers, Kok).

A cone penetration test was carried out at the Building Research Station in a laboratory prepared sample. This sample, with 1.0 m height and 0.76 m diameter and set up inside a cylindrical testing chamber, consisted of a sand prepared to the same grading as that reported by Bjerrum (1973). Great care was taken to saturate the sand, but the large sample was not particularly dense. A lorry mounted, autographic cone penetrometer was used for the test. The cone passed through a gland in the top of the test cylinder and a water pressure was applied to the surface of the sand to simulate 70 m head of sea water. The standard rate of 2 cm/sec was used for cone penetration but unfortunately the cone used was too insensitive for the loose sand, making the results difficult to interpret.

A second sample of saturated sand was consolidated by applying pressure to it through a layer of bentonite and the use of mechanical vibrators acting on the walls of the test cylinder. The same water pressure was applied

to the surface of the sand as in the first test and a cone of greater sensitivity was used. Analysis of the results were made difficult in this case because the cone was overloaded by the dense sand. The penetration test was carried out using a 5 tonne equipment, giving a maximum cone resistance of 500 Kg/cm^2.

It had been hoped that these tests would demonstrate the effects of dilation on cone resistance. On land a fall of pore pressure to a value approaching -1 atmosphere causes cavitation, so limiting the increase of resistance due to dilation. Under a pressure of sea water however, and with high rates of strain which limit the time for drainage, it was thought that much higher penetration resistance might be developed. It became clear that satisfactory conclusions would not result from these ad hoc tests with the lorry-mounted rig and that a laboratory equipment would have to be built so that a more complete series of controlled tests could be carried out.

As a result from the parametric analysis, see Section 3.2, it was indicated that the excess pore pressure at the point of an advancing cone penetrometer can be represented as:

$$U = F_1(\Delta)q_c + F_2(\Delta)\sigma_i \qquad (3.23)$$

where $F_n(\Delta)$ are functions depending on the volumetric strain occurring in the plastic zone

σ_i is the overburden pressure

q_c is the cone resistance

In a homogeneous granular soil and for a given rate of penetration, Eq. 3.23 indicates that the induced excess pore pressure would depend, at least, on the permeability and the compressibility-strain behaviour of the soil. For cohesionless soils these factors are strongly dependent on density, confining pressure and stress history.

In order to better investigate the effect of density, confining pressure and stress history upon the excess pore pressure surrounding and advancing cone penetrometer an apparatus was developed, consisting basically of:

a) Testing chamber

b) Driving system

c) Electrical cone penetrometer with pore pressure measurement device

The preliminary tests promptly indicated the difficulties in obtaining useful and correlative information. Most of the initial results were abandoned as a consequence of an inadequate performance of the equipment, see Appendix A3. Modifications to testing techniques and adaptations of the apparatus were mostly made as an outcome of failures rather than based on previous experiences. This caused an excessive consumption of time which affected the initial testing programme. It was decided to reduce the number of cone tests and to obtain extra information from the saturated sample. Hence the research program was extended to include the study of factors affecting the relationship between cone resistance and compressibility, for normally - and over -consolidated conditions.

CHAPTER 5

DESCRIPTIONS OF THE APPARATUS

5.1 GENERAL

Large testing chambers have been used to assist with the calibration and development of basic correlations for in situ test equipment. Thus, samples under controlled conditions can be obtained and may provide a basis for understanding the effects caused by the varying factors. As a very important application, the use of these large calibration chambers may permit separate the similar effects of increased effective stress level and increased density.

With respect to the boundary conditions, there are two types of design: a flexible wall or a rigid wall testing chamber.

Plantema (1953) describes one of the first flexible wall testing chambers developed. Basically, it consists of a double wall cylinder. The outer wall of the chamber is formed by a rigid steel cylinder and the inner consists of a rubber membrane. There exists water with pressure control filling the space between the outer and inner wall. Thus, lateral and vertical stresses can be independently applied. The chamber houses a cylindrical sample of 0.95 m diameter and 0.75 height.

Schultze and Melzer (1965) give details of a rigid wall chamber consisting basically of a test pit with 3.0 m diameter and 5.5 m effective depth.

A rigid wall design will impose a boundary condition of zero lateral displacement and consequently boundary effects may interfere in the calibration results. In order to avoid this interference, a large chamber-testing instrument diameter ratio is required. A flexible wall chamber provides a more versatile design, can be made much smaller and as stressed by Holden (1971) it will provide a boundary condition closer to the field conditions.

Chapman (1974) describes a well instrumented triaxial testing chamber which can be used to measure accurately and control stresses and strains at the sample boundaries in both the lateral and vertical directions. This flexible wall chamber can impose two different boundary conditions: a constant stress or a zero average lateral displacement.

The use of this well equipped large triaxial testing chamber, for calibration purposes, has been proved successfully and this can be exemplified by the works of Veismanis (1974) and Laier et al (1975).

All the published information on the works carried out so far indicate that tests have been only performed on dry material.

For this research a very simple testing chamber has been used. Fig. 5.1 provides a general layout of the equipment and it comprises four major components: testing chamber, driving system, pressure unit and penetrometer; each of which is described in more details in the subsequent sections.

5.2 TESTING CHAMBER

The testing chamber consists basically of a cylinder and removable top and bottom plates, see Fig. 5.1.

A rigid thick wall steel cylinder, with 0.76 m internal diameter and 1.57 m height, is used. It is fitted at the upper and lower edge with 0-ring seals.

The top plate, see Fig. 5.2, sealing off the top of the chamber, enables fluid pressure to be applied through a connexion. The central part of the top plate forms a removable gland, with two attached 0-ring seals, through which a rigid tube can slide. The 0-ring seal attached to the gland and in contact with the sliding tube should provide minimum friction and efficiency against leakage. For calibration purposes, it has been found that the lubricated tube falls slowly under its own weight. There exists at the bottom end of the rigid

tube a fixed and a sliding circular ring. The sliding ring can be bolted to the fixed one, tightening in between the edge of the rubber membrane cap. The tube and the double plates form a rigid system and is used for plate bearing tests. A "0"- ring seal is attached internally at the top end of the rigid tube, see Fig. 5.2.

The dimension of the external ring diameter is a compromise between opposing requirements. The ratio between its external and internal diameters should be big enough to avoid the influence of the ring effect. Thus the results of the plate bearing test can be treated as proceeding from a solid plate. However the ratio between plate external-cylinder internal diameter should be small enough to minimize the boundary effects on the plate bearing test results. The minimum possible internal ring diameter is limited by the clearance needed for the free movement of the penetrometer and rods passing through. Inside these requirements, the circular ring has been designed with an internal and external diameters of 44.2 mm and 150 mm respectively.

The rubber membrane cap, forms a flexible piston and is used for applying load on the top of the sample. Its outer edge is tightened against the cylinder upper edge and the top plate.

The bottom plate, see Fig. 5.3, sealing off the lower end of the cylinder is a solid rigid plate containing four independent connexions. Each of these connexions contains a porous stone in the internal end and serves as a drainage system, when connected to a single tap, or as pressure connexion, when connected to a pressure supply. These connexions can also be connected to a volume change apparatus for measuring the volume of water expelled out from the sample during the consolidation process, see Fig. 5.1.

5.3 DRIVING SYSTEM

The driving system comprises the loading frame, the hydraulic jack and the jack control, see Fig. 5.1.

The loading frame consists of two vertical rods fixed to the chamber top plate and a thick horizontal bar, with adjustable level positioning, bolted to the top end of the rods, see Fig. 5.3. This loading frame provides the reaction for the hydraulic jack which is used to push the penetrometer into the sample.

The hydraulic jack which is fixed to the horizontal bar, is a double acting power cylinder with approximately 0.75 m travel. It is controlled by two valves. The flow control valve which determines the driving speed of the ram, giving a range from 1.5 cm/sec to 2.5 cm/sec, and the action control valve controlling the action and direction of movement. The system is electrically power operated.

5.4 PRESSURE UNIT

The pressure unit consists basically of an oil pressure maintainer with a minimum load increment of 0.35 Kg/cm^2, connected to the removable top of a cylindrical container, see Fig. 5.1. This cylinder container is filled with water. Thus the pressure is applied from the load maintainer to the water through the flowing oil. The cylindrical container is connected from a tap controlled opening, placed at its lower part, to a manual hydraulic pump. This pump serves to inject extra water into the system and also reversing the flow, pumping the oil back into the load maintainer. Before reaching the connexion provided at the testing chamber top plate the system is connected to a volume change apparatus. Therefore, the volume of the water entering the testing chamber can be measured. There are three Bourdon gauges along the pressure line, see Fig. 5.1, their locations are: pressure maintainer, manual hydraulic pump and testing chamber top plate. There is an extra Boudon gauge connected to the bottom of the testing chamber and can be used when the drainage system is closed, to measure pore pressure change (at the bottom of the sample) caused by variation in total stress (applied at the top of the sample).

5.5 ELECTRICAL PENETROMETER

5.5.1 DESCRIPTION

Fig. 5.4 provides details of the electrical penetrometer which comprises three major components: the porous conical tip, the friction sleeve and the corresponding load cells. Except for the adapted porous conical tip, the penetrometer is similar to the Fugro electric type which has been described by De Ruiter (1971). Basically, it consists of two independent strain gauge load cells which enable the measurement of the resistance developed at the conical tip and along the sleeve during the penetration process.

The conical tip has been modified for measuring the induced excess pore water pressure during the penetration process. Fig. 5.5 shows the separable base and nose, which form the adapted conical tip. The base and nose can be screw coupled enclosing in between a pressure transducer. Rubber sheet washers are provided and efficient sealing is obtained by tightening the two coupled parts. One third of the nose, at the point, is made of coarse porous stone.

A DRUCK type pore water pressure transducer is located in the prepared cavity existing between the screw coupled parts (conical tip). This pressure transducer has 10.7 mm diameter and 11.9 mm length and is commercially provided with a porous disc in front of the diaphragm. For the series of tests this porous disc has been removed.

The penetrometer has an apex angle of 60°, a diameter of 35.6 mm giving a base area of 10 cm^2 and a friction sleeve of 150 cm^2 lateral surface area.

5.5.2 RECORDING SYSTEM

The loads and pressure registered respectively by the load cells and the pressure transducer are transferred to the recording system by the corresponding set of wires passing through the hollow penetrometer and rods.

The recording system consists basically of two Solartron type chart recorders with two channels each. Transducer supplies and digital voltimeters are also provided. Therefore, the three measured quantities (point and sleeve loads and tip excess pore pressure) can be automatically registered.

For convenience, it has been adopted as test procedure to record in one chart recorder the point resistance and pore pressure and in the other point and sleeve resistances.

5.5.3 CALIBRATION OF THE PENETROMETER LOAD CELLS

For the calibration of the respective point and friction sleeve load cells, a calibration rig was used which consists of two vertical rods and four horizontal plates, see Fig. 5.6. The vertical rods are fixed on the two external horizontal plates forming a rigid frame. The two internal horizontal plates, provided with ball bearing, can slide along the vertical rods. A load cell is attached to the external top plate. A hydraulic jack, connected to a manual pump, is fitted between the internal top plate and the rig load cell.

The calibration rig can optionally be provided with an extra load cell which can be fixed to the external bottom plate, see Fig. 5.6.

For the present calibration procedure, only the top load cell has been used.

The penetrometer rests on a conical recess fixed on the internal bottom plate and is fitted at the top to a cylindrical recess fixed on the internal top plate.

The calibration procedure is done by applying load with the hydraulic jack and recording the loads registered by the rig load cell (previously calibrated) and the penetrometer load cells. For the calibration of the friction sleeve, the conical point of the penetrometer is removed and the lower edge of the friction sleeve is fitted in the conical recess. The calibration procedure is the same as above.

Calibration curves of the rig, point and friction sleeve load cells are shown in Figs. 5.7, 5.8 and 5.9 respectively.

Fig. 5.8 indicates that a value CF = 253.3 Kg/mv can be assumed as the calibration factor for the point load cell. Thus, the cone end resistance is obtained by transforming the electric impulse in load and dividing this value by a factor of 10 corresponding to the base area in cm^2. The result will be obtained in Kg/cm^2. The maximum working load of the point load cell is 2 tons, giving a maximum working cone resistance of 200 Kg/cm^2

For the friction sleeve load cell, Fig. 5.9 indicates that a value of CF = 191.0 Kg/mv can be assumed as the calibration factor. The friction sleeve resistance is obtained dividing the estimated load by a factor of 150 corresponding to the lateral surface area in cm^2. The results will be obtained in Kg/cm^2. The maximum working load of the friction sleeve resistance of 6.67 Kg/cm^2.

In order to prevent point loads being partially transferred to the friction sleeve, a modification was introduced in the original cylindrical sleeve, see Fig. 5.10. This partial load transfer is likely to occur when fine soil particles can enter the existing space between the friction sleeve lower edge and the base of the conical tip. The confined particles can be the transfer element as the conical tip subjected to loads moves towards the friction sleeve, see Fig. 5.10.

This particular problem, has been observed during a calibration performed after a penetration test having been carried out. The obtained calibration curve corresponding to the point load cell is shown in Fig. 5.11. The partial load transferred to the friction sleeve was also recorded and this value has been converted in terms of the point load. The calibration curve based on the registered point load plus the converted friction sleeve load indicated a calibration factor equal to the actual calibration curve, see Fig. 5.11. For comparison purposes, the actual calibration curve is also

indicated in the same figure. The fine soil particles confined into the existing space was washed out and the calibration repeated. The repeated calibration indicated for the cleaner penetrometer no load transference and a calibration factor equal to the actual calibration curve.

The modification consisted in transforming the original lower edge into a knife shape end, see Fig. 5.10.

Several calibrations have indicated a good performance of the modified sleeve in respect to the load transfer problem. Due to the small dimension of the proposed wedge, any possible contribution of the lower edge end bearing to the sleeve lateral resistance can be neglected.

All the presented results have been obtained with the modified friction sleeve.

5.5.4 SATURATION AND CALIBRATION OF THE PORE PRESSURE DEVICE

For saturating the porous conical tip, the vacuum technique has been used. The normal procedure consists in placing the removable nose inside a container filled with deaired water and applying a vacuum at the top of this container. A transparent set is used, which enables visual inspection of trapped air bubbles being expelled from the porous part of the nose and indicates the period required to achieve almost full saturation. After saturation, the nose is screw coupled to its base under deaired water.

For the calibration of the pore water pressure transducer, the penetrometer with the saturated conical tip is placed inside a calibration pressure cylinder filled with deaired water, see Fig. 5.12. The cylinder top gland is provided with a pressure connexion. Thus, a known water pressure is applied through the provided connexion and the corresponding transducer output signal is registered. Fig. 5.13 indicates the calibration curve of the

transducer used in the presented series of tests. A value of CF = 7.07×10^{-2} Kg/cm^2/mv can be assumed as the calibration factor. The maximum working pressure for this transducer is 7.0 Kg/cm^2.

Depending upon the application, the pressure range can be selected by changing the tip transducer.

It has been observed that for a high water pressure value, above 15 Kg/cm^2, leakage is likely to occur between the sleeve and the point load cell.

During the application of the water pressure, the point and sleeve loads have also been recorded. It has been indicated that approximately 70% of the total applied water pressure (U) was transferred to the point load cell. The friction sleeve load cell indicated a value equal to 30% of the total applied water pressure. This load distribution is consequence of the geometrical configuration of the penetrometer, see Fig. 5.12. The penetrometer base area is 10 cm^2 and the cross sectional area of the hollow cylindrical sleeve is 2.98 cm^2. Therefore, these figures indicate that approximately 30% of the total hydraulic pressure will be acting on the sleeve lower edge.

As discussed in Chapter II, during a penetration process, the induced excess pore pressure will be bigger around the conical tip than at the lower edge of the sleeve. Therefore, the extra load resulting from the excess pore pressure will not be distributed in the same manner as in the case of an applied all-round calibration pressure, i.e., 70% to the point and 30% to the sleeve. The distribution of the extra load will depend upon the values of the excess pore pressure surrounding the conical tip and at the sleeve lower edge. Hence, results proceeding from a penetrometer with the specified geometrical configuration can present serious interpretation problems. Such problems will be more pronounced in deposits indicating relatively high excess pore pressure values compared with the point and sleeve resistances. This fact can impose a limitation in the use of this penetrometer in such deposits.

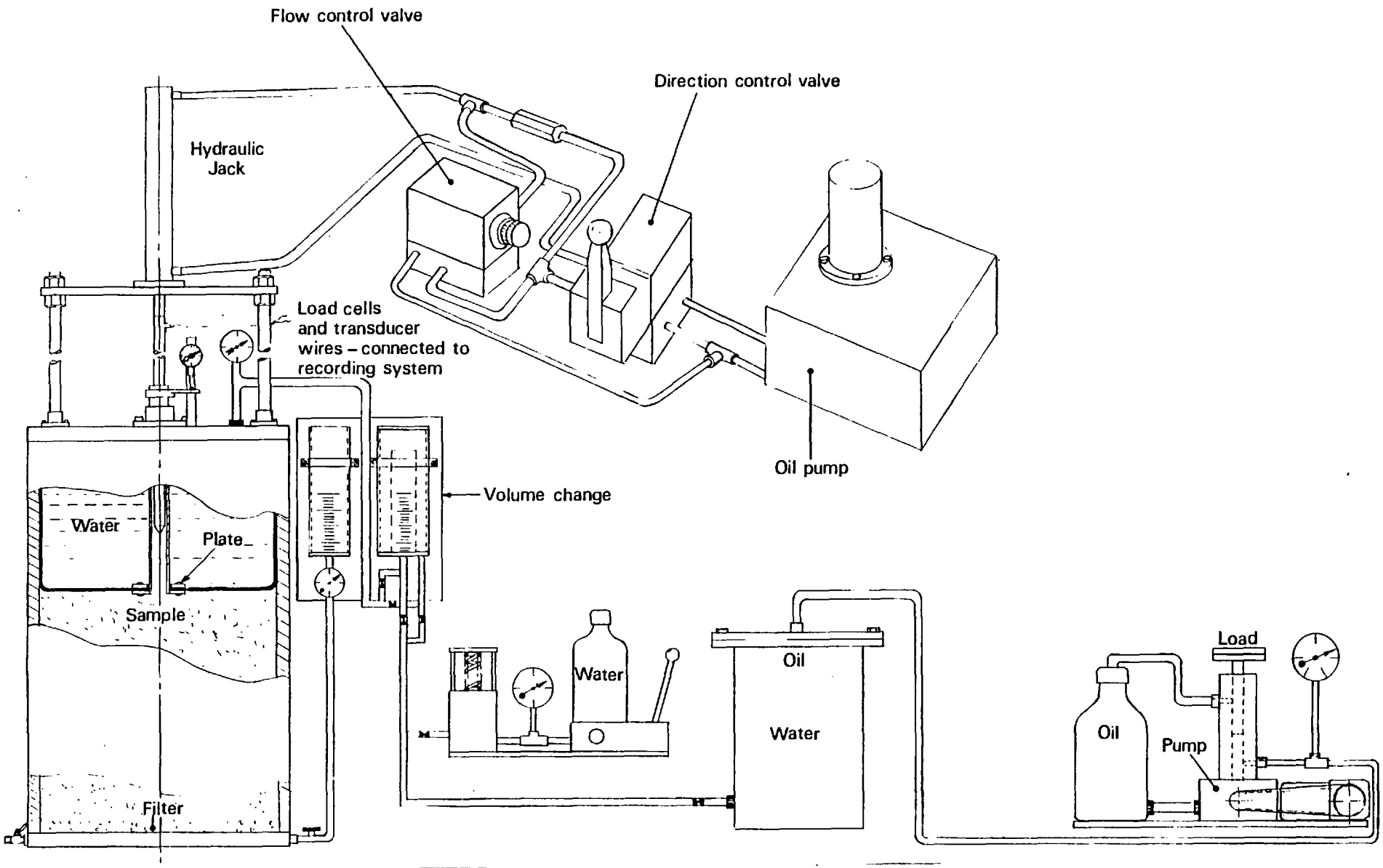
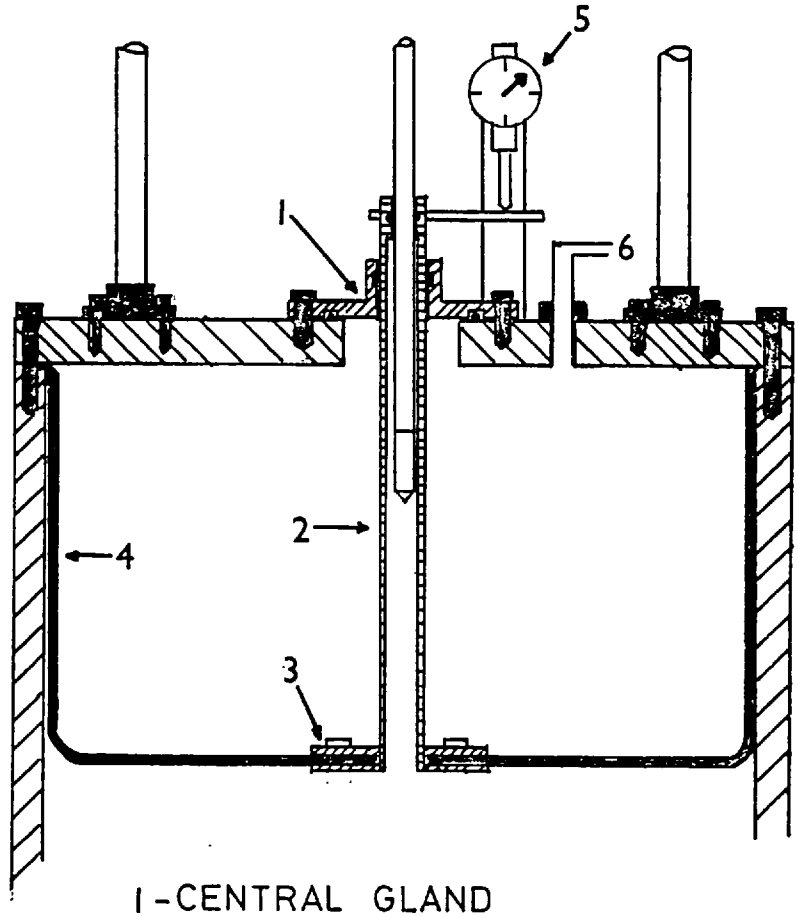
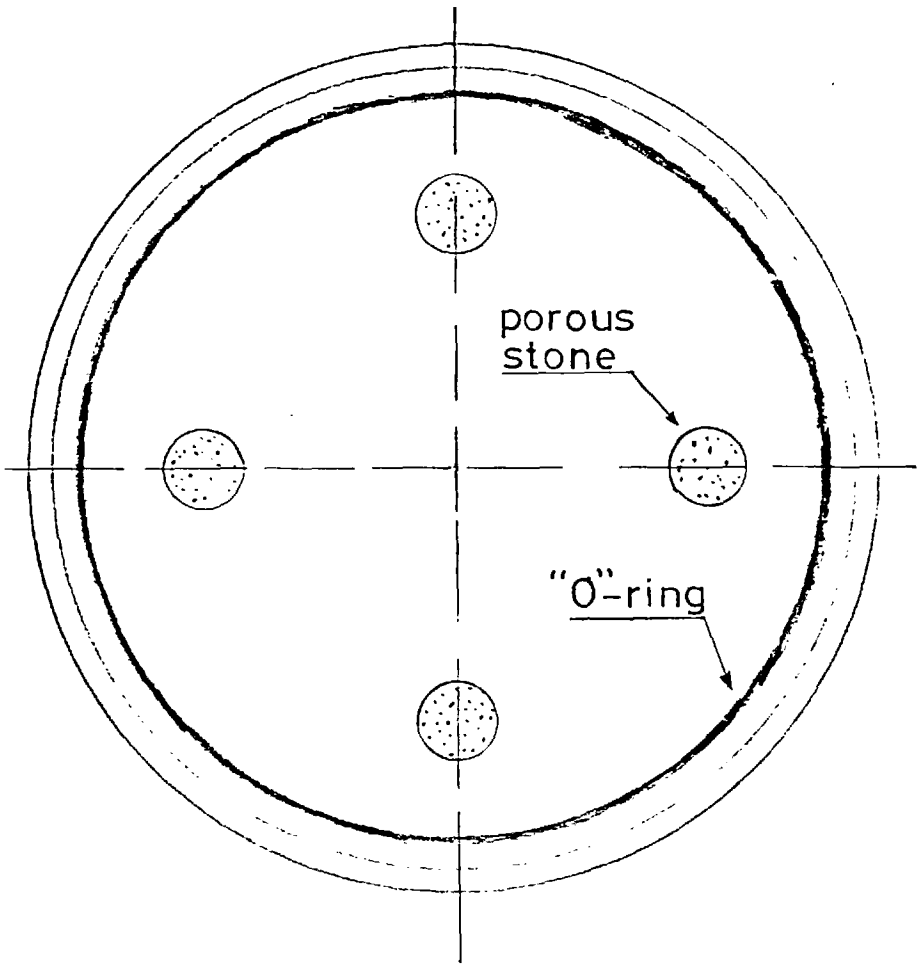


FIGURE 5.1 - LAYOUT OF THE APPARATUS.



1-CENTRAL GLAND
2-RIGID TUBE
3- " RING
PLATE TEST DEVICE
4-RUBBER MEMBRANE
5-DIAL GAUGE
6-PRESSURE CONNEXION

FIGURE 5.2 - DETAILS OF THE TOP PLATE.



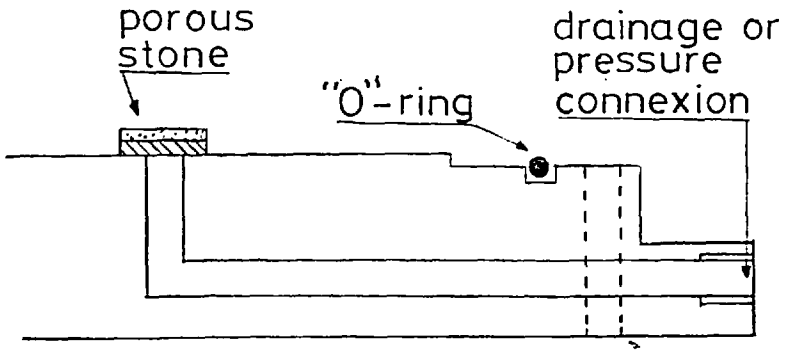


FIGURE 5.3 - DETAILS OF THE BOTTOM PLATE.

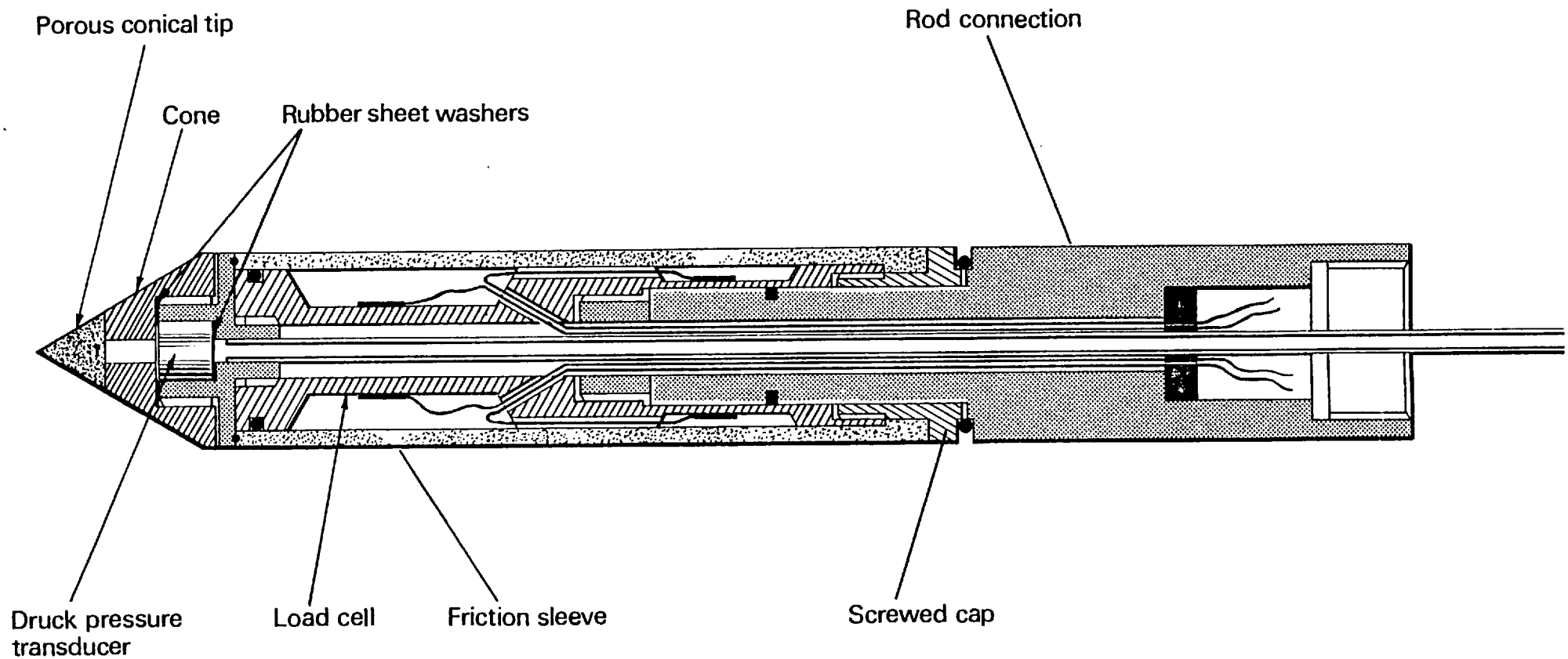


FIGURE 5.4 - ELECTRICAL PENETROMETER WITH PORE PRESSURE DEVICE.

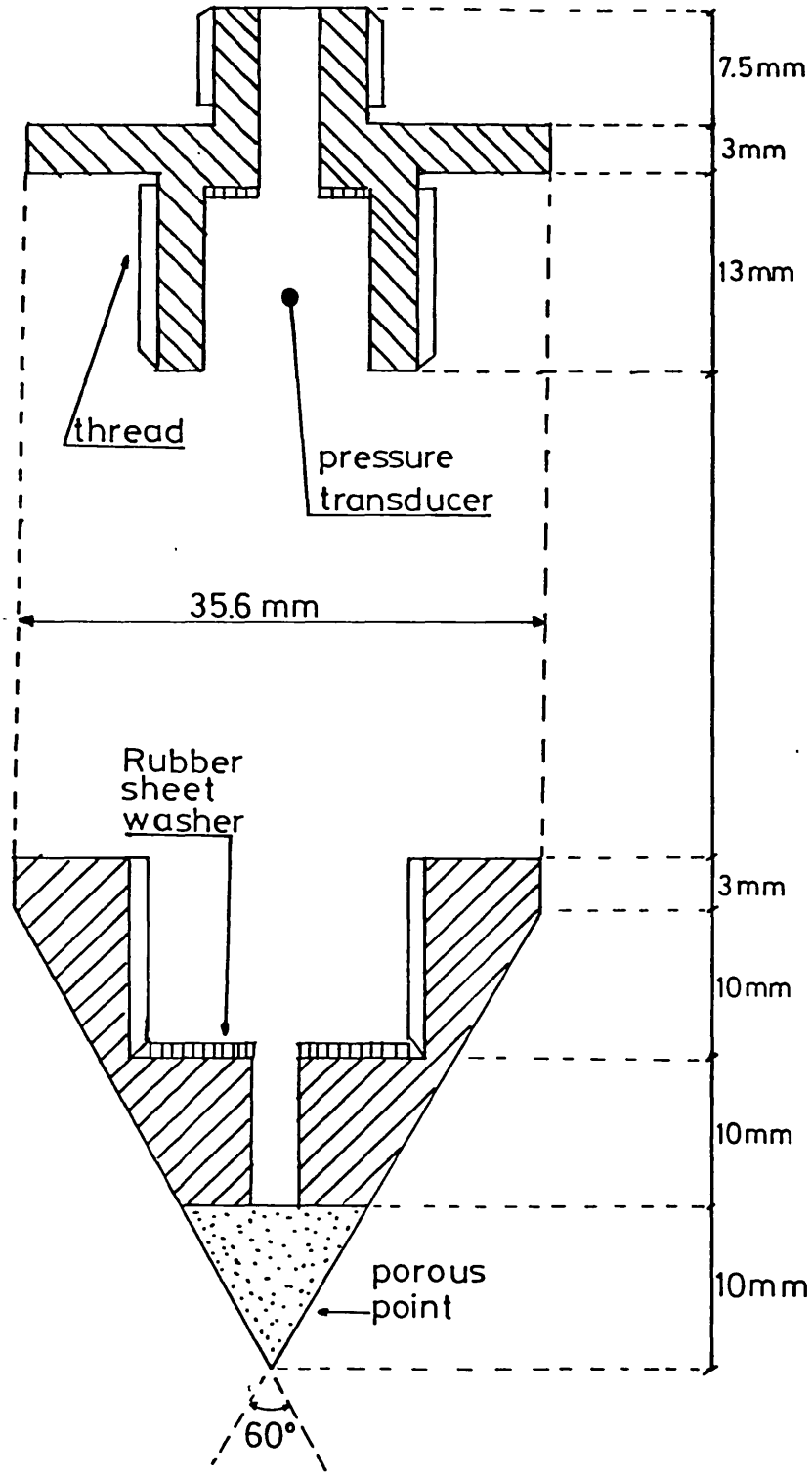


FIGURE 5.5 - DETAILS OF THE POROUS TIP.

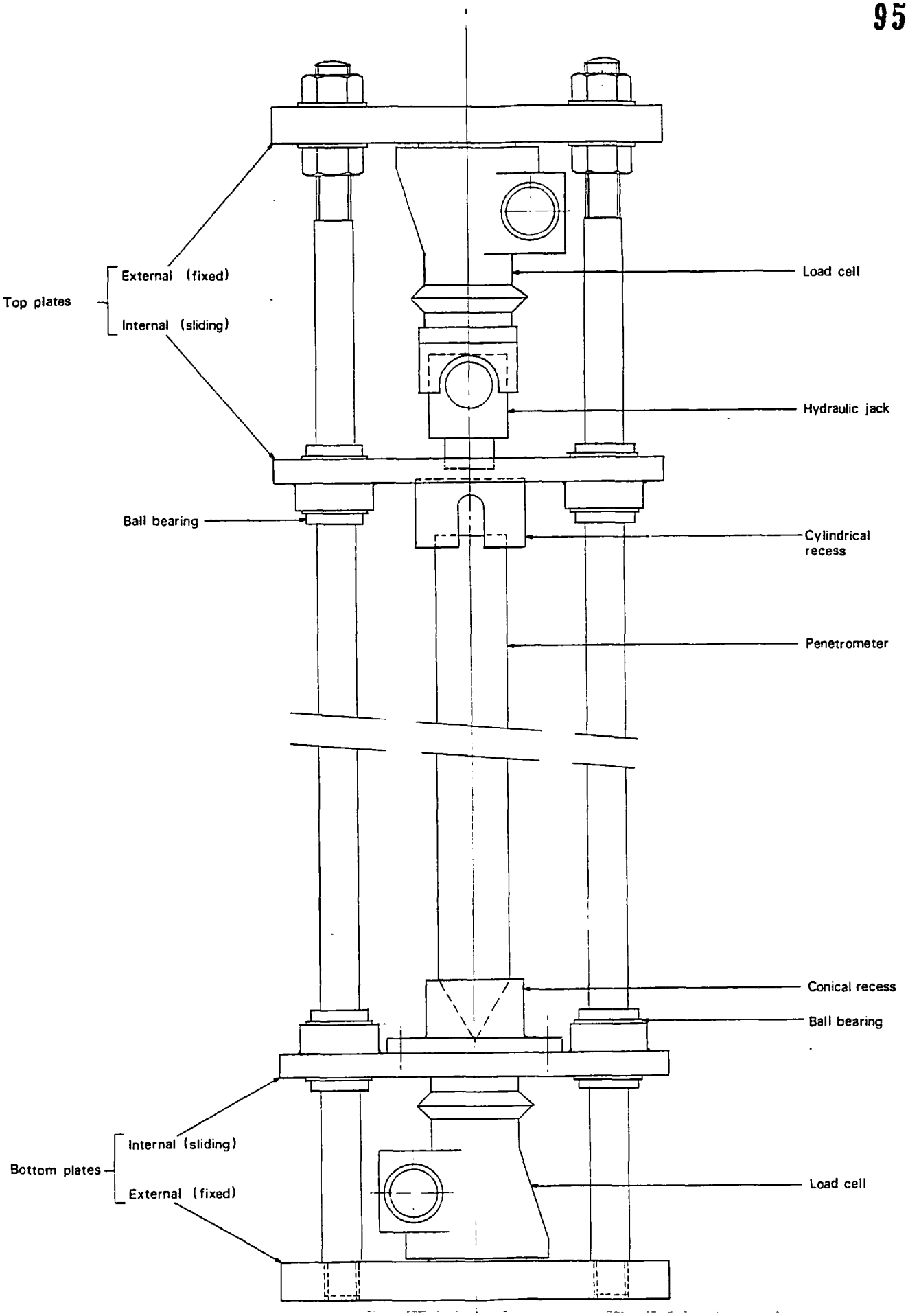


FIGURE 5.6 - CALIBRATION RIG.

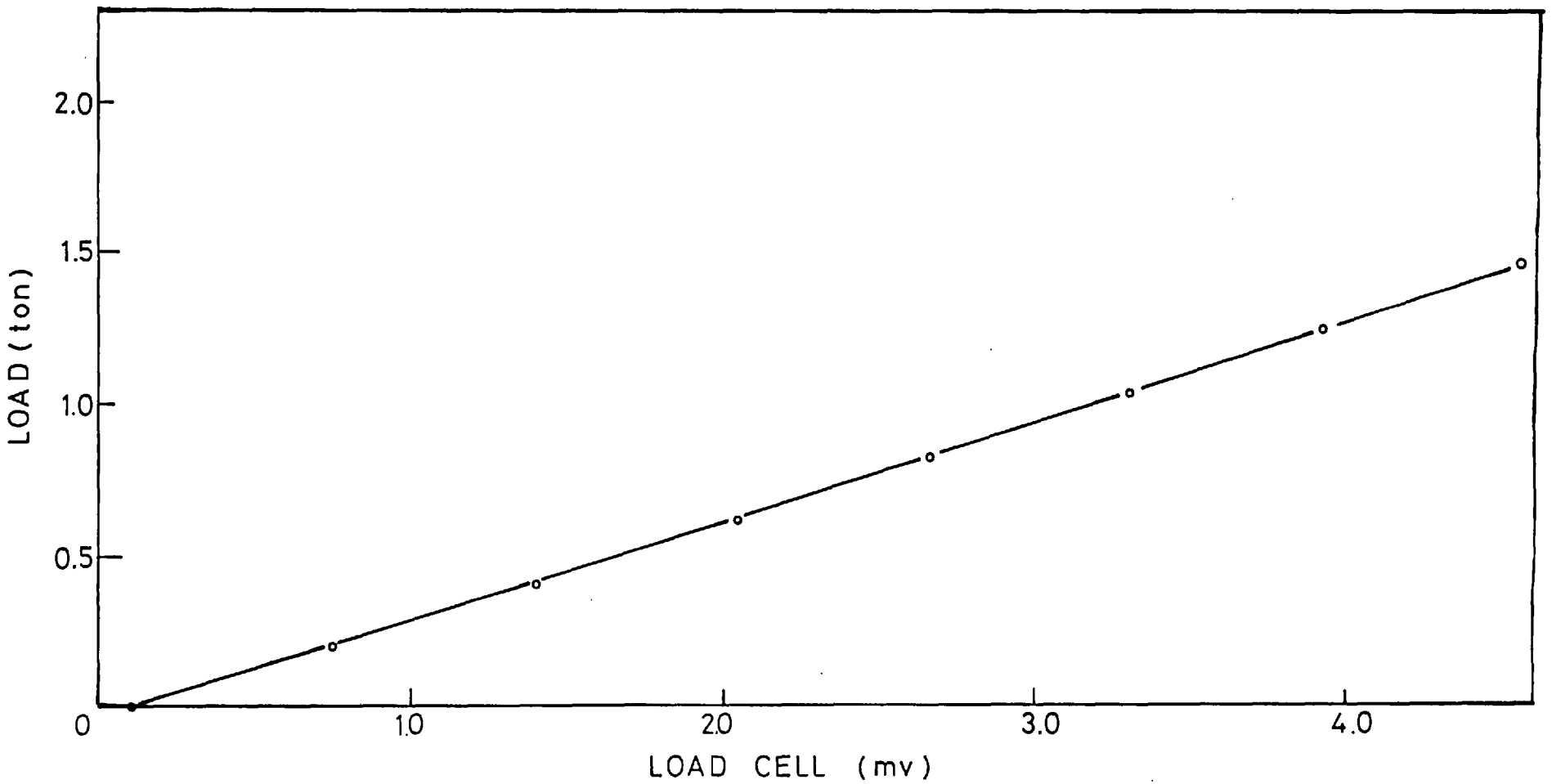


FIGURE 5.7 - CALIBRATION CURVE OF THE RIG LOAD CELL.

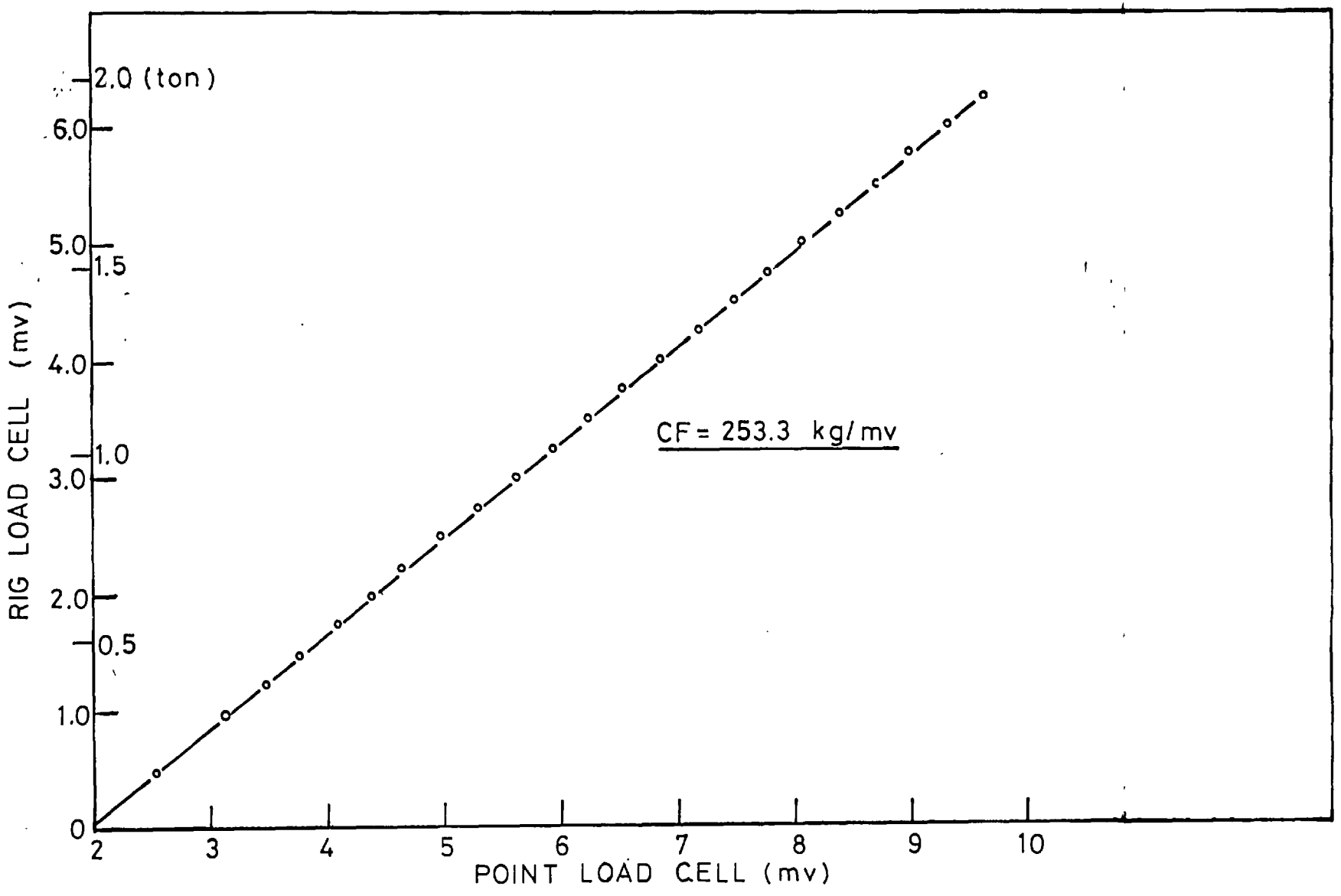


FIGURE 5.8 - POINT LOAD CELL CALIBRATION CURVE.

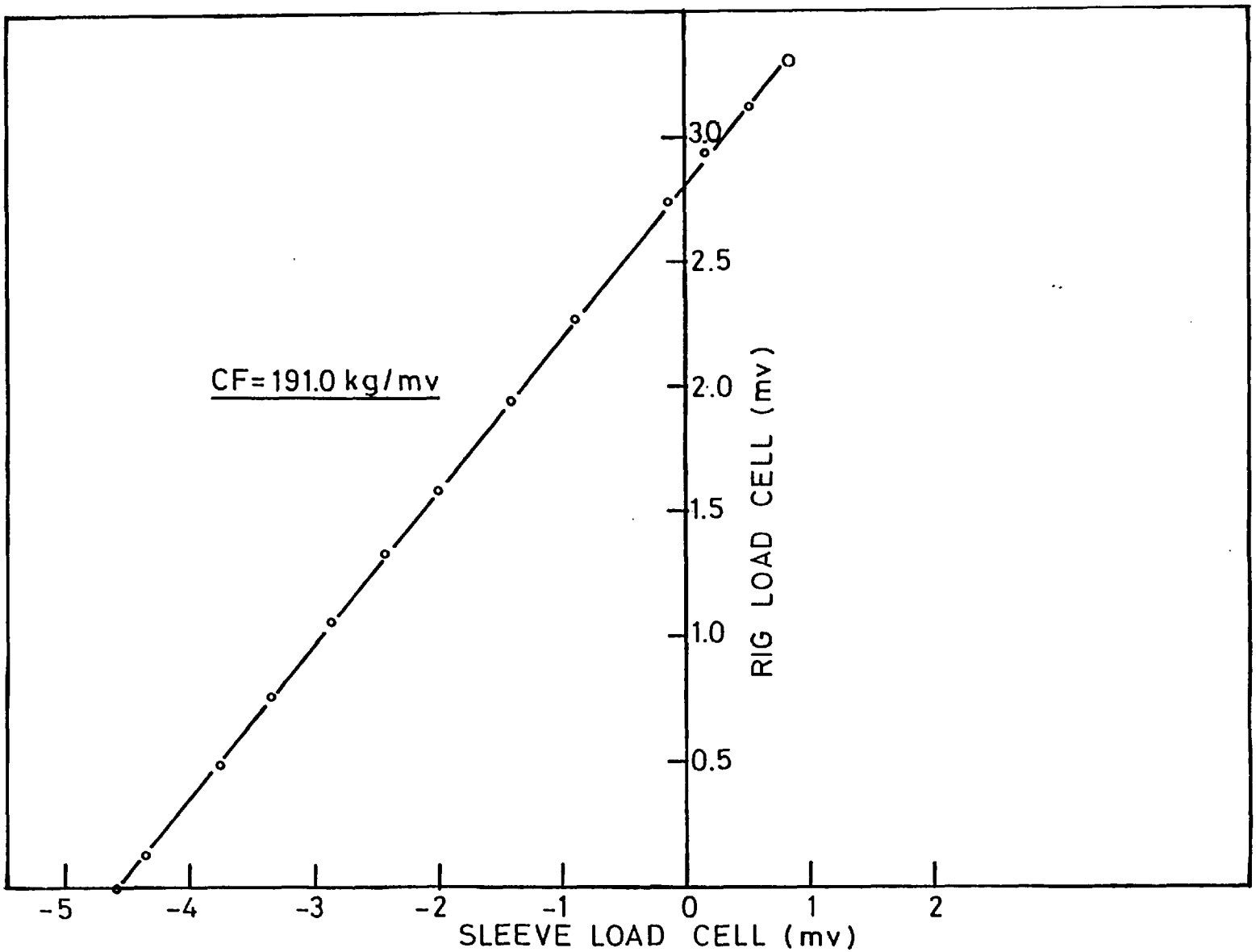


FIGURE 5.9 - SLEEVE LOAD CELL CALIBRATION CURVE.

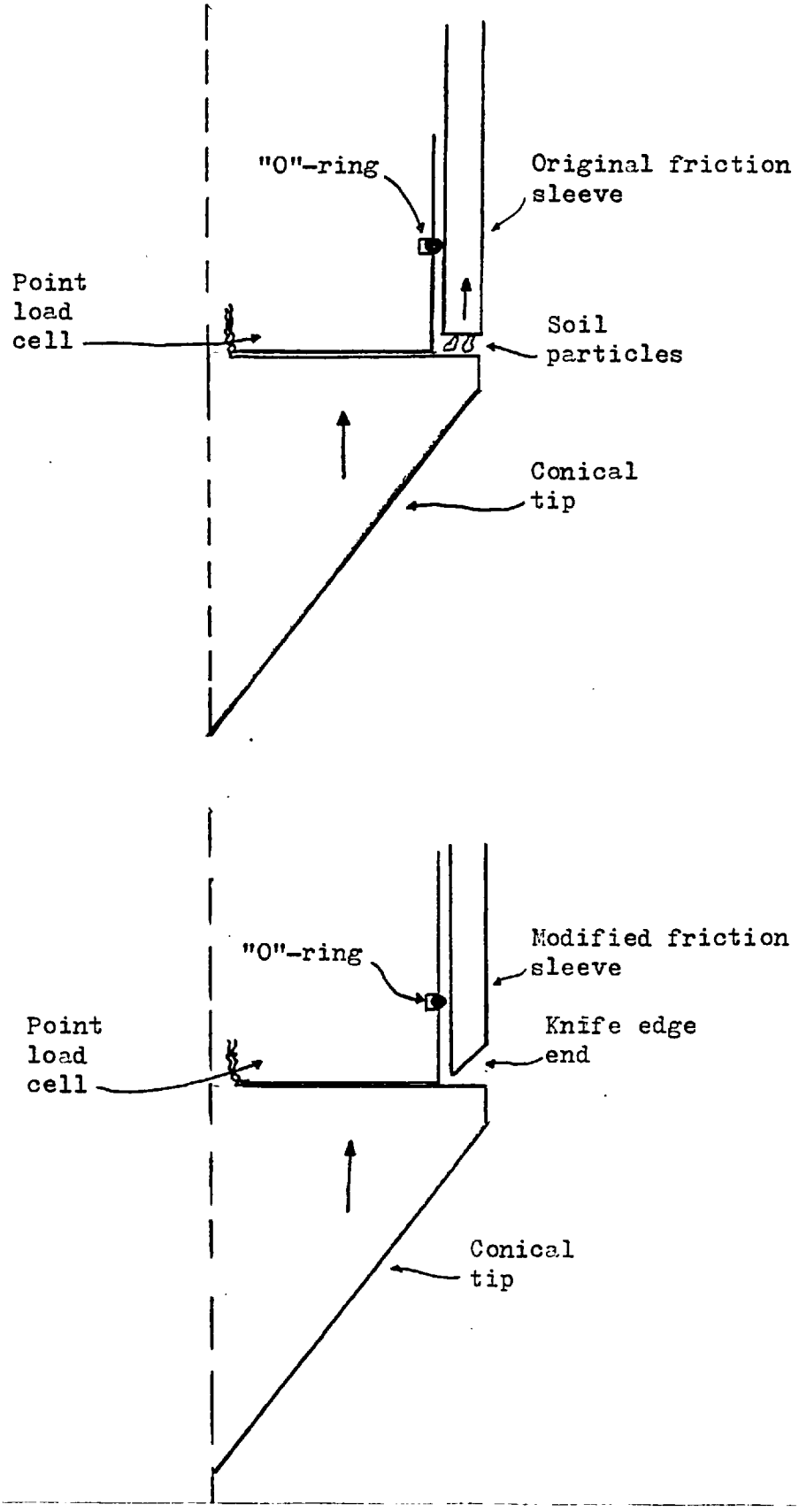


FIGURE 5.10 - PARTIAL LOAD TRANSFER.

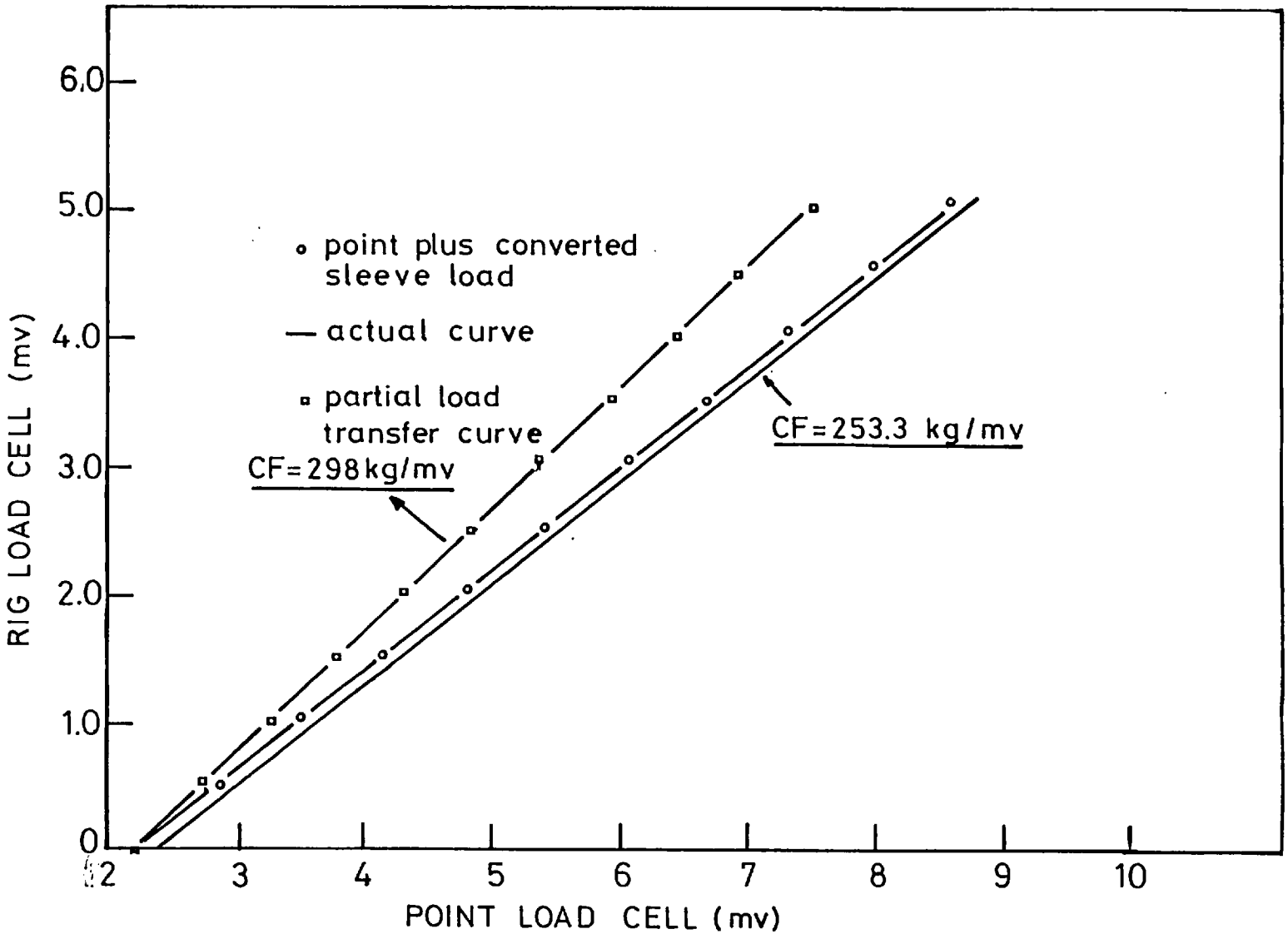


FIGURE 5.11 - CALIBRATION OF POINT LOAD CELL WITH PARTIAL LOAD TRANSFER.

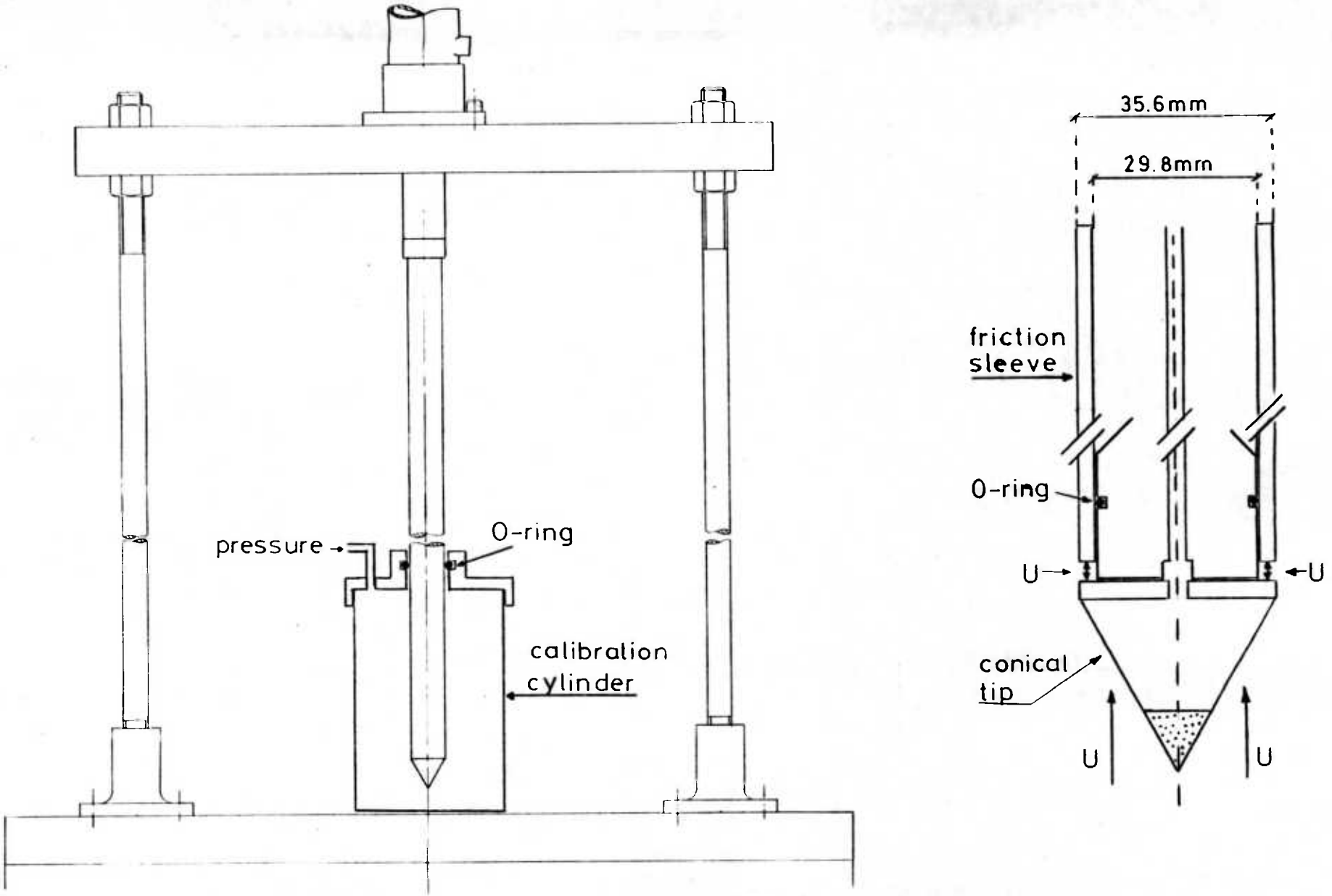


FIGURE 5.12 - CALIBRATION OF TIP PRESSURE TRANSDUCER.

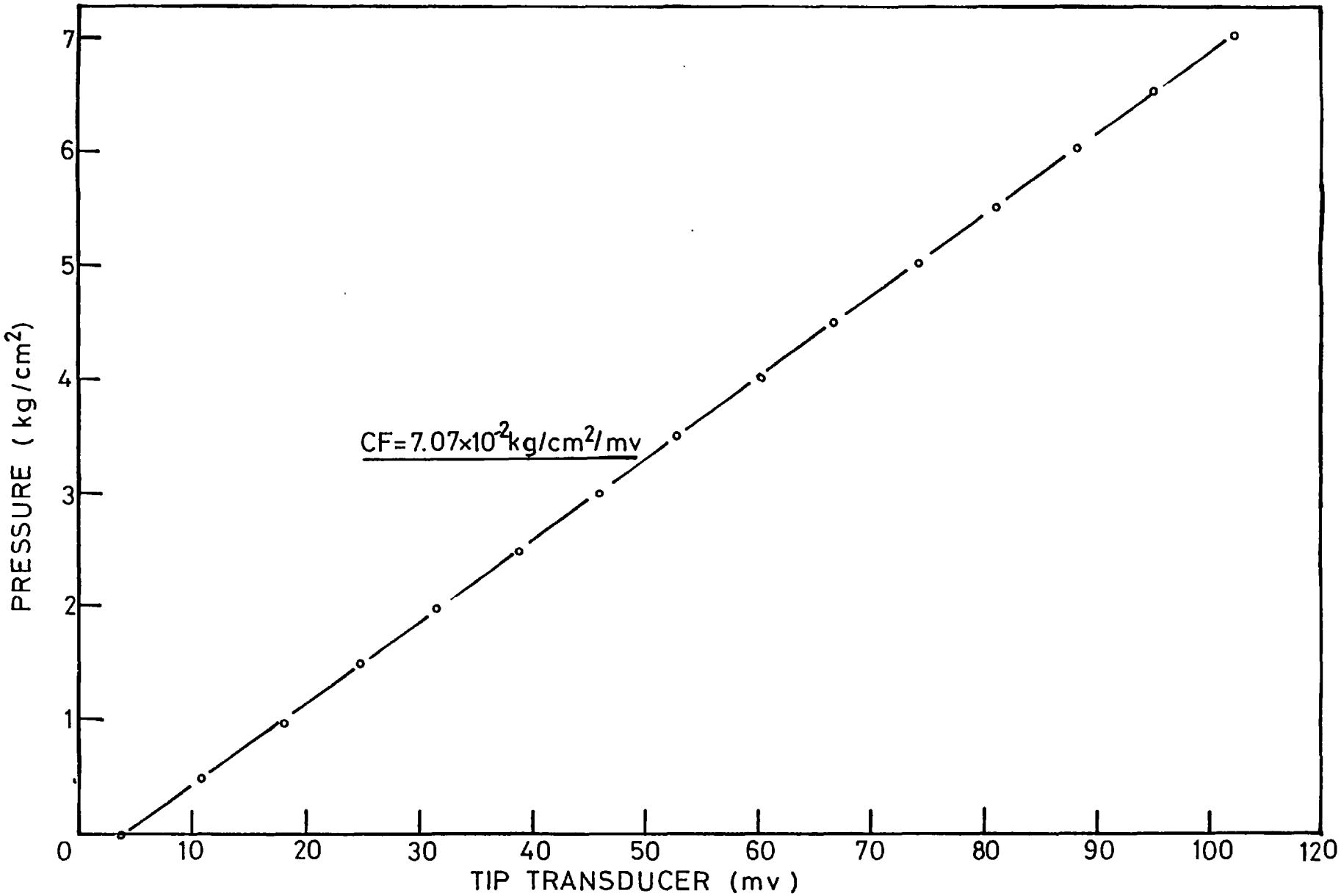


FIGURE 5.13 - PRESSURE TRANSDUCER CALIBRATION CURVE.

CHAPTER 6

DESCRIPTION OF THE SAND

6.1 GRADING CURVE

The sand used in the cone penetration test series was processed to the specified grading by the Structures Laboratory at the Building Research Station.

One of the basic requirements in specifying the grading curve was that the sand to be tested should have a particle size distribution similar to the curves obtained from the sand samples taken at shallow depths in the North Sea. Other requirements were concerned with dilatancy and permeability.

Bjerrum (1973) shows grain-size distribution of four sand samples obtained at shallow depths at various locations in the North Sea, see Fig. 6.1. The different locations corresponding to each sand is indicated in Fig. 6.2.

It can be observed that, excepting the Brent site, the grading curves are very similar and indicate a uniform to fine sand with little or no fines. The Brent site indicated a silty sand.

Concerning with dilatancy, the sand to be tested should indicate a structure favouring the development of negative pore water pressure or positive dilatancy when subjected to displacement. Results reported by Eggestad (1974) suggests that the dilatancy characteristics are independent of particle size distribution. He measured the surface heave caused by a rod being vertically driven in a compacted sand sample. Fig. 6.3 indicates the principle of the method and gives details of the apparatus used to measure the surface heave volume. Fig. 6.4 shows the grading curves and the corresponding classification index values of the four sands used in the testing programme. Fig. 6.5 presents values of heave ratio, defined as the ratio between the volumes of surface heave and of penetrated rod, plotted against relative density corresponding to 0.12 m rod penetration. He concluded that there

exists a clear relationship between the heave ratio and compactness and that this relationship was almost independent of grain size distribution and of the water content, as long as the sand was moist.

Finally, the permeability of the sand to be tested should indicate a value which would impose rate effects during a normal 2 cm/sec penetration rate and such effect could be quantified by varying the test speed within practical limits. A clean uniform sand, such as presented in Fig. 6.1, would indicate a coefficient of permeability around 10^{-2} cm/sec. Hence, in such deposits, a 2 cm/sec penetration test would either occur under drained conditions or the induced excess pore pressure quickly dissipate. In the second case, significant values of induced excess pore pressure would be difficult to monitor.

Fig. 6.6 indicates the grading curve of the sand used in the cone test series. The particle size distribution corresponding to the sands presented in Fig. 6.1 is also indicated. Table 6.2 presents values of the main classification index for these sands.

TABLE 6.2

SAND	D_{60} (mm)	D_{10} (mm)	D_{60}/D_{10} (mm)	CLASSIFICATION
USED SAND	190	38	5.1	- Well graded medium to fine silty sand
FRIGG	212	120	2.3	- Medium to fine uniform clean sand
EKOFISK	125	55	2.8	- Medium to fine uniform sand with little fine
BRENT	110	39	2.8	- Poorly graded silty sand
FORTIES	84	47	1.8	- Medium to fine uniform sand with little fine

6.2 SPECIFIC GRAVITY

The specific gravity of the soil particles has been determined using the two methods described in the B.S. 1377:1975, method 6(A) for fine-, medium-

and coarse-grained soils and method 6(B) for fined-grained soils. Method 6(A) utilises a 1 litre gas jar and the determination is made on a sample of oven-dry soil weighing 200 g - 400 g approximately. The gas jar with soil-water suspension is mechanically shaken to remove the air. Method 6(B) utilises a 50 ml density bottle and 10 g weight of an oven-dry soil sample. The air is removed by placing the density bottle under vaccum.

TABLE 6.3

METHOD	6(A)	6(B)
Specific Gravity (1)	2.955	2.918
Specific Gravity (2)	2.956	2.932
Specific Gravity (3)	2.951	-
Average	2.954	2.925

Krawczyk (1969) presents an examination of alternative methods of measuring the specific gravity of soil particles. He concluded that method 6(B) can indicate too low values owing to difficulties associated with a complete removal of air.

According to Sherwood (1970) the values indicated by Method 6(A) in table 6.3 present a very good repeatability. Hence, the specific gravity of the soil particles has been assumed as 2.954.

6.3 MAXIMUM AND MINIMUM VOIDS RATIOS

The maximum voids ratio (loosest condition) has been determined by pouring the sand through air inside a 152 mm diameter x 127 mm height and weighing the volume required to fill the mould.

The minimum voids ratio (densest condition) has been determined by vibrating with an electric hammer the top of a three layer dry sample inside a

steel compaction mould. The hammer has a circular foot of 145 mm diameter and vibration is applied for a period of 60 sec, during which the hammer is subjected to a firm downward pressure.

The methods used for determining the maximum and minimum voids ratios have been described by Kolbuszewski (1948).

Table 6.4 indicates values measured during two determinations.

TABLE 6.4

	MAXIMUM VOIDS RATIO	MINIMUM UNIT WEIGHT	MINIMUM VOIDS RATIO	MAXIMUM UNIT WEIGHT
(1)	1.095	1.410 g/cm^3	0.411	2.093 g/cm^3
(2)	1.085	1.415 g/cm^3	0.409	2.096 g/cm^3
Average	1.090	1.413 g/cm^3	0.410	2.095 g/cm^3

6.4 TRIAXIAL TEST RESULTS

Results of triaxial consolidated undrained tests on normally consolidated specimens have been carried out. Samples of approximately 7.5 cm (3 in.) diameter have been carefully prepared in order to avoid segregation of fine particles. The main steps involved in the sample preparation are similar to the process described by Bishop and Henkel (1972) for saturated cohesionless samples. Thus, sufficient sand to form the sample is weighed out and saturated by mixing in a container with enough water to cover the sand. The mixture is then boiled with a constant stirring to remove trapped air. The sample is built up by placing the saturated sand with a spoon in the former clamped to the base of the triaxial cell. The former consists of a split mould which encloses the rubber membrane and the lower sealing rings. After removing the split mould and measuring the sample dimensions the test is carried out in a normal procedure.

It has been found that a large amount of fine particles segregation has occurred by depositing the saturated sand under water using the funnel and stopper technique.

The rate of test used throughout the test series was 1.3×10^{-2} mm/sec.

Fig. 6.7 shows typical stress-strain curves for the undrained triaxial tests with pore pressure measurements. The corresponding effective stress paths are indicated in Fig. 6.8. Details of the presented tests and main characteristics of the samples are indicated on Table 6.5.

Table 6.6 indicates values of the main parameters obtained from these tests.

TABLE 6.5

TEST	1	2	3	4
e_i	0.87	0.85	0.85	0.78
D_{Ri}%	32	35	35	46
Cons. Pressure (Kg/cm^2)	1.4	4.2	5.6	7.0
e_f	0.84	0.73	0.71	0.65
D_{Rf}%	37	53	56	65
Cell Pressure (Kg/cm^2)	1.4	4.2	5.6	7.0

TABLE 6.6

TEST	1	2	3	4
$E_s(\frac{1}{2})$ (Kg/cm^2)	80.0	100.0	115.0	160.0
$E_s(\frac{1}{3})$ (Kg/cm^2)	95.0	155.0	160.0	270.0
E_t (Kg/cm^2)	160.0	220.0	220.0	350.0
ϕ'	44°	43°	43°	43°
A_f	-	0.3	0.46	0.34

Bjerrum (1973) has reported that typical undrained value of the friction angle observed in triaxial tests on the fine sand from the North Sea is 34^{o}; compared with a value of 43^{o} observed in drained triaxial tests.

The symbols presented on tables 6.5 and 6.6 are:

e_i is the void ratio value before the consolidation

e_f is the void ratio value after the consolidation

D_{Ri} and D_{Rf} are the corresponding relative density values defined as:

$$D_R = \frac{e_{(max)} - e}{e_{(max)} - e_{(min)}} \times 100\%$$

E_s ($\frac{1}{2}$) is the secant deformation modulus corresponding to $(\sigma_1 - \sigma_3)_{max}/2$, from Fig. 6.6

E_s ($\frac{1}{3}$) is the secant deformation modulus corresponding to $(\sigma_1 - \sigma_3)_{max}/3$, from Fig. 6.6

E_t is the tangent deformation modulus corresponding to the initial linear portion of the stress-strain curve, from Fig. 6.6.

ϕ' is the value of the effective friction angle, from Fig. 6.7

A_f is the Skempton's pore pressure parameter corresponding to $(\sigma_1 - \sigma_3)_{max}$, from Fig. 6.6.

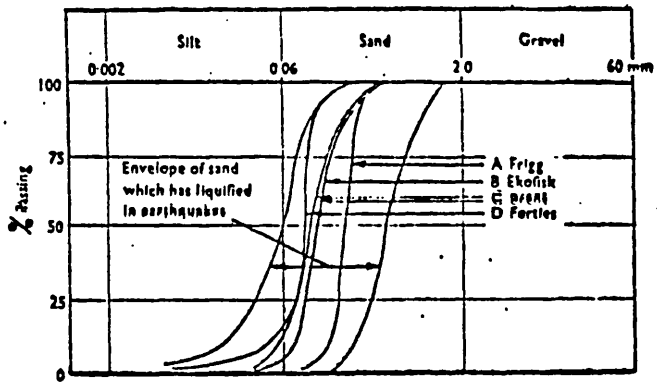


FIGURE 6.1 - GRAIN-SIZE DISTRIBUTION OF SAND SAMPLES OBTAINED AT SHALLOW DEPTHS AT DIFFERENT SITES IN NORTH SEA (AFTER BJERRUM 1973)

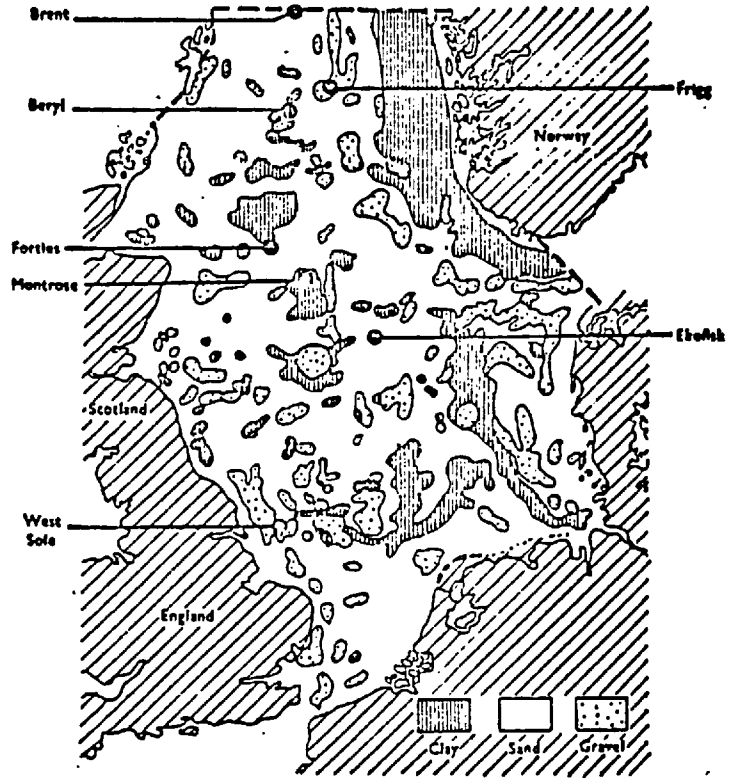


FIGURE 6.2 - MAP OF NORTH SEA WITH DISTRIBUTION OF BOTTOM SEDIMENTS (AFTER BJERRUM, 1973).

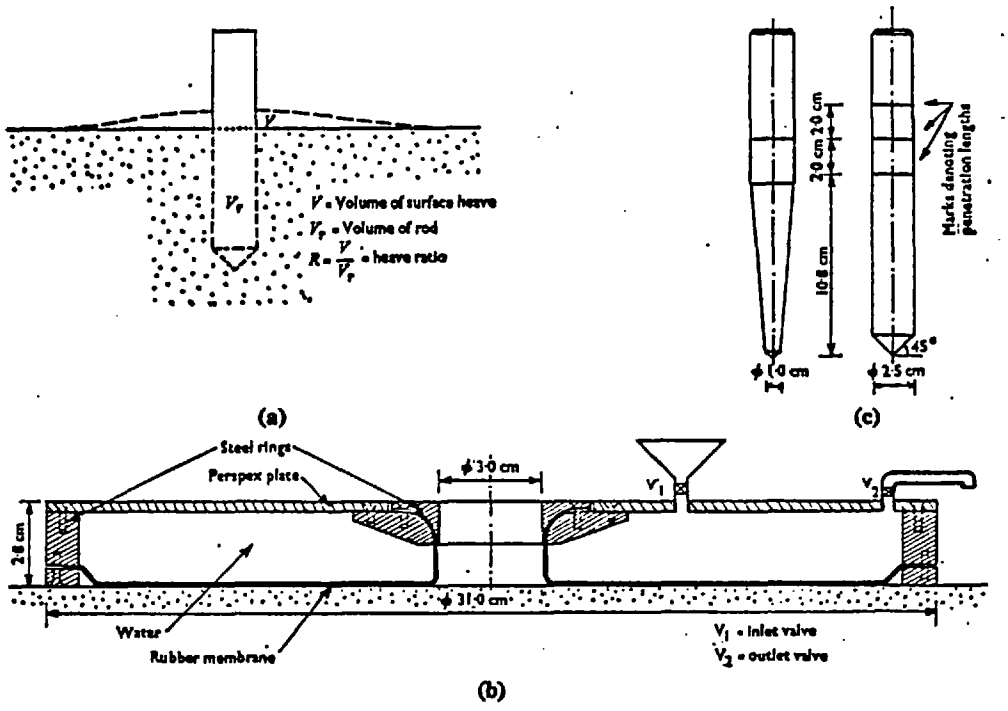


FIGURE 6.3 - (a) PRINCIPLE OF METHOD; (b) DIAGRAM SHOWING A CROSS SECTION THROUGH THE APPARATUS; (c) PENETRATING RODS. (FROM EGGESTAD, 1974).

Sand	D_{60}	D_{60}/D_{10}	γ_{dmax}	γ_{dmin}	100% Proctor Standard
A	0·80	1·9	1·78	1·40	1·71
B	0·15	2·2	1·70	1·33	1·62
C	0·35	3·0	1·94	1·47	1·81
D	1·30	4·3	2·03	1·65	1·93

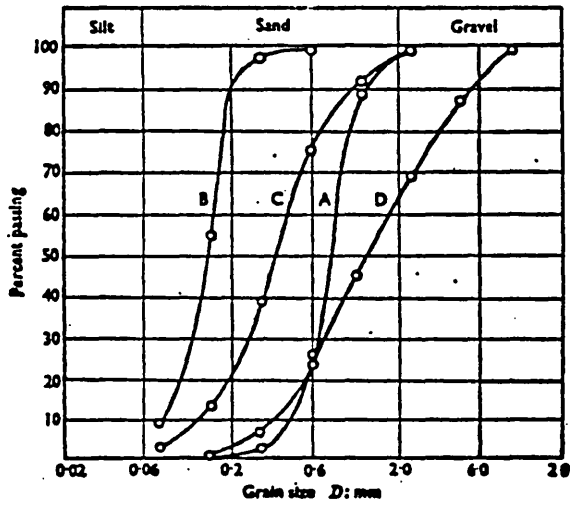


FIGURE 6.4 - GRAIN SIZE DISTRIBUTION FOR SANDS USED IN TESTING PROGRAMME (FROM EGGESTAD, 1974).

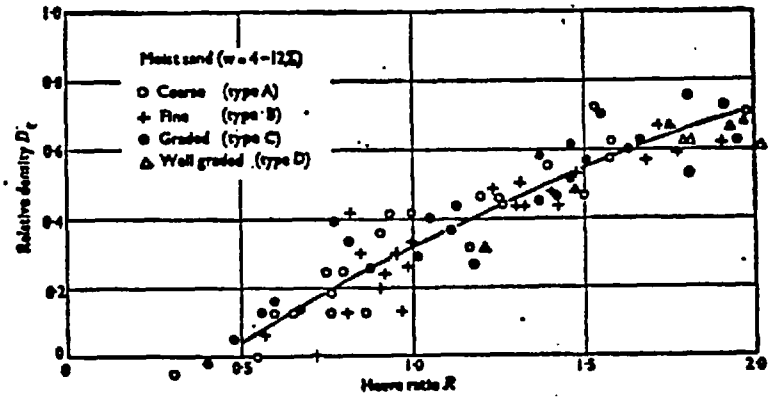


FIGURE 6.5 - HEAVE RATIO AGAINST RELATIVE DENSITY FOR ALL TESTS WITH MOIST SAND AND CYLINDRICAL ROD. (FROM EGGESTAD, 1974).

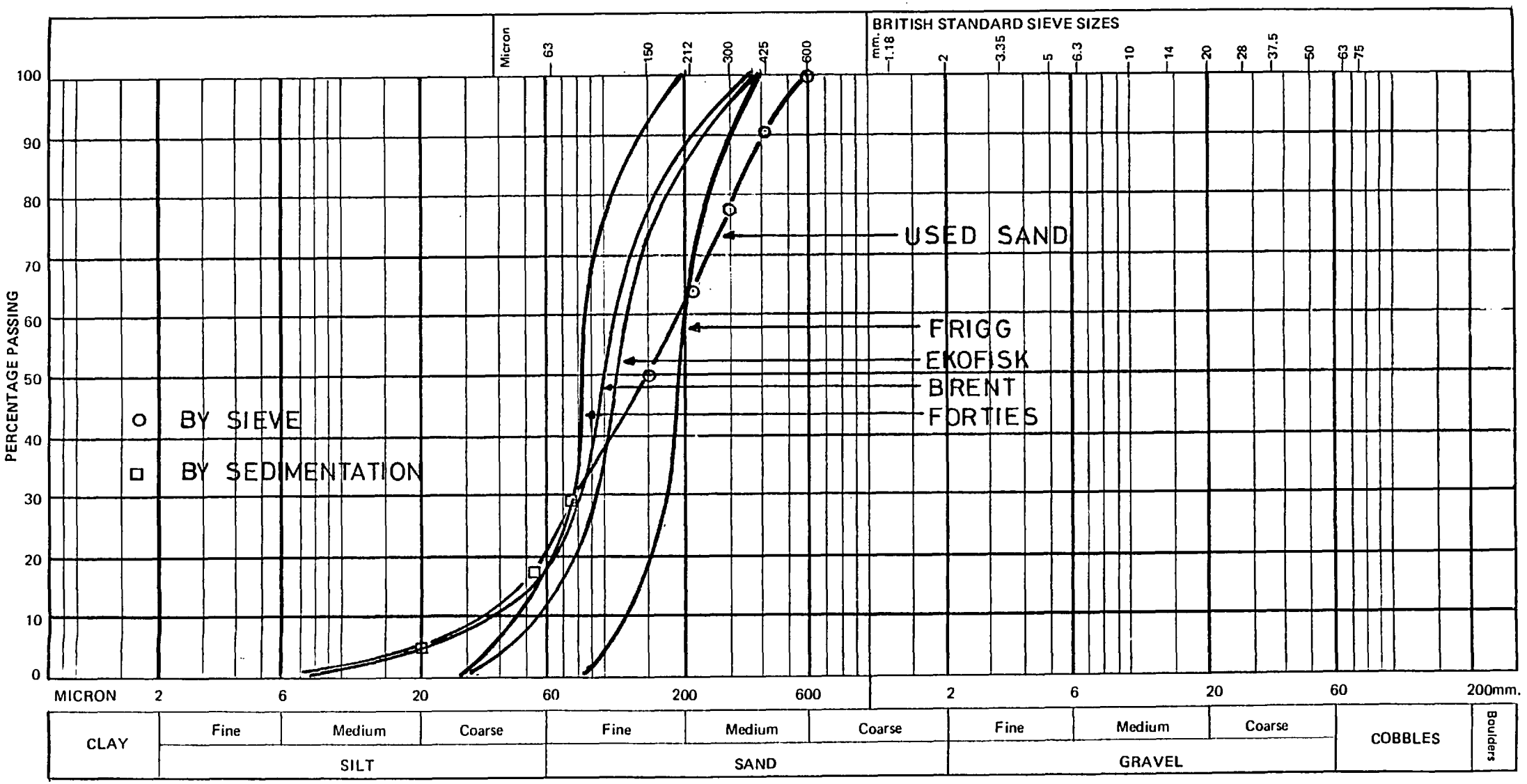


FIGURE 6.6 - GRADING CURVE.

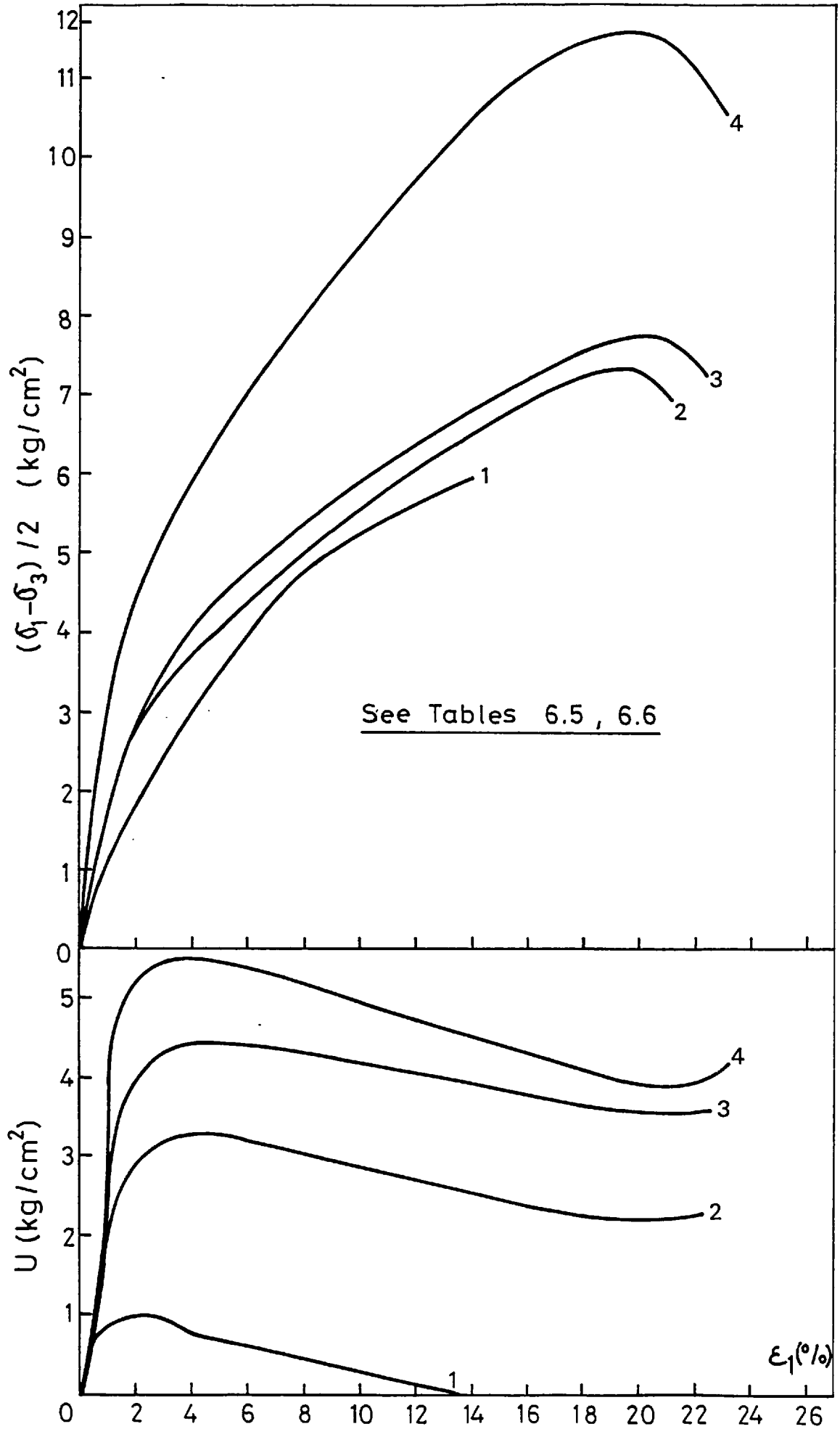


FIGURE 6.7 - STRESS - STRAIN CURVES.

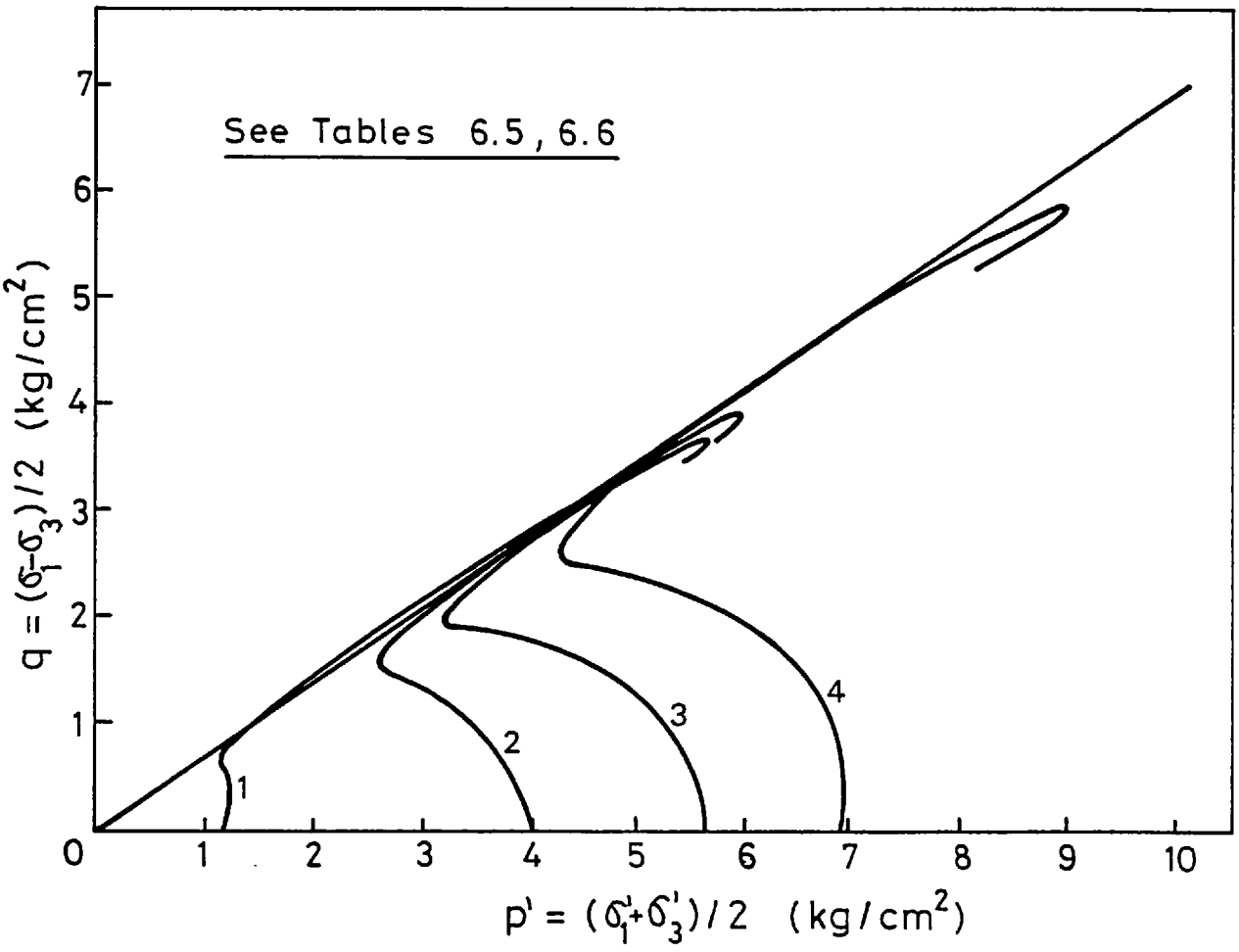


FIGURE 6.8 - EFFECTIVE STRESS PATH.

CHAPTER 7

SAMPLE PREPARATION AND TESTING PROCEDURE

7.1 PREPARATION OF THE SAMPLE

Owing to the big volume of sand required to set up the sample, usually 0.76 m diameter and 1.0 m height, the process involved in the preparation should provide a quick and efficient saturation.

The process of saturating a small volume by boiling the sand-water mixture and then depositing the saturated sand in the testing cylinder, has been found laborious and time consuming.

The adopted process consists of depositing dry sand inside the testing cylinder and subsequent flooding. It has been found that this procedure enables a sample to be quickly set up. However, it is extremely difficult to ensure a complete saturation of the sample.

Before filling the testing cylinder with dry sand, a filter of approximately 0.1 m thickness, grading from coarse sand to fine gravel, is formed at the bottom, see Fig. 5.1. The sand is then deposited in small portions using a metal bin provided with a "drop bottom". The metal bin is filled with dry sand and placed inside the testing chamber. The "drop bottom" is disconnected and the sand allowed to fall out. The procedure is repeated until a sample of approximately 1.0 m height is formed, see Fig. 7.1. During each stage the sand should be placed with the same height of fall to ensure a uniform density throughout the sample.

To saturate the sample, the top plate with the sealed central gland is fixed on top of the chamber and vacuum is applied inside the chamber through the connexion at the top plate. After ensuring that the maximum vacuum have been achieved at the top and bottom of the sample, the bottom water supply is then opened. Thus, the filter is quickly flooded and a uniform slow upwards flow follows. Complete saturation can be indicated by the presence of water on the transparent vacuum connexion. After the saturation is completed the vacuum supply is disconnected, the top plate removed and the water inside the

chamber lowered to a minimum above the top of the sample. It has been found that this process gives a neglected amount of fine particles segregation.

For the presented series of tests, the procedure described above has only been used for the two initial tests. The volume of dry sand available was sufficient to form two samples. Hence, the sample already tested should be dried out and made available for the next sample preparation. The time and operation involved in drying out the tested sample has been found not convenient for the testing programme. Therefore, for the remaining tests of the presented series, this procedure has been abandoned.

The new process which was adopted consists of digging out the sample already tested from the testing chamber and depositing the sand-water mixture in small metal bins. For this operation a scoop is used and care is taken to avoid air entering the saturated sand. After reaching some depth, the excavation process becomes difficult due to the limited space available. The remaining sample is disturbed using a spade while being subjected to an upwards flow of water. The sand-water mixture from the metal bins is then placed back in small portions into the testing chamber and mixed using a spade. During this operation the water level inside the testing chamber should be sufficient just to cover the saturated sand and to avoid segregation of fine particles during deposition. One of the drawbacks in using the described sample preparation process is associated with difficulties in obtaining a uniform density throughout the sample. It has been observed that there is a tendency to produce samples relatively dense at the bottom and relatively loose at the top.

7.2 TESTING PROCEDURE

7.2.1 GENERAL

After the sample is prepared, the normal testing procedure consists of the following major steps: sample consolidation and/or additional overconsolidation; plate load test; continuous cone penetration test; static

penetrometer load test; "aside" continuous cone penetration test, and finally the determination of the sample compactness.

It has been found that the plate load test can strongly affect the cone measurements. Therefore, for some tests the plate bearing test has been eliminated from the sequence, this fact is indicated in the presentation of the cone penetration test results.

Each of the major steps is described in more detail in the following sections.

7.2.2 CONSOLIDATION OF THE SAMPLE

To consolidate the sample, the rubber membrane cap, with the attached accessories, see Fig. 5.2, is placed on the top of the sample and filled with water. During the operation, trapped air between the membrane and the sample should be removed. The top plate without the central gland, leaving free clearance for the central rigid tube, is fixed on the top of the testing cylinder. The pressure system is connected and using the manual hydraulic pump the water inside the membrane is then levelled to the top plate external surface. The central gland, with the two attached "O"-ring seals, is fixed on the top plate and a displacement gauge is attached at the top end of the rigid tube, see Fig. 5.2. The rigid tube is filled with water and a metal plug, reacting against the penetrometer push rods, forms the seal at the top end. The sample consolidation is carried out by increasing the water pressure inside the membrane, measuring the induced sample excess pore pressure, indicated in the bottom Bourdon gauge, and then opening the bottom drainage system. Generally, during the penetration process, the hydraulic pressure increments and the corresponding volumes of water entering the chamber and expelled from sample and the plate vertical displacement are recorded.

Comparing the deformation values indicated by the vertical movement of the reference plate and by the expelled volume of water, the top deflexion of the sample can be calculated.

The lateral part of the rubber membrane is formed with convolutions to avoid interference of the rubber strength on the consolidation process.

7.2.3 PLATE LOADING TEST

For the plate load test, a proving ring and a hydraulic jack connected to a manual pump are fixed on the top of the rigid tube. The loading frame, through the penetrometer push rods, provides the reaction support. A given load, the value of which is indicated by the proving ring, is applied and the corresponding plate settlement, indicated by the displacement gauge mounted on the rigid tube top end, is then measured, see Fig. 7.2a. For each load increment the corresponding plate settlement is measured as a function of time. The adopted plate settlement value is assumed as that indicated by a time corresponding to approximately 95% of the total plate vertical movement.

7.2.4 CONTINUOUS CONE PENETRATION TEST

For the continuous cone penetration test, the metal plug and the internal "O"-ring seal are removed from the rigid tube. The penetrometer, with the saturated porous tip, is fixed on the push rods and advanced through the rigid tube to the sample surface. The wires from the pressure transducer and load cells are connected to the recording system and the sensitivity of the chart recorders channels are selected.

The right selection of the equipment sensitivity is very difficult and can constitute the main source of problems during the penetration process. The range of the recording unit should not be relatively wide, giving a slow sensitivity characteristic, that for significant small variation on the measured values could be measured. On the other hand it should not be narrow ranging, giving a high sensitivity characteristic, as unpredictable high values could be bigger than the established system upper limit. This second problem has

occurred particularly during cone penetration tests carried out after plate load test. During plate load tests, compaction occurs and the influenced zone under the plate indicates relatively high penetration values compared to measurements obtained for further penetration.

The continuous cone penetration test is carried out at a constant speed of 2 cm/sec, during which the point end and friction sleeve resistances and the tip excess pore pressure are automatically recorded.

After the penetration process is stopped, the rate of the induced excess pore pressure dissipation with time is recorded.

7.2.5 STATIC PENETROMETER LOAD TEST

For the static penetrometer load test, the penetrometer and the extension rods are disconnected from the hydraulic jack driving piston. A proving ring and hydraulic jack connected to a manual pump are fixed on the top of the extension rod. The loading frame provides the reaction support. A given load, the value of which is indicated by the proving ring, is applied and the corresponding penetrometer-extension rods settlement, indicated by the displacement gauge mounted at the top of the extension rod, is then measured, see Fig. 7.2.b. Values of the point and sleeve resistances and the tip pore pressure corresponding to a given load increment are also automatically recorded. The load increment should be applied at a speed which indicates no excess pore water pressure. For a given load increment, these measurements are obtained as a function of time.

The interpretation of the penetrometer-extension rods settlements are similar to the analysis presented for the plate load tests, see section 7.2.2.

7.2.6 "ASIDE" CONTINUOUS CONE PENETRATION TEST

This corresponds to continuous penetration test carried out half way between the sample centre and the cylinder wall. Generally, four adjacent equi-spaced tests are carried out at different penetration rates ranging from

1.5 cm/sec (minimum) to 2.5 cm/sec (maximum). The purpose of these tests is to investigate qualitatively the rate effect on the cone measurements. For this speed range, little difference among the results have been found.

For this series of cone penetration tests, the rubber membrane is removed and the top plate dislocated, locating the driving system to the required position.

The test procedure is similar to the described for the continuous cone penetration test carried out at the sample centre, see section 7.2.4.

Saturation of the porous tip is repeated for each individual test.

7.2.7 DETERMINATION OF THE SAMPLE COMPACTNESS

For the determination of the sample compactness, open thin wall cylindrical samplers, with cutting edge, are pushed into the soil in a fast continuous movement. To reduce the friction, the internal sampler wall is lubricated. Each sample is cut free from the remaining soil by undercutting and inserting a spade under the sampler. The sample is oven-dried, weighed out and hence its dry unit weight deduced.

In order to better investigate the influence of sampler dimensions on the sample disturbance, four cylindrical samplers with different height-diameter ratio have been used. Table 7.1 indicates their dimensions.

TABLE 7.1

SAMPLER	HEIGHT (mm)	DIAMETER (mm)	H/D
1	92.78	101.58	0.91
2	50.84	120.74	0.42
3	100.28	53.54	1.87
4	152.61	74.58	2.05

These four cylinders have been driven at a common depth in a uniform prepared layer, the corresponding relative density determined and an average value calculated. It has been found that the four samples give an

approximately ± 12% band limits compared to the average value.

This process has been repeated for the same sand layer. This time the sampler has been pushed in an intermittent slow movement after a rough advance trimming of the soil in front of the cutting edge. This process indicated a band limit of ± 9%. Relative density values obtained by the same sampler during the two determinations have been compared. Sampler 1 indicated more consistent values.

Finally, a "block" sample, which dimensions are 56.28 x 43.53 x 49.88 mm, has been carefully obtained for the same layer and the corresponding relative density value deduced. This value has been compared to the values indicated by the four samplers. Sampler 1 indicates the closest value with a difference around + 4%.

It must be emphasized, that this observation has been carried out in a layer indicating a relative density of 70%, corresponding to the average values. Therefore, bigger difference in values than the indicated should be expected for loose materials.

As a result of this observation, sampler 1 with the intermittent push method has been adopted for determining the sample compactness. Generally, two determinations at a common depth are obtained and the average value assumed.

For the sampler 1, it has been found that errors on the relative density value could be involved due to:

1. determination of the representative sampler dimensions, corresponding to ± 2.5%.
2. determination of the sample weight, directly from the oven or a natural cool-down in a temperature controlled laboratory, corresponding to ± 5%.

Hence, the assumed relative density value, should be considered with an error of at least ± 5% involved.

7.3 SUMMARY AND INDEXING OF TESTS

Table 7.2 presents the summary and indexing of the series of tests which have been considered in the presented analysis. The main information provided in this table are related to:

a. Stress history

Normally consolidated and overconsolidated samples have been tested. $\sigma_{v'(max)}$ represents the consolidation pressure while $\sigma_{v'(test)}$ indicates the "overburden" pressure during the test. Both values correspond to the "oedometric" hydraulic pressure applied on the top of the sample. Hence, equality of $\sigma_{v'(max)}$ and $\sigma_{v'(test)}$ implies normal consolidation, see Test 1 for an example. An overconsolidated sample is indicated by different consolidation and "overburden" pressure values. Test 7, which values of $\sigma_{v'(max)}$ and $\sigma_{v'(test)}$ are 7.0 Kg/cm^2 and 1.4 Kg/cm^2 respectively, corresponds to an overconsolidated sample with an overconsolidation ratio equal to 5.

b. Sample compactness

The relative density values indicated in table 7.2 correspond to an average of two determinations. These values should be considered with an error of at least $\pm$ 5% involved, see section 7.2.7. Generally, for each sample the relative density has been obtained for different depths, corresponding to:

1. top = 0.0 m to 0.1 m
2. medium = 0.25 m to 0.35 m
3. bottom = 0.40 m to 0.50 m

TABLE 7.2

TEST	$\sigma_v'(max)$ Kg/cm^2	$\sigma_v'(test)$ Kg/cm^2	PLATE TEST	CONE TEST	STATIC TEST	"ASIDE" TEST	STRESS HISTORY	RELATIVE DENSITY* % TOP/MEDIUM/BOTTOM
1	1.4	1.4	PT 1	CPT 1	SPLT 1	ACPT 1A	NC	41 / 39.5 / 35
2	2.8	2.8	PT 2	CPT 2	SPLT 2	ACPT 2A	NC	46 / 45 / 50
3	"O"	"O"	PT 3	CPT 3	SPLT 3	ACPT 3A	NC	25 / 27 / -
4	1.4	"O"	PT 4	CPT 4	SPLT 4	ACPT 4A	OC	42.5 / 36 / -
5	1.4	"O"	-	CPT 5	-	-	OC	43 / - / -
6	1.4	1.4	-	CPT 6	-	ACPT 6A	NC	43.5 / 40 / 46
7	2.8	2.8	-	CPT 7	-	ACPT 7A	NC	38 / 33.5 / 55
8	7.0	1,4	PT 5	-	-	-	OC	57.5 / 61 / -
9	7.0	1.4	-	CPT 8	SPLT 5	ACPT 8A	OC	60 / 56 / 78

* $\pm$ 5% error involved. Top = 0.0 m to 0.1 m/Medium = 0.25 m to 0.35 m/Bottom = 0.4 m to 0.5m.

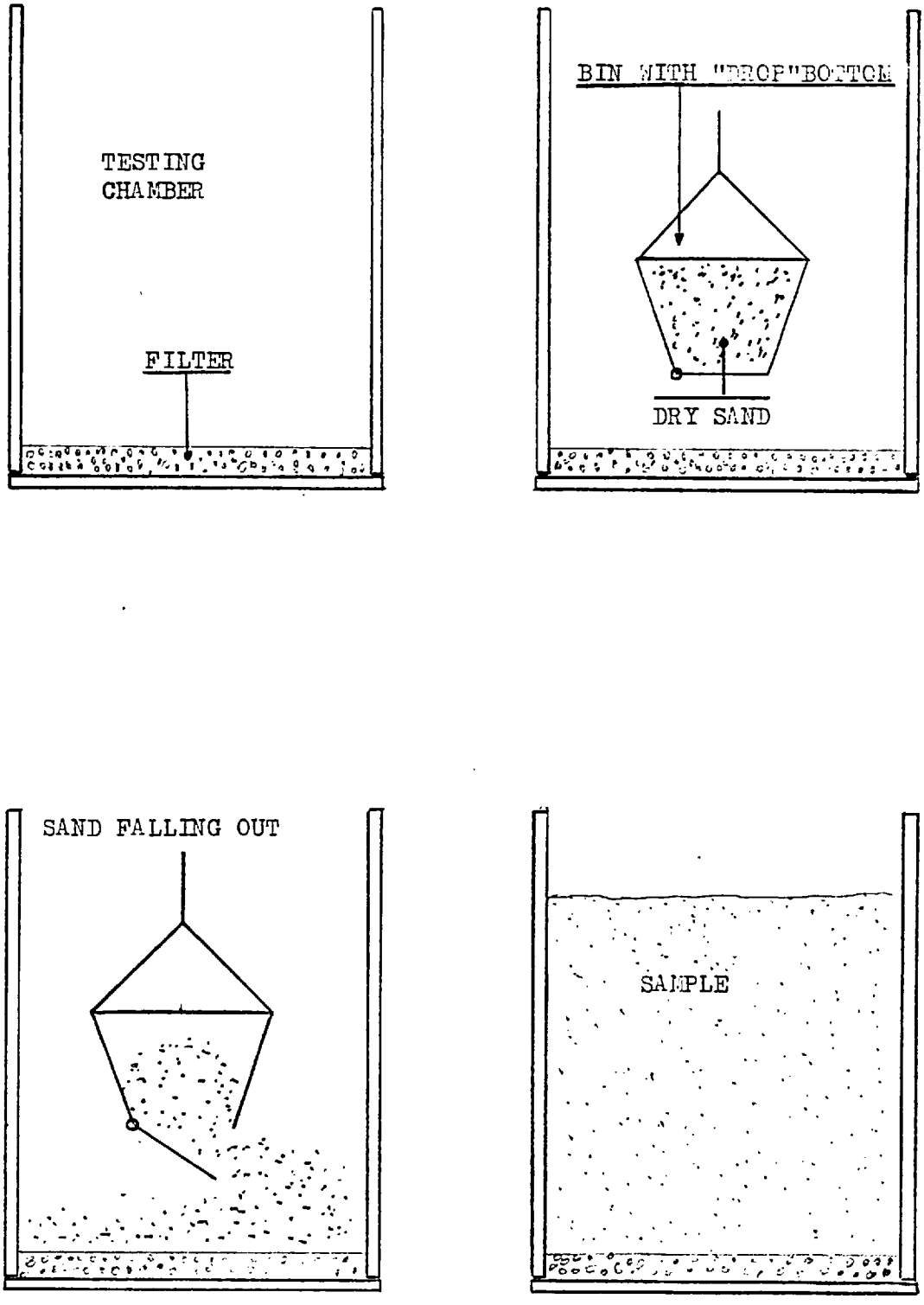


FIGURE 7.1 - PREPARATION OF THE SAMPLE

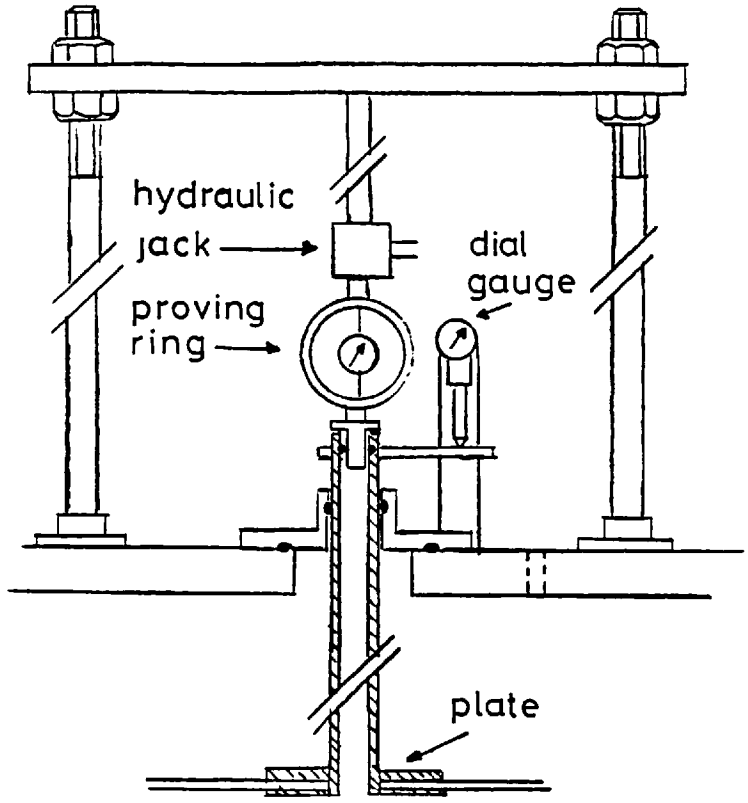


FIGURE 7.2.a - PLATE LOADING TEST

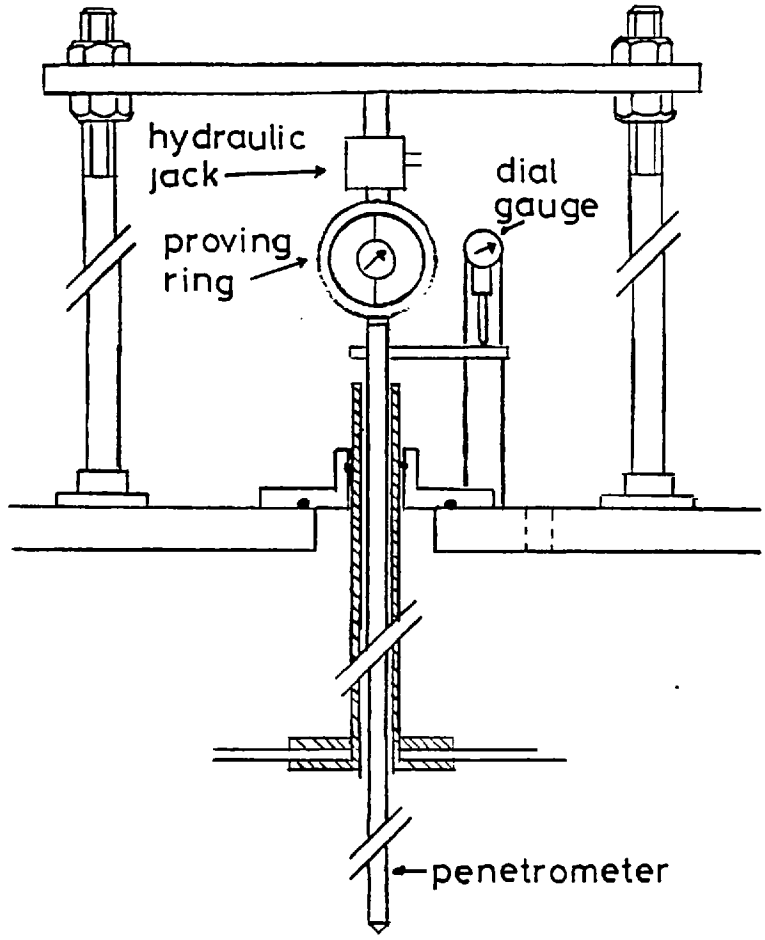


FIGURE 7.2.b - PENETROMETER LOADING TEST

CHAPTER 8

ANALYSIS I - INTERPRETATION OF CONE PENETRATION TEST RESULTS

8.1 GENERAL

In this chapter, results obtained from cone penetration tests during continuous penetration and during the static penetrometer load test, have been analysed.

The analysis carried out has considered the experimental and the interpreted results only qualitatively. Clearly, for the present series of tests, problems associated with:

a) difficulty in controlling the initial void ratio;

b) wall friction, imposing a very complex state of stress and compactness, during the consolidation process;

c) inexactness in determining the final void ratio;

preclude the possibility of any approach considering these results quantitatively.

Possible boundary effects, imposed by the rigid wall testing chamber (see Section 5.1), would be difficult to take into consideration and such effect also contributes for considering the obtained results as relative values.

As a general observation, it can be noted that cone penetration results are very sensitive to any variation in density. This fact can be more noticeable from the cone penetration tests results carried out after a plate load test. During the plate load test, compaction had occurred and the influenced zone under the plate can be sensed by the cone results, see Figs. 8.1, 8.2 and 8.4, see Section 5.2 for the plate dimensions.

8.2 RESULTS FROM CONTINUOUS CONE PENETRATION TESTS

Continuous cone penetration tests have been carried out with a rate of penetration around 2 cm/sec. During the continuous cone penetration test,

the point resistance, the friction sleeve resistance and the tip excess pore pressure have been recorded.

Figures 8.1 to 8.8 present results from the series of tests carried out at the centre of the sample. Four additional tests have been carried out half way between the centre of the sample and the chamber wall, see Section 7.2.6. Little difference among these four tests have been found. Figures 8.9 to 8.15 present results obtained for one test as representative of each series.

8.2.1 ANALYSIS OF THE POINT RESISTANCE

Point resistance values obtained from the continuous penetration tests have been compared with the limiting pressure required to expand a spherical cavity. Fig. 8.16 indicates values of the experimental results and of the spherical cavity limit pressure plotted against the overburden pressure.

For the spherical cavity expansion approach it has been assumed that:

a) according to Vesic (1973)[2], the ultimate pressure in a cohesionless material can be computed from:

$$p_u = q\frac{3(1+\sin\phi)}{(3-\sin\phi)}\left[I_r \times \xi_v\right]^{4\sin\phi/3(1+\sin\phi)} = q\,F_q \qquad 8.1$$

for drained conditions; and:

$$p_u = \frac{4}{3}\tau_f (L_n I_r + 1) + q \qquad 8.2$$

for undrained conditions.

where $q = \frac{1}{3}(1 + 2K_o)\sigma'_v$ (mean normal stress), 8.3

$$I_r = \frac{E}{2(1+\nu)\,q\tan\phi} \text{ (rigidity index)} \qquad 8.4$$

ξ_v is the volume change factor, depending on the average volumetric strain at failure in the plastic zone.

b) from the triaxial tests results, see Section 6.4;

$$E = 160 \text{ Kg/cm}^2 \text{ (loose)} = 350 \text{ Kg/cm}^2 \text{ (dense)}$$

$\phi = 35^{o}$ (loose) $\phi = 40^{o}$ (dense)

and considering $K_o = 1 - \sin \phi$ 8.5

$$\nu = K_o/(1 + K_o) \quad 8.6$$

Using these values, Eq. 8.4 gives:

$I_r = 75$ (loose) $= 180$ (dense)

~~Assuming possible values of ξ_v or~~ consulting Fig. 2 from Vesic (1972), we have:

$F_q = 15$ (loose) $= 37$ (dense)

Hence, for normally consolidated conditions ($K_o = 1 - \sin\phi$), the ultimate cavity pressure can be expressed as:

$p_u = 9.3\ \sigma'_v$ - (loose) - lower limit 8.7

$p_u = 21.1\ \sigma'_v$ - (dense) - upper limit 8.8

for drained conditions, and:

$p_u = 3.7\ \sigma'_v$ - (loose) - lower limit 8.9

$p_u = 4.6\ \sigma'_v$ - (dense) - upper limit 8.10

for undrained conditions.

The upper limit for drained and undrained cases can be extended by considering the effect of overconsolidation. Thus by assuming $K_o = 1$, we have:

$p_u = 37\ \sigma'_v$ - (dense) upper limit OC - drained 8.11

$p_u = 8\ \sigma'_v$ - (loose) upper limit OC - undrained 8.12

For the continuous cone penetration test, four values of the point resistance have been considered as follows:

a) A maximum value resulted from the influence of plate load test. It has been considered as overconsolidated subjected to an overburden pressure equal to σ'_v (test), See Table 7.2.

b) A minimum value obtained below the plate test influence zone or below 0.3 m depth of penetration for cases of no plate tests. Subjected to an overburden pressure equal to 0.7 $\sigma'_{v\,(test)}$. The analysis of the reduction in the overburden pressure ($\sigma'_{v\,(test)}$), with depth, caused by the wall friction is presented in Appendix A.2.2.

c) A maximum value obtained near the surface of the sample resulted from the consolidation process. Subjected to an overburden pressure equal to $\sigma'_{v\,(test)}$, see Table 7.2.

d) A maximum value obtained at the end of the penetration process. High values resulted from recompaction and the possible boundary effect. Subjected to a maximum overburden pressure equal to 0.7 $\sigma'_{v\,(test)}$, see Appendix A.2.2.

Despite the limited qualitative nature of the experimental and theoretical information obtained, some conclusions can be drawn from Fig. 8.16, as follows:

1) The cone penetration tests are likely to have occurred under or close to drained conditions.

2) Most of the results are inside the limits predicted by the spherical cavity expansion approach. These values have been obtained on samples with loose to medium density subjected to an overburden pressure varying from 1.0 Kg/cm^2 to 2.8 Kg/cm^2.

3) For medium-dense to very dense samples subjected to an overburden pressure less than 1.0 Kg/cm^2, the obtained results are much greater than those predicted by the spherical cavity approach. These high values may be due to very high lateral stress developed as a consequent of overconsolidation or boundary effects.

8.2.2 ANALYSIS OF FRICTION SLEEVE RESISTANCE

For the interpretation of the friction sleeve resistance, it has been assumed that:

$$f_s = K_o \times \sigma'_v \times \tan \delta \qquad 8.13$$

where K_o is the at-rest coefficient of earth pressure.

δ is the soil - steel friction angle.

σ'_v is the overburden pressure.

Maximum and minimum values have been predicted assuming that:

a) normally consolidated lower limit:

$$K_o = 1 - \sin\phi, \ \phi = 35^o, \ \delta = 0.7\,\phi.$$

b) normally consolidated upper limit:

$$K_o = 1 - \sin\phi, \ \phi = \delta = 40^o$$

c) overconsolidated upper limit:

$$K_o = 1, \ \delta = 40^o$$

Four values of the friction sleeve resistance have been considered in the same manner than for cone end resistance.

Fig. 8.17 indicates the experimental and predicted friction sleeve resistance values plotted against overburden pressure. These results also provide similar information as indicated by the cone end resistance analysis.

8.2.3 ANALYSIS OF THE EXCESS PORE PRESSURE

The excess pore pressure induced by a penetration process has been analysed in Chapter 3. From a simplified parametrical study, it has been found that the induced excess pore pressure can be expressed as:

$$\Delta U = F_1(\Delta)\, q_c + F_2(\Delta)\, \sigma_i \qquad (3.23)$$

or

$$\frac{\Delta U}{q_c} = F_1(\Delta) + F_2(\Delta)\, \frac{\sigma_i}{q_c} \qquad 8.14$$

The derivation of equation 3.23 is presented in Section 3.2. These parameters are defined as:

ΔU - excess pore pressure induced during a penetration process.

q_c - cone end resistance

$F_1(\Delta)$ and $F_2(\Delta)$ - functions of the volumetric strain occurring in the plastic zone

σ_i - confining stress

The ratio between confining pressure and cone end resistance is very small, therefore, the second term of this expression can be neglected and Eq. 8.14 becomes:

$$\frac{\Delta U}{q_c} = F_1(\Delta) \qquad 8.15$$

Values of the excess pore pressure/cone end resistance ratio have been calculated for all tests and plotted against depth of penetration. Fig. 8.18 indicates values obtained in normally consolidated samples. It should be emphasized that cone tests 1, 2 and 3 have been carried out after the plate load test (See Table 7.2), therefore the influenced zone should be considered as overconsolidated. Fig. 8.19 presents values obtained for overconsolidated samples. Fig. 8.20 indicates values obtained for the series of tests carried out half way between the sample centre and the chamber wall, these conditions should be considered as heavily overconsolidated subjected to a low overburden pressure.

These results indicate:

a) for normally consolidated loose-medium samples:

$$0.25 < F_1(\Delta) < 0.35 \qquad 8.16$$

b) for normally consolidated medium-dense samples.

$$0.025 < F_1(\Delta) < 0.1 \qquad 8.17$$

c) for lightly overconsolidated medium-dense samples:

$$0.05 < F_1(\Delta) < 0.1 \qquad 8.18$$

d) for lightly overconsolidated very dense samples:

$$0.05 < F_1(\Delta) < 0.1 \qquad 8.19$$

e) for heavily overconsolidated loose-medium samples:

$$-0.025 < F_1(\Delta) < 0.05 \qquad 8.20$$

Obviously, due to the limited number of tests and to not having taken into consideration the confining stress effect, these defined limits should only be treated as a qualitative indication.

8.3 STATIC PENETROMETER LOAD TESTS RESULTS

8.3.1 GENERAL

Static loading tests have been performed after some of the continuous cone penetration tests. During the static loading tests, the total load (proving ring), the displacement at the push rods top end, the cone end resistance and the friction sleeve resistance have been recorded. The pore pressure unit was constantly monitored and showed no excess value during the test, See Section 7.2.5.

Fig.s 8.21, 8.22, 8.23, 8.24 and 8.25 indicate results from static penetrometer load tests carried out after the continuous cone penetration tests 1, 2, 3, 4 and 8 respectively, See Table 7.2. These figures also indicate the corresponding cone end resistance, $q_{c(c)}$, and friction sleeve resistance, $f_{s(c)}$, values obtained at the common depth during the continuous cone penetration test.

The static loading conditions indicated two distinct type of failure. According to Vesic (1963) these failure patterns can be defined as: 1) local shear failure (tests 1, 2, 3 and 4), the ultimate load is basically defined on the rate of settlement rather than on the peak resistance; 2) general shear failure (test 5), the ultimate load corresponds to a well defined peak resistance.

8.3.2 ANALYSIS OF RESULTS

It can be observed that for all investigated cases, the cone end requires little displacement to develop almost full resistance. For the friction sleeve

excepting for general shear failure conditions(test 5), it requires a big vertical movement to mobilize any resistance.

The minimum movement necessary to mobilize the cone end and the friction sleeve resistances can be better observed during the 0.1 m continuous penetration test performed after the penetrometer load test 2, See Fig. 8.22. For this test, the full cone end resistance has been achieved in less than 1.0 mm vertical movement, while the friction sleeve resistance required 100 mm for full development.

The difference between the quantities measured during the static penetrometer load test, T - P, has been compared with the summation of the friction sleeve resistance developed during the continuous penetration test, $\Sigma f_{s(c)}$. Table 8.1 indicates these values.

TABLE 8.1

TEST	A $(T - P)_s$ (Kg)	B $\Sigma f_{s(c)}$ (Kg)	$\frac{A}{B}$ %	$\frac{A}{0.75\ B}$ %
1	49.0	48.9	100	136
2	150.0	574.0	26	35
3	20.0	257.2	8	10
4	53.5	321.3	17	22
5	775.0	1124.8	70	92

The results have shown that, excepting test 1, the friction capacity indicated during the continuous cone penetration tests have not been mobilized, along the shaft, during the static penetrometer load test. It is interesting to note that, even for test 5 where the local friction sleeve resistance has indicated bigger values for the penetrometer load test than the continuous cone penetration test (See Fig. 8.25), only 70 percent of the indicated continuous friction capacity have been mobilised.

Nottingham (1975) developed a cone penetration and model pile study to evaluate the cone penetration test prediction methods for pile capacity. His method for estimating drained pile-soil friction capacity, consists basically in taking the local friction measurements, f_s, and correct them for the type of penetrometer used, the type of soil penetrated, the pile material and taper, and the relative depth of pile penetration. According to Nottingham's method, the values indicated in column B, Table 8.1, should be corrected by a factor of 0.75. Even considering this drained correction factor, the results still indicate discrepancy between the continuous and static friction capacity values.

8.4 INFLUENCE OF EXCESS PORE PRESSURE ON MEASURED VALUES

8.4.1 GENERAL

In Chapter 3, the difficulties involved in considering any theoretical approach to predicting the excess pore pressure and its effect during the penetration process have been discussed.

Comparisons between values measured during a penetration rate generating excess pore pressure and at a speed with no excess pore pressure, would at least indicate a quantitative influence of this factor on the measured quantities.

The rate effect can introduce two interdependent phenomena: 1) inducing excess pore pressure and consequently varying the effective stress, 2) mobilization of viscous resistance. These two interdependent phenomena may have opposite effects. As an example, in a collapsible soil, generation of excess positive pore pressure reducing the effective stress would indicate a decrease on the measured values. However, the mobilization of viscous resistance would contribute to an increasing in such measured values. Results obtained by Bemben and Myers (1974), see Fig. 3.25, indicated this combined effect.

8.4.2 INFLUENCE OF EXCESS PORE PRESSURE ON CONE END RESISTANCE

Fig. 8.26 indicates the ratio between the cone end resistance measured during static condition, $q_{c(s)}$, and during the continuous penetration test, $q_{c(c)}$. Also, in the same figure, there is a rough indication of limits defining the compactness of the samples.

Two distinct type of behaviour can be observed, as follows:

1) For static loading condition, carried out on the sample indicating a local shear failure behaviour, the cone end resistance showed a smaller value than the continuous penetration test. Therefore, for a material showing this type of failure mode, the rate effect is related to the mobilization of the viscous resistance rather than reduction of the effective stress.

2) For static loading condition, carried out on the sample indicating a general shear failure, the cone end resistance showed a bigger value than the continuous cone penetration test. Therefore, for this case, the reducing effective stress effect predominates over the effect of the mobilization of viscous resistance.

Fig. 8.26 indicates the ratio between the excess pore pressure and the continuous cone end resistance.

For the cases observed, the pore pressure ratio, $\Delta U/q_{c(c)}$, does not vary significantly. All the values obtained are inside the limits 4% to 7%. Therefore, regarding to the magnitude and sense (positive) there is a good agreement among the measured values. Hence, it should be expected that the excess pore pressure would influence these results equally. However, the cone end resistance, as a measure of the shear strength, is not a function of any localized excess pore pressure surrounding the advancing tip but a function of the excess pore pressure developed along the failure surface.

The pore pressure measurement at the penetrometer conical end point will provide an indication of the maximum absolute value surrounding the tip. This value associated with the cone end resistance, would at least,

qualitatively, indicate the influence of the rate effect on the penetration process.

In general, the rate effect can be related to predominating viscous resistance or effective stress variation effects. The first of these phenomena will occur in soils exhibiting a local shear failure criterion. The effective stress variation effect will occur in soils exhibiting a general shear failure criterion and this condition can be followed by two distinct types of behaviour: reduction or increasing effective stress. The reduction in effective stress is associated with collapsible structures and increasing will occur in dilating materials. These different behaviours can be related to the compactness of the deposit. Clearly, the very important stress level and stress history effects, should be taken into consideration when analysing the influence of rate effect on the penetration process. High confining stress will reduce the possibility of dilating effects. High overconsolidation ratio will increase the dilating tendency. These observations will be considered in Section 8.5.2, Fig. 8.29.

8.4.3 INFLUENCE OF EXCESS PORE PRESSURE ON FRICTION SLEEVE RESISTANCE

Results from static loading conditions carried out on samples indicating a local shear failure behaviour have shown that the friction sleeve resistance has not been mobilized. For the penetrometer load test 5, it has been found that the local friction sleeve resistance has indicated a value 40 percent greater than that indicated by the continuous penetration test. Therefore, it appears that a rate effect analagous to that for cone end resistance can be adopted for friction sleeve resistance.

8.5 RELATIVE DENSITY AS INDICATED BY THE CONE END RESISTANCE

8.5.1 GENERAL

The use of cone end resistance as an indication of the relative density has been investigated by other authors for different purposes.

Mitchell and Gardner (1975) summarize the most relevant investigations carried out with the objective of establishing a relationship between cone end resistance and in situ relative density, See Fig. 8.27. These quoted relationships refer to various series of tests carried out on laboratory sand samples prepared to a known relative density value. Results from Turnbull et al (1960) are applicable to saturated fine sand. The relationship proposed by Schultze and Melzer (1965) have been obtained from statistical analysis of many test results on dry samples. Results from Thomas (1968) are based on a 3/8 in. penetrometer diameter and are applicable to uniform medium dry sands. Finally the correlations proposed by Schmertmann (1971) are applicable to silty fine dry sands and uniform medium dry sands.

These tests were carried out in normally consolidated samples.

The results on Fig. 8.27 show a wide scatter of values, however, each specific set of curves can be approximately represented as:

$$D_r = A \text{ Log } q_c + B \sigma_v' + C \qquad 8.21$$

where: σ_v' is the vertical effective stress,

A, B and C are empirical parameters.

It should be noted that any investigation proposing correlations between cone end resistance and relative density may be strongly affected by errors involved in determining the maximum, the minimum and the actual density values.

8.5.2 ANALYSIS OF THE RESULTS

Fig. 8.28 presents values of relative density and cone end resistance obtained at a common depth. This figure, shows the results from Tests 1, 2, 6 and 7 carried out in normally consolidated conditions, see Table 7.2. For a penetration below approximately 0.35 m the overburden pressure has been assumed as 0.7 σ_v', see Appendix A.2.2. The method of determinating the relative density value has been explained in Section 7.2.7.

These results indicated that the relative density can be approximately indicated by the following expression:

$$D_r\,(\%) = 57\,\mathrm{Log}_{10}\,q_c - 12\,\sigma_v' - 11 \qquad 8.22$$

q_c and σ'_v in Kg/cm^2

Fig. 8.28 also presents the relationships obtained by Turnbull et al (1960), for saturated fine sand, and by Schmertmann (1971), for uniform medium dry sand.

Despite these results being obtained for soils with different grading curves, some conclusions may be drawn as follows:

1) For loose condition, there is an agreement between the two relationships obtained for the saturated sands. For the same relative density, the saturated sands indicated a lower cone end resistance than the dry sand. Therefore, it can be argued that, for this condition, saturation will reduce the cone resistance value. Apparently, this fact may be contradicting the viscous resistance effect, which indicated a higher cone resistance for continuous than for static tests, see Fig. 8.26. It appears that, for this condition a loss of strength is likely to occur in the affected area surrounding the advancing penetrometer. Hence, a static test carried out afterwards will not represent the dry condition, for the same initial void ratio.

2) As the density increases, the results obtained by Turnbull et al (1960) showed relatively high cone end resistance values. For a relative density above 40% - 45% these values are bigger than for the dry sand. This fact suggests that the effect of negative excess pore pressure may account for the increase in the resistance value. For the sand used in this research this fact was not observed and the negative pore pressure effect would be expected for higher density values than the above indicated.

In general, it can be said that:

a) For saturated loose-medium sands, there will be a loss of strength (liquefaction) in the affected area surrounding the advancing penetrometer. A static test carried out afterwards may indicate a resistance value smaller than for dry conditions for the same initial void ratio.

b) For saturated medium-dense-very dense sands (collapsible structures), there will be a gain of strength (consolidation) in the affected area surrounding the advancing penetrometer. A static test carried out afterwards may indicate a resistance value bigger than for dry condition, for the same initial void ratio.

c) For saturated very dense sands (dilating structures) there will be a loss of strength (swelling) in the affected area surrounding the advancing penetrometer. A static test carried out afterwards may indicate a resistance value smaller than for dry conditions for the same initial void ratio.

These observed facts together with the information indicated in Fig. 8.26, see Section 8.4.2, may suggest that the rate effect influencing the penetrometer resistance can be qualitatively represented as indicated in Fig. 8.29. This figure indicates the importance of relative density considering the effect related to penetration process. As a result, it can be said that, a relationship between cone resistance and relative density established for dry sands, cannot be extrapolated to saturated conditions.

8.6 FRICTION RATIO AS AN INDICATION OF SOIL CLASSIFICATION

8.6.1 GENERAL

The measurement of the local friction sleeve resistance, in addition to providing a basis for the evaluation of pile friction resistance, may be used to identify soil types by the concept of friction ratio. The friction ratio is

defined as the ratio between cone end and friction sleeve resistances. The use of this value to indicate the soil classification is at the present well recognized. It use, implies the recognition that the friction ratio does not depend on stress level but is a function of soil type.

Begemann (1965, 1969) has shown that there is a relationship between the ratio of unit friction resistance, f_s, to unit cone resistance, q_c, and the soil type.

Vesic (1967) has found for sands that:

$$0.6 < FR\ (\%) < 1.65$$

Sanglerat (1972) reports results supporting the relationship proposed by Begemann (1965, 1969) and by Schmertmann (1967). His findings can be summarized as in Table 8.2.

TABLE 8.2

Soil Type	FR (%)
Soft Rocks, Shells or Loose Gravel Fill	0.0 - 0.5
Sands or Gravel	0.5 - 2.0
Clay-Sand Mixture and Silts	2.0 - 5.0
Clays	5.0

8.6.2 ANALYSIS OF THE RESULTS

Fig. 8.30 summarizes all the friction ratio values obtained during the continuous cone penetration tests. It can be observed that most of the results are inside the limits 1% to 4%. There is a tendency for this upper limit to reduce with an increase in the sample compactness. For a penetration depth below 0.55 m, in predominantly dense material, the lower and upper limits are 1% and 2% respectively.

8.7 DISSIPATION OF EXCESS PORE PRESSURE

8.7.1 GENERAL

In this section it will be discussed how to make use of the dissipation rate of induced excess pore pressure with time. This information can be obtained after the penetration process has stopped. It is essential that this data should be measured with no movement of the penetrometer. Any movement occurring would induce a different excess pore pressure value and disturb the entire dissipation process.

As pointed out by Milligan (1975): "These measurements may indirectly permit estimates of permeability, but are primarily directed to an evaluation of volume compressibility in relation to strain".

From the consolidation theory, (Terzaghi (1943), the time necessary for almost full dissipation of the excess pore pressure in an homogeneous media can be expressed as:

$$t = \frac{m_v}{K} \gamma_w H^2 \qquad 8.23$$

where: m_v is the coefficient of volume change

K is the coefficient of permeability

γ_w is the unit weight of water, it will be taken as unity

$1\ g/cm^3 = 10^{-3}\ Kg/cm^3$.

H is the geometrical factor defining the volume of the soil mass involved per drainage surface.

Difficulties associated with the evaluation of the geometrical factor during the penetration process, may lead to the impossibility of solving this problem theoretically.

8.7.2 CONSIDERATIONS ON THE GEOMETRICAL FACTOR VALUE

The volume of the pertubed pore pressure zone surrounding an advancing penetrometer, for undrained conditions, can be approximately

estimated using the cavity expansion approach. In Section 3.2, it has been shown that the relative radius of the plastic zone (See Fig. 3.1) can be expressed as follows:

$$\frac{R_p}{R_u} = \frac{E_u}{3\tau_o}^{\frac{1}{3}} \quad \ldots \text{spherical cavity} \tag{3.10}$$

$$\frac{R_p}{R_u} = \frac{E_u}{3\tau_o}^{\frac{1}{2}} \quad \ldots \text{cylindrical cavity} \tag{3.11}$$

Vesic (1972) reports typical values of the rigidity index for sands, subjected to an isotropic confining stress of 1 Kg/cm^2, ranging from 70 to 150 (loose to dense). These values give:

$$\frac{R_p}{R_u} = 4 \text{ to } 6 \text{ (loose to dense)} \ldots \text{spherical cavity} \tag{8.24}$$

$$\frac{R_p}{R_u} = 9 \text{ to } 15 \text{ (loose to dense)} \ldots \text{cylindrical cavity} \tag{8.25}$$

Eq. 8.23 has been obtained assuming that the initial excess pore pressure is uniform within the affected soil mass. However, the excess pore pressure may show large variations within the affected zone surrounding the advancing penetrometer. The initial excess pore pressure distribution can be represented as, See Section 3.2,:

$$\frac{\Delta U}{\tau_f} = 0.943_{\,f} + 4 \text{ Ln } \left(\frac{R_p}{r}\right) \ldots \text{spherical cavity} \tag{3.2}$$

$$\frac{\Delta U}{\tau_f} = 0.817_{\,f} + 2 \text{ Ln } \left(\frac{R_p}{r}\right) \ldots \text{cylindrical cavity} \tag{3.6}$$

or assuming an idealised elastic soil model ($\alpha_f = 0$), these equations become respectively:

$$\frac{\Delta U}{\tau_f} = 4 \text{ Ln } \left(\frac{R_p}{r}\right) \tag{8.26}$$

$$\frac{\Delta U}{\tau_f} = 2 \text{ Ln } \left(\frac{R_p}{r}\right) \tag{8.27}$$

These equations may need to be modified when the analysis of the cavity expansion is carried out for a non-linear soil model. However, as observed by Randolph (1977), the logarithmic variation is a reasonable interpretation, see Fig. 8.31.

The distribution of the initial excess pore pressure has been solved by Massarch (1976), See Fig. 8.32.

Assuming: 1) zero excess pore pressure outside the plastic zone; 2) that the penetration problem lies in between the spherical and cylindrical solution, Al - Awkati (1975); 3) the radial excess pore pressure distribution as represented in Fig. 8.33, it follows that:

$$\frac{R_p}{R_u} = \frac{H}{R_u} = 3 \text{ to } 5 \text{ (loose to dense)} \qquad 8.28$$

Eq. 8.28 indicates that the geometical factor (H) is proportional to the penetrometer radius (R_u). Because, this is a squared factor, one can argue that the horizontal dimension of the penetrometer can be more important than the characteristics of the soil surrounding it.

8.7.3 CONSIDERATIONS ON THE PERMEABILITY AND COMPRESSIBILITY EFFECT UPON THE DISSIPATION TIME

For the same geometrical problem (penetrometer dimensions and boundary conditions), eq. 8.23 becomes:

$$t = f\left(\frac{m_v}{K}\right) \qquad 8.29$$

Eq. 8.29 indicates that the dissipation time increases with increasing compressibility and decreases with increasing permeability. Consequently, the dissipation time will have relatively high values for clay deposits and relatively low values for sands. Silty soils will indicate an intermediate value. Hence, this indicates an immediate application of the rate of excess pore pressure dissipation with time as a qualitative indication of the soil type being penetrated.

In order to better investigate the influence of the compressibility and permeability on dissipation time, the variation of these parameters with void ratio will be considered for the same soil. This analysis will be carried out only for granular materials. Thus if t_1 and t_2 are the dissipation time corresponding to the loosest (e_{max}, $D_r = 0$) and densest (e_{min}, $D_r = 100$) conditions respectively, we have:

$$\frac{t_1}{t_2} = \left(\frac{m_{v1}}{m_{v2}}\right) / \left(\frac{K_1}{K_2}\right) \qquad 8.30$$

Table 8.3 indicates typical values of the compressibility (secant determination) for several granular soils during virgin loading obtained by Hassib (1951).

For the consideration of the permeability ratio factor, it will be assumed that:

a) From Taylor (1948) the coefficient of permeability can be expressed as:

$$K = D_s^2 \frac{\gamma}{\mu} \frac{e^3}{1+e} C \qquad 8.31$$

where: D_s is the effective particle diameter

γ is the unit weight of permeant

μ is the viscosity of permeant

e is the void ratio

C is the shape factor

b) Other conditions being the same, we have:

$$\frac{K_1}{K_2} = \frac{e^3_{max}}{1+e_{max}} / \frac{e^3_{min}}{1+e_{min}} \qquad 8.32$$

Table 8.4 indicates typical values of maximum and minimum void ratio for granular soils reported by Hough (1957). The variation of the coefficient of permeability as a function of the relative density has also been indicated by Burmister (1954), See Fig. 8.34.

Values presented in Tables 8.3 and 8.4 have shown that for granular material the dissipation time is more susceptible to changes in permeability than in compressibility. The influence of permeability can be at least 4 times greater than the influence of compressibility,.

From the reported values and eq. 8.28, it can be established that:

$$t_{(e_{min})} = (9 \text{ to } 14)\, t_{(e_{max})} \qquad 8.33$$

Equation 8.33 suggests a possible application of the dissipation time as an indicator of the compactness of granular materials.

TABLE 8.3

SOIL TYPE	DR%	m_v'(cm^2/Kg x 10^3) A $\Delta\sigma_1$ (Kg/cm^2) 0.6 - 1	m_v'(cm^2/Kg x 10^3) B $\Delta\sigma_1$ (Kg/cm^2) 2 - 5	A m_{v1}/m_{v2}	B m_{v1}/m_{v2}
UNIFORM GRAVEL	0	3.2	1.6	3.8	3.0
1 mm< D <5 mm	100	0.84	0.55		
WELL GRADED SAND	0	7.1	3.86	3.7	4.7
0.02 mm <D <1 mm	100	1.9	0.81		
UNIFORM FINE SAND	0	6.8	2.8	3.5	3.4
0.07 mm < D < 0.3 mm	100	1.9	0.82		
UNIFORM SILT	0	3.6	5.7	12.8	4.4
0.02 mm < D <0.07 mm	100	2.8	1.3		

TABLE 8.4

SOIL TYPE	$e_{(max)}$	$e_{(min)}$	$e^3_{max}/(1+e_{max})$	$e^3_{min}/(1+e_{min})$	K_1/K_2
UNIFORM SPHERES	0.92	0.35	0.4056	0.0318	12.75
STANDARD OTTAWA SAND	0.80	0.50	0.2844	0.0833	3.41
CLEAN UNIFORM SAND	1.0	0.40	0.5000	0.0457	10.94
UNIFORM INORGANIC SILT	1.1	0.40	0.6338	0.0457	13.87
SILTY SAND	0.90	0.30	0.3837	0.0208	18.45

TABLE 8.4 (Continued/...)

SOIL TYPE	$e_{(max)}$	$e_{(min)}$	$e^3_{max}/(1+e_{max})$	$e^3_{min}/(1+e_{min})$	K_1/K_2
FINE TO COARSE SAND	0.95	0.20	0.4397	0.0067	65.63
MICACEOUS SAND	1.2	0.40	0.7855	0.0457	17.19
SILTY SAND AND GRAVEL	0.85	0.14	0.3320	0.0024	138.33
USED SAND	1.09	0.41	0.6196	0.0489	12.7

8.7.4 ANALYSIS OF THE RESULTS

Fig. 8.35 indicates measurements of the rate of dissipation of excess pore pressure with time, for the series of tests carried out at the centre of the sample. Fig. 8.36 presents the same measurement corresponding to the series of tests carried out half way between the centre of the sample and the chamber wall. In Fig. 8.37 and Fig. 8.38 these results have been presented as percentages of the respective cone end resistances.

After the penetration process has stopped, a decrease in the cone end and friction sleeve resistances have been observed. This decrease, observed in all tests, corresponded to an average of 15 percent and has taken place in less than 0.5 sec. After this 15 percent quick reduction, the cone end and the friction sleeve have indicated a constant value, during which the dissipation of excess pore pressure has occurred.

These results have indicated that the dissipation of excess pore pressure have occurred in less than 6 sec. This can be considered a very quick time. As stressed by Schmertmann (1974a) refering to dissipation time of excess pore pressure induced during penetration tests in sands: "Such a rapid effect would likely also go unreported, which might also lead to the erroneous conclusion that significant pore pressure did not exist during the q_c measurements".

Using eq. 8.23 and assuming:

1) t = 2 sec. (loose) = 5.6 sec. (dense) - From Fig. 8.35

2) $m_v = (1/100)cm^2/Kg$ (loose) = $(1/300)cm^2/Kg$ (dense) - From Fig. 9.3.b

3) $H = 3R_u$ (loose) = $5R_u$ (dense)

4) $R_u = 1.78$ cm (penetrometer radius)

we have:

$$K = 1.4 \times 10^{-4} \text{ cm/sec (loose)}$$

$$K = 4 \times 10^{-5} \text{ cm/sec (dense)}$$

This indirectly estiamted values of the coefficient of permeability are typical values for silty sands.

For sands, indirect assessment of permeability can be obtained from the simple relationship between this value and the effective particle size as follows:

$$K = N (D_{10})^2 \text{ cm/sec} \qquad 8.34$$

where D_{10} is the particle diameter (in cm) at which 10% of the soil weight is finer.

N is an empirical value

Eq. 8.34 applies for sands indicating a coefficient of uniformity ranging from 2 to 20. For the sand used the coefficient of uniformity is around 5 and D_{10} equal to 3.5×10^{-3} cm, see Fig. 6.6

For the indirectly estimated permeability values, eq. 8.34 gives N = 11 and N = 3 for loose and dense conditions respectively.

Lane and Washburn (1946) indicated that this value N may vary from 1 to 42, for granular soils. For medium sand, they indicated a value of N = 7.

The variation of the permeability as a function of the relative density is not considered in eq. 8.34, therefore, an average value is obtained.

8.8 SUMMARY AND CONCLUDING REMARKS

Results from continuous cone penetration and static penetrometer load tests have been analysed. Due to uncontrollable factors, mainly concerned with void ratio and state of stress, these results have only been considered qualitatively. Some conclusions can be drawn as follows:

1) The cone penetration tests are likely to have occurred under or close to drained conditions.

2) The ratio between pore pressure and cone end resistance show a maximum value for normally consolidated loose-medium samples (0.35) and a minimum value for heavily overconsolidated loose-medium samples (-0.025).

3) The rate effect may introduce two interdependent phenomena, affecting the measured values: 1) inducing excess pore pressure and consequently varying the effective stress; 2) mobilization of viscous resistance. The first is likely to occur in samples indicating general shear failure behaviour. For samples indicating a local shear failure criterion, the effect of viscous resistance will predominate.

4) Due to rate effects, the relationship between cone resistance and relative density established for dry sand cannot be extrapolated to saturated condition.

5) During a continuous penetration test, the affected area surrounding the advancing penetrometer will be subjected to rate effects. Hence, a static test, with no excess pore pressure, carried out afterwards will not represent the dry condition, for the same initial void ratio.

6) The measurement of the rate of excess pore pressure dissipation provides a basis for an estimation of the coefficient of permeability.

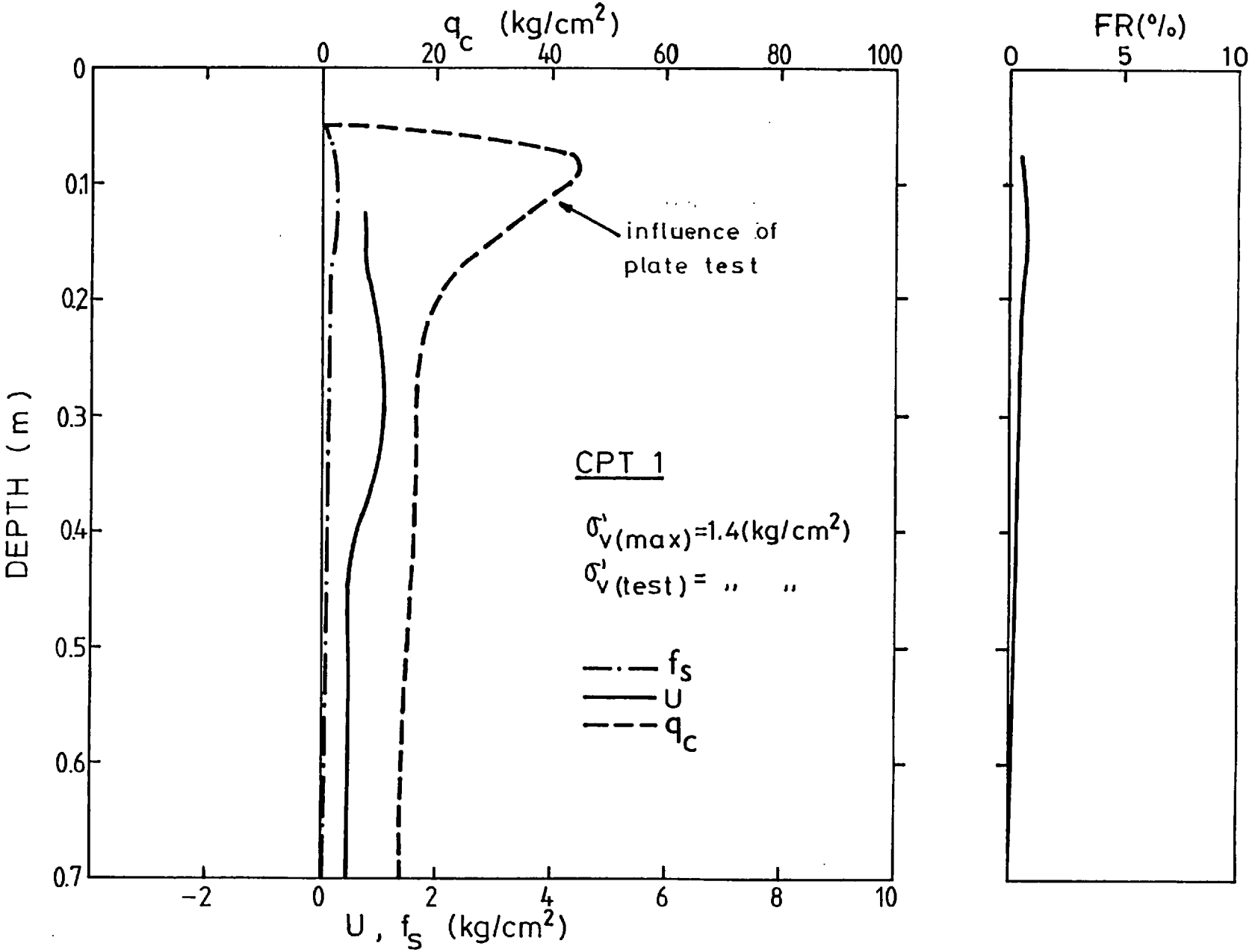


FIGURE 8.1 - CONTINUOUS CONE PENETRATION TEST.

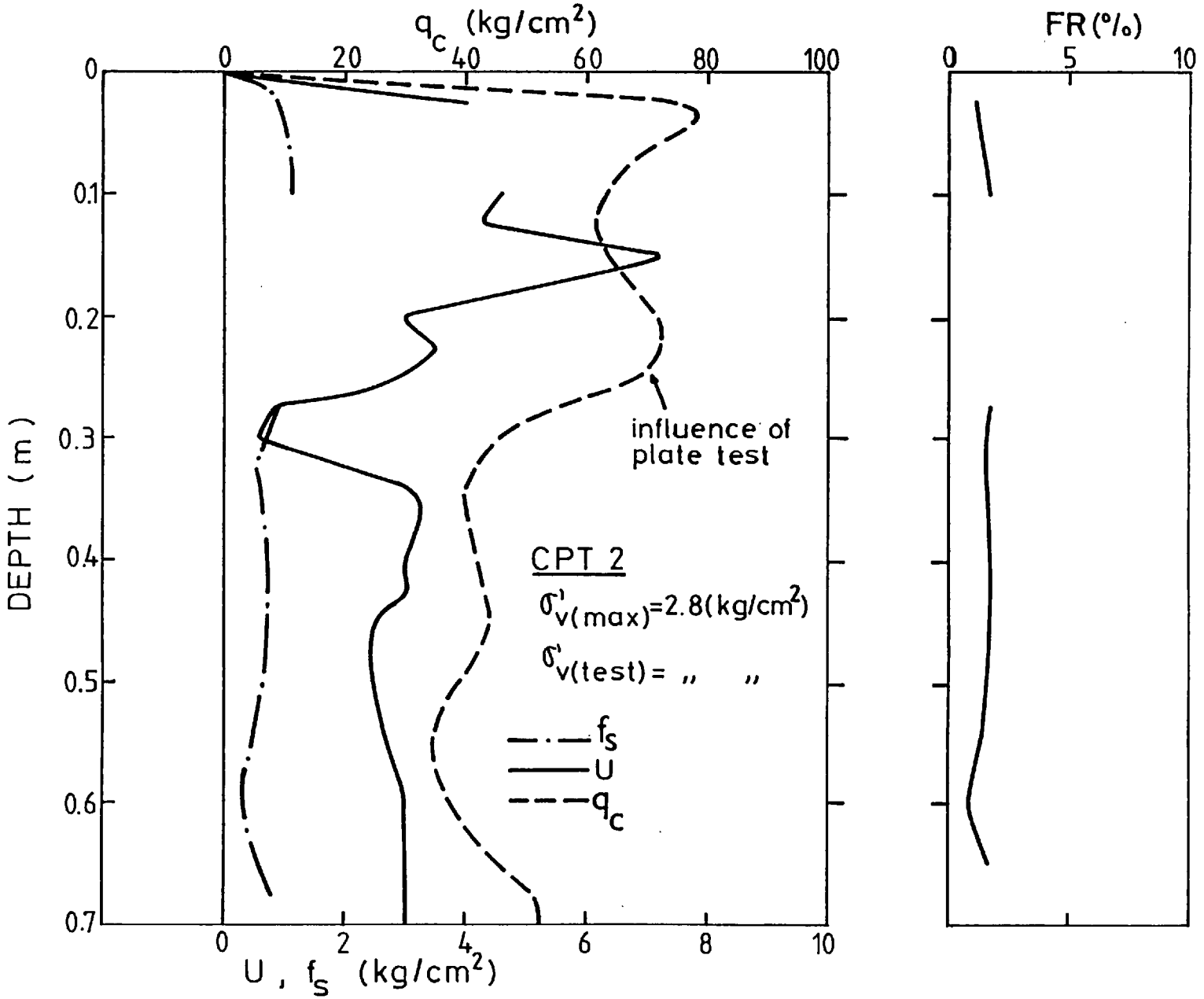


FIGURE 8.2 - CONTINUOUS CONE PENETRATION TEST.

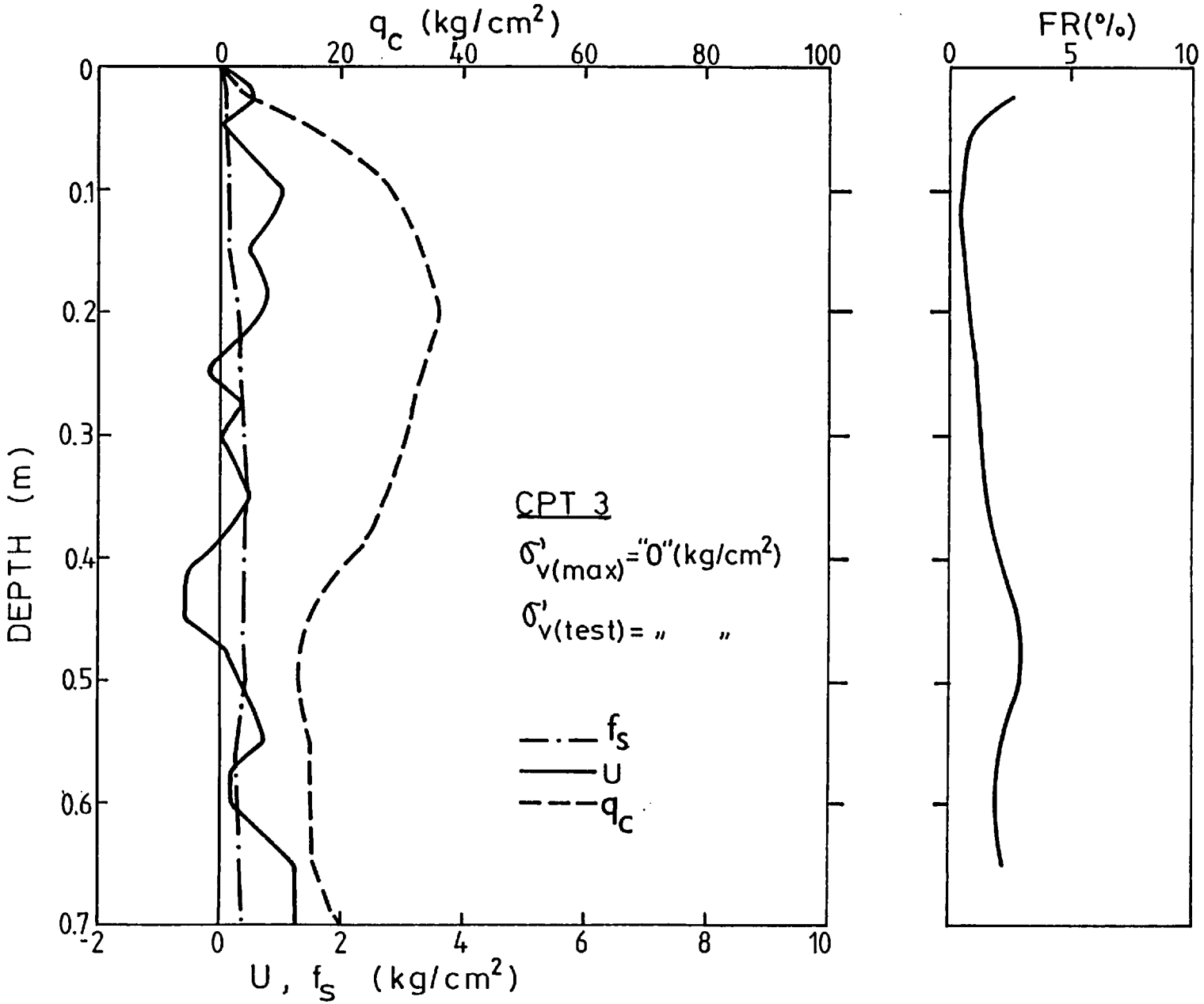


FIGURE 8.3 - CONTINUOUS CONE PENETRATION TEST.

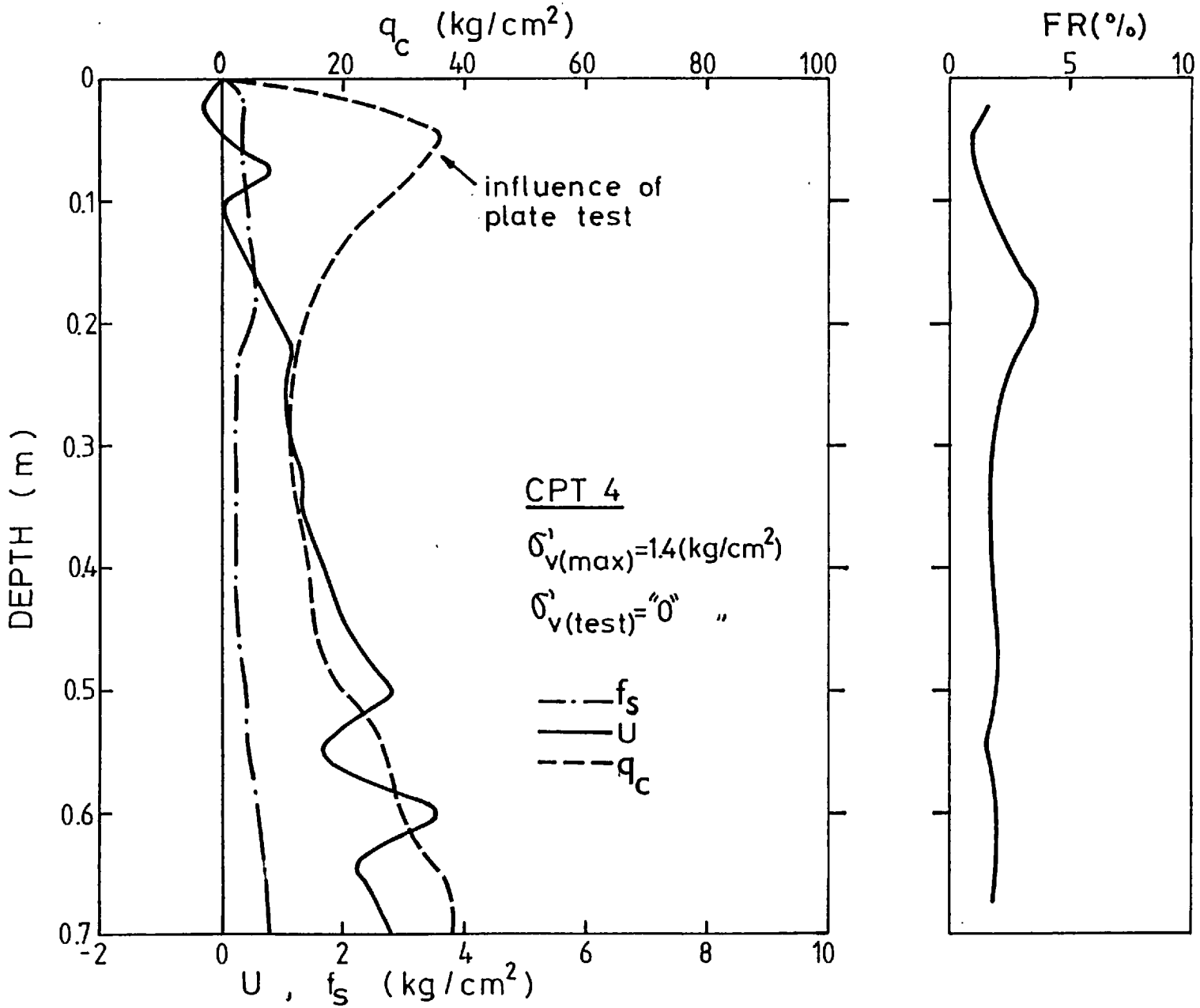


FIGURE 8.4 - CONTINUOUS CONE PENETRATION TEST.

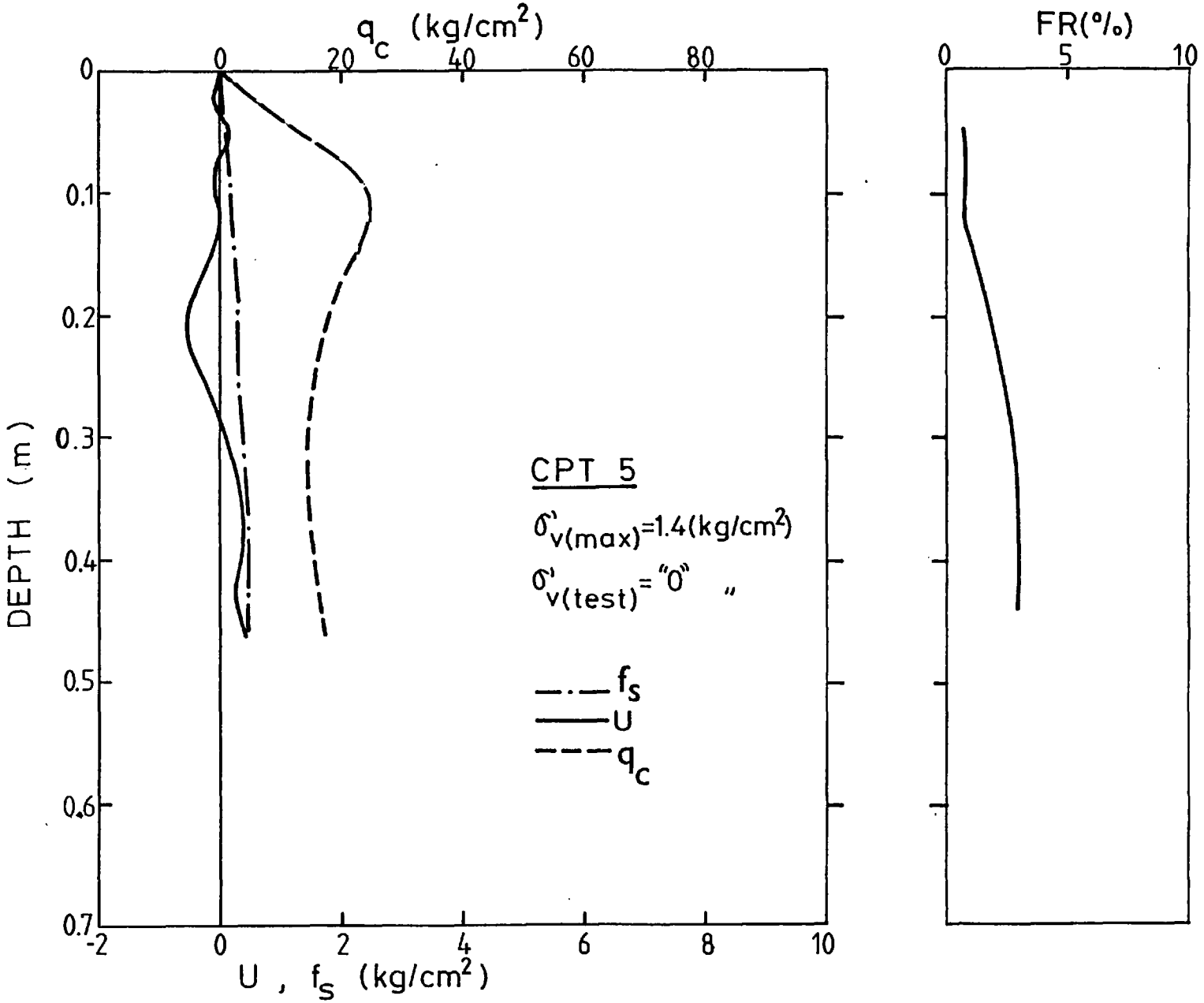


FIGURE 8.5 - CONTINUOUS CONE PENETRATION TEST.

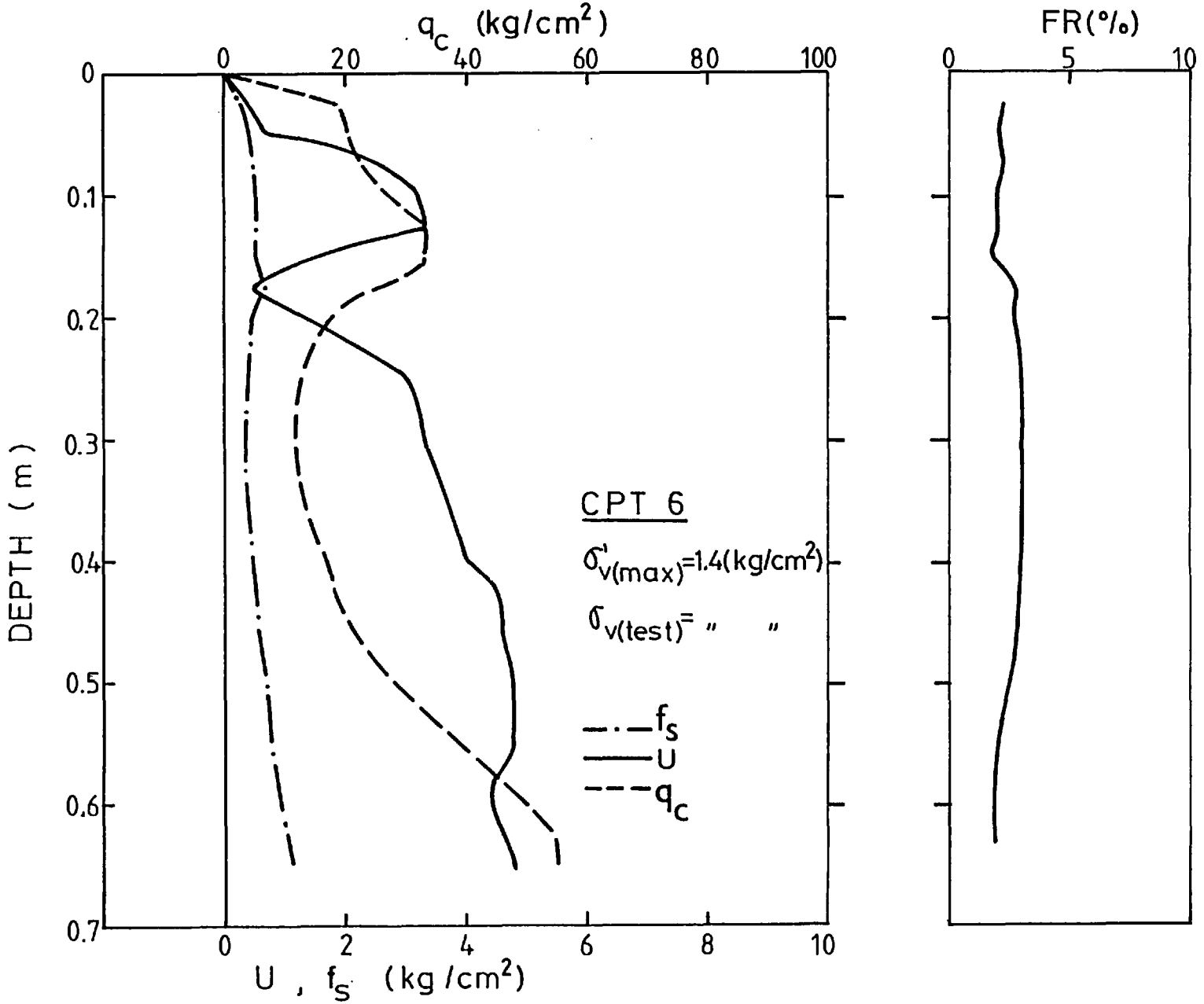


FIGURE 8.6 - CONTINUOUS CONE PENETRATION TEST.

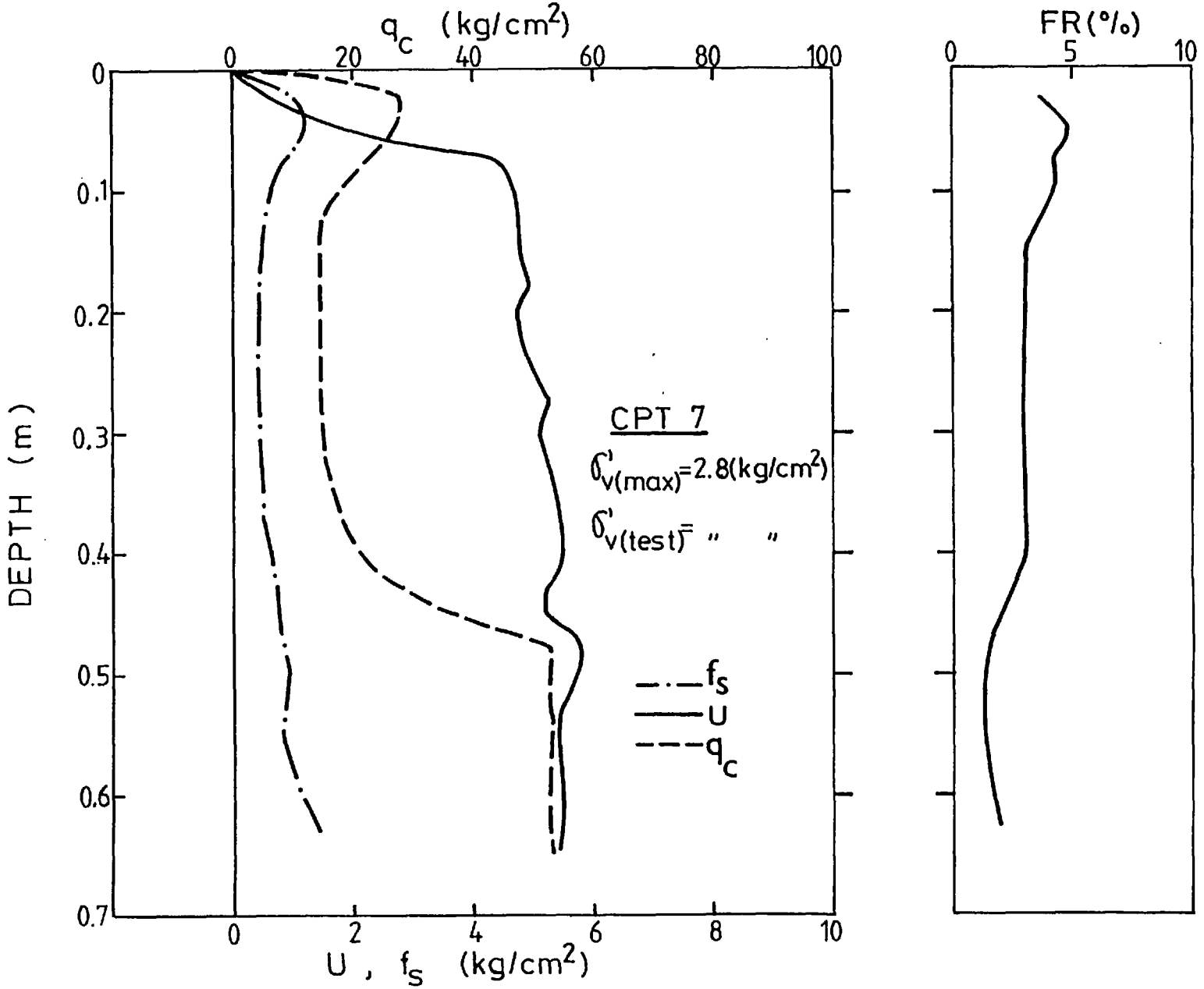


FIGURE 8.7 - CONTINUOUS CONE PENETRATION TEST.

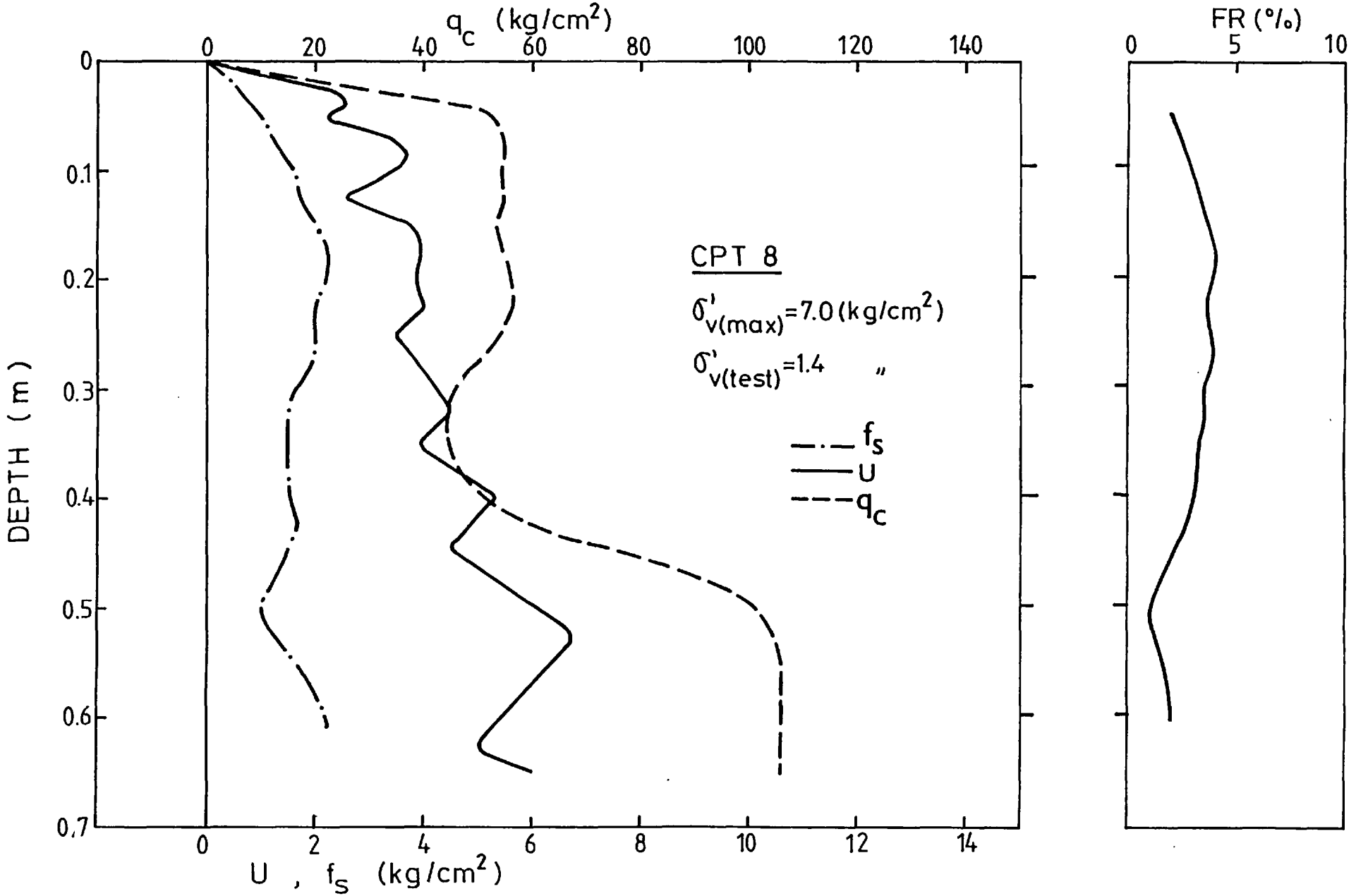


FIGURE 8.8 - CONTINUOUS CONE PENETRATION TEST.

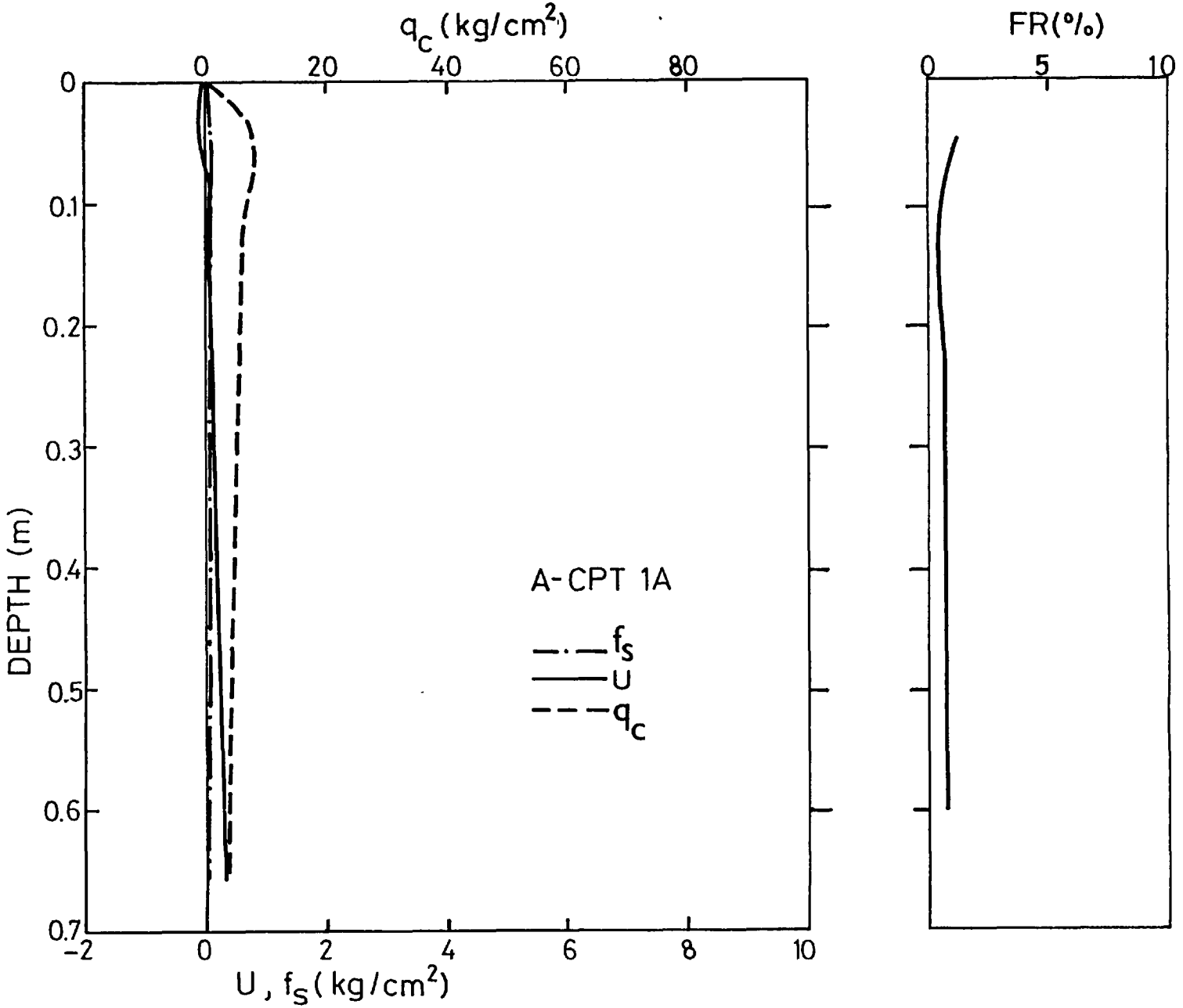


FIGURE 8.9 - CONTINUOUS CONE PENETRATION TEST-'ASIDE'.

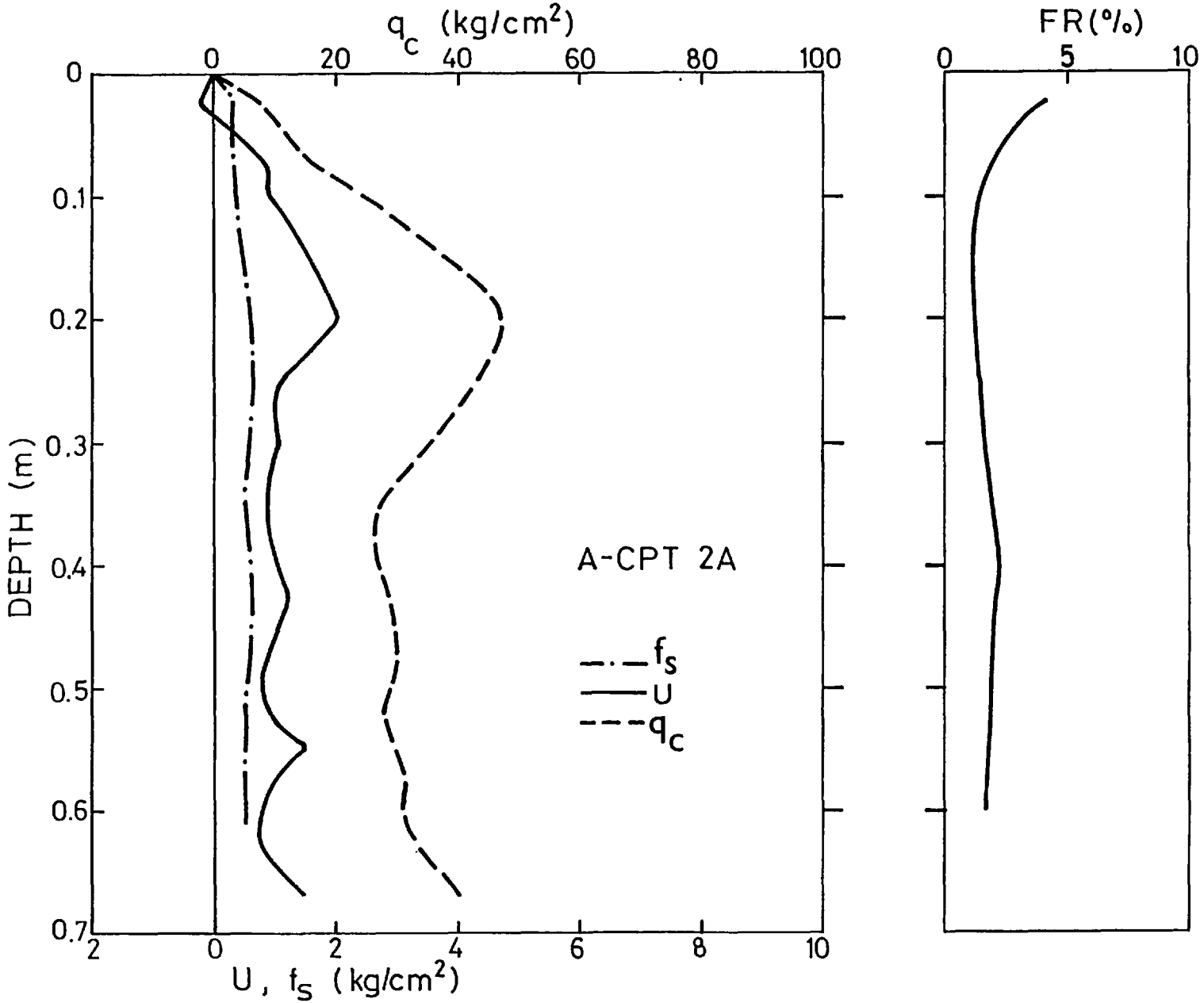


FIGURE 8.10 - CONTINUOUS CONE PENETRATION TEST-'ASIDE'.

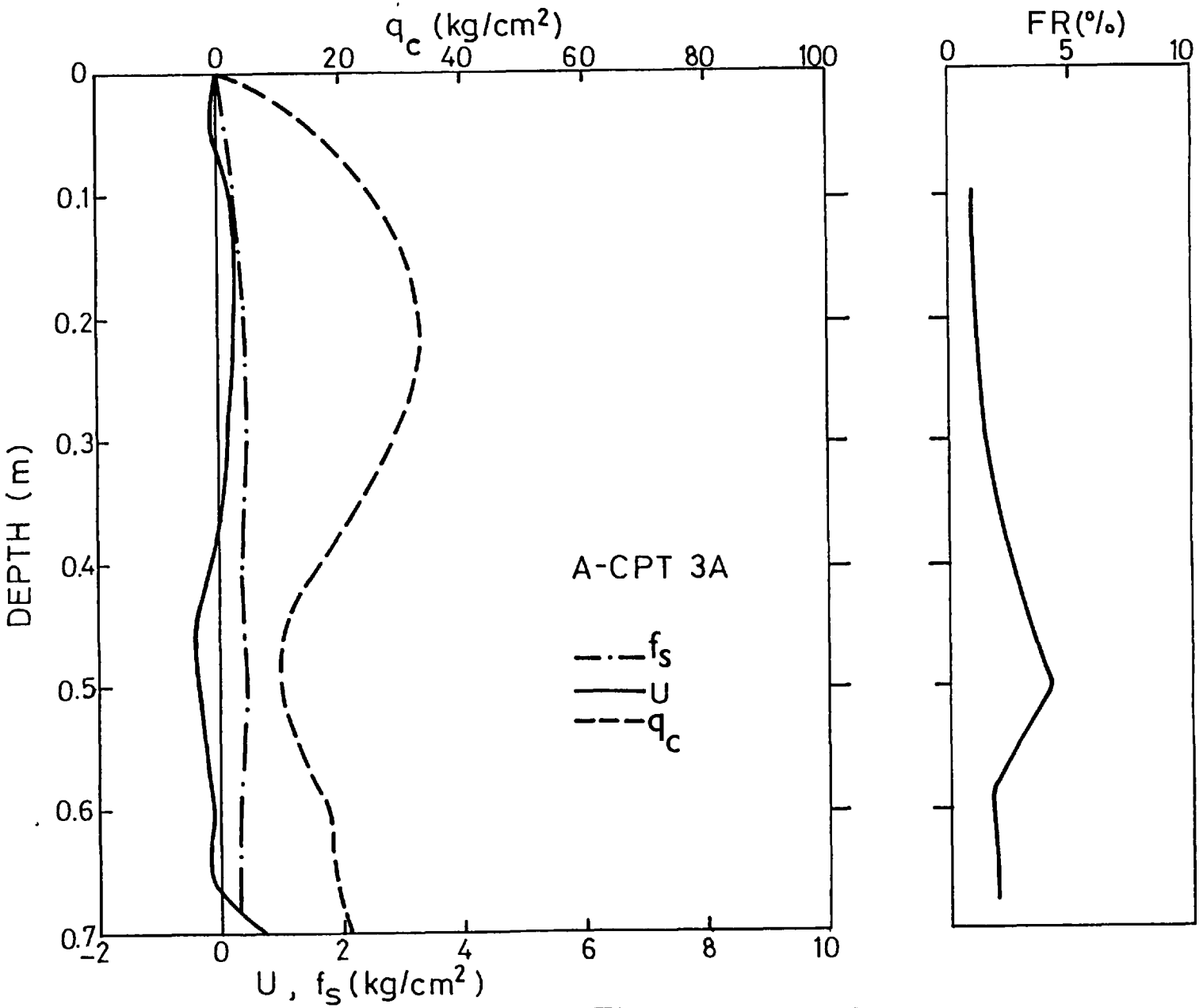


FIGURE 8.11 - CONTINUOUS CONE PENETRATION TEST-'ASIDE'.

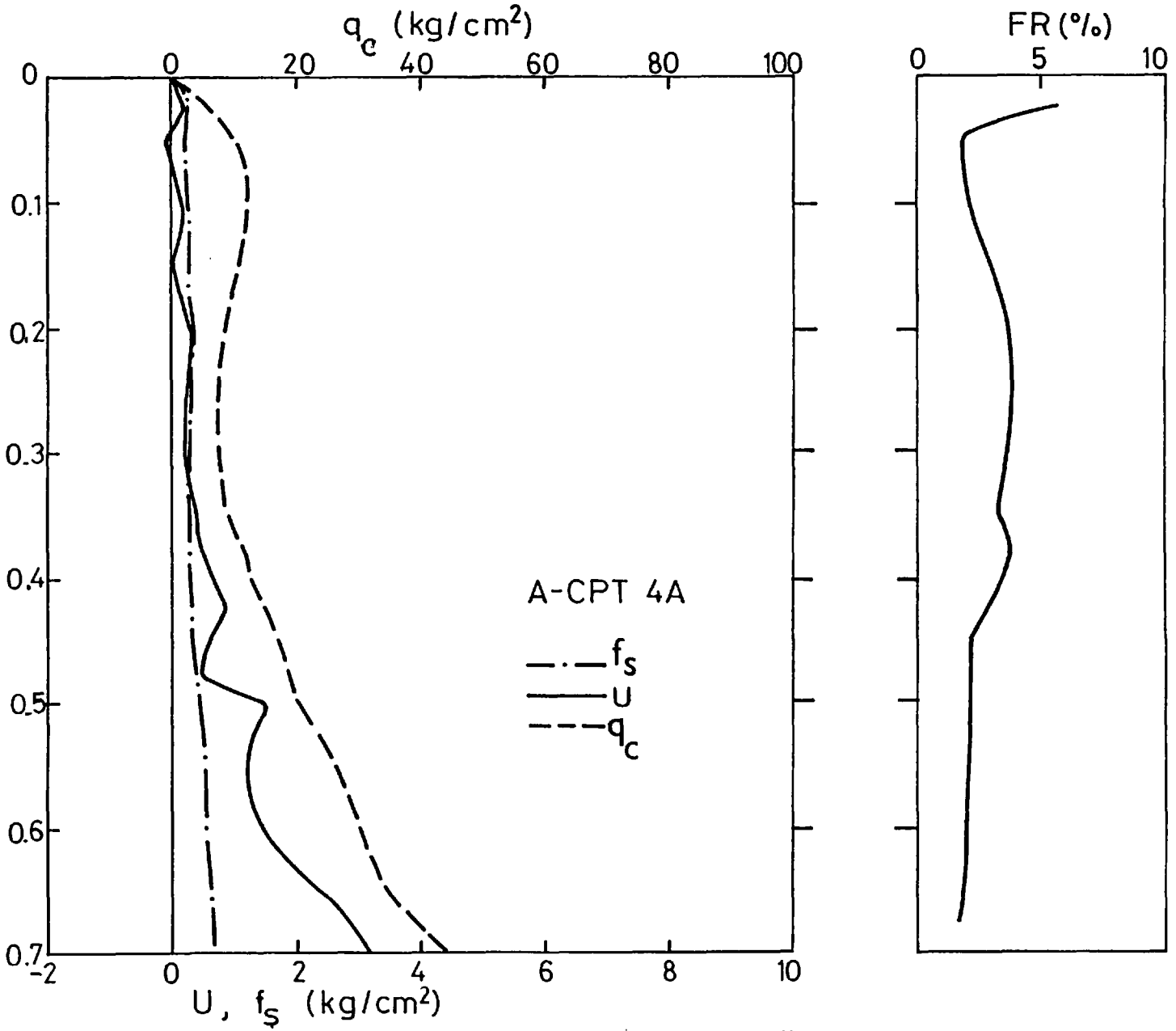


FIGURE 8.12 - CONTINUOUS CONE PENETRATION TEST-'ASIDE'.

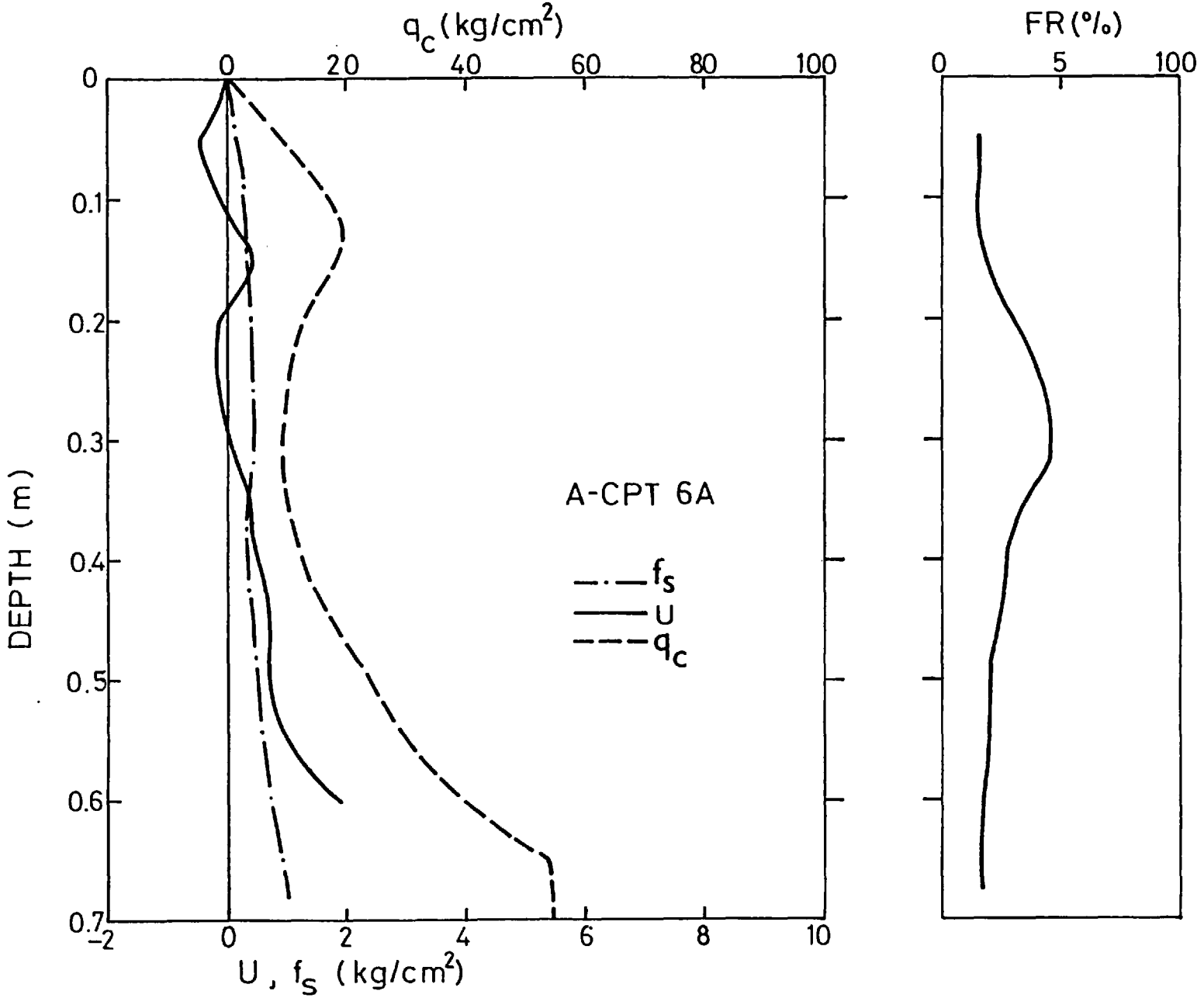


FIGURE 8.13 - CONTINUOUS CONE PENETRATION TEST-'ASIDE'.

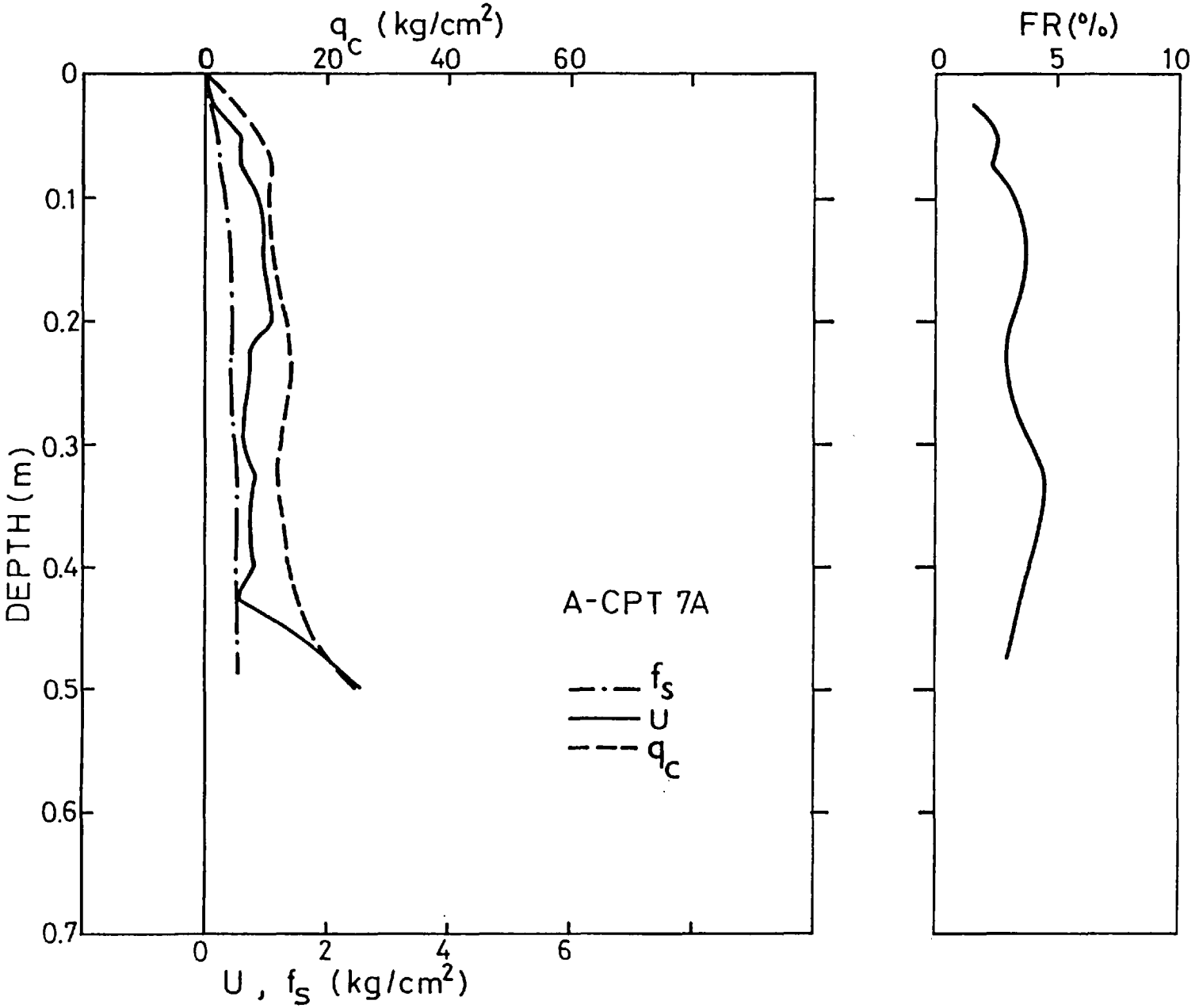


FIGURE 8.14 - CONTINUOUS CONE PENETRATION TEST-'ASIDE'.

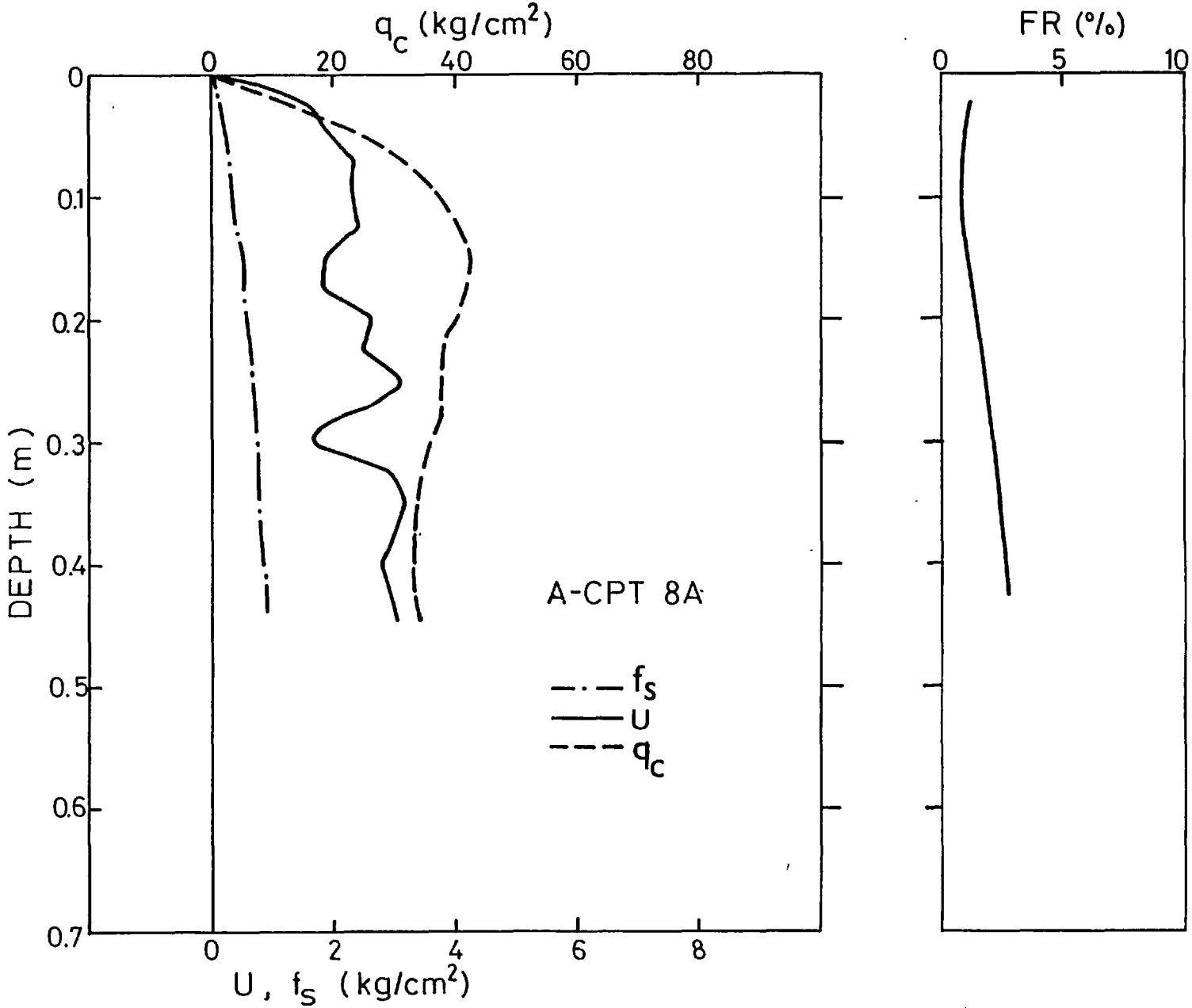


FIGURE 8.15 - CONTINUOUS CONE PENETRATION TEST-'ASIDE'.

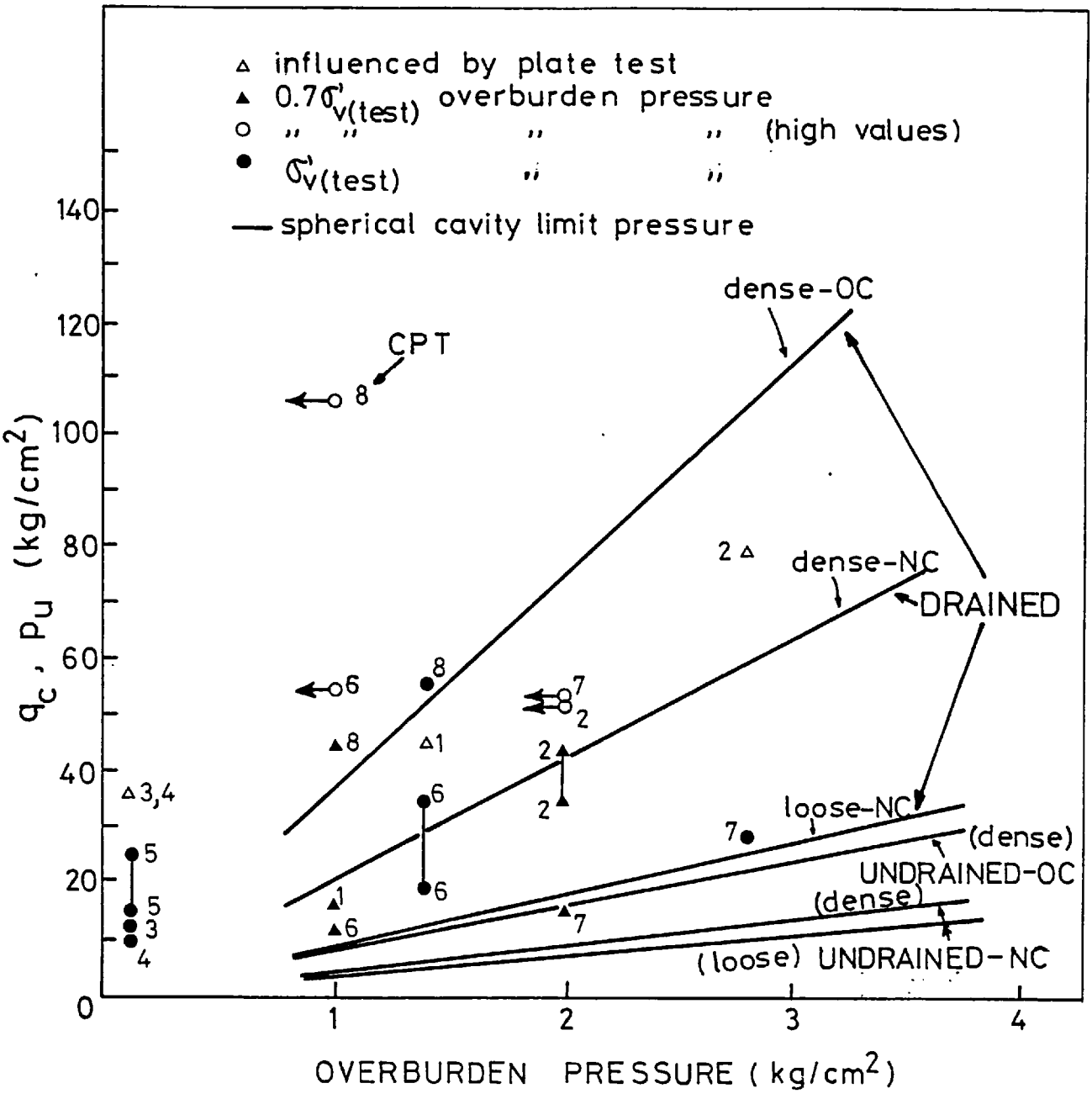


FIGURE 8.16 - EXPERIMENTAL AND PREDICTED POINT BEARING CAPACITY VALUES.

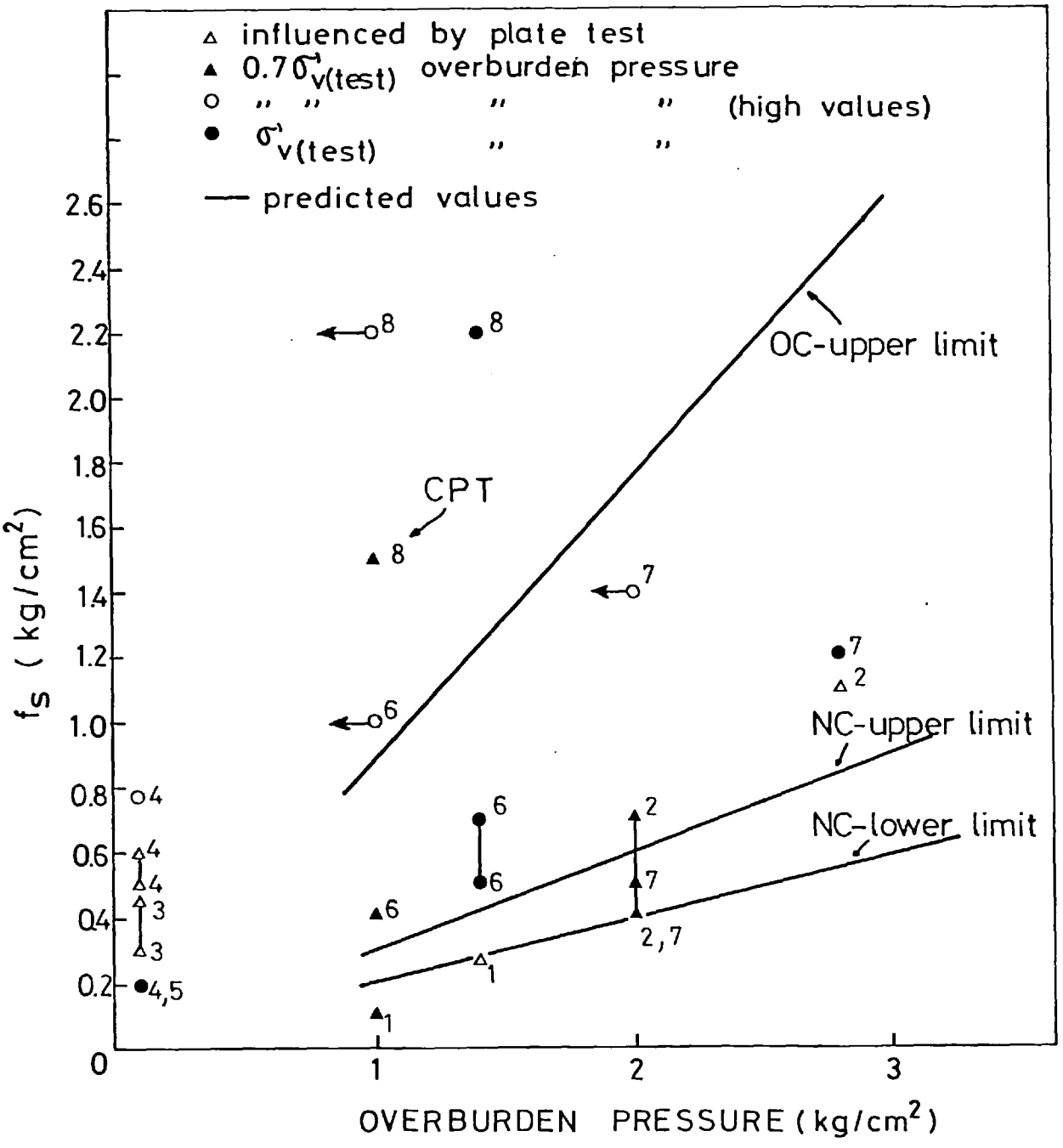


FIGURE 8.17 - EXPERIMENTAL AND PREDICTED FRICTION SLEEVE RESISTANCE VALUES.

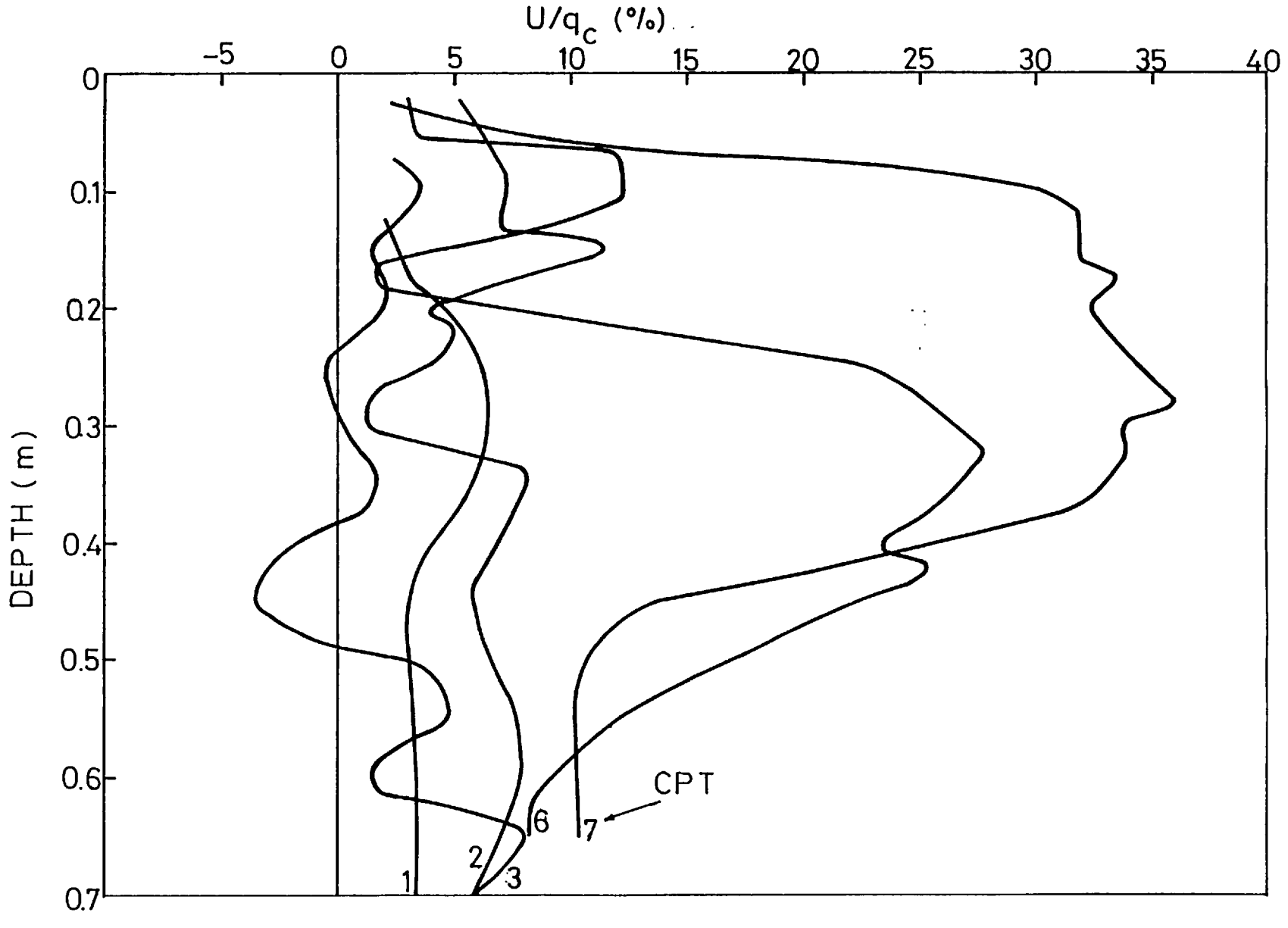


FIGURE 8.18 - PORE PRESSURE RATIO FOR NC SAMPLES.

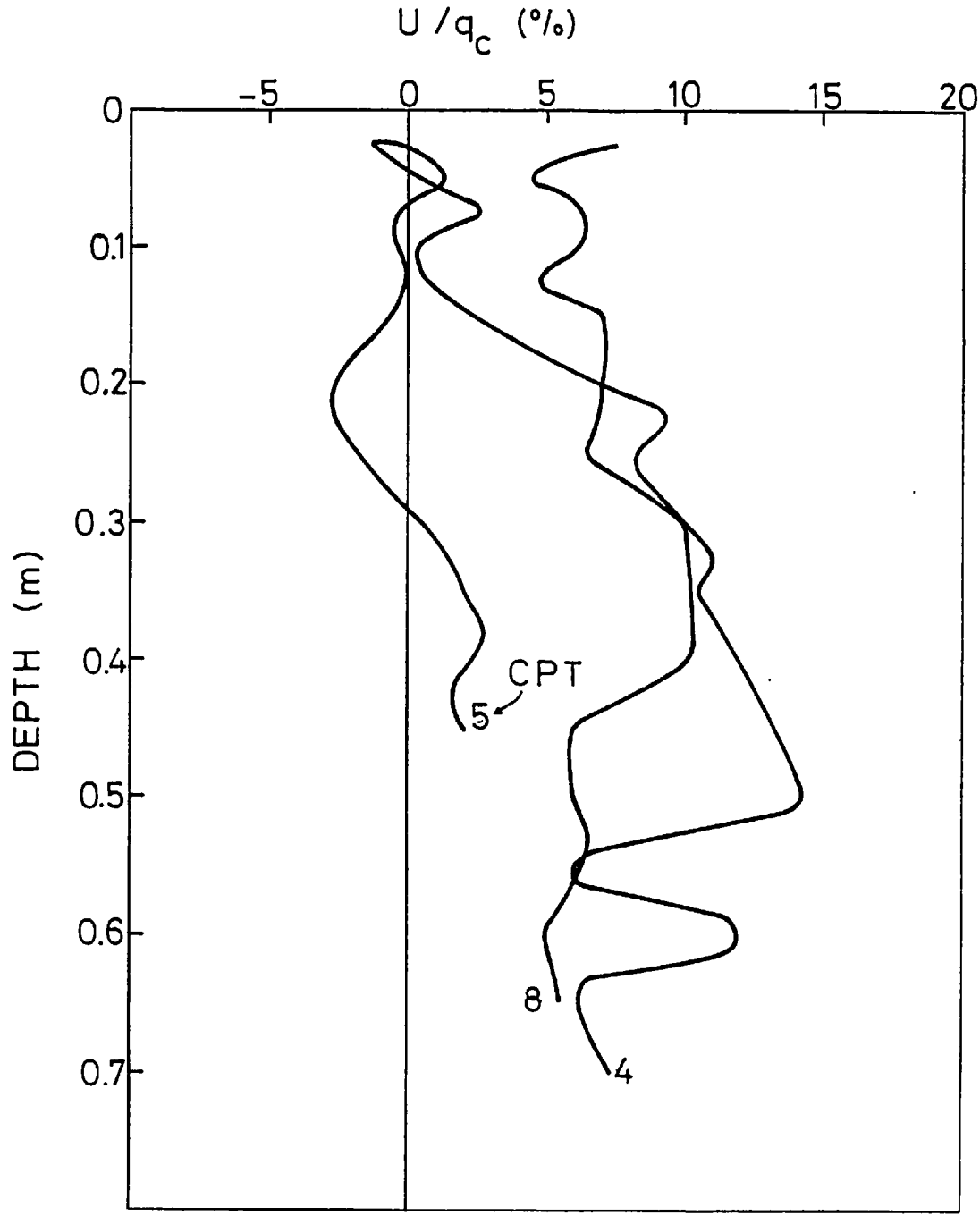


FIGURE 8.19 - PORE PRESSURE RATIO FOR OC SAMPLES.

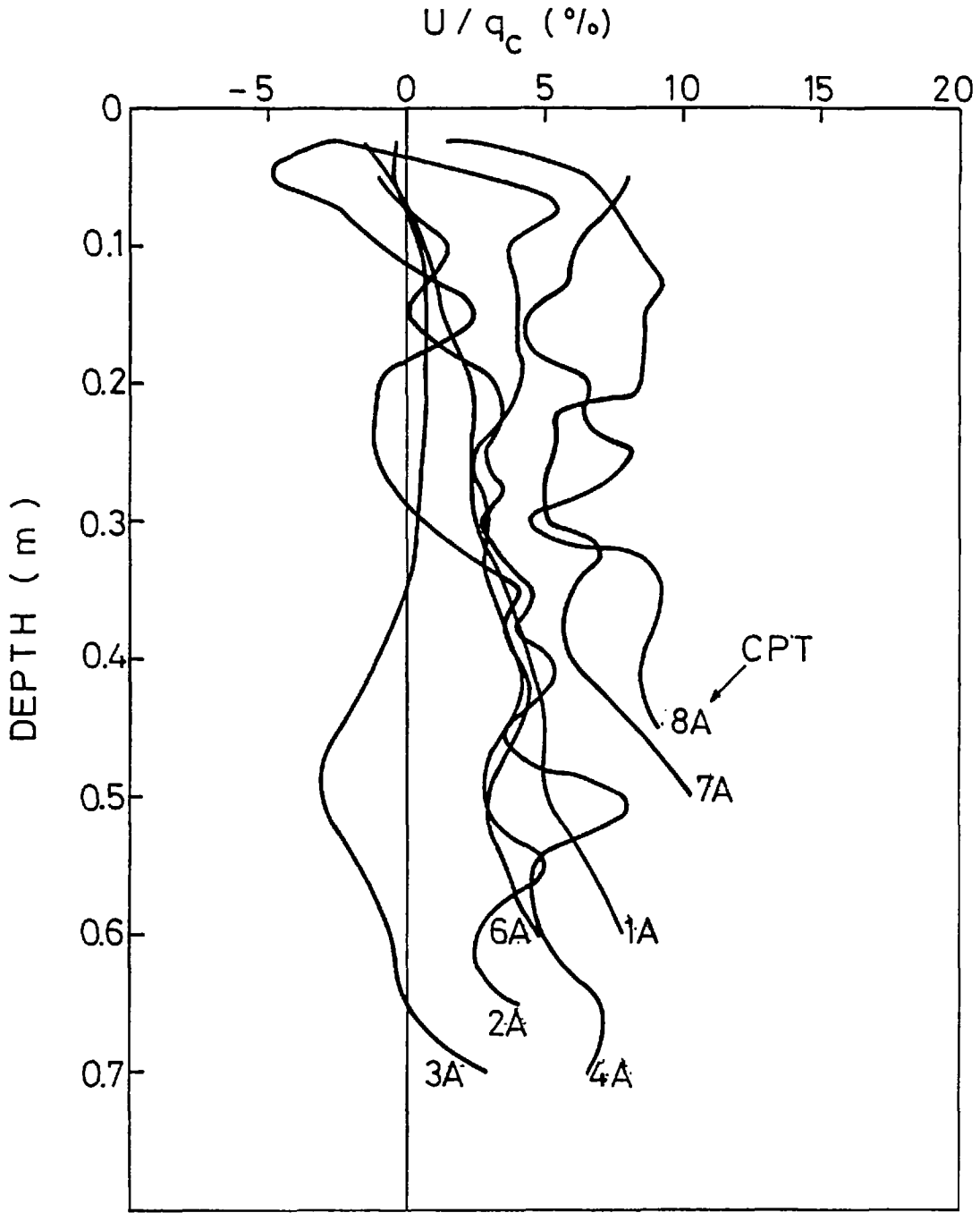


FIGURE 8.20 - PORE PRESSURE RATIO FOR OC SAMPLES-'ASIDE' TESTS.

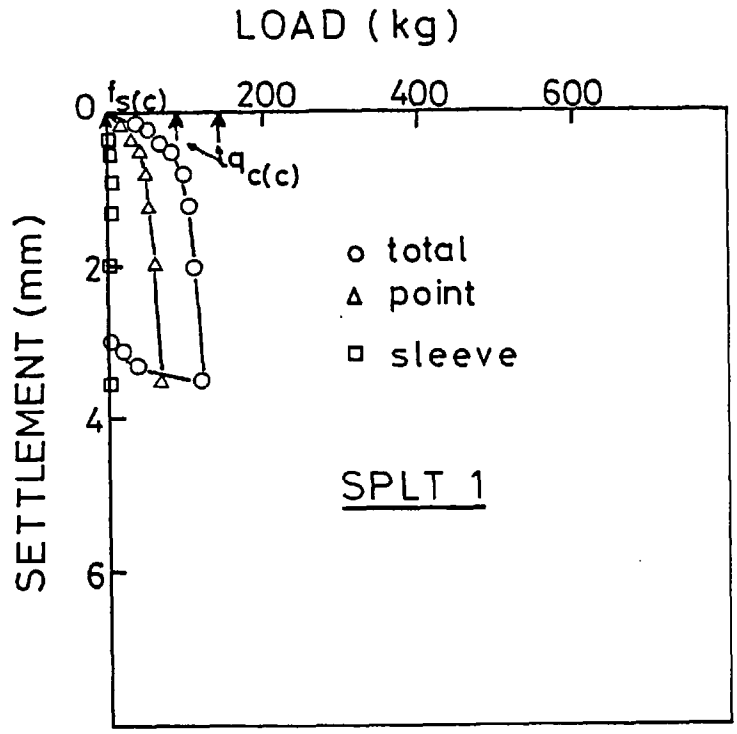


FIGURE 8.21 - STATIC PENETROMETER LOADING TEST.

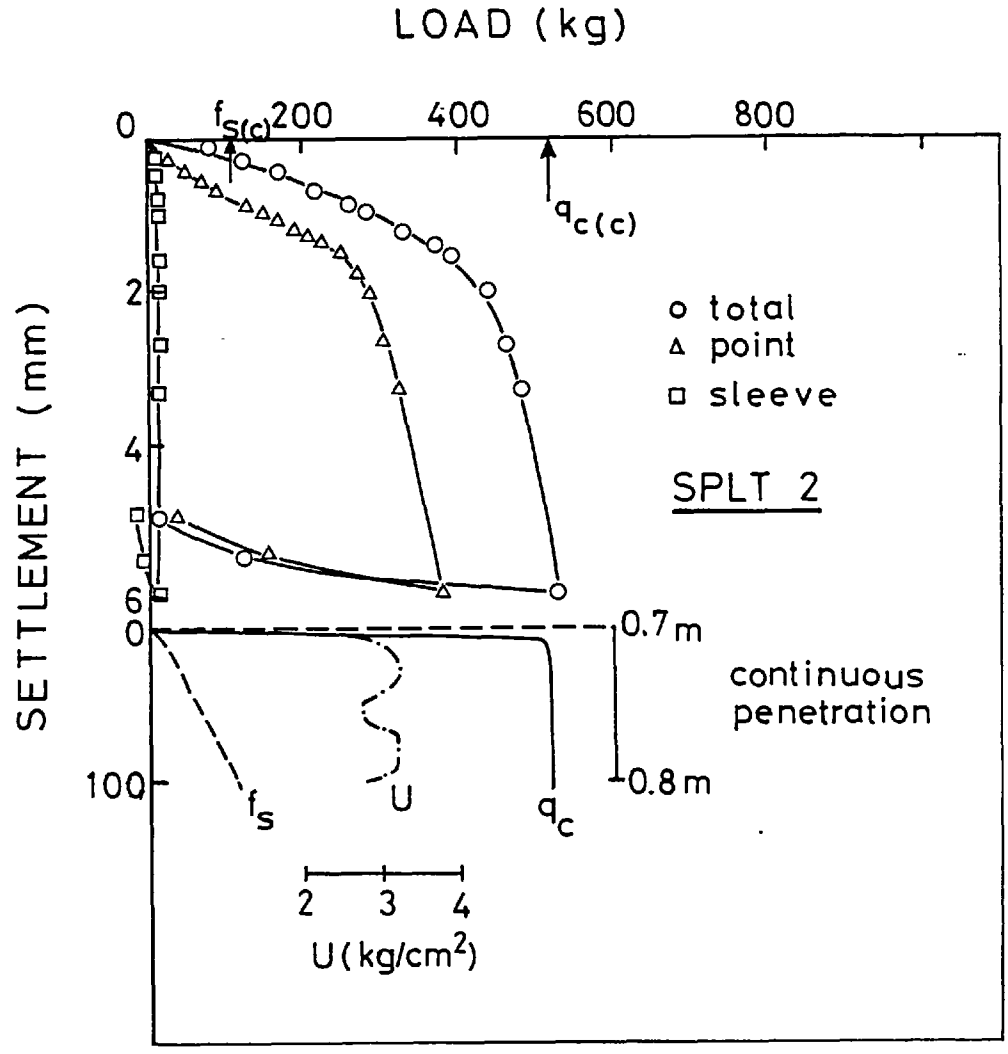


FIGURE 8.22 - STATIC PENETROMETER LOADING TEST.

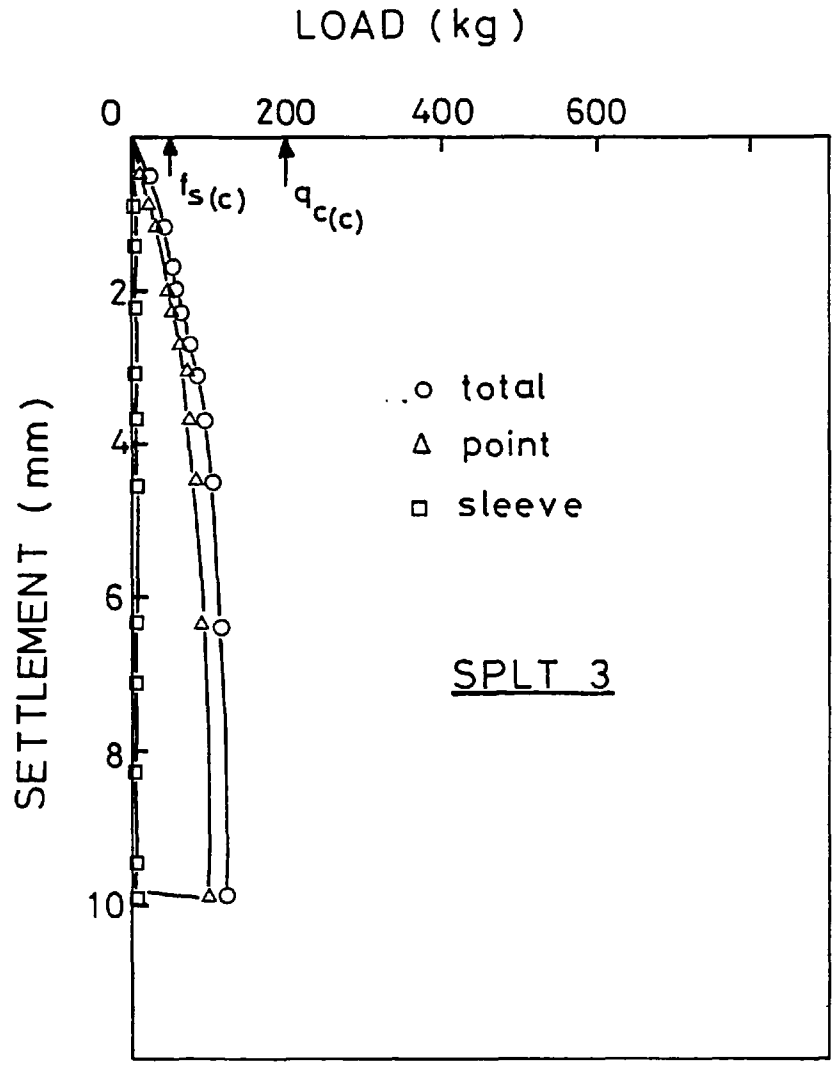


FIGURE 8.23 - STATIC PENETROMETER LOADING TEST.

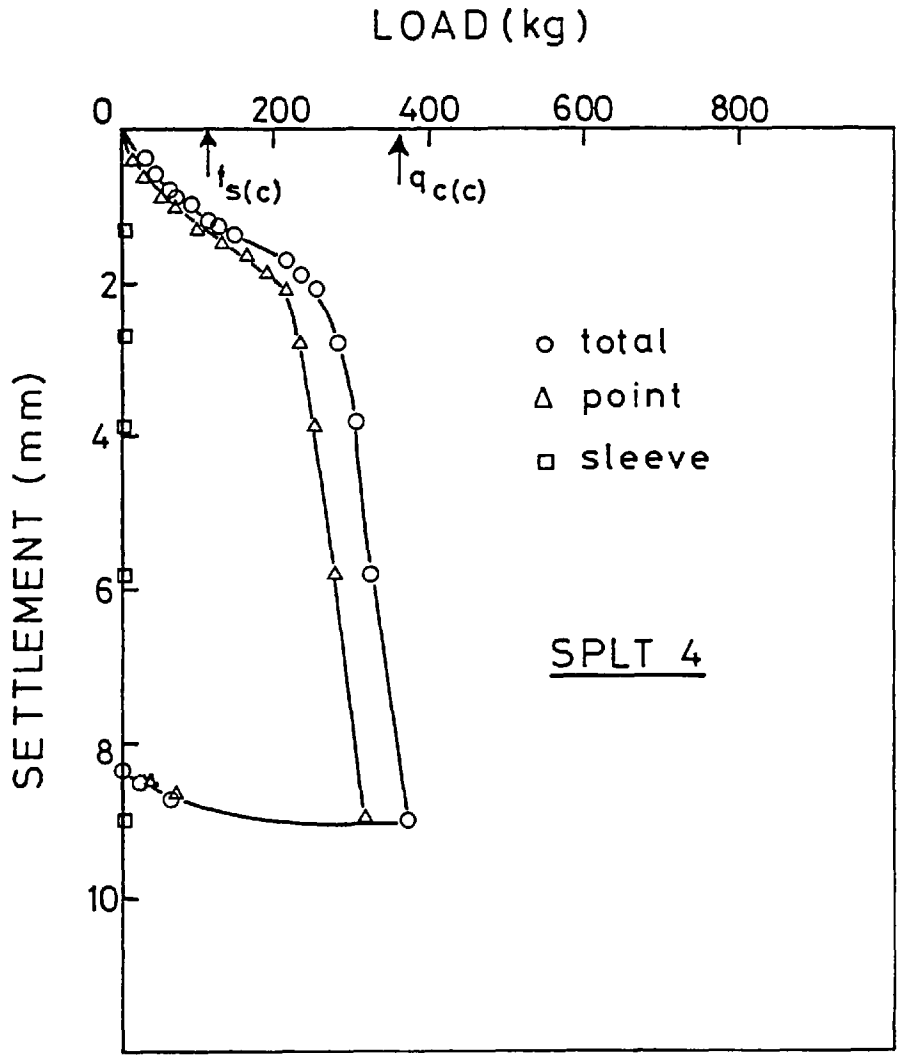


FIGURE 8.24 - STATIC PENETROMETER LOADING TEST.

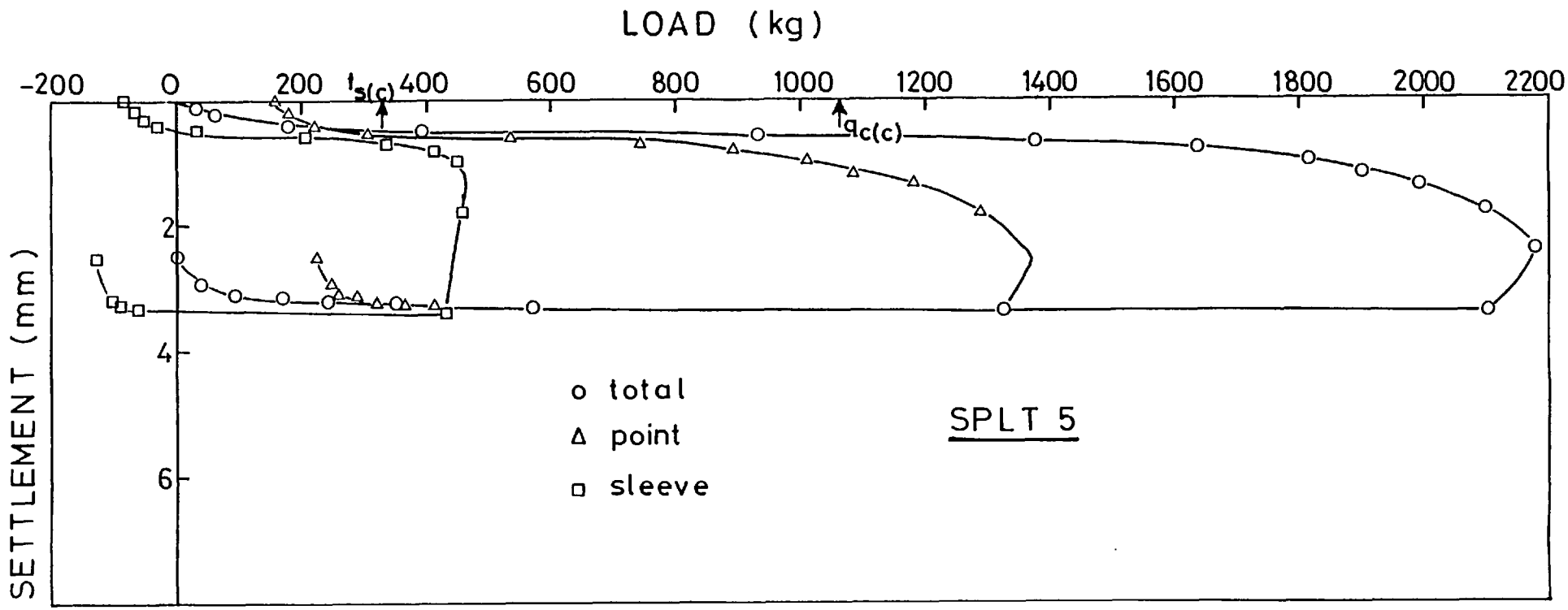


FIGURE 8.25 - STATIC PENETROMETER LOADING TEST.

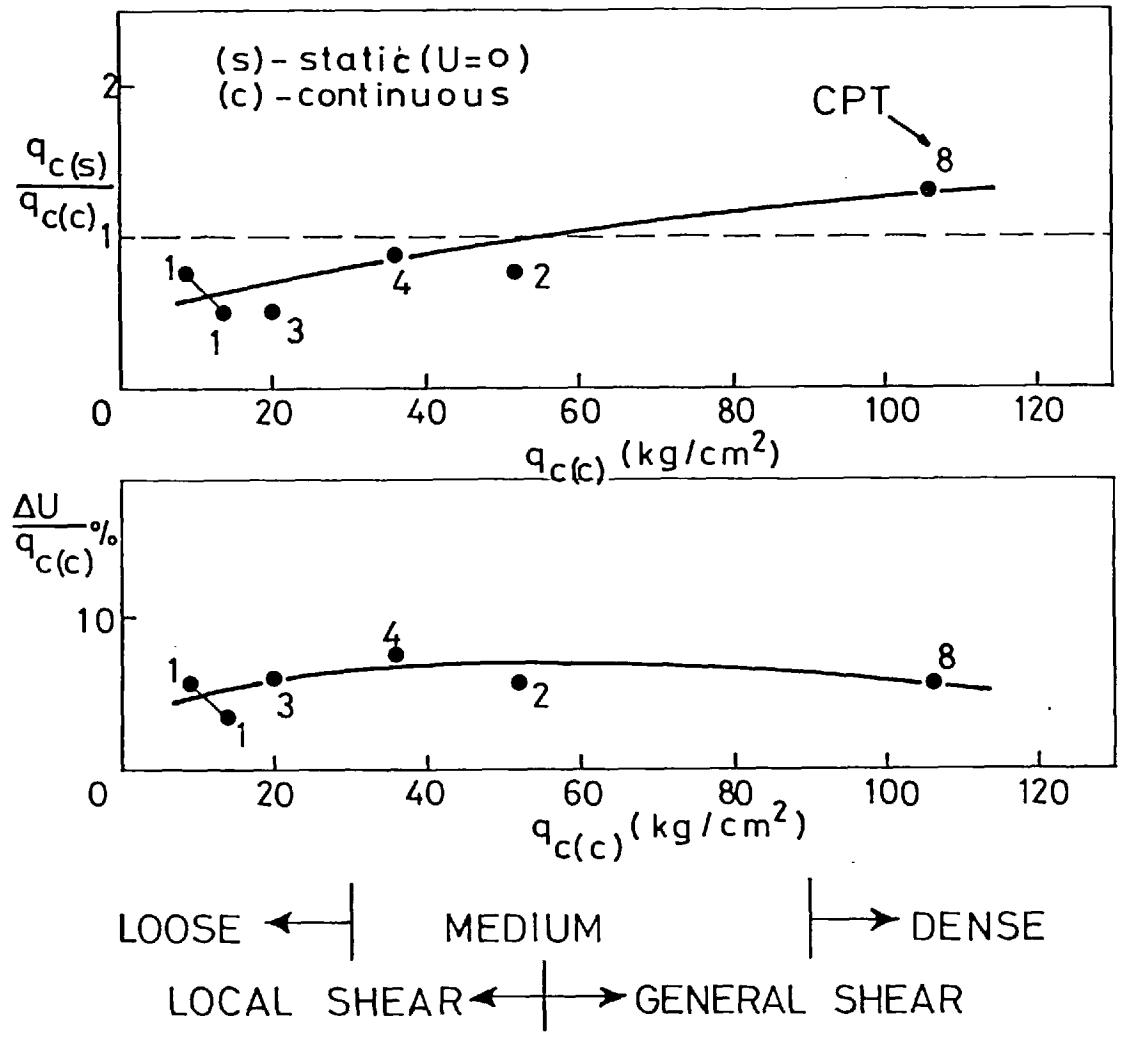


FIGURE 8.26 - COMPARISON BETWEEN STATIC AND CONTINUOUS CONE RESISTANCE.

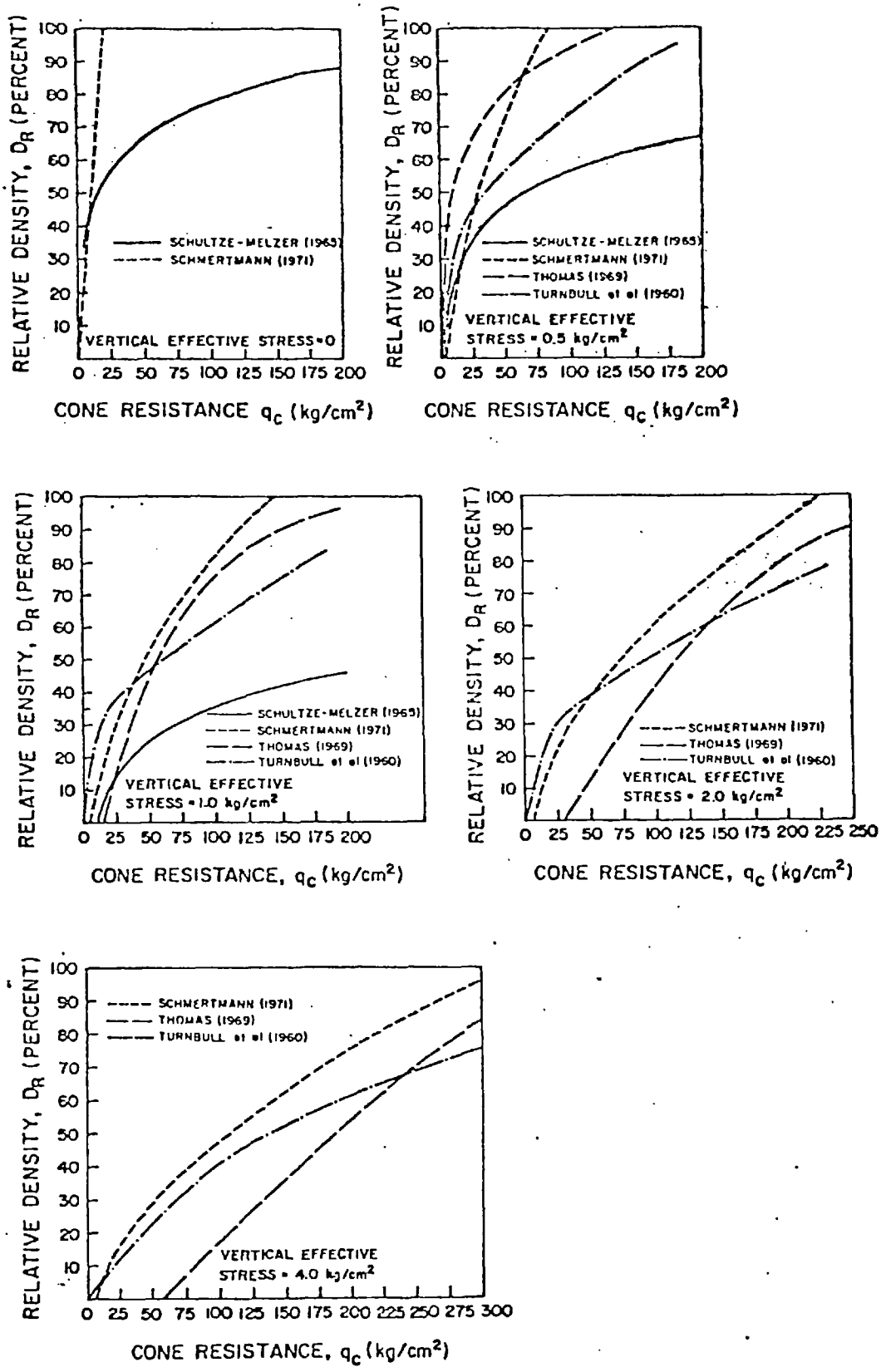


FIGURE 8.27 - CORRELATIONS BETWEEN STATIC CONE RESISTANCE, VERTICAL EFFECTIVE STRESS, AND RELATIVE DENSITY (AFTER MITCHELL & GARDNER, 1975).

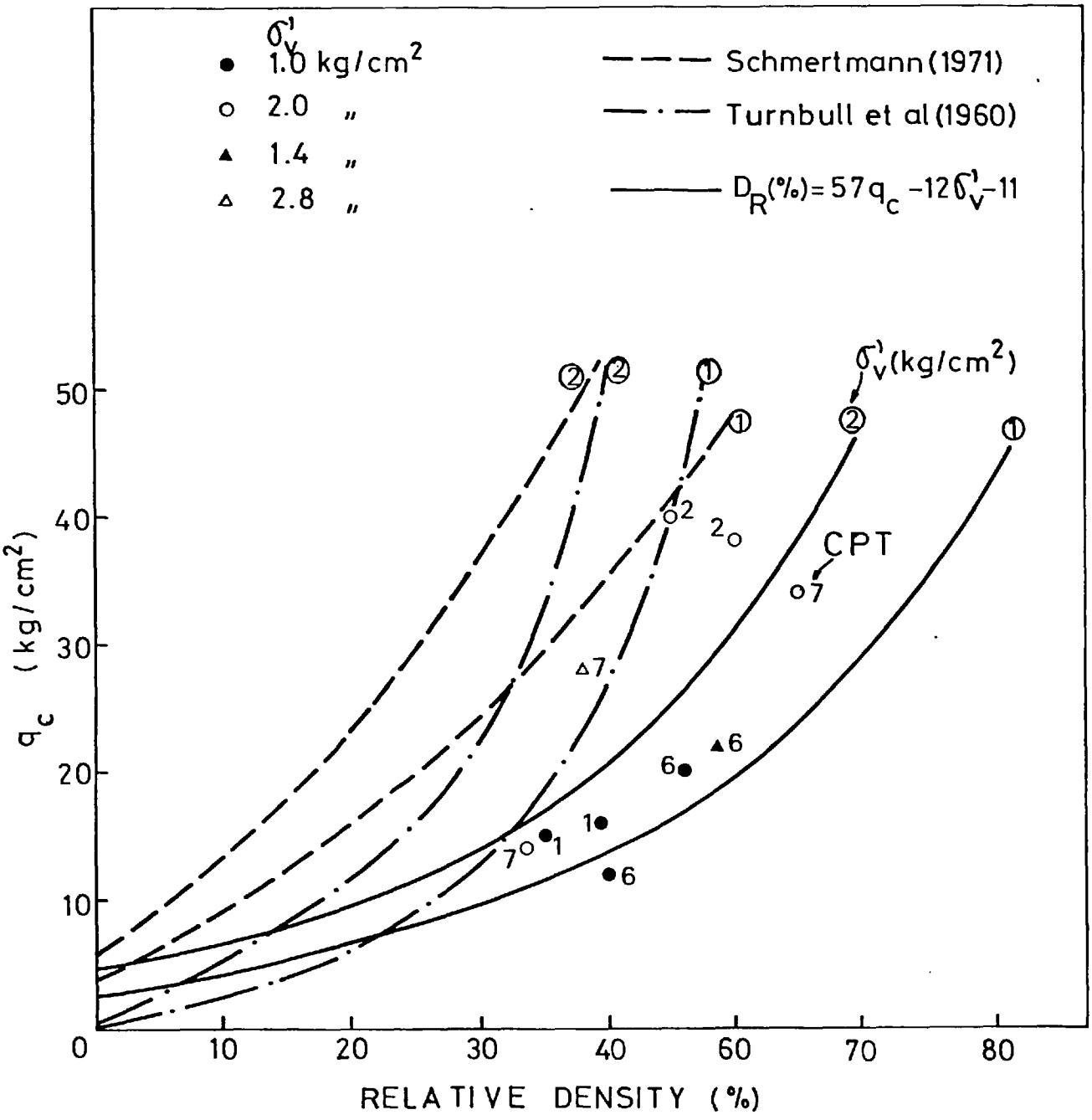


FIGURE 8.28 - RELATIONSHIP BETWEEN CONE RESISTANCE AND RELATIVE DENSITY.

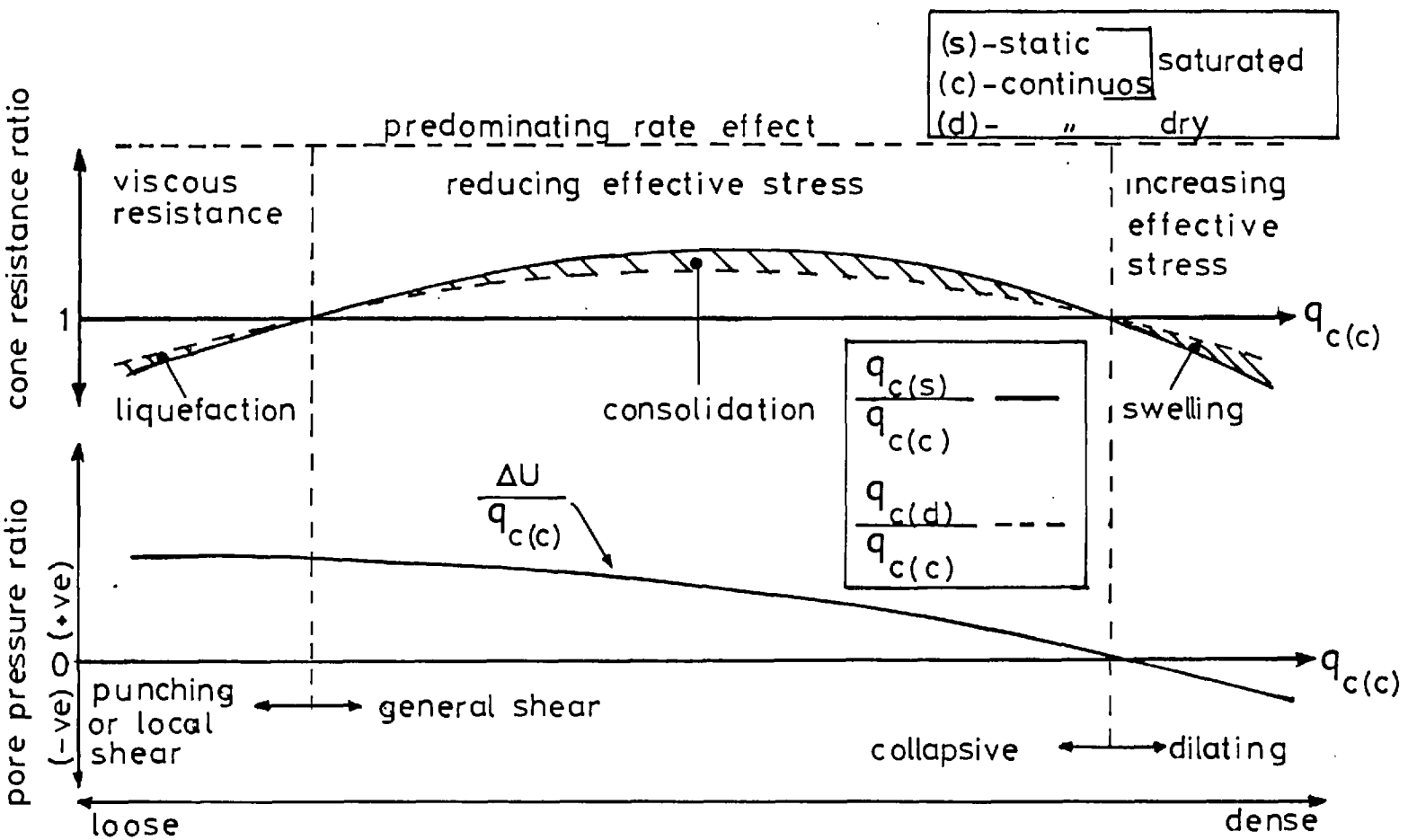


FIGURE 8.29 - RATE EFFECT ON PENETRATION RESISTANCES.

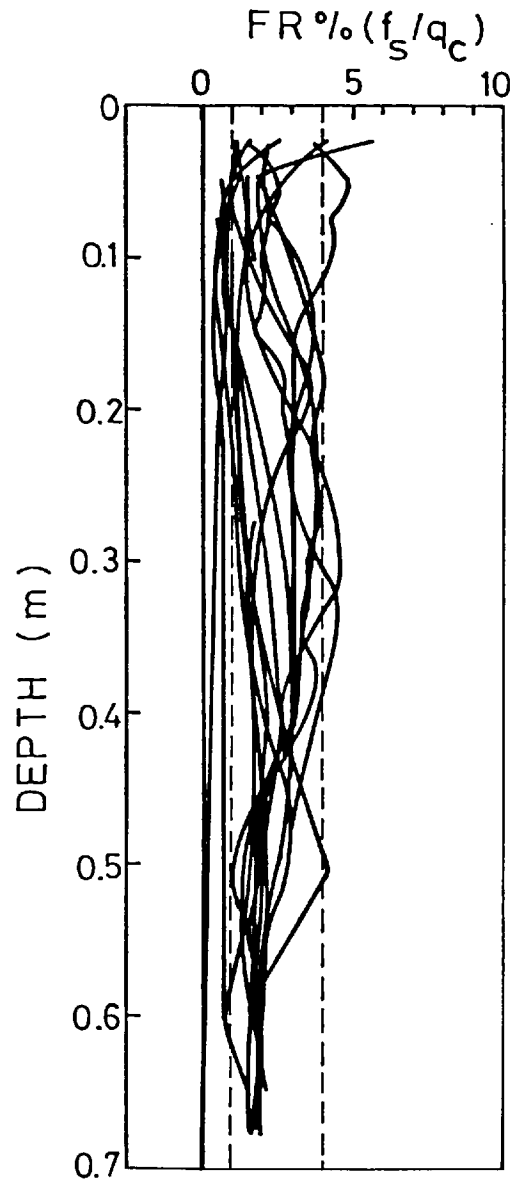


FIGURE 8.30 - FRICTION RATIO.

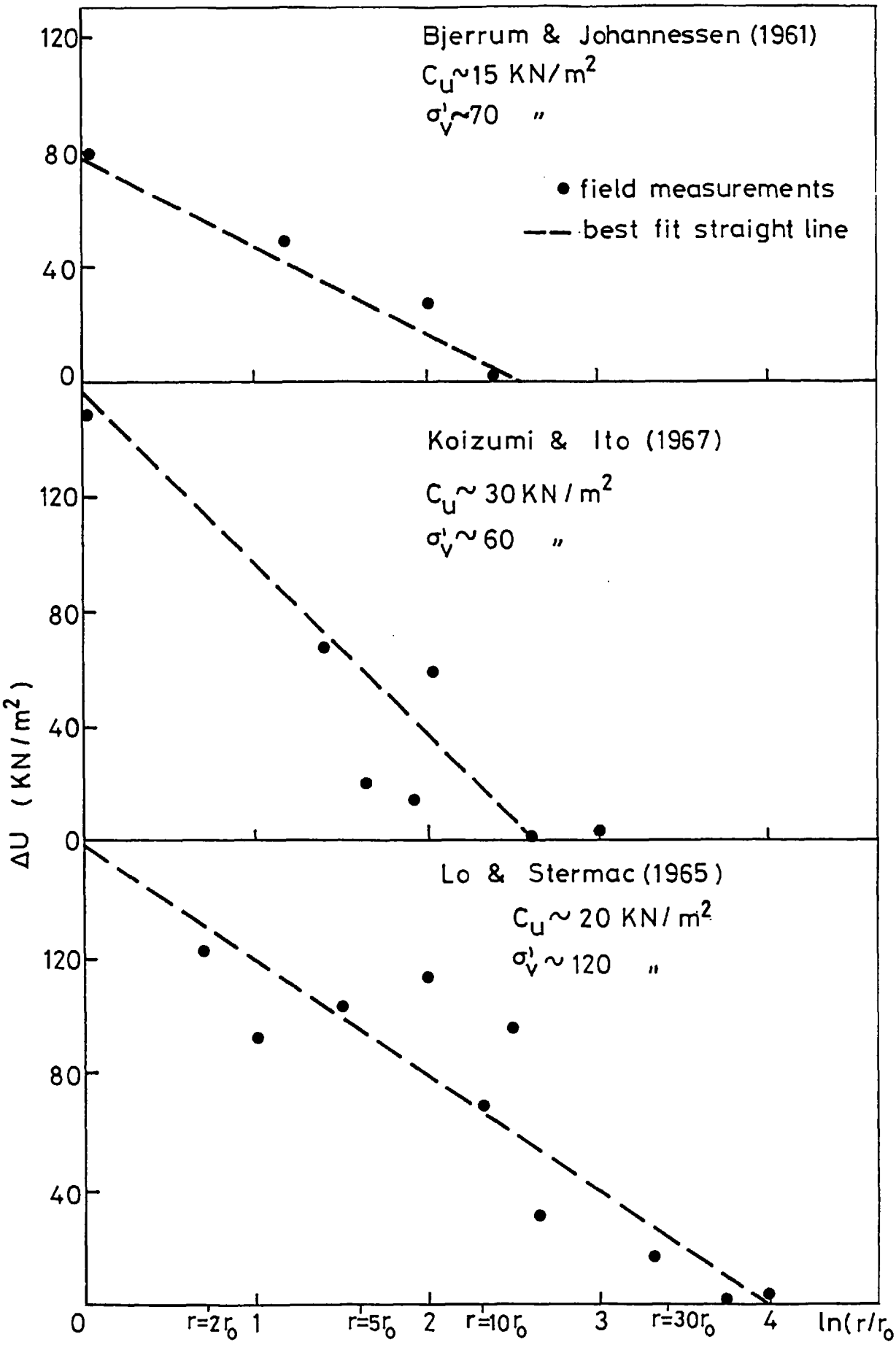


FIGURE 8.31 - FIELD MEASUREMENTS OF EXCESS PORE PRESSURE RESULTING FROM PILE DRIVING (AFTER RANDOLPH, 1977).

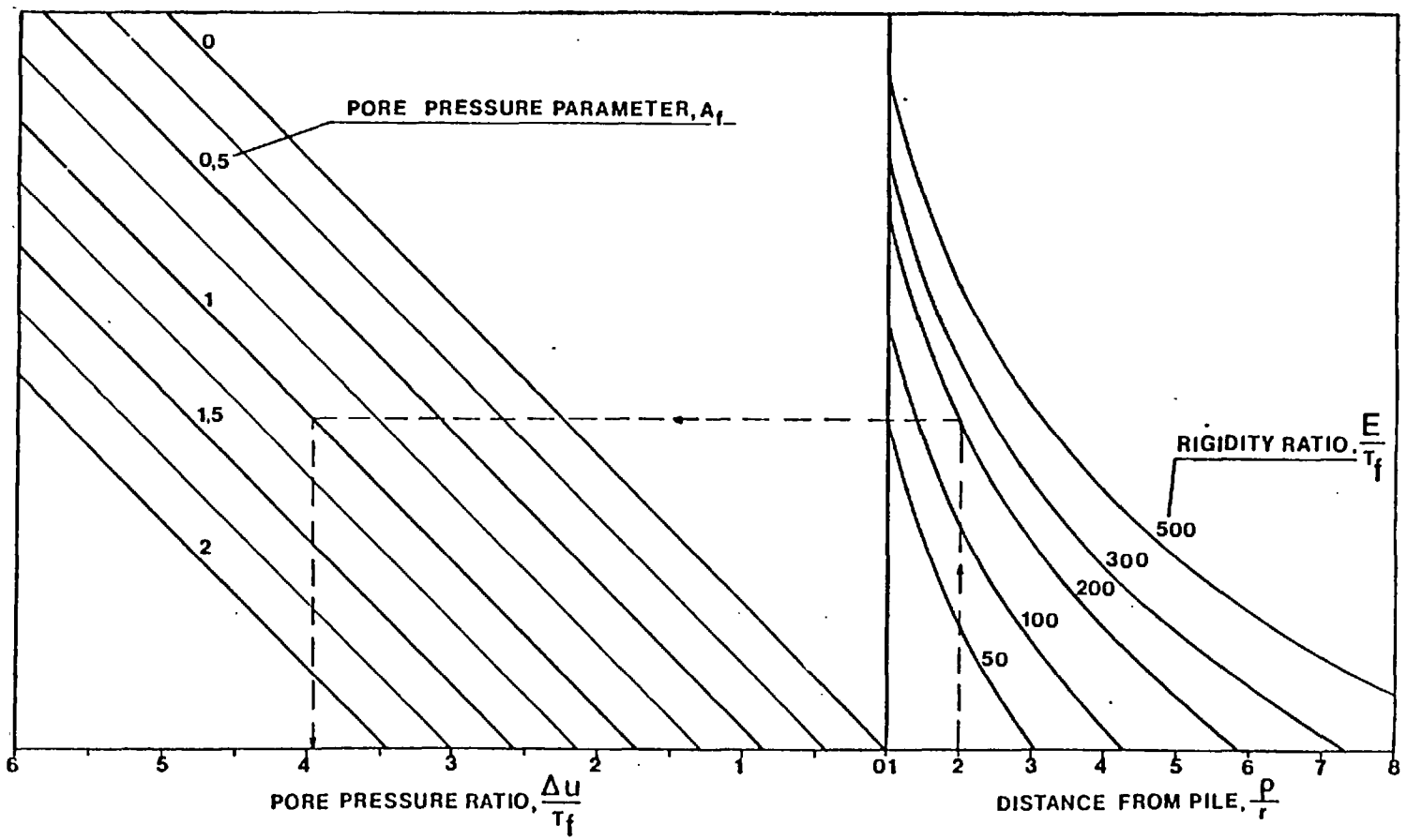


FIGURE 8.32 - VARIATION OF EXCESS PORE PRESSURE AS A FUNCTION OF THE SOIL RIGIDITY RATIO AND THE PORE PRESSURE PARAMETER A_f.

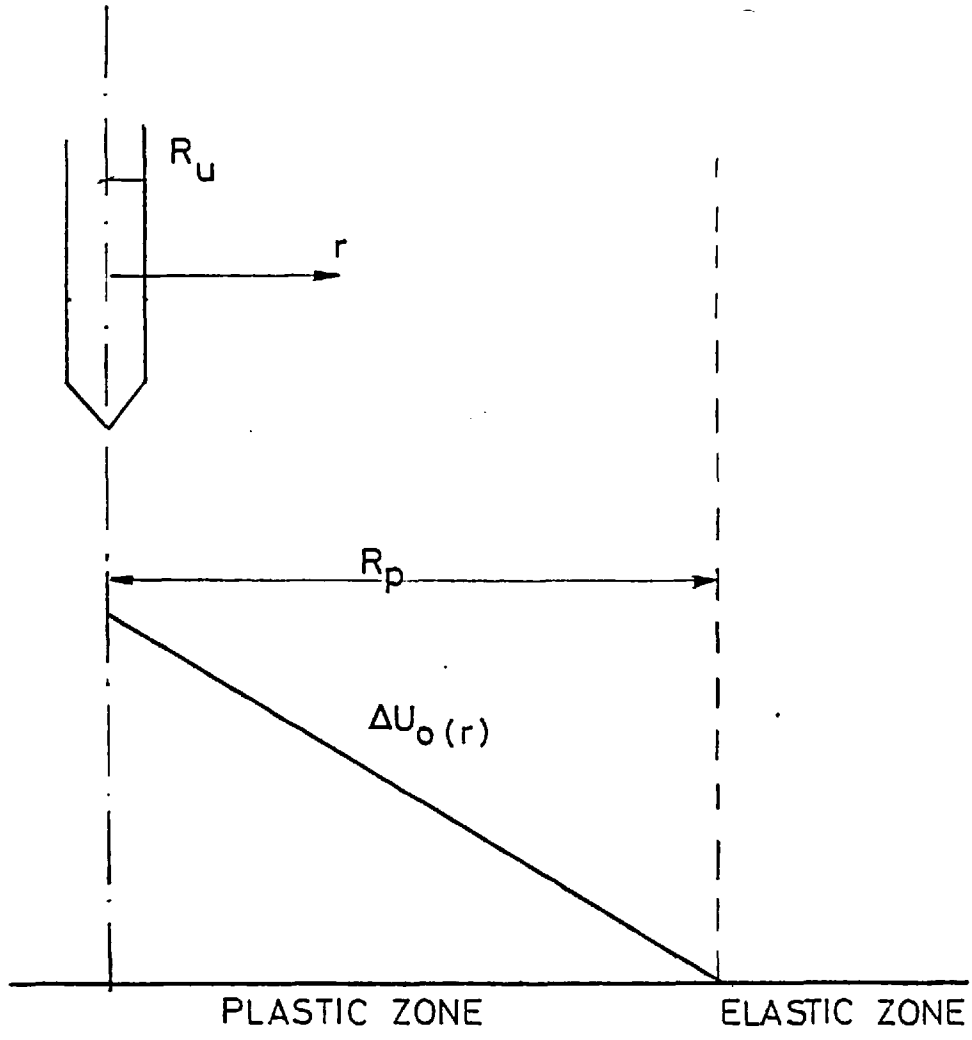
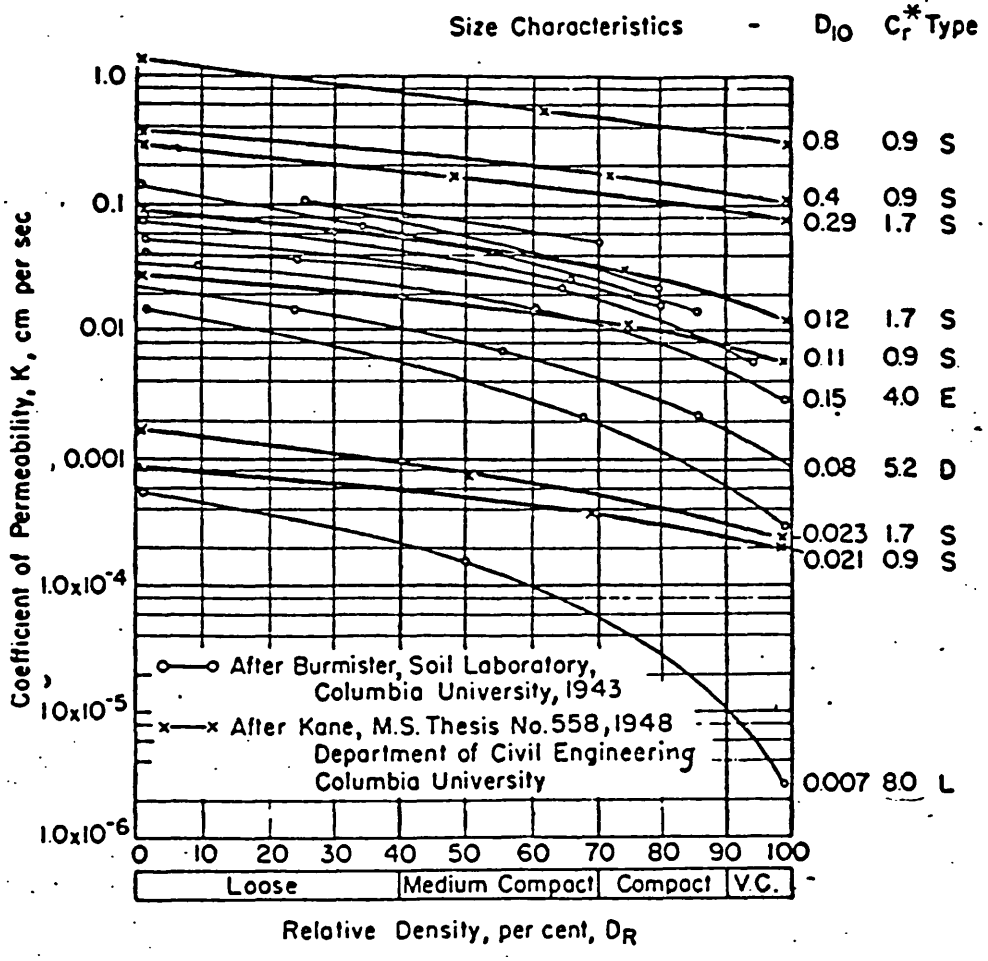


FIGURE 8.33 - PORE PRESSURE DISTRIBUTION WITHIN THE PLASTIC ZONE.



D_{10} = Hazen's effective size.
C_r = range of grain size defined by mean slope.
Type = letter designation of symmetric or asymmetric shape of grain size curves.

FIGURE 8.34 - PERMEABILITY-DENSITY RELATIONSHIPS (AFTER BURMISTER, 1954).

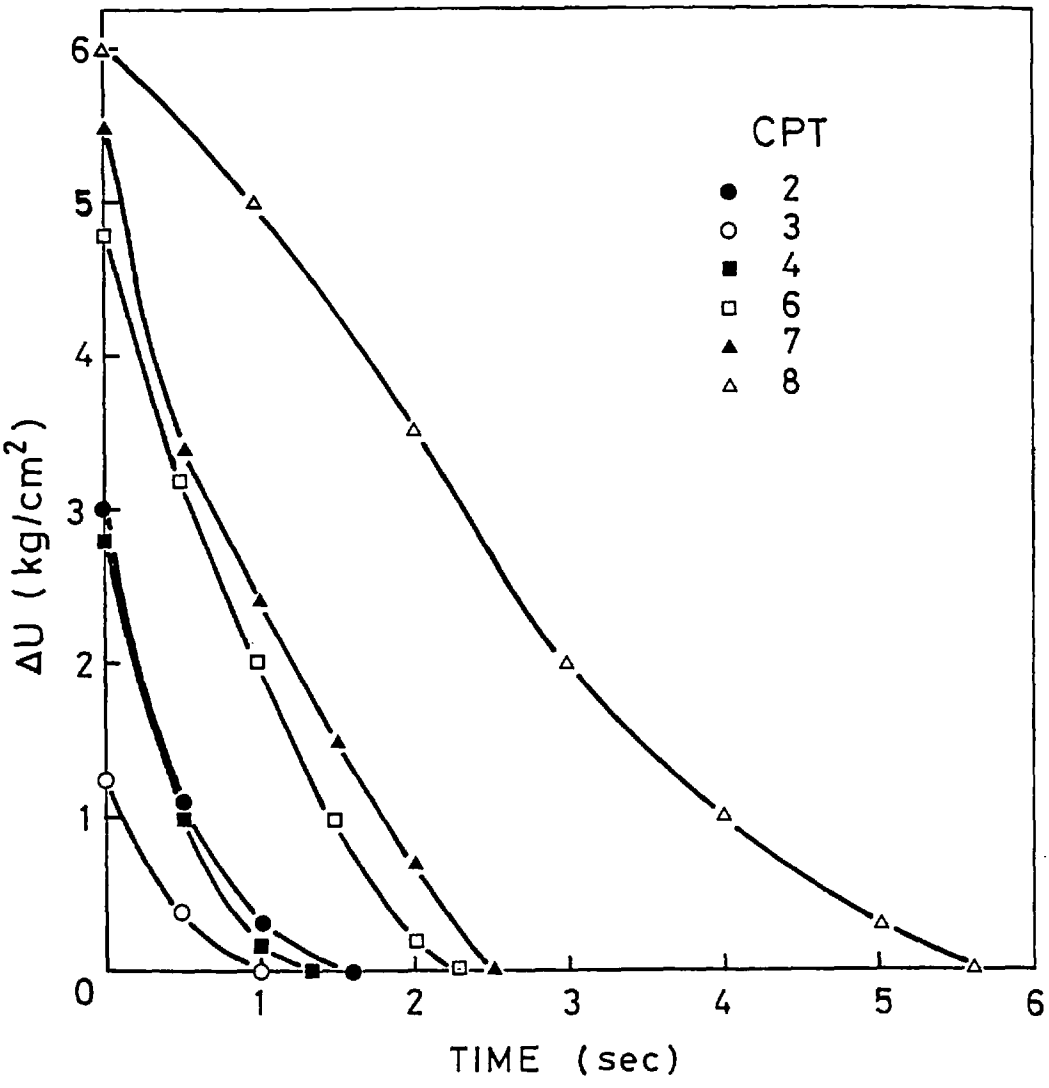


FIGURE 8.35 - DISSIPATION RATE OF EXCESS PORE PRESSURE WITH TIME.

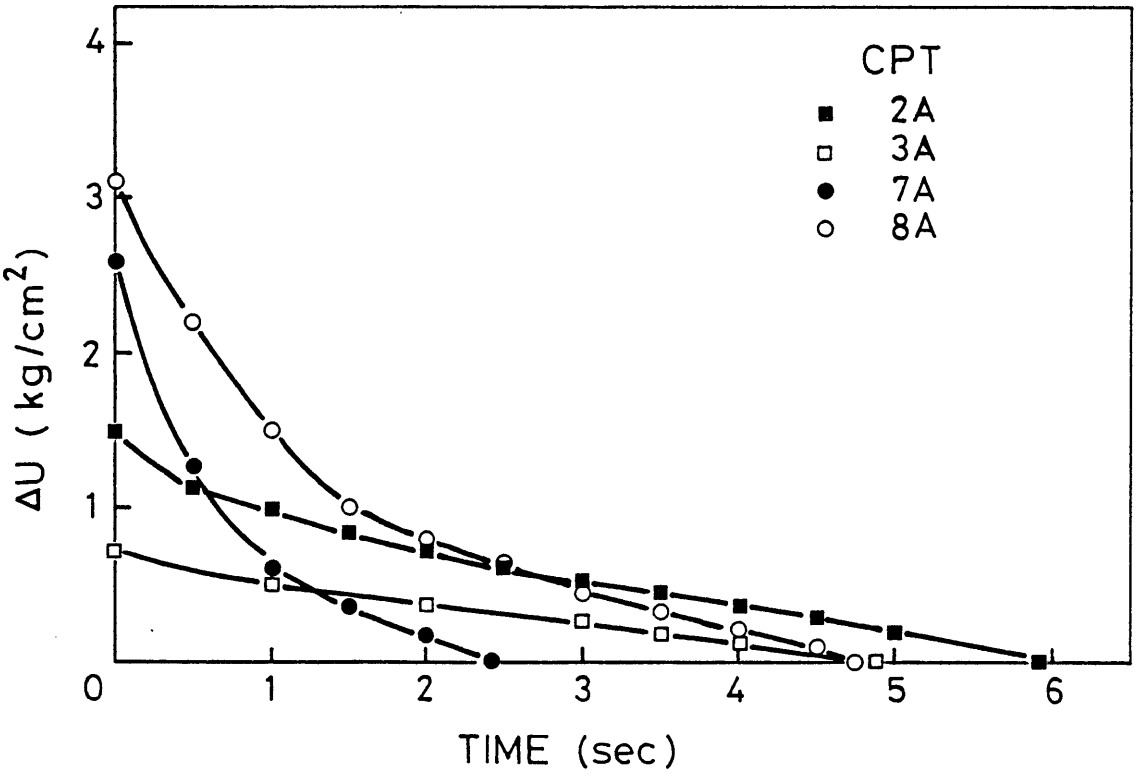


FIGURE 8.36 - DISSIPATION RATE OF EXCESS PORE PRESSURE WITH TIME-'ASIDE' TESTS.

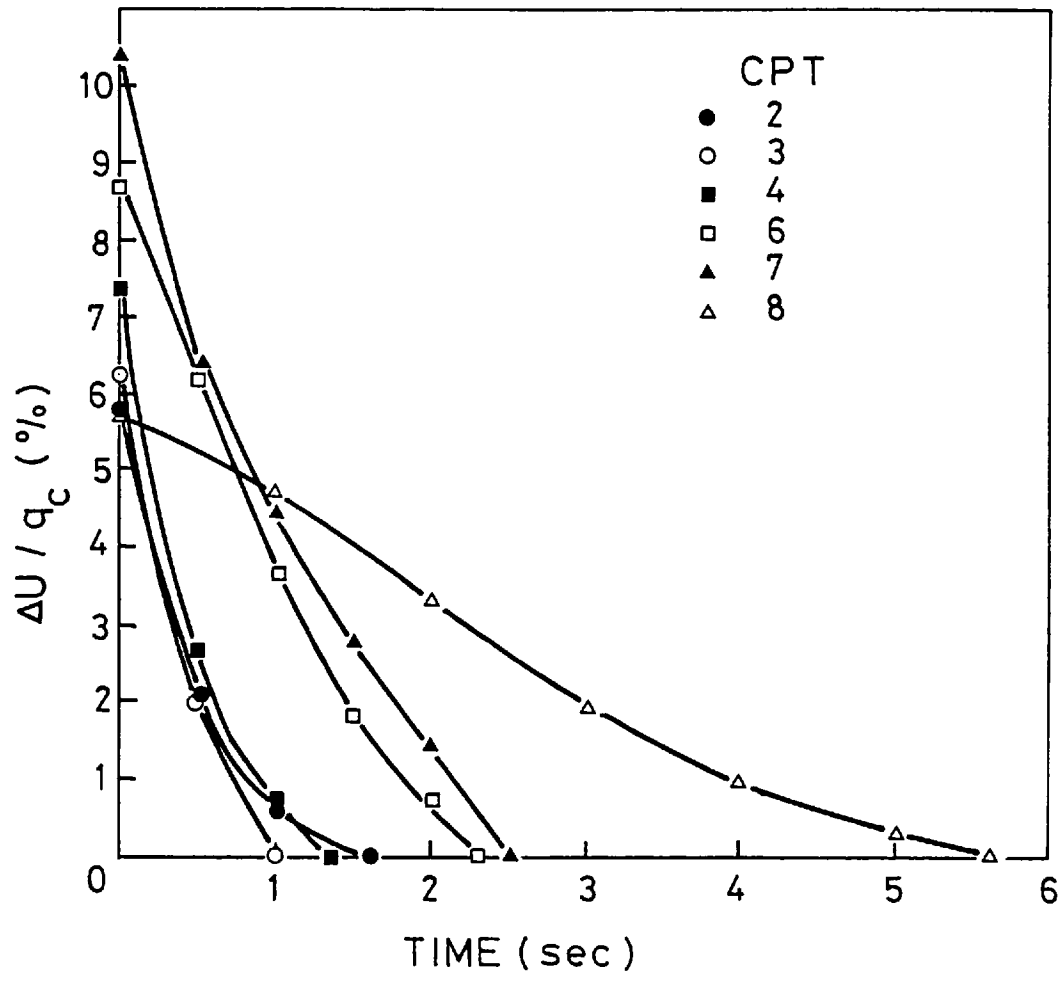


FIGURE 8.37 - DISSIPATION RATE OF EXCESS PORE PRESSURE WITH TIME-NORMALISED PLOT.

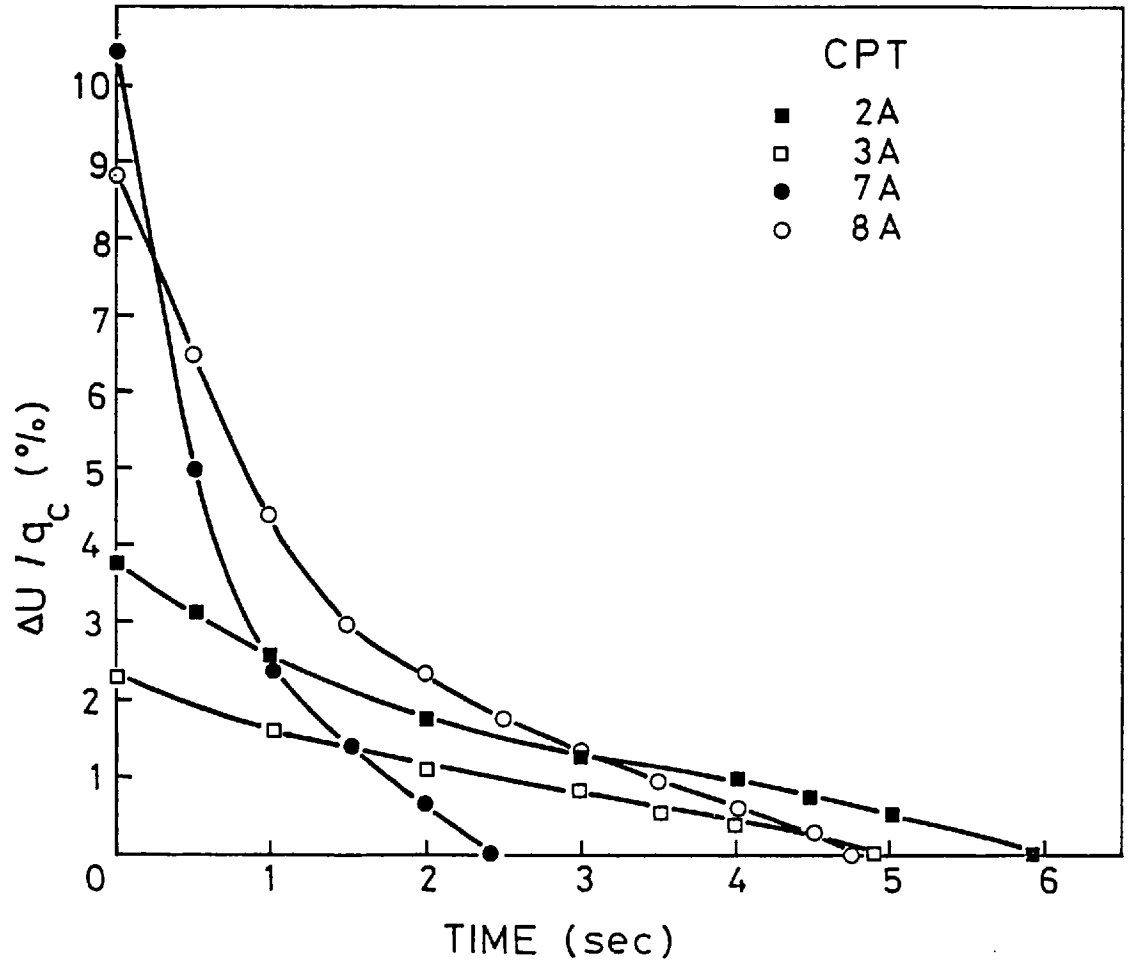


FIGURE 8.38 - DISSIPATION RATE OF EXCESS PORE PRESSURE WITH TIME-NORMALISED PLOT-'ASIDE' TESTS.

CHAPTER 9

ANALYSIS I - RELATIONSHIP BETWEEN COMPRESSIBILITY AND CONE END RESISTANCE

9.1 GENERAL

As discussed in Chapter 2, one of the most commonly used application of the cone penetration tests is the indication of the compressibility characteristics of granular materials.

In this chapter, the experimental values obtained are used to investigate the correlation between compressibility and cone resistance.

The deformability characteristics of the sand used in the cone tests could be estimated from the results obtained during one dimensional consolidation and plate load tests.

The compressibility characteristics as indicated from the one dimensional consolidation results have been taken only as a comparative value. Due to the wall friction, which can lead to substancial non-uniformity in stress and strain within the sample as consolidation proceeds, the interpretation of these results would require more elaborate analysis. Hence, the results obtained from plate load tests have been taken as indicative of the true compressibility characteristics of the sand. These values have been compared with cone resistance values leading to an empirical relationship. This empirical relationship is used for analysing the limitation and errors involved when using the cone penetration test as an indicator of compressibility.

9.2 INTERPRETATION OF THE ONE-DIMENSIONAL CONSOLIDATION TESTS

Figure 9.1 indicates the vertical movement of the reference plate plotted against consolidation pressure. The vertical movement of the reference plate indicates the variation in thickness corresponding to the central part of the sample, see Section 7.2.2 for testing procedure. By

comparing this value with the average value given by the total volume of water expelled from the sample, the deflection at the top of the sample could be estimated, see Appendix A.3. The results indicate a very small deflexion. Hence, the vertical movement of the reference plate will be taken as indicative of the thickness variation for the calculation of the constrained deformation modulus.

In order to take into consideration the influence of the wall-friction on the consolidation process, a reduction factor has been defined by considering the variation in vertical and radial stresses at the centre line, see Appendix A.2.2.

The value of the reduction factor as a function of the consolidation pressure has been determined by adopting a simplified stress distribution and considering an effective depth of consolidation as indicated by the cone penetration test, see Fig. 9.2.

Thus, the secant oedometer (constrained) modulus is given as:

$$\Delta E_s = \Delta\sigma_c \frac{H_o R_{(\sigma c)}}{\Delta L} \qquad 9.1$$

where, ΔE_s is the secant oedometer modulus as indicated in Fig. 9.3a

$\Delta\sigma_c$ is the incremental variation of consolidation pressure

H_o is the initial height of the sample

$R_{(\sigma_c)}$ is the reduction factor obtained from Fig. 9.2 for a given consolidation pressure

ΔL is the corresponding vertical movement of the reference plate due to $\Delta\sigma_c$

Fig. 9.3b indicates the variation of the secant constrained modulus with consolidation pressure.

9.3 INTERPRETATION OF PLATE LOADING TESTS

9.3.1 GENERAL

The five plate load tests carried out, see Section 7.2.3 for testing procedure, can be classified in two groups:

1) Plate load tests carried out on a normally consolidated sample.

2) Plate load tests carried out on an overconsolidated sample.

Figures 9.4, 9.5, and 9.6 show results obtained from plate load tests in normally consolidated samples.

Figures 9.7 and 9.8 show results obtained from plate load tests in overconsolidated samples.

These figures, also indicate the corresponding results obtained during one dimensional consolidation.

Elastic solutions have been assumed for the interpretation of the plate load test. Thus, for a rigid plate:

$$E = q\frac{R}{\delta}\frac{\pi}{2}(1 - \nu^2)\, I \qquad 9.2$$

where: E is the deformation modulus

q is the total load divided by the plate area

R is the plate radius

δ is the plate settlement

ν is the Poisson's ratio, which value for the analysis will be taken as 0.24 corresponding to $K_o/(1 + K_o)$, where $K_o = 1 - \sin 43^o$

I is the influence factor depending on the geometry of loading area and boundary conditions.

9.3.2 INFLUENCE OF THE CENTRAL HOLE

Figure 9.9 shows the solution obtained by Egorov (1965) for settlements of rigid ring on an elastic semi-infinite mass. The settlement is given by:

$$\delta = q\frac{R}{E}\pi(1 - \nu^2)\, W(n) \qquad 9.3$$

where: W(n) is function of the ratio between the internal and external radius

for: D_i = 4.42 cm

D_e = 15 cm

n = 0.29

and from Figure 9.7 we have:

W(0.29) = 0.5045

for: R_i = 0 (solid plate); n = 0, W(0) = 0.5

and

$$\frac{\delta\,(\text{HOLE})}{\delta\,(\text{SOLID})} = \frac{W(0.29)}{W(0)} = \frac{0.5045}{0.5} = 1.009 \qquad 9.4$$

Thus, for this geometric conditions the error involved by considering the testing plate as solid will be less than 1%.

9.3.3 INFLUENCE OF THE WALL CONFINEMENT

Figure 9.10 presents results indicating the influence of the wall confinement on the deformability characteristic of the sand. These results have been obtained by using finite elements analysis, see Appendix A.2.3.

The induced stress below the plate has been determined for a fixed plate settlement considering different boundary radius-plate radius ratios. The effect of the wall friction has been considered by assuming two boundary conditions:

a) no wall friction (free vertical displacement);

b) no vertical displacement (infinite wall friction).

In all these analysis the ratio between plate radius and depth of layer has been taken as 0.075 corresponding to 0.075 m and 1.0 m respectively.

Thus, for a boundary radius equal to 0.38 m and a plate radius of 0.0755 m, we have:

$$1.03 < \frac{E}{E_{100}} < 1.08 \qquad 9.5$$

where E_{100} is the deformation modulus corresponding to a boundary - plate ratio equal to 100. E_{100} will be assumed here as the value with no influence of the wall confinement.

Thus, for this boundary condition an error around 5% can be involved in the determination of the deformation modulus.

9.3.4 EVALUATION OF THE DEFORMATION MODULUS

For each load increment the corresponding plate settlement has been measured as a function of time. The adopted plate settlement value is assumed as that indicated by a time corresponding to approximately 95% of the total plate movement. This value has been used to compute the drained deformation modulus.

Figure 9.11b indicates the variation of the drained deformation modulus during the plate load tests.

The values of the drained deformation modulus have been obtained using the following expression:

$$\Delta E'_p = \Delta q \times \frac{R}{\Delta \delta} \times \frac{\pi}{2} \times (1 - \nu^2) \times I_\delta \times 0.95 \qquad 9.6$$

where: $\Delta E'_p$ is the drained secant deformation modulus, as defined in Fig. 11a

Δq is the incremental variation in the applied stress

R is the plate radius

$\Delta \delta$ is the incremental plate settlement due to Δq

0.95 is the reduction factor accounting for the wall confinement influence

I_δ is the influence factor account for a rigid finite layer, this value can be estimated from Poulos and Davis (1973), Fig. 7.19, solutions for rigid loaded area, circle on finite layer. From this reference, we have:

for $\nu = 0.24$

and $R/H = 0.075$

$$\frac{\pi}{2}(1 - \nu^2) I_\delta = 1.4 \qquad 9.7$$

So, the expression 9.2 becomes:

$$\Delta E'_p = \Delta q \frac{R}{\Delta \delta} \times 1.33 \qquad 9.8$$

Some interesting conclusions may be drawn for Figure 9.11b as follows:

a) for plate load tests carried out in normally consolidated samples (PT1, PT2 and PT3) the variation of the deformation modulus with loading is not significant.

b) Comparing tests PT1 and PT2, the difference between the two deformation modulus is not significant. However test PT2 stayed longer in the range of elastic behaviour. This could be due to higher values of consolidation pressure and relative density for test PT2.

c) for plate load tests carried out in overconsolidated samples (PT4 and PT5) there is a considerable variation of the deformation modulus with loading up to the point where behaviour like that of the normally consolidated sand is reached. For test PT4 the point has been reached faster than for test PT5, as indicated by a higher gradient for the curve corresponding to test PT4. Hence, the point corresponding to "like normally-consolidated behaviour" is a function of the pre-consolidation pressure and overconsolidation ratio. The deformation behaviour of overconsolidated sand samples subjected to a K_o - loading - unloading condition has been more deeply investigated by Daramola (1978). Figure 9.12, presents his results obtained from a series of laboratory tests. Stress paths corresponding to tests PT4 and PT5, are also presented in Fig. 9.12. Thus, Daramola's results explain the reason why test PT4 reached the "like normally consolidated behaviour" faster than test PT5.

As a result of these observations, the dependence on the stress level should be noted when determining the deformation modulus.

For normally consolidated conditions this problem will be bigger for materials presenting a pronounced curved stress-strain relationship.

For overconsolidated conditions this problem will be associated with factors controlling the point corresponding to the "like normally consolidated behaviour".

Dahlberg (1974) estimated from in situ screw plate load test in a preloaded natural sand deposit the deformation modulus for the pre-compression range and for the normally consolidated range. The deformation modulus corresponding to the normally consolidated range was obtained by carrying out the screw plate tests beyond the preconsolidation pressure. Fig. 9.13a, indicates the definition of precompression and virgin compression range used in his analysis. Fig. 9.13b presents values of the deformation modulus obtained for the precompression and virgin compression range. However, these values have been obtained for different stress levels under the screw-plate. As indicated by the results presented in Fig. 11b the deformation modulus corresponding to the point when the applied pressure exceeds the overconsolidated-pressure cannot be taken as representative of the normally consolidated conditions.

Let us assume that a normally consolidated sample having the same relative density and overburden pressure as tests PT4 and PT5 would follow a corresponding path indicated by the dashed line in Fig. 9.11b. The secant deformation modulus for test PT4 corresponding to the initial 1.0 Kg/cm^2 loading would have a value around 80 Kg/cm^2. The value of the secant deformation modulus corresponding to 1.0 Kg/cm^2 exceeding the precompression pressure, σ'_c = 1.4 Kg/cm^2, would be around 50 Kg/cm^2. In this case, the virgin precompression range would give a value corresponding to 62.5% of the actual secant deformation modulus. The same values as indicated from PT5 would be: 105 Kg/cm^2 for the initial loading and 45 Kg/cm^2 for loading beyond the precompression pressure, and this last value represents only 43% of the initial loading.

Thus, a value of deformation modulus obtained for the virgin compression range in a preloaded sand should be corrected when extrapolated to the normally consolidated conditions. The correction factors will be dependent on the relative density, precompression pressure and overconsolidation ratio.

9.4 COMPARISON BETWEEN DEFORMATION MODULUS FROM ONE DIMENSIONAL CONSOLIDATION AND PLATE LOAD TEST

For a sample with the same initial void ratio the stress-deformation curve corresponding to a plate load test will be in between the stress-deformation curves for the confined and uniaxial compression tests. Thus, a deformation modulus obtained from a plate load test would have a value within the limits given by the confined and uniaxial compression tests. Hence:

$$E_c < E_p < E_s \qquad 9.9$$

where E_c, E_p and E_s represent the deformation modulus corresponding to uniaxial compression, plate load and confined compression tests respectively.

From the elasticity theory the uniaxial compression modulus and the confined compression modulus are related as:

$$E_c = E_s\left[1 - \frac{2\nu^2}{1-\nu}\right] \qquad 9.10$$

hence

$$E_s\left[1 - \frac{2\nu^2}{1-\nu}\right] < E_p < E_s \qquad 9.11$$

let us assume:

a) $\nu = 0.24$ corresponding to $\phi' = 43^\circ$, giving $\left[1 - \frac{2\nu^2}{1-\nu}\right] = 0.85$

b) $\nu = 0.30$ corresponding to $\phi' = 35^\circ$, giving $\left[1 - \frac{2\nu^2}{1-\nu}\right] = 0.74$

and we have:

$$(0.74 \text{ --- } 0.85)\, E_s < E_p < E_s \qquad 9.12$$

For 1.0 Kg/cm^2 additional loading in excess of the consolidation pressure, the values of the constrained and plate load deformation modulus can be obtained from Fig. 9.3b and Fig. 9.11b respectively. Thus, we have:

	E_s (Kg/cm^2)	E'_p (Kg/cm^2)	0.74 E_s	0.85 E_s
TP1 (σ'_c = 1.4 Kg/cm^2)	95	85	70	81
TP2 (σ'_c = 2.8 Kg/cm^2)	135	110	100	115

From these results, a good agreement, for the initial loading conditions, can be observed between the constrained and plate load deformation modulus. The comparison between the two moduli has only been made for the normally consolidated condition.

9.5 CORRELATION BETWEEN COMPRESSIBILITY AND CONE RESISTANCE

9.5.1 GENERAL

A relationship between compressibility and cone resistance for normally consolidated conditions has been established by direct use of the results. For the overconsolidated condition this empirical correlation has been determined by an indirect approach.

It must be emphasized that in this series of tests, the very important relative density and overburden pressure effects have not been considered properly, hence, the proposed empirical relationship should be only used as an indicative value. The limitations of these correlations will be commented on in subsequent sections.

9.5.2 THE DETERMINATION OF REPRESENTATIVE VALUE OF COMPRESSIBILITY

Results from plate load tests will be taken as representative of the compressibility characteristics of the sand.

As previously discussed, the importance of the stress level should be noted when defining the deformation modulus. For this analysis, the deformation modulus obtained for a plate stress equal to 1 Kg/cm^2 will be considered as representative value.

Thus, from Fig. 9.11.b, we found:

TEST PT1 --- E'_p = 85.0 Kg/cm^2

TEST PT2 --- E'_p = 110.0 Kg/cm^2

TEST PT3 --- E'_p = 20.0 Kg/cm^2

TEST PT4 --- E'_p = 125.0 Kg/cm^2

TEST PT5 --- E'_p = 270.0 Kg/cm^2

9.5.3 THE DETERMINATION OF REPRESENTATIVE VALUE OF THE CONE RESISTANCE

As indicated in Chapter 8, the cone resistance values were strongly influenced by the plate load tests. An attempt was made to reproduce similar samples (density and stress history) and additional cone penetration tests were carried out, see Table 7.2.

Representative values of cone resistance have been assumed as:

1) Indicated by the reproduced sample, when this sample shows similarity to the corresponding sample with a preceding plate load test.

2) Estimated from a combination between the values indicated during tests with and without a preceding plate test, when the corresponding samples show difference in compactness.

In order to take into account the loosening of the soil with depth, the representative value of cone resistance has been determined using the simplified influence factor distribution proposed by Schmertmann et al (1978). Thus, we have:

$$q_{cm} = 0.25q_{c1} + 0.4q_{c2} + 0.25q_{c3} + 0.1q_{c4} \qquad 9.13$$

where; q_{c1}, q_{c2}, q_{c3} and q_{c4} represent the average values of the cone resistance within the intervals, O to R, R to 2R, 2R to 3R and 3R to 4R respectively. R is the plate radius.

Thus, representative cone resistance values have been found as:

Corresponding to PT1 --- q_c = 25 Kg/cm^2 (from CPT1 and CPT6) — See Table 7.2

Corresponding to PT2 --- q_c = 36 Kg/cm^2 (from CPT2 and CPT7)

Corresponding to PT3 --- q_c = 8 Kg/cm^2 (from CPT3 - bottom)

Corresponding to PT4 --- q_c = 20 Kg/cm^2 (from CPT4 and CPT5)

Corresponding to PT5 --- q_c = 53 Kg/cm^2 (from CPT8)

9.5.4 CORRELATION FOR NORMALLY CONSOLIDATED CONDITIONS

Using the following expression, $E_{pnc} = \alpha \; q_{cnc}$ to represent the relationship between compressibility and cone resistance for normally

consolidated conditions, we have:

	E_{pnc} (Kg/cm^2)	q_{cnc} (Kg/cm^2)	σ'_v (test) (Kg/cm^2)	α	RELATIVE DENSITY %
TEST 1	85	25	1.4	3.4	41 ± 5 - Medium
TEST 2	110	36	2.8	3.1	46 ± 5 - Medium
TEST 3	20	8	"O"	2.5	25 ± 5 - Loose

For these results, it could be observed that the effect of overburden pressure was not too significant on the value of α. Thus with some approximation a value 3.25 and 2.5 can be assumed as representative of α for medium and loose conditions respectively. Consequently, it follows that:

$$\alpha \sim 1.2\,(3D_R^2 + 2) \qquad 9.14$$

Thus, the relationship obtained shows that the empirical factor increases with an increase in relative density. Therefore, the relative density of the deposit should be evaluated in order to use equation 9.14. This could represent a practical limitation of the proposed relationship. For this analysis, the in situ relative density will be estimated from the measured cone resistance value as:

$$D_R\,(\%) = 57 \log q_{cnc} - 12\,\sigma'_v - 11 \qquad (8.22)$$

q_{cnc} and σ'_v in Kg/cm^2

This equation has been established from the experimental results as described in Section 8.5.2. It should be noted that this relationship has been established for the normally consolidated condition and its validity is limited to an effective overburden pressure, σ'_v, not exceeding 3 Kg/cm^2.

9.5.5 CORRELATION FOR OVERCONSOLIDATED CONDITIONS

The empirical factor correlating the compressibility and cone resistance for the overconsolidated condition in the form of $E_{poc} = \beta\, q_{coc}$ has been found as:

	E'_{poc} (Kg/cm^2)	q_{coc} (Kg/cm^2)	β	Relative Density %	OCR
TEST 4	125	20	6.25	42.5±5 - Medium	5<<
TEST 5	270	53	5.1	57.5±5 - Medium	5

In this case, the extrapolation cannot be done by direct use of the results, as the β value has only been determined for the medium condition, therefore, an indirect approach will be used.

Daramola (1978) estimated the settlement of a footing on normally and overconsolidated sand for different initial void ratios based on the stress path method. He determined the vertical movement below the centre line of the footing due to an external load of 100 KN/m^2. For the overconsolidated condition the overconsolidation ratio for three points (See Fig. 9.14) were 7, 3.5 and 1.75, the values decreasing with depth. He integrated the values of the vertical movement under the centre line and obtained the settlement for each specific situation (See Fig. 9.14). By comparing the settlement obtained for normally and overconsolidated conditions, he found that the ratio between the compressibility for these two conditions to be:

$$\frac{E_{oc}}{E_{nc}} = 3.45 \text{ (loose)} = 2.60 \text{ (medium)} = 2.15 \text{ (dense)} \qquad 9.15$$

These results are plotted as function of relative density in Fig. 9.15. Using Fig. 9.11b, a ratio of 2.71 and 2.63 can be obtained for test PT5 for plate stresses, of 0.5 Kg/cm^2 and 1 Kg/cm^2 respectively. This result is plotted on Fig. 9.15, showing a good agreement with Daramola's results. For test PT4 this ratio has been found as 2.5 for a plate stress of 0.5 Kg/cm^2, however it should be noted the very high overconsolidation ratio and very small confining pressure for this test. Hence, it is not in agreement with the results in Fig. 9.15 obtained for low value of overconsolidation ratio and relatively high confining pressure.

In order to proceed with the extrapolation, the relationship between cone resistance values for normally and overconsolidated condition should be established. From equation 2.39, 2.45 and 2.56 (Chapter 2) we have:

$$\frac{q_{coc}}{q_{cnc}} = (1.9\, D_R + 0.15)\, OCR^{\frac{0.44\,(1 - D_R)}{L_n D_R + 1.61}} \qquad \text{for } D_R > 40\% \quad 9.16$$

$$\frac{q_{coc}}{q_{cnc}} = 0.88\, OCR^{0.38} \qquad \text{for } D_R < 40\% \quad 9.17$$

Thus, by considering 9.15, 9.16 and 9.17 we have:

$$K_{D_R} E_{nc} = \beta q_{cnc} (1.9 D_R + 0.15)\, OCR^{\frac{0.44\,(1 - D_R)}{L_n D_R + 1.61}} \qquad \text{for } D_R > 40\% \quad 9.18$$

$$K_{D_R} E_{nc} = \beta q_{cnc}\, 0.88\, OCR^{0.38} \qquad \text{for } D_R < 40\% \quad 9.19$$

and putting $E_{nc} = \alpha q_{cnc} = 1.2\,(3D_R^2 + 2)$ into 9.18 and 9.19 and eliminating q_{cnc} we found:

$$\beta = \frac{K_{D_R}\, 1.2\,(3D_R^2 + 2)}{(1.9\, D_R + 0.15)\, OCR^{\frac{0.44\,(1-D_R)}{L_n D_R + 1.61}}} \qquad \text{for } D_R > 40\% \quad 9.20$$

$$\beta = \frac{K_{D_R}\, 1.2\,(3\, D_R^2 + 2)}{0.88\, OCR^{0.38}} \qquad \text{for } D_R < 40\% \quad 9.21$$

where K_{D_R} is equal to 3.45, 2.6 and 2.15 for loose, medium and dense sand respectively.

The use of equation 9.20 and 9.21 should be limited for settlement analysis of shallow foundation or of foundations located at depth with maximum overburden pressure value of 3 Kg/cm^2. It also should be noted that equations 9.20 and 9.21 only apply for lightly overconsolidated sands.

Fig 9.16 presents the variation of β with relative density obtained from equations 9.20 and 9.21 for an overconsolidation ratio value equal to 5. The experimental value obtained using results of the plate load PT5 and cone test

CT5 shows a good agreement with the values obtained from the indirect approach.

Fig. 9.17 presents values of the compressibility plotted against relative density for normally consolidated and overconsolidated conditions. These values have been calculated assuming the overburden pressure equal to 1 Kg/cm^2 and 3 Kg/cm^2. The results indicated an increasing of 50% in the compressibility value as the overburden pressure increases from 1 Kg/cm^2 to 3 Kg/cm^2, for the same relative density. For the overconsolidated condition, the overconsolidation ratio has been taken as 5.

9.6 ERRORS INVOLVED IN THE COMPRESSIBILITY EVALUATION IF THE STRESS HISTORY IS NOT KNOWN

Generally, during a cone penetration test the information available includes the direct measured value of cone resistance and the indirect estimation of the overburden pressure from the penetration depth and the average unit weight of the strata.

In this section, the error that could be involved in estimating the settlement from this available information will be analysed. Thus, for a given cone resistance value and overburden pressure the settlement for a normally consolidated and for an overconsolidated condition will be estimated using the approach described in the previous sections.

Let us first consider that the sand is normally consolidated, and the compressibility can be obtained as (See Fig. 9.18):

a) from q_c, σ_v' and assuming $q_c = q_{cnc_1}$;

$$D_{R_1} = f(q_{cnc_1}, \sigma_v') \tag{8.22}$$

b) from D_{R_1}; $\alpha = f(D_{R_1})$ (9.14)

c) from q_c and α;

$$E_{nc} = \alpha\, q_c$$

Now, let us assume that the deposit is overconsolidated, the compressibility will be obtained as (See Fig. 9.18):

a) from q_c, σ_v' and assuming $q_c = q_{coc}$

$$\frac{q_{coc}}{q_{cnc_2}} = f(OCR, D_{R_2}) \quad D_{R_2} > 40\% \tag{9.16}$$

$$\frac{q_{coc}}{q_{cnc_2}} = f(OCR) \qquad D_{R_2} < 40\% \tag{9.17}$$

$$D_{R_2} = f(q_{cnc_2}, \sigma_v') \tag{8.22}$$

It should be noted that the values of q_{cnc} and D_{R_2} must satisfy these two equations. The q_{cnc_2} obtained indicates the cone resistance value that would have this overconsolidated deposit for a normally consolidated condition. Thus, the value of q_{cnc_2} is smaller than the q_c value and consequently D_{R_2} will be smaller than D_{R_1}.

b) from D_{R_2}; $\beta = f(D_{R_2}, OCR)$ (9.20 and 9.21)

c) from q_c and β, $E_{oc} = \beta q_c$

Hence, the settlement due by considering the deposit as normally consolidated will be given as:

$$\delta_{nc} = f\left(\frac{1}{E_{nc}}\right) \tag{9.22}$$

however, if this deposit is overconsolidated the settlement due will be as:

$$\delta_{oc} = f\left(\frac{1}{E_{oc}}\right) \tag{9.23}$$

Thus, by ignoring the stress history of the deposit and assuming a normally consolidated condition, the error involved can be computed as:

$$\frac{\delta_{nc}}{\delta_{oc}} = \frac{E_{oc}}{E_{nc}} = \frac{\beta q_c}{\alpha_{q_c}} = \frac{\beta}{\alpha} \tag{9.24}$$

$$\delta_{nc} = \frac{\beta}{\alpha} \delta_{oc} \tag{9.25}$$

It should be stressed here, that α and β are determined for different values of relative density. For a given value of the cone resistance and overburden pressure the normally consolidated condition will be in a denser state than the overconsolidated condition, See Fig. 9.18.

Following the described procedure and assuming an overconsolidation ratio of 5, these values have been computed and they are:

D_{R_1}	40%	55%	65%	75%	80%
α	2.98	3.49	3.92	4.43	4.7
D_{R_2}	25%	40%	50%	57%	61%
β	6.7	6.2	5.55	5.3	5.2
β/α	2.2	1.8	1.4	1.2	1.1

Fig. 9.19 presents the β/α ratio plotted against the relative density of the overconsolidated deposit, D_{R_2}.

It can be observed that the error involved by considering the deposit as normally consolidated decreases with an increasing in the compactness of the deposit. Thus, for this assumption, the settlement can be overestimated by a factor of 2.2 and 1.1 for the loosest and densest conditions respectively.

The results, also indicated that for a relative density greater than 50%, the error involved is less than 40%. From a practical viewpoint this error is not too significant for settlement analysis. Therefore, the cone penetration test would indicate the same value of the settlement independent of considering the stress history of the deposit, for a compact material.

This analysis has been carried out considering a preloaded deposit with an overconsolidated ratio of 5. The errors involved would tend to decrease or increase as the overconsolidation ratio decreases or increases respectively. However, these values can be considered as representative for a lightly overconsolidated condition.

9.7 SUMMARY AND CONCLUDING REMARKS

In this chapter, the experimental results have been used to indicate the relationship between compressibility determined from the plate load test and the cone resistance value. The main points observed are:

1) For normally consolidated condition, a relationship between compressibility and cone resistance has been obtained directly from the experimental values. The empirical number expressing this relationship increases with an increasing in the relative density value.

2) For lightly overconsolidated conditions, an indirect approach has been used for establishing the relationship between compressibility and cone resistance. The empirical number expressing this relationship decreases with an increase of the relative density value.

3) For lightly overconsolidated conditions, the error involved by considering the deposit as normally consolidated has been computed. This error can be affected by a factor of 2.2 and 1.1 for the loosest and densest conditions respectively.

4) For a compact material, it has been found that the cone penetration test would indicate almost the same settlement value independent of considering the stress history of the deposit.

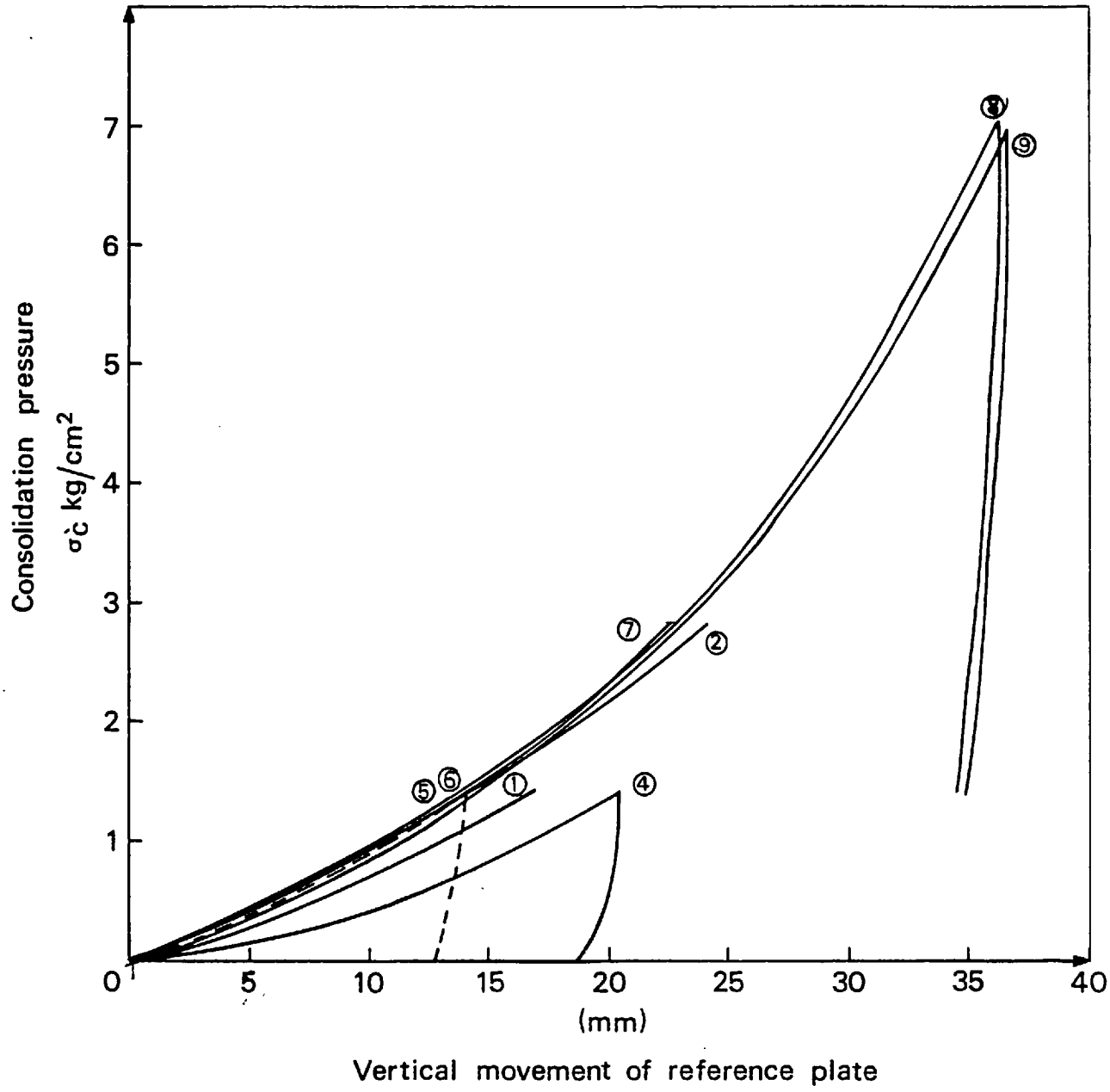


FIGURE 9.1 - ONE-DIMENSIONAL CONSOLIDATION RESULTS.

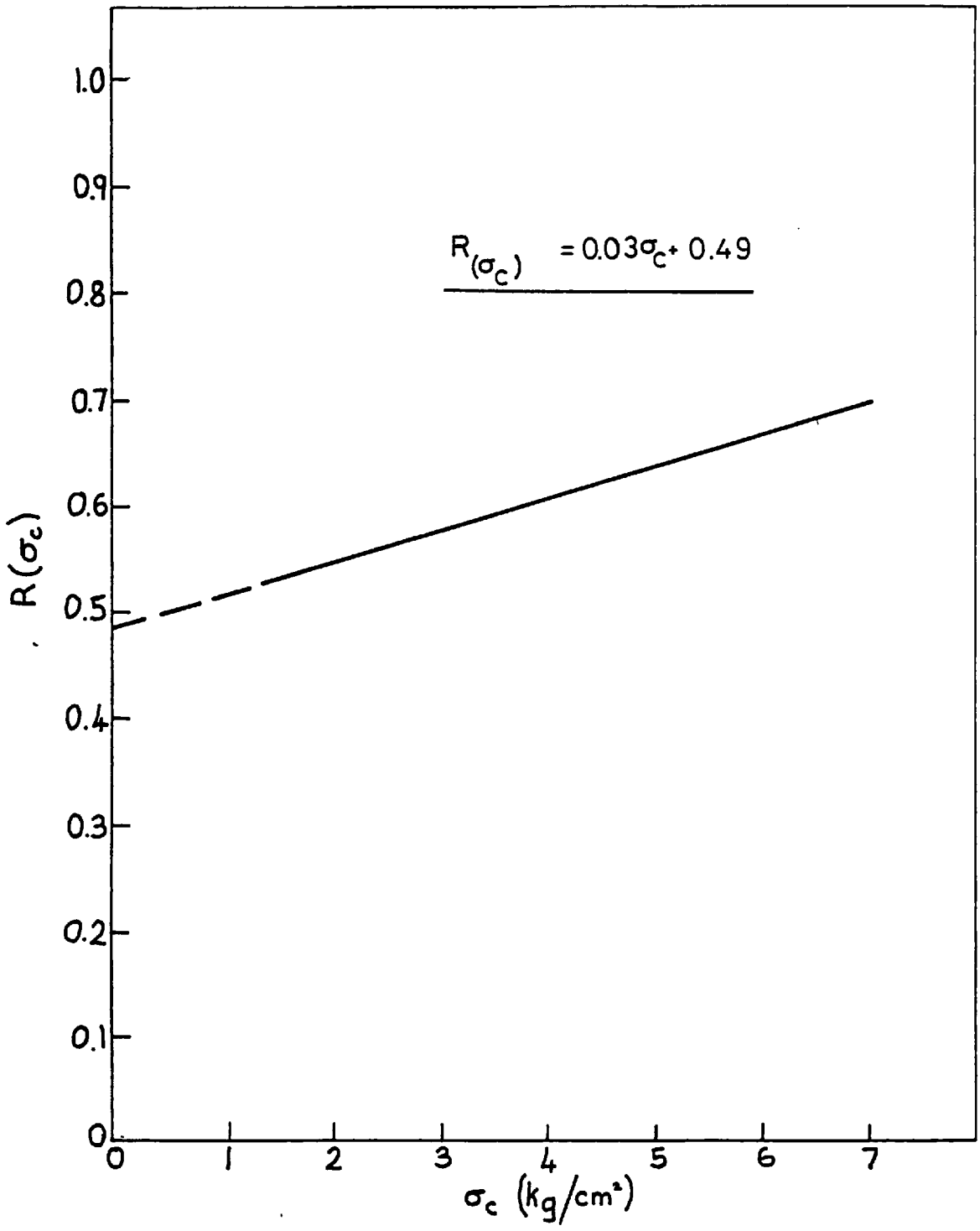
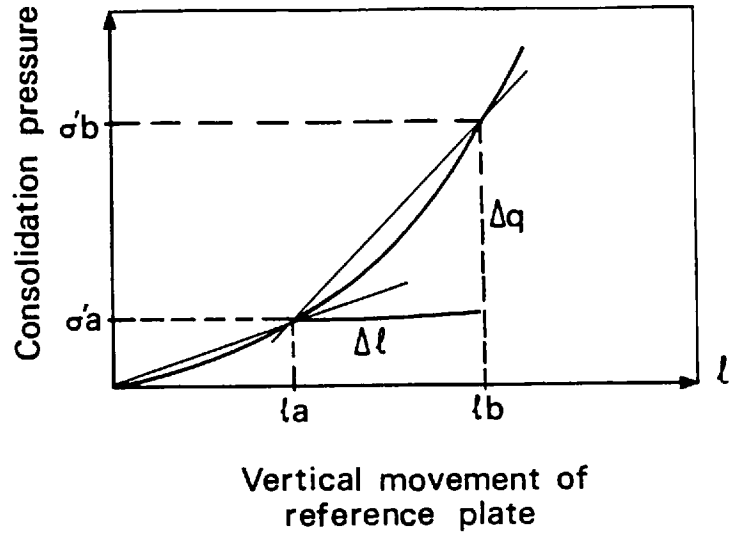


FIGURE 9.2 - REDUCTION FACTOR.



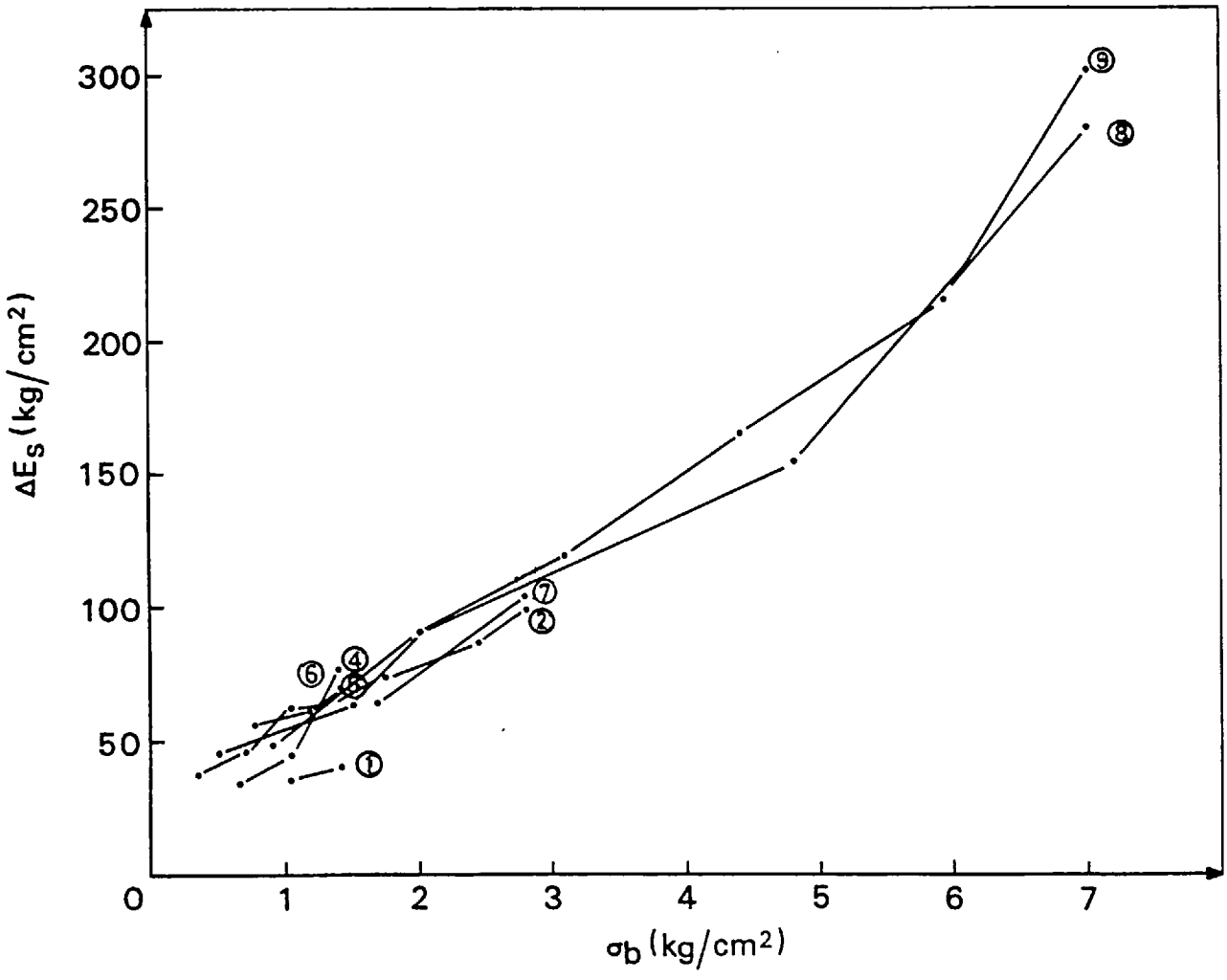


FIGURE 9.3 - (a) DEFINITION OF ΔE; (b) SECANT CONSTRAINED MODULUS VS CONSOLIDATION PRESSURE.

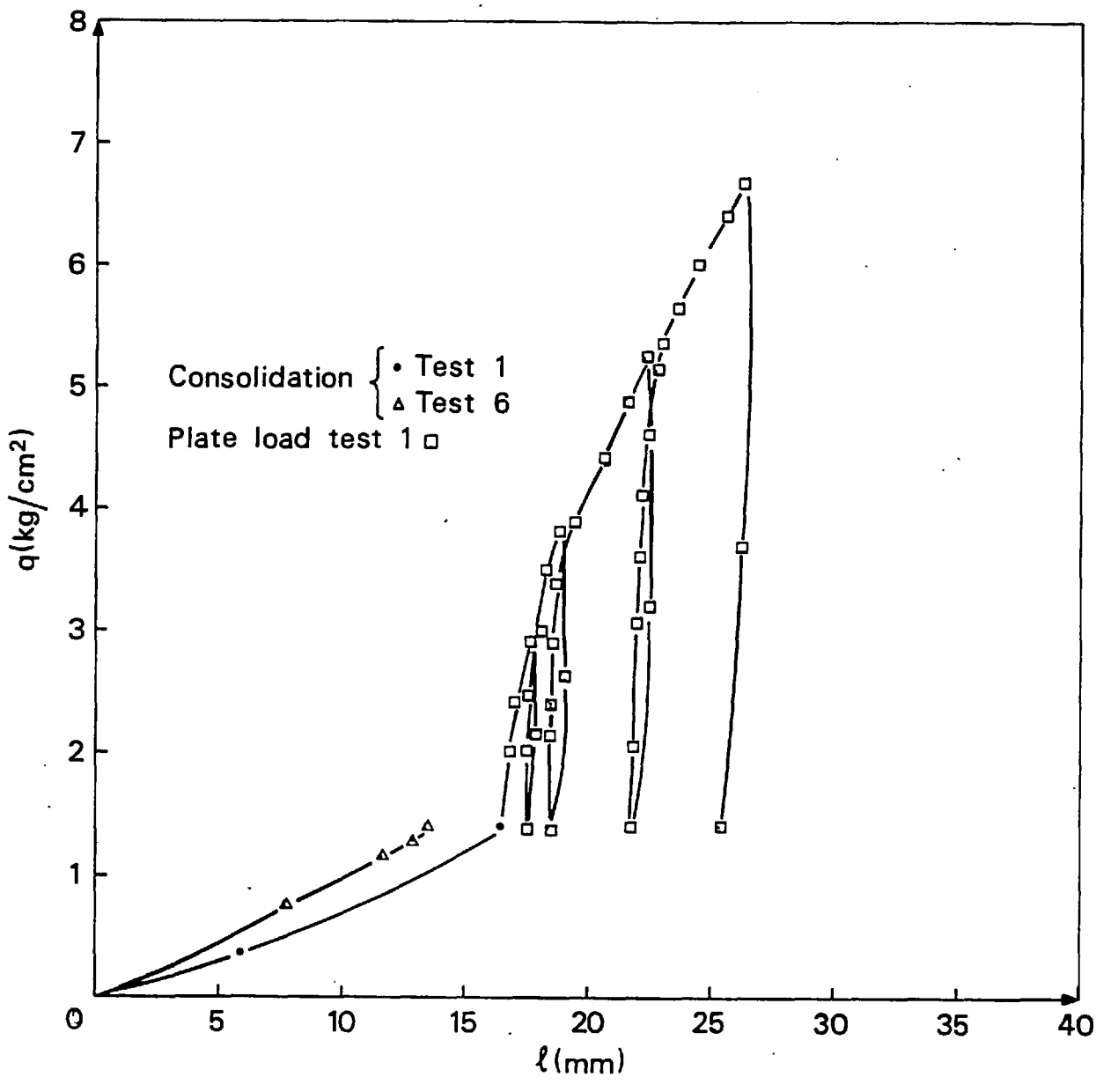


FIGURE 9.4 - VERTICAL MOVEMENT OF PLATE VS PRESSURE (CONSOLIDATION-PLATE LOADING TEST).

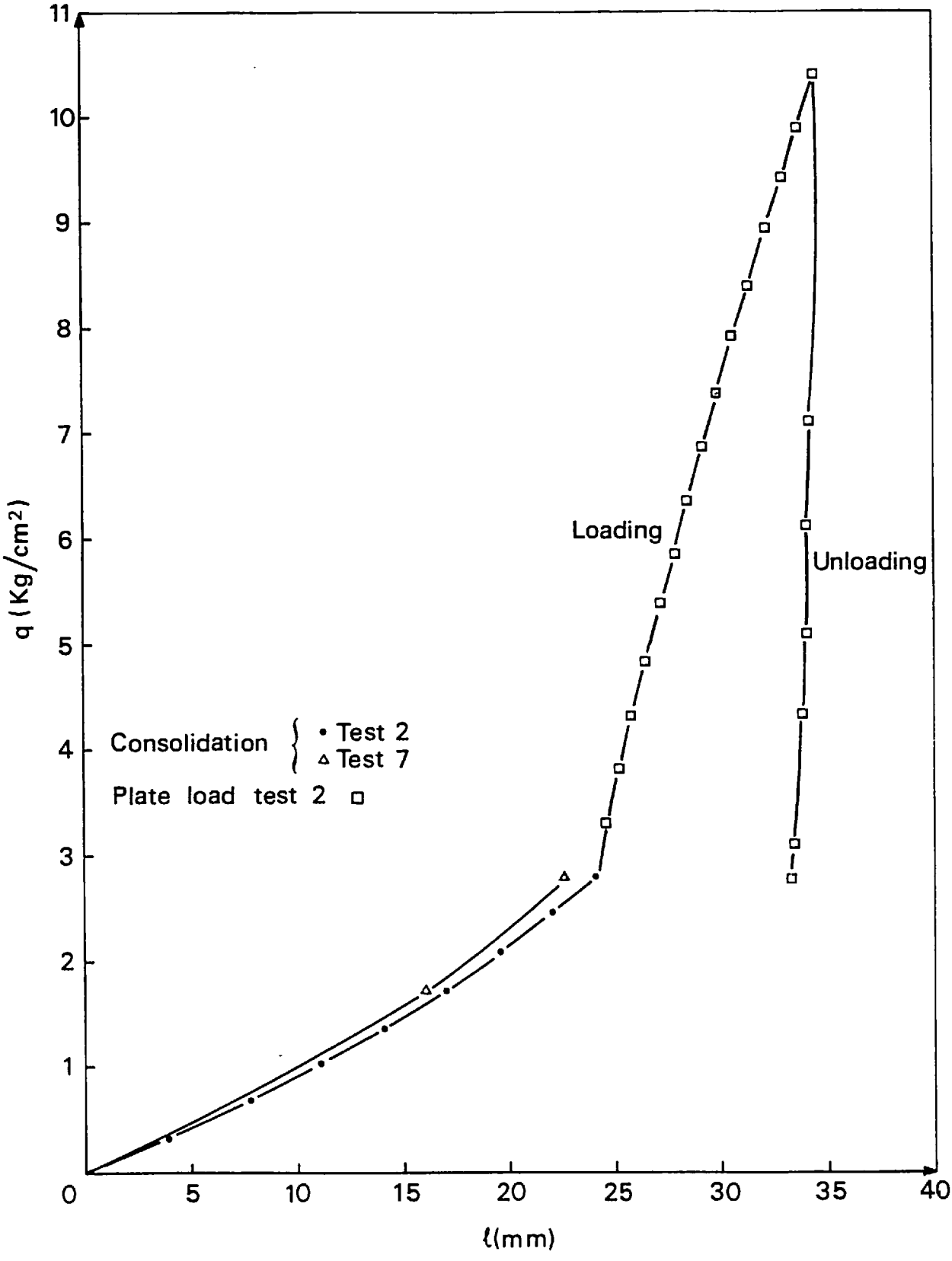


FIGURE 9.5 - VERTICAL MOVEMENT OF PLATE VS PRESSURE (CONSOLIDATION-PLATE LOADING TEST).

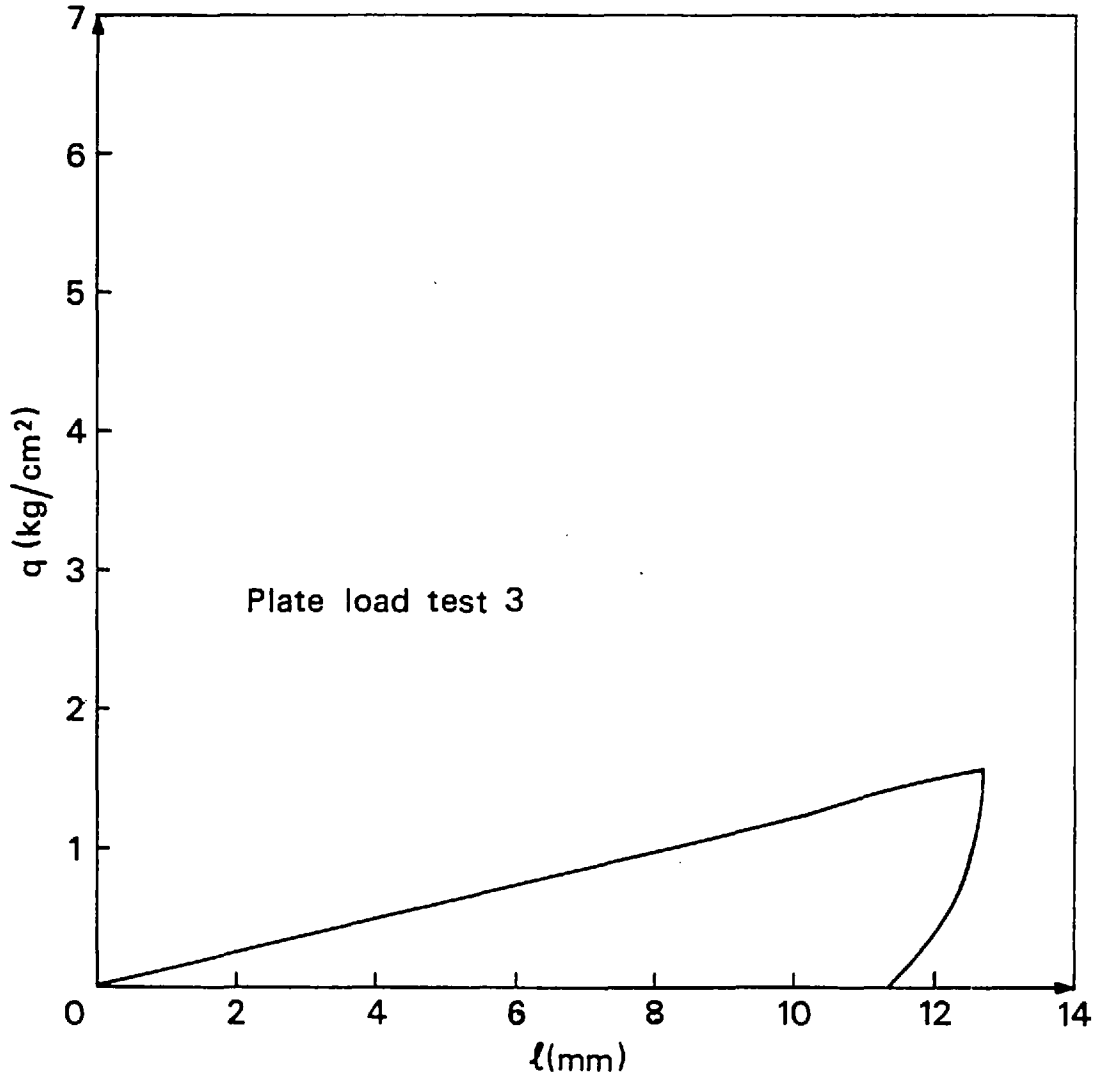


FIGURE 9.6 - VERTICAL MOVEMENT OF PLATE VS PRESSURE (PLATE LOADING TEST).

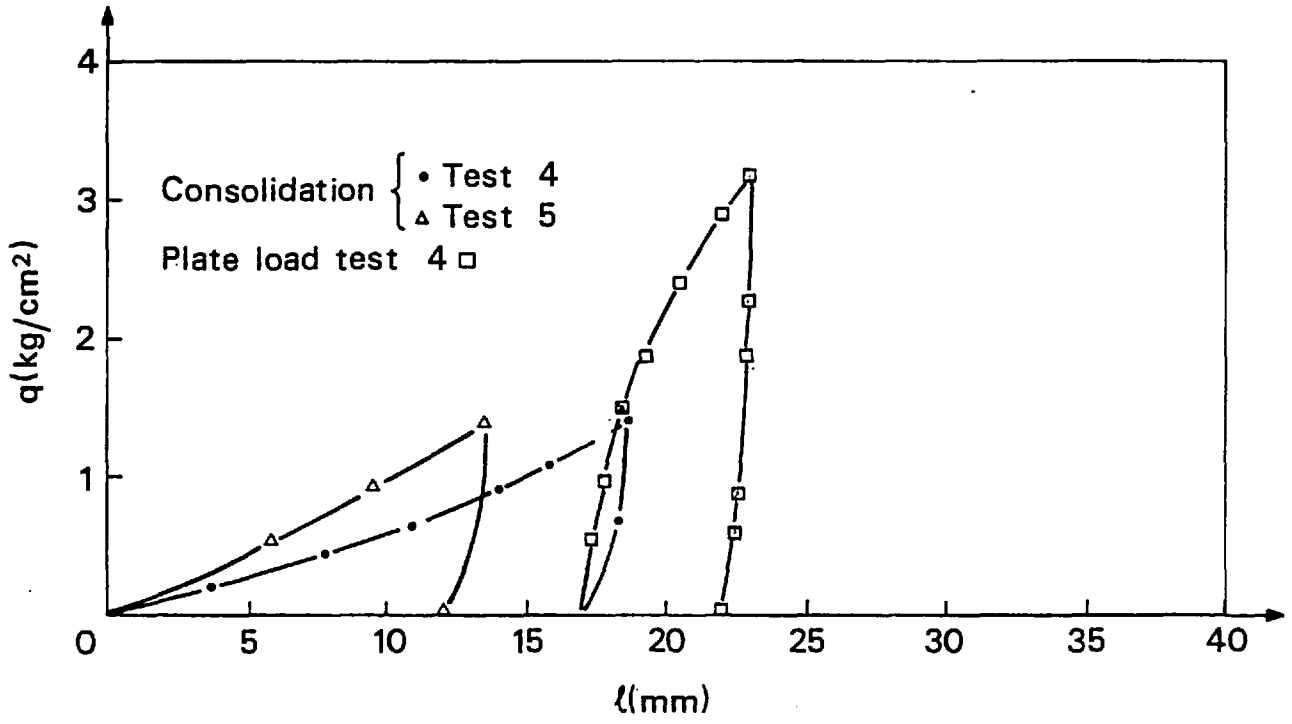


FIGURE 9.7 - VERTICAL MOVEMENT OF PLATE VS PRESSURE (CONSOLIDATION-RELEASE-PLATE LOADING).

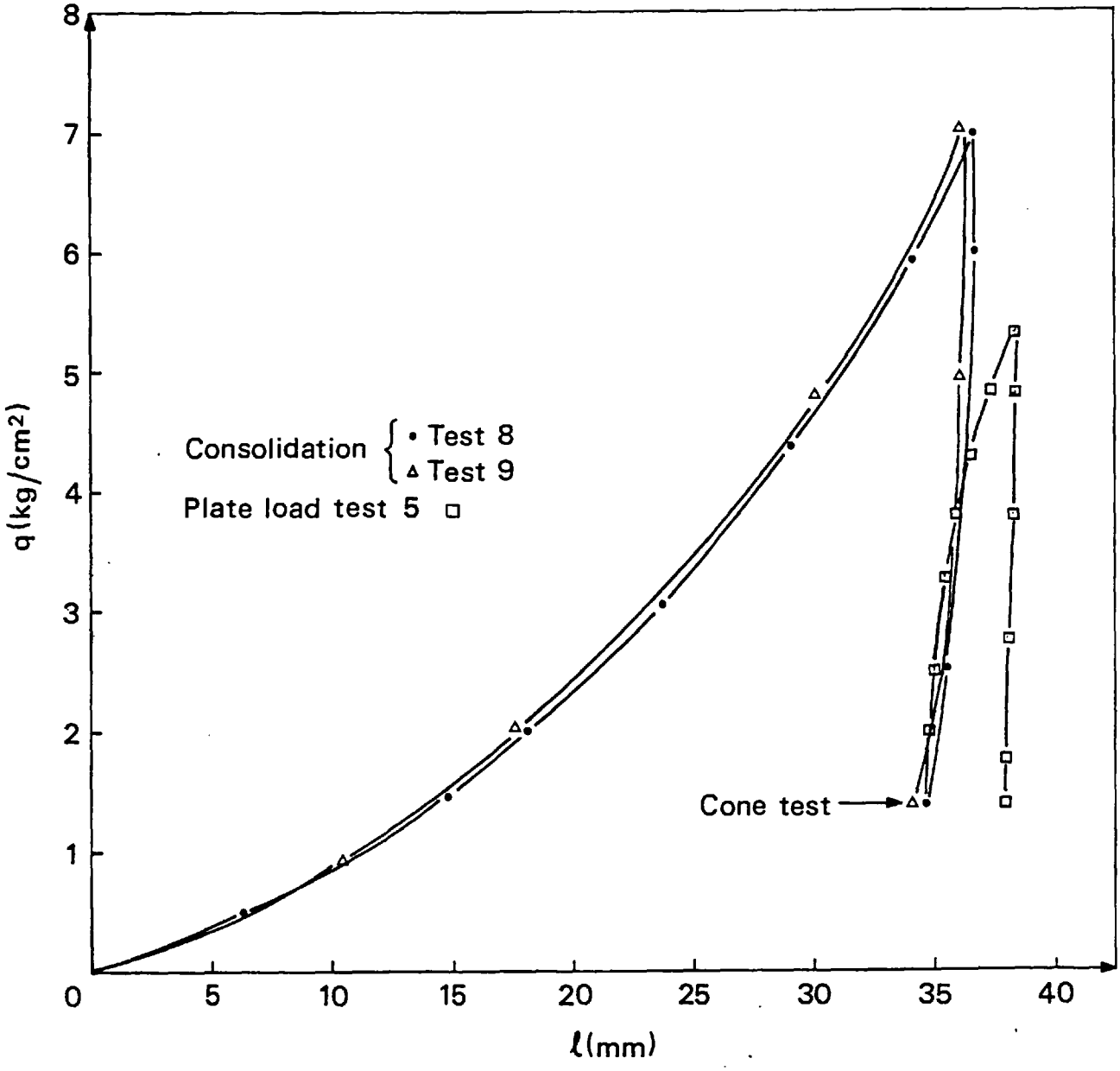


FIGURE 9.8 - VERTICAL MOVEMENT OF PLATE VS PRESSURE (CONSOLIDATION-RELEASE-PLATE LOADING).

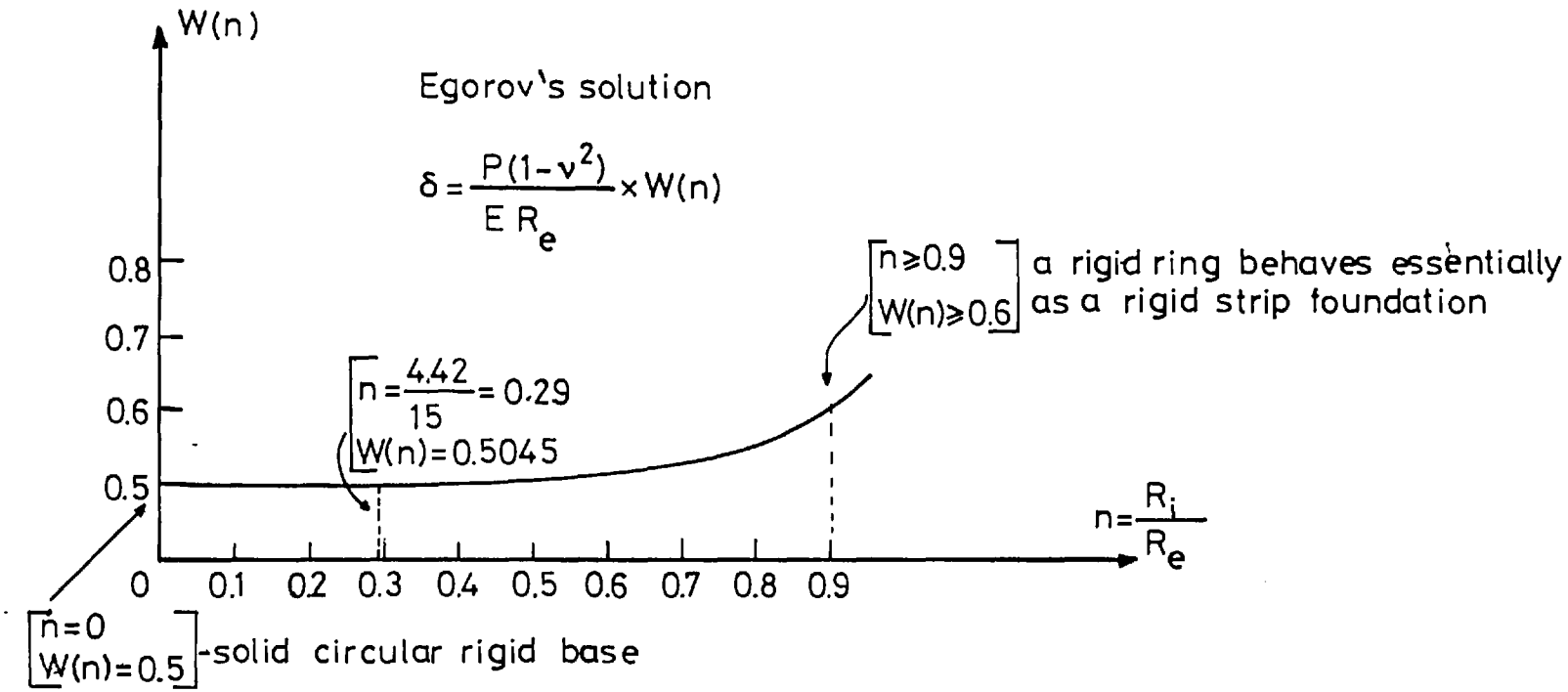


FIGURE 9.9 - SOLUTION FOR RIGID RING ON AN ELASTIC SEMI-INFINITE MASS (FROM EGOROV, 1965).

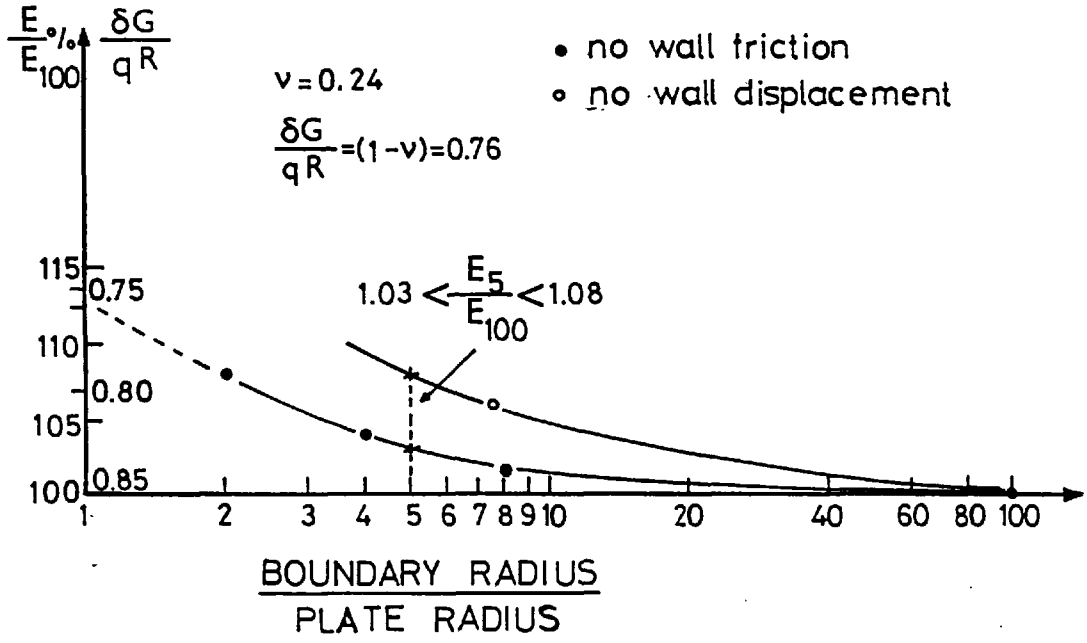
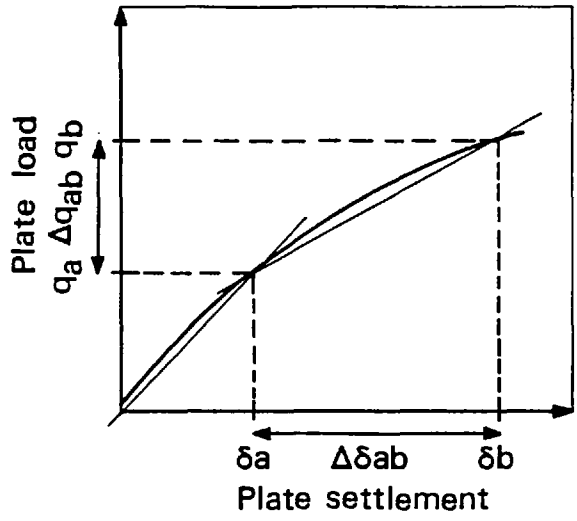


FIGURE 9.10 - INFLUENCE OF WALL CONFINEMENT ON THE DEFORMATION MODULUS.



$$\Delta E_{ab} = \Delta q_{ab} \times \frac{R}{\Delta \delta ab} I$$

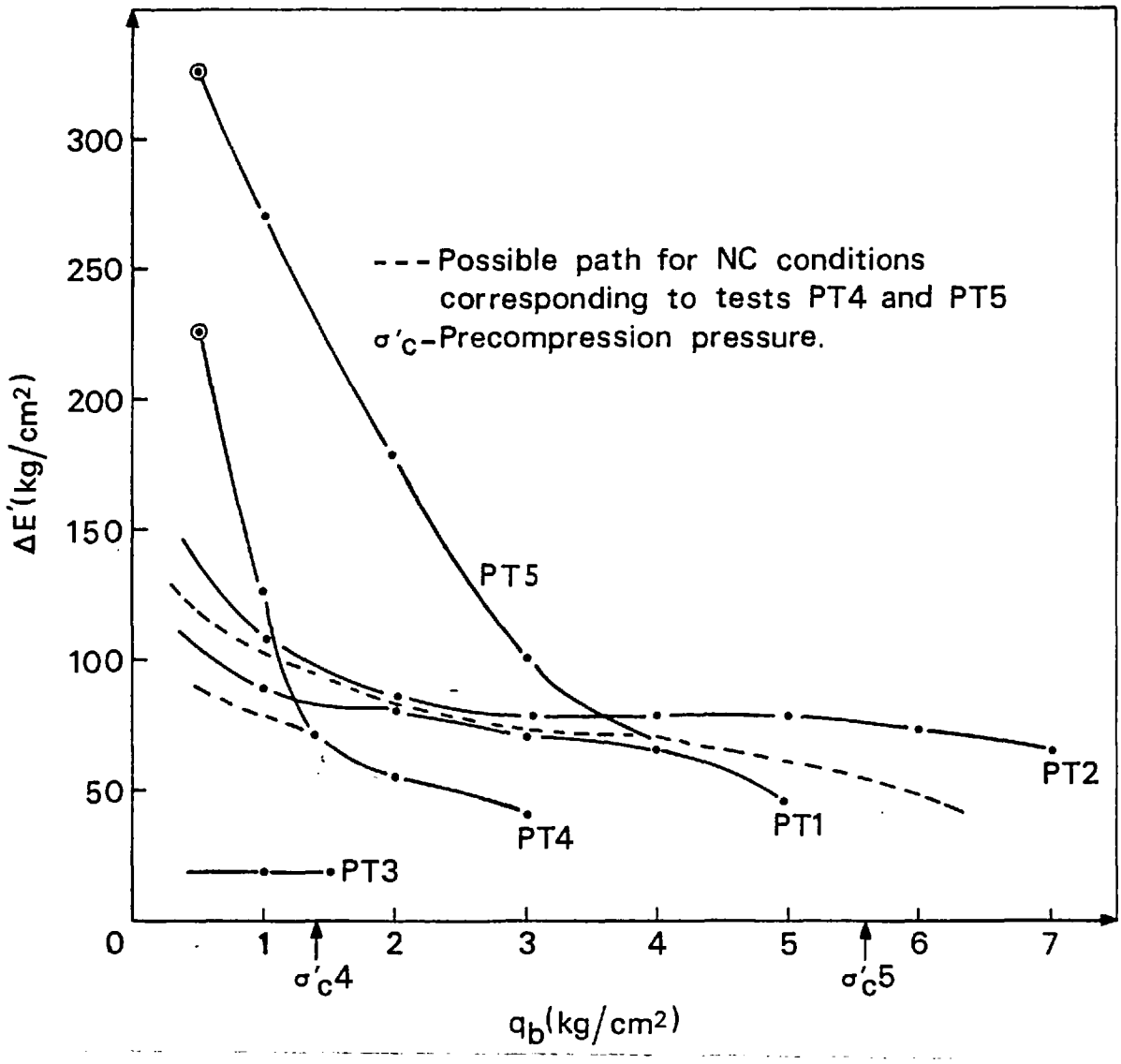


FIGURE 9.11 - VARIATION OF SECANT DEFORMATION MODULI WITH LOADING.

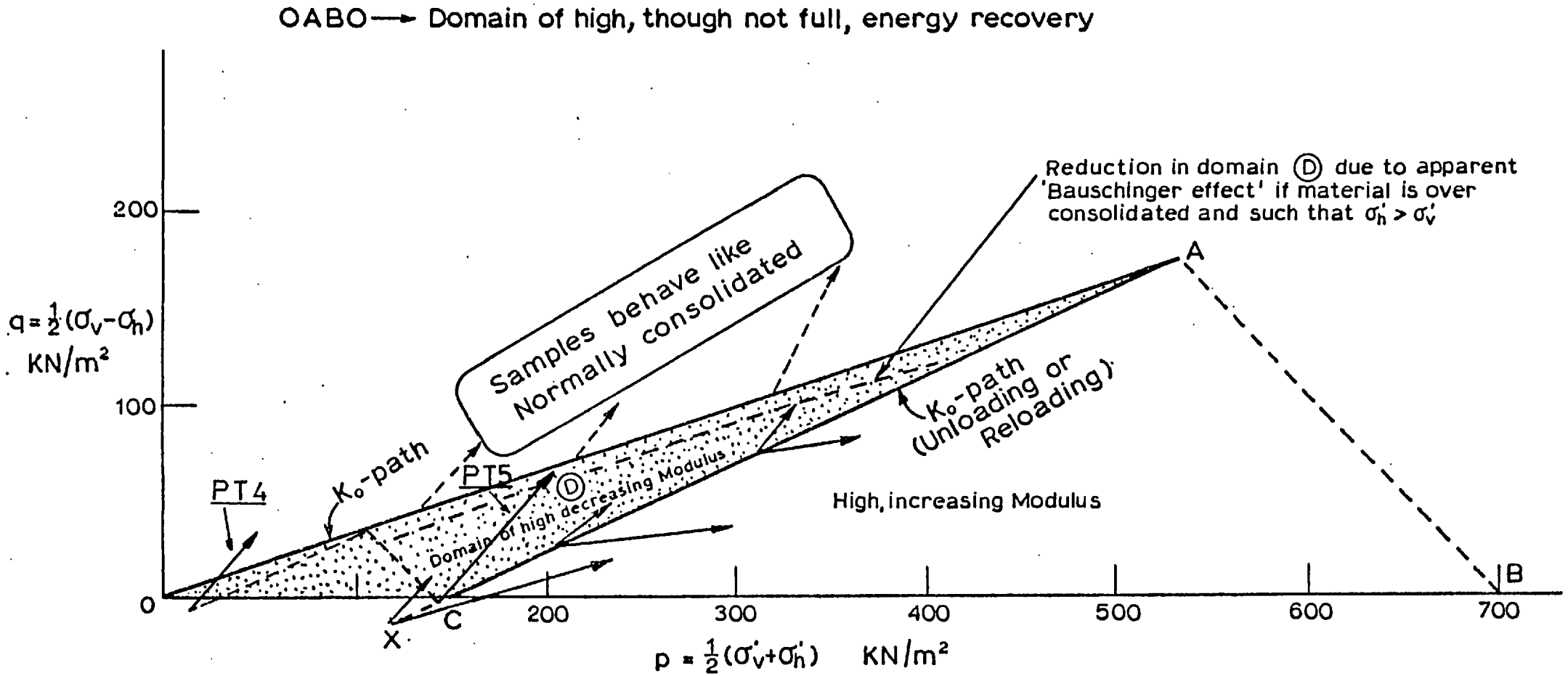
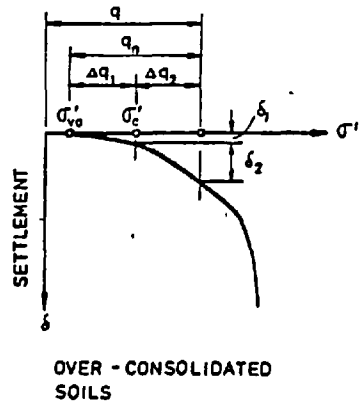


FIGURE 9.12 - ON THE DEFORMATION BEHAVIOUR OF K_o -OVERCONSOLIDATED SAMPLES (FROM DARAMOLA, 1978).



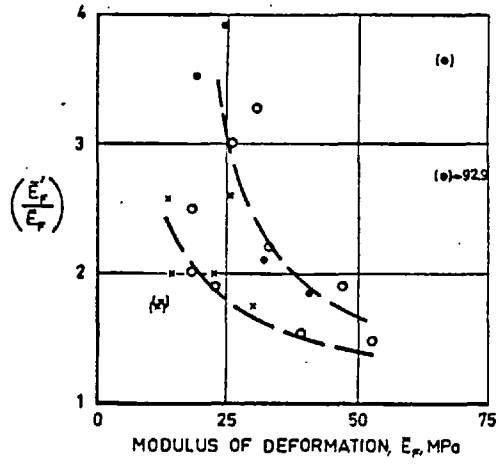


FIGURE 9.13 - (a) DEFINITION OF SYMBOLS; (b) RATIO BETWEEN DEFORMATION MODULI IN THE PRECOMPRESSION RANGE (E'_F) AND IN THE VIRGEN COMPRESSION RANGE ($\overline{E}_F$).

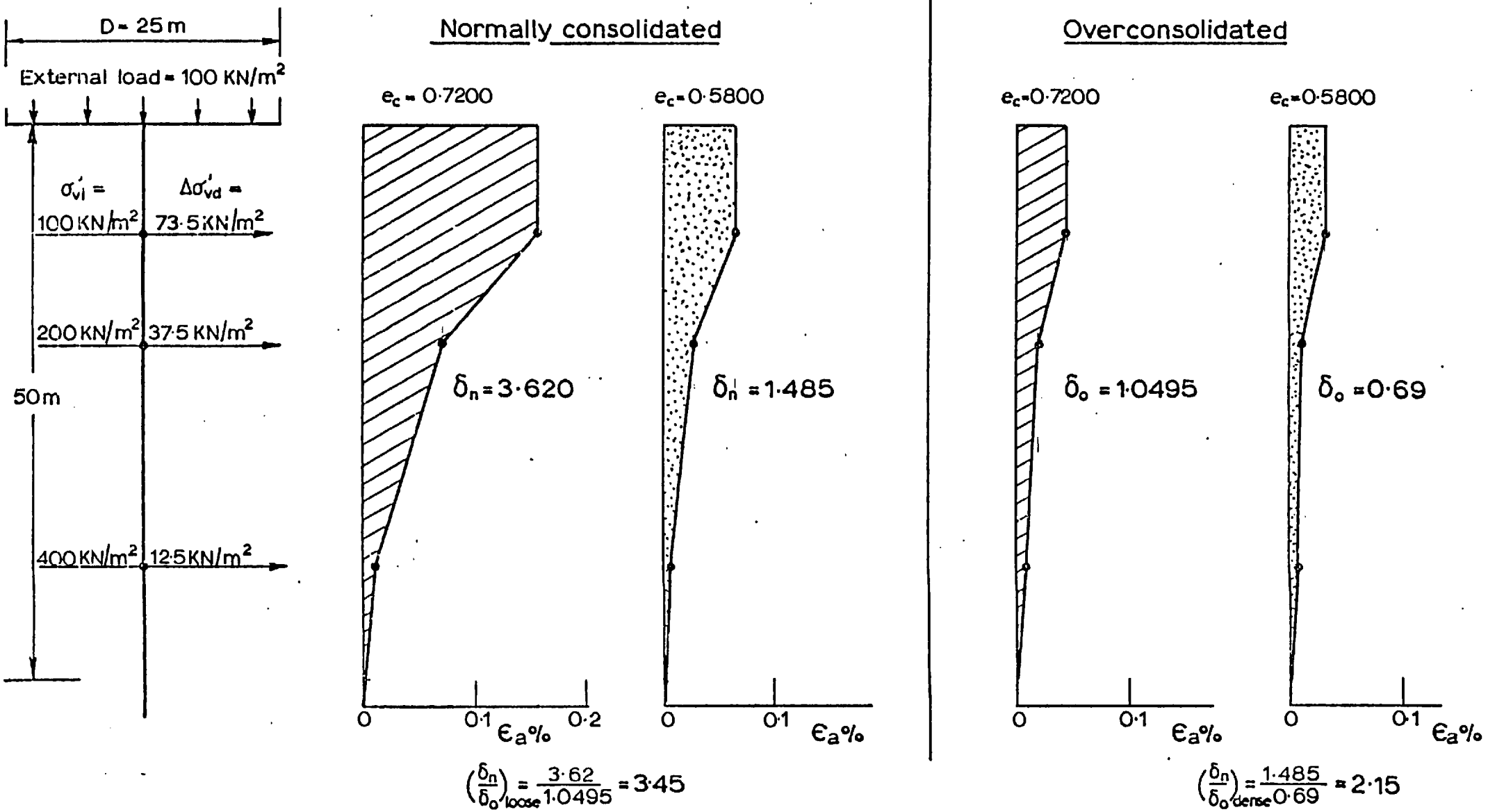


FIGURE 9.14 - SETTLEMENT COMPUTATIONS (FROM DARAMOLA, 1978).

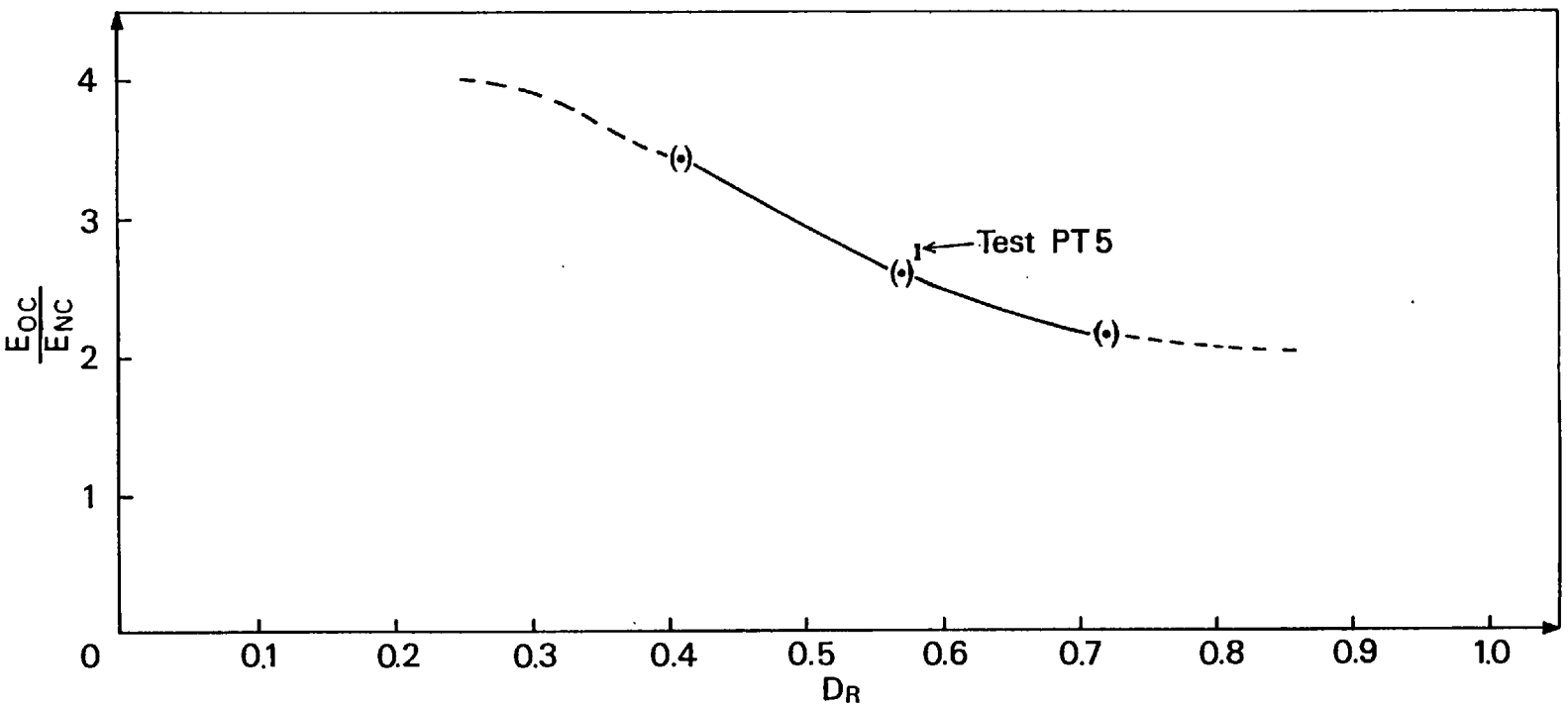


FIGURE 9.15 - COMPRESSIBILITY RATIO VS RELATIVE DENSITY.

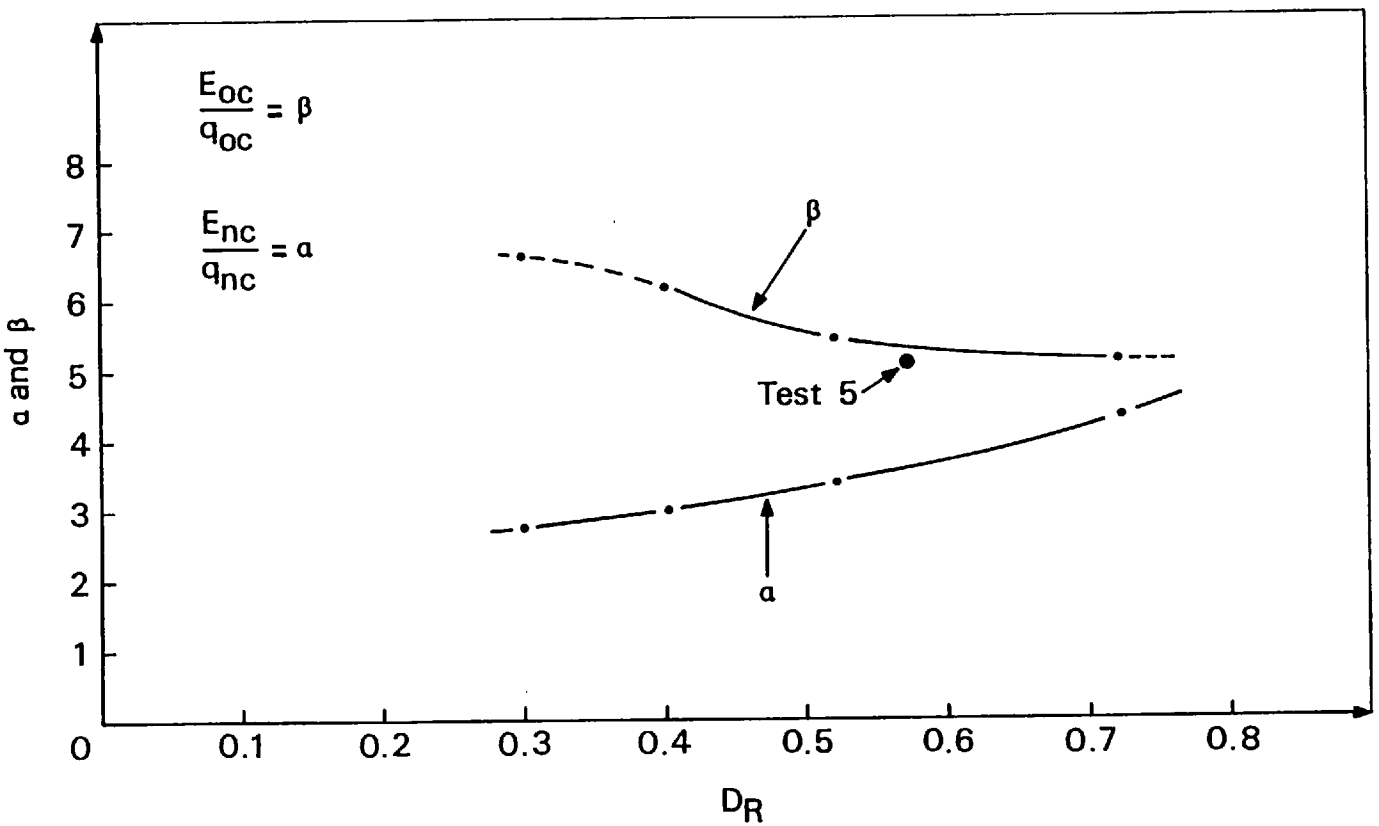


FIGURE 9.16 - α & β FACTORS VS RELATIVE DENSITY.

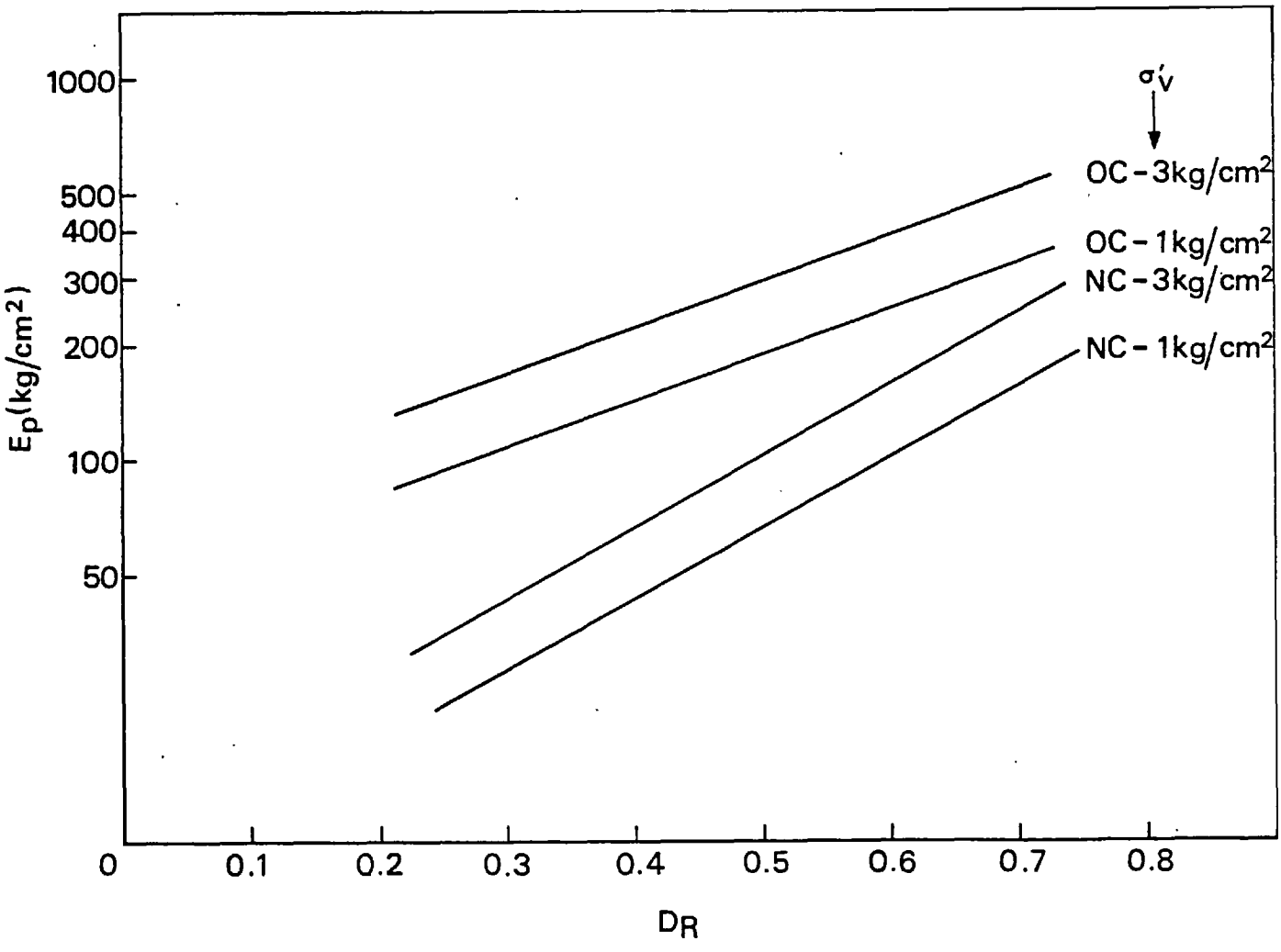


FIGURE 9.17 - PLATE DEFORMATION MODULI VS RELATIVE DENSITY.

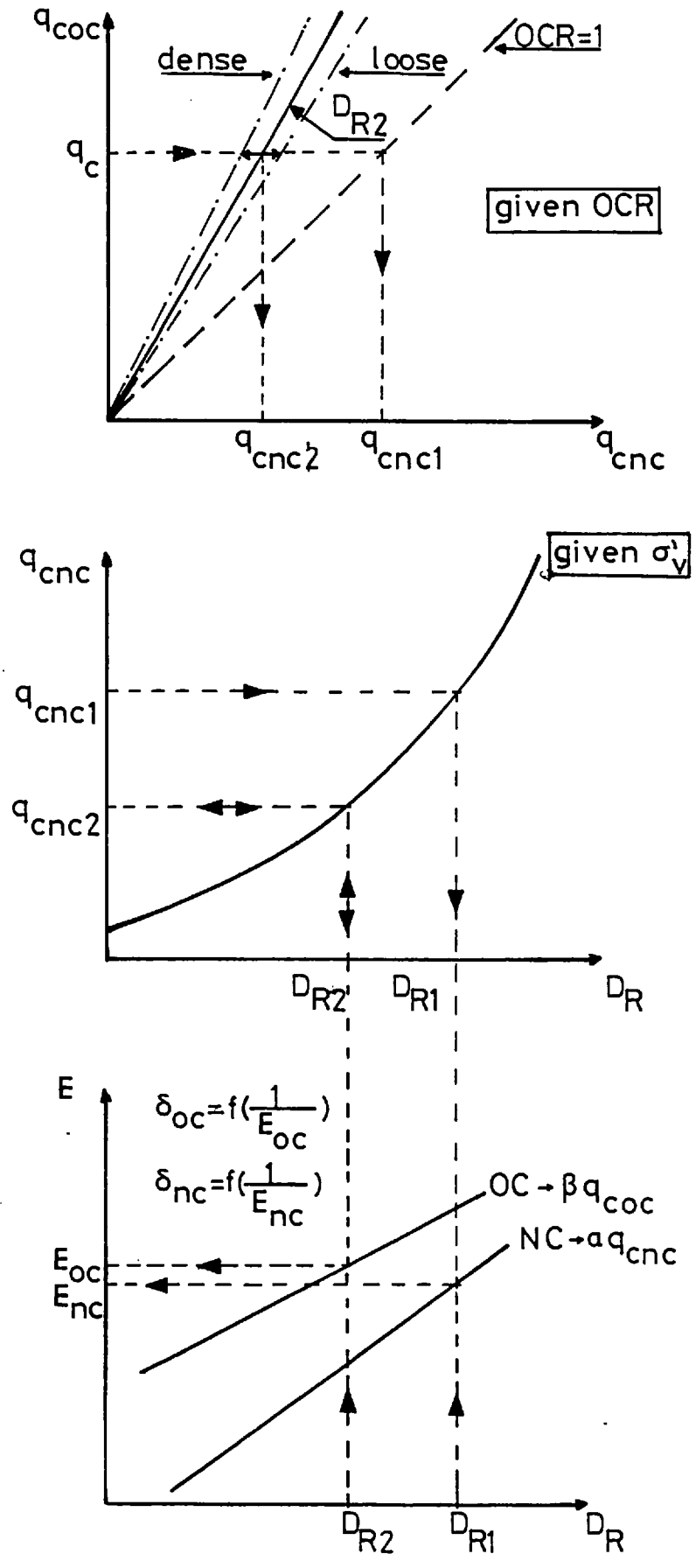


FIGURE 9.18 - ON THE CONSIDERATION OF STRESS HISTORY ON SETTLEMENT COMPUTATIONS.

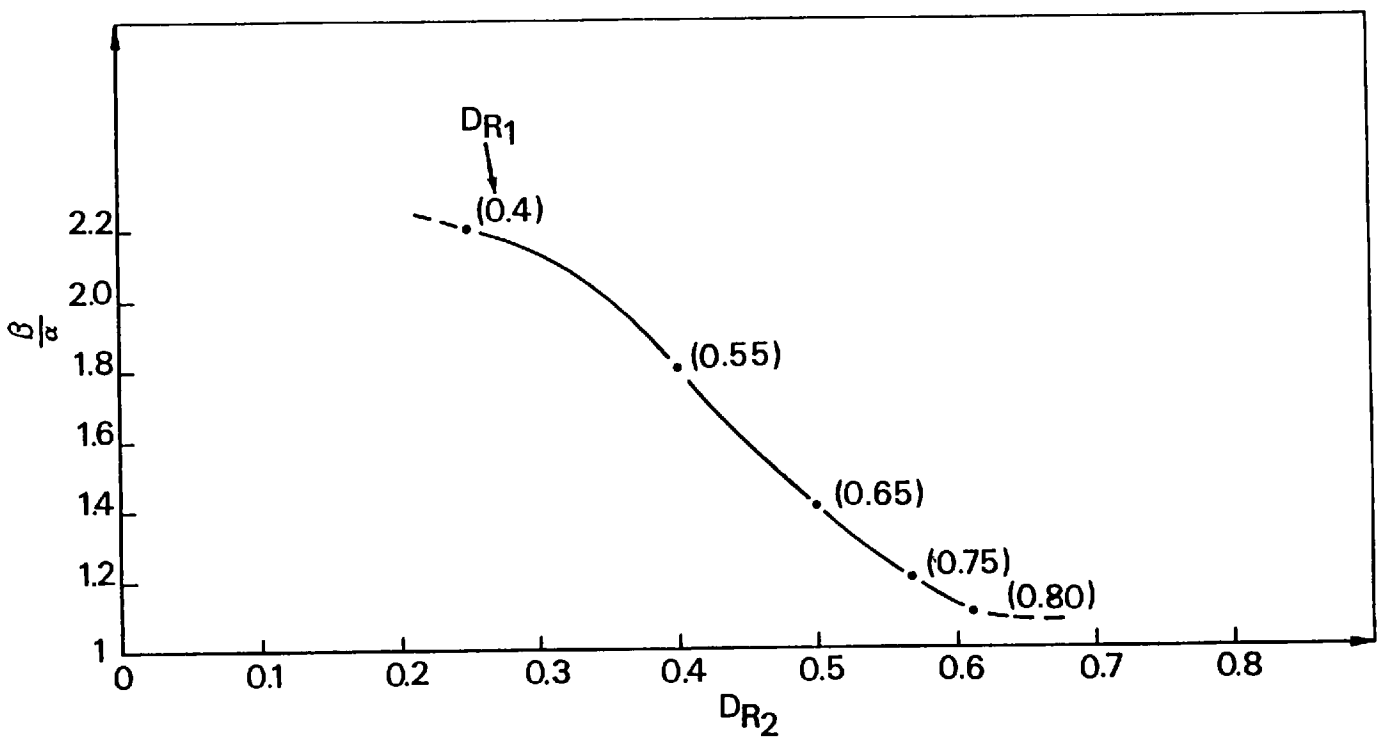


FIGURE 9.19 - SETTLEMENT RATIO VS RELATIVE DENSITY.

CHAPTER 10

CONCLUSIONS AND SUGGESTIONS FOR FURTHER RESEARCH

10.1 GENERAL

This work has attempted to improve the understanding of the excess pore pressure effects upon the cone penetration measurements. Most of the important findings are summarized at the end of the corresponding chapters. In this chapter, the relevant aspects of the results which suggest to areas for future research are outlined.

10.2 CONE PENETROMETER

Calibration tests have indicated that the geometrical configuration of the penetrometer used in this work may introduce significant errors on the point and sleeve measurements. This fact is due to:

a) partial load transmission from the point to the sleeve resistance;

b) difficulties in estimating the contribution of the pore pressure, which acts in front of the penetrometer, to the cone resistances.

It is suggested that the measurement of the friction sleeve resistance should be abandoned in favour of including pore pressure measurements along the penetrometer rods.

10.3 RATE EFFECT

The excess pore pressure generated during the penetration process may strongly influence the magnitude of the cone penetration test measurements. The rate effect may introduce two interdependent phenomena: 1) inducing excess pore pressure and consequently varying the effective stress; 2) mobilizing the viscous resistance. The dissipation of the excess pore pressure may cause

liquefaction, consolidation or swelling within the pertubed zone surrounding the advancing penetrometer. Hence, a static test, with no excess pore pressure, carried out afterwards will not represent the dry condition for the same initial void ratio.

It is suggested that cone penetration tests should be carried out in dry and saturated samples, having the same initial void ratio. In the saturated sample, the excess pore pressure induced during the penetration process should be measured at different points, both in the penetrometer apparatus and within the soil mass. The different effects of relative density, "overburden" pressure and stress history should be considered in the investigation.

10.4 CONE RESISTANCE AS AN INDICATOR OF COMPRESSIBILITY

For normally consolidated granular soils, the relationship between cone resistance and compressibility is not linear and depends at least on the relative density and confining pressure. For preloaded granular soils this relationship is strongly affected by the overconsolidation ratio plus the factors influencing the normally consolidated conditions. For a compact material, it has been found that the cone penetration test would indicate almost the same settlement value independent of considering the stress history of the deposit.

It is suggested that series of cone penetration tests should be carried out in laboratory prepared samples, which compressibility characteristics are previously known. The influence of relative density and "overburden" pressure upon the relationship between cone resistance and compressibility, should be investigated for normally - and over - consolidated conditions. The sequential analysis proposed in Fig. 9.18 should be followed in order to quantify errors involved in the settlement computation if the stress history of the deposit is not known.

APPENDIX A.1

ROUTINE FOR THE SOLUTION OF THE NON-LINEAR EQUATION

The non-linear equation 2.42 was solved by the technique which uses the combined method of linear interpolation and extrapolation, and bisection to locate a root of a continuous function in a given interval.

The main steps of the solution are presented as follows:

a) Non-linear equation

$$m\left[\frac{3(1-K_{onc})}{1+2K_{onc}} - \frac{3(1-K_{ooc})}{1+2K_{ooc}}\right] = Ln\left[\frac{OCR\,(1+K_{onc})}{1+2K_{ooc}}\right] \qquad (2.42)$$

solved for:

$$K_{onc} = 0.7 - 0.4\,D_R$$

b) Listing of the program, see Table A.1

c) Input

D_R, OCR and m.

d) Output, see Table A.2

$$\frac{K_{ooc}}{K_{onc}}$$

TABLE A.1

```
1   'BEGIN'
2   'REAL' Q, CONST, THREE M;
3   'PROC' F = ('REAL' Q) 'REAL' :
4   (LN (Q) - THREE M * (3 - Q) / (Q + Q) - CONST);
5
6   SPACES 'OF' NUMBERSTYLE := 3;
7   SIGN 'OF' NUMBERSTYLE := 0;
8   BEFORE 'OF' NUMBERSTYLE := 2;
9   AFTER 'OF' NUMBERSTYLE : = 2;
10  EXP 'OR' NUMBERSTYLE : = 0;
11
12  'FOR' I 'FROM' 1 'TO' 2 'DO' (
13  THREE M : = 3 * (I = 1 ! 1.5 ! 2.0);
14  PRINT ( (NEWPAGE, "M =", THREE M / 3, NEWLINE, NEWLINE) );
15  'FOR' J 'FROM' 0 'TO' 10 'DO' (
16  'REAL' DR = J / 10;
17  PRINT ( (NEWLINE, DR, "      ") );
18  'REAL' K = 0.7 - 0.4 * DR;
19  'REAL' K CONST = LN (1 + K) - THREE M * (1 - K) / (1 + K + K);
20  'FOR' LOOP 'FROM' 4 'TO' 13 'DO' (
21  CONST : = K CONST + LN ( (LOOP = 13 ! 50 !:
    LOOP = 12 ! 25 !: LOOP = 11 ! 15 ! LOOP) );
22  Q : = CO5AAB (1.0, 100.0, 1&-5, 1&-11, F, NAGHARD);
23  PRINT ( (Q - 1) / (K + K)  )
24  ) 'C' OD 'C'
25  ) 'C' OD 'C'
26  ) 'C' OD 'C'
27  'END'
28  'FINISH'
29
```

TABLE A.2

M = 2.0

DR/OCR → ↓	4	5	6	7	8	9	10	15	25	50
0.00	1.47	1.60	1.71	1.82	1.92	2.01	2.10	2.48	3.11	4.36
0.10	1.47	1.60	1.71	1.82	1.91	2.00	2.09	2.47	3.08	4.28
0.20	1.47	1.60	1.71	1.82	1.91	2.00	2.09	2.46	3.02	4.20
0.30	1.47	1.60	1.71	1.82	1.91	2.00	2.08	2.45	3.00	4.13
0.40	1.48	1.61	1.72	1.82	1.91	2.00	2.08	2.44	2.99	4.07
0.50	1.49	1.61	1.72	1.82	1.92	2.00	2.08	2.43	2.97	3.01
0.60	1.50	1.62	1.73	1.83	1.92	2.01	2.09	2.44	2.97	3.97
0.70	1.51	1.63	1.74	1.84	1.94	2.02	2.10	2.44	2.97	3.94
0.80	1.52	1.65	1.76	1.86	1.95	2.04	2.12	2.46	2.98	3.92
0.90	1.54	1.67	1.78	1.89	1.98	2.06	2.14	2.49	3.00	3.93
1.00	1.57	1.70	1.82	1.92	2.01	2.10	2.18	2.53	3.05	3.96

TABLE A.2 (Continued/...)

M = 1.50

DR/OCR → ↓	4	5	6	7	8	9	10	15	25	50
0.00	1.61	1.79	1.95	2.11	2.25	2.39	2.52	3.13	4.17	6.44
0.10	1.61	1.79	1.95	2.11	2.25	2.38	2.51	3.11	4.13	6.31
0.20	1.62	1.79	1.96	2.11	2.25	2.38	2.51	3.09	4.08	6.18
0.30	1.62	1.80	1.96	2.11	2.25	2.38	2.51	3.07	4.04	6.07
0.40	1.63	1.81	1.97	2.11	2.25	2.38	2.51	3.06	4.01	5.96
0.50	1.64	1.82	1.98	2.12	2.26	2.39	2.51	3.06	3.98	5.86
0.60	1.65	1.83	1.99	2.13	2.27	2.40	2.52	3.06	3.96	5.78
0.70	1.67	1.85	2.01	2.15	2.29	2.42	2.54	3.07	3.95	5.71
0.80	1.69	1.87	2.03	2.18	2.31	2.44	2.56	3.09	3.96	5.67
0.90	1.72	1.90	2.06	2.21	2.35	2.48	2.60	3.13	3.99	5.66
1.00	1.75	1.94	2.11	2.26	2.40	2.53	2.65	3.19	4.05	5.69

APPENDIX A.2
APPLICATIONS OF THE FINITE ELEMENT METHOD

A.2.1 INTRODUCTION

The finite element program used in this thesis belongs to the Geotechnical Division of the Building Research Station.

The package analyses the stresses and strains in structures which satisfy the following conditions:

A) The materials have elastic properties

B) The analysis can be reduced to two-dimensional problems (plane strain, plane stress or axially simetric).

The method is based on the use of triangular finite elements with nodes at the vertices and the mid-points of the sides. Thus, components of the displacement at any point within any element are quadratic polinomials in the spatial coordinates. The mathematics of the method can be found in "The finite element method in Engineering Science", O.C. Zienkiewicz.

The forces applied to the structure may consist of body forces proportional to the density at the given point or given forces at some specified nodes.

The displacements, zero or non-zero, of some nodes may also be specified. It is also possible to specify that some nodes may be constrained by external elastic supports.

The computer will calculate the displacement of each node and obtain the constants in the expression for the displacement at any point in each element, so that the stresses, strains and their principal components may be printed.

A.22. WALL-FRICTION EFFECT ON THE CONSOLIDATION PROCESS

Fig. A.1 indicates the distribution of vertical and radial stresses at the centre of the sample induced by a uniform surface load. Fig. A.2 indicates the same results corresponding to the stress distribution at the wall.

Three specific boundary conditions have been considered:

1) No displacement at the wall
2) The wall nodes are subjected to a uniform vertical force (simulating friction) equal to $K_o \times q_c \times \tan \phi$ ($K_o = 1 - \sin \phi$, $\phi = 40^o$)
3) The wall nodes are subjected to a vertical force (simulating friction) equal to $K_o \sigma_R$ (σ_R is the radial stress, which distribution with depth is indicated in Fig. A.2 for no displacement condition at the wall and from 0 to 0.15 m depth $\sigma_R = 0$)

For this analysis a simplified vertical stress distribution has been assumed, see Fig. A.1. The reduction factor due to the wall friction was determined based on the ratio between the delimited areas corresponding to each stress distribution, for example (See Fig. A.1):

$$R = \frac{S_{OAEFGC}}{S_{OABC}} \quad \text{or} \quad R = (1 - S_{EFGB}) \quad (\text{Assuming } S_{OABC} = 1)$$

The computer program used in this analysis assumes the material having elastic properties, hence, the possibility of failure occurring at the boundary is not taken into consideration. As the applied stress on the top of the sample increases, failure is likely to occur along the wall. In order to take this fact into account, the effective depth of consolidation was assumed as that indicated by the corresponding cone penetration test results. Fig. A.1 shows the value of the effective depth of consolidation as indicated by the cone test results, for consolidation pressures corresponding to 1.4 Kg/cm^2 and 7 Kg/cm^2. From these points an equivalent simplified stress distribution was considered and the corresponding delimited area determined. Thus, the reduction factor was determined as a function of stress distribution and consolidation pressure.

A.2.3 WALL CONFINEMENT EFFECT ON PLATE LOADING RESULTS

Fig. A.3 indicates the induced stresses below the plate for a given settlement considering different boundary radius - plate radius ratios.

The influence of the wall confinement was considered as follows:

a) From the elastic solution

$$E_p = \frac{q}{\delta} I$$

where E_p is the deformation modulus

q is the stress

is the settlement

I is the influence factor depending on the geometry of loading area and boundary condition.

For a given geometry of the loading area and a given settlement value, and putting $E_p/I = E$, we have:

$$E = f(q)$$

b) From Fig. A.3, and assuming that there is no influence of the wall confinement for a boundary radius - plate radius ratio equal to 100, it follows:

$$\frac{E}{E_{100}} = \frac{\int q \times ds}{\int (q \times ds)_{100}}$$

where s is the delimited area below the plate in Fig. A.3. As the delimited areas have the same geometrical configuration, we have:

$$\frac{E}{E_{100}} = \frac{\Sigma q}{\Sigma q_{(100)}}$$

APPENDIX A.3

DEFLEXION OF THE TOP OF THE SAMPLE

The deflexion on the top of the sample as consolidation proceeds can be estimated by considering the total volume of water expelled from the sample and the vertical movement of the reference plate. Table A.3 gives the deflexion values (θ) and Fig. A.4 indicates the determination procedures.

TABLE A.3

TEST	CONSOLIDATION PRESSURE (Kg/cm^2)	H(P) cm	H(V) cm	θ degrees
1	1.4	1.684	1.60	0.27
2	2.8	2.421	2.530	
3	"0"	-	-	-
4	1.4	2.016	1.916	0.32
5	1.4	2.154	-	-
6	1.4	1.3345	1.279	0.20
7	2.8	2.251	2.043	0.67
8	7.0	3.6155	3.069	1.74
9	7.0	3.607	-	-

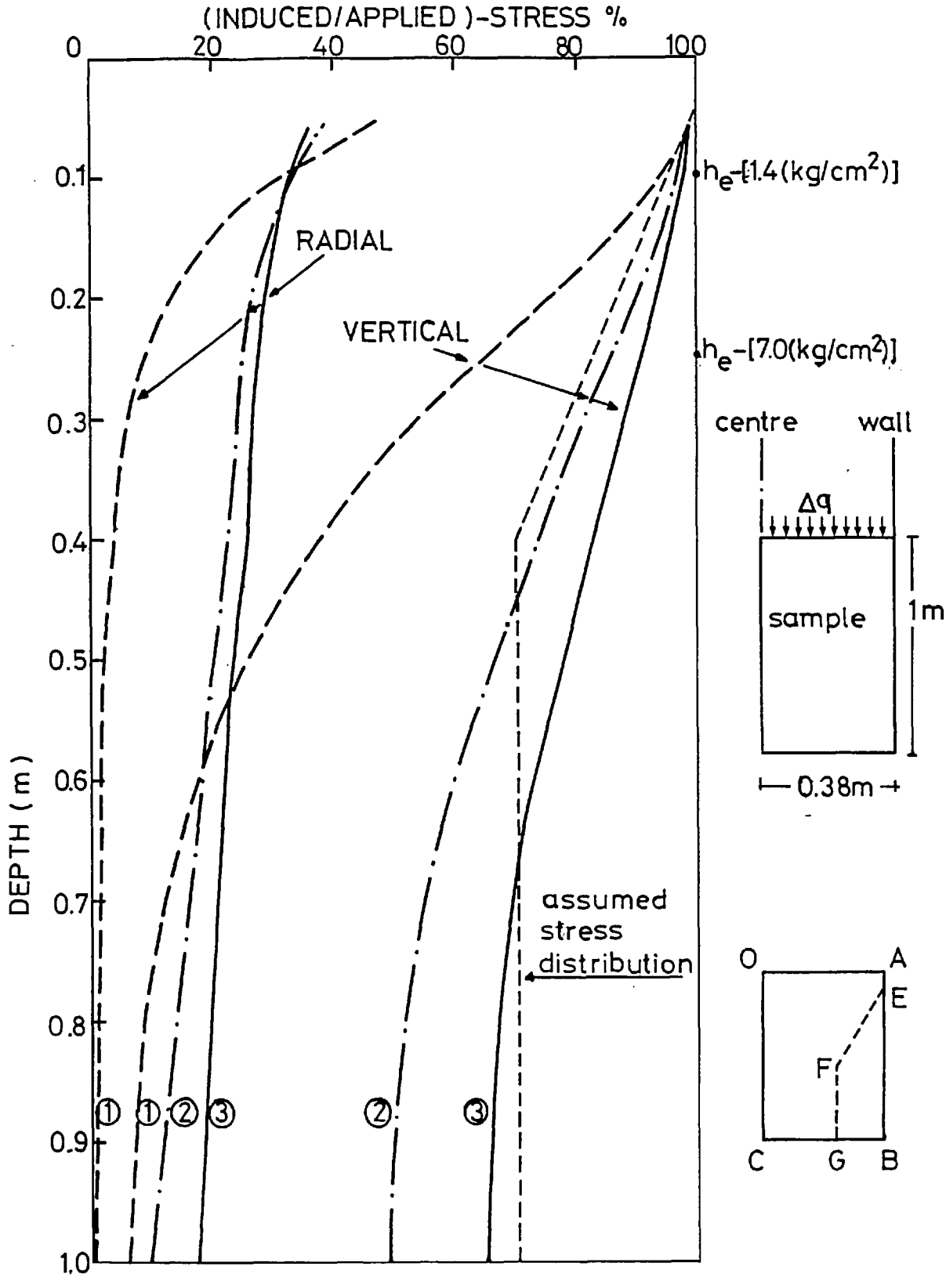


FIGURE A.1 - STRESS VARIATION AT SAMPLE CENTRE

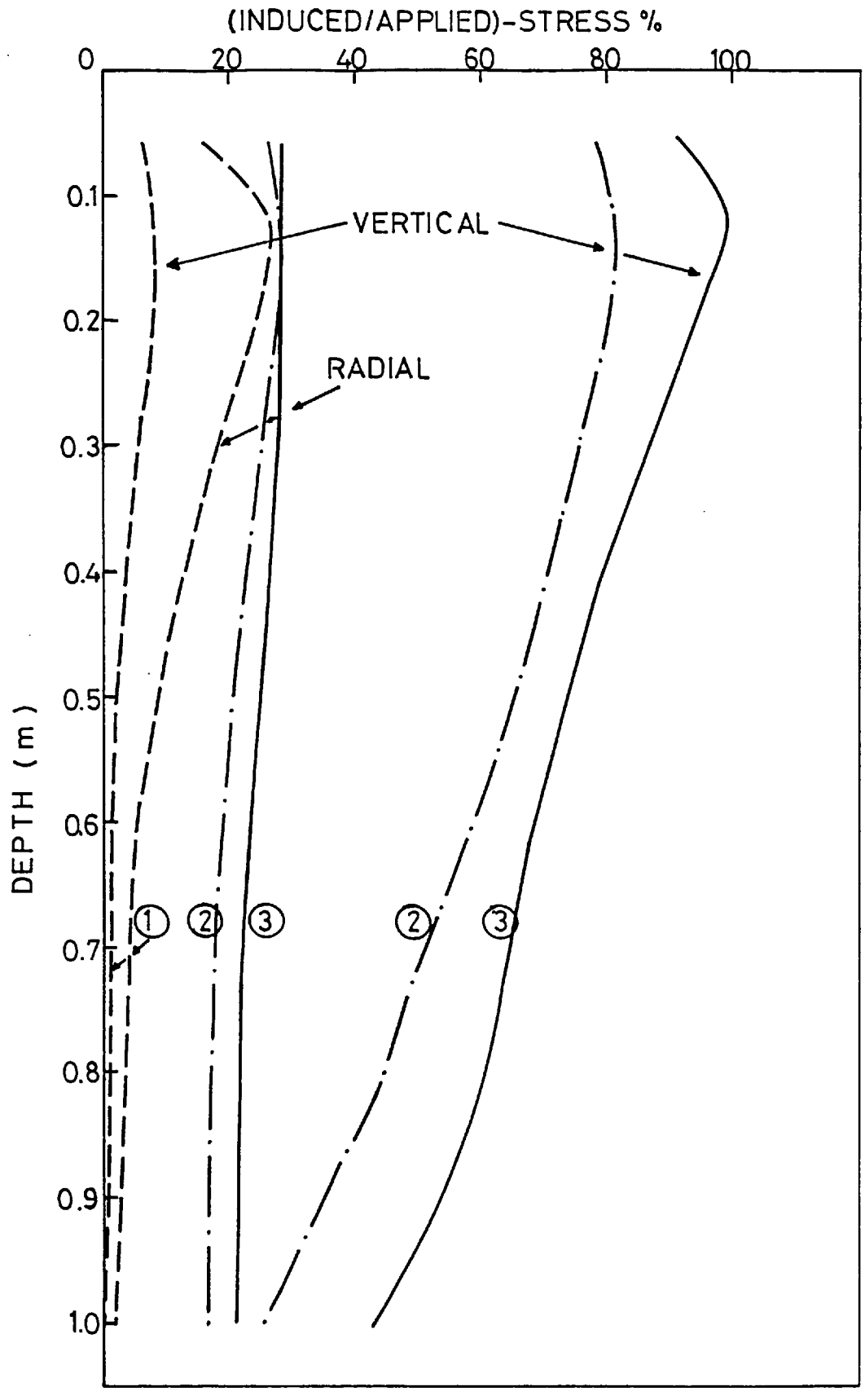


FIGURE A.2 - STRESS VARIATION AT SAMPLE BOUNDARY

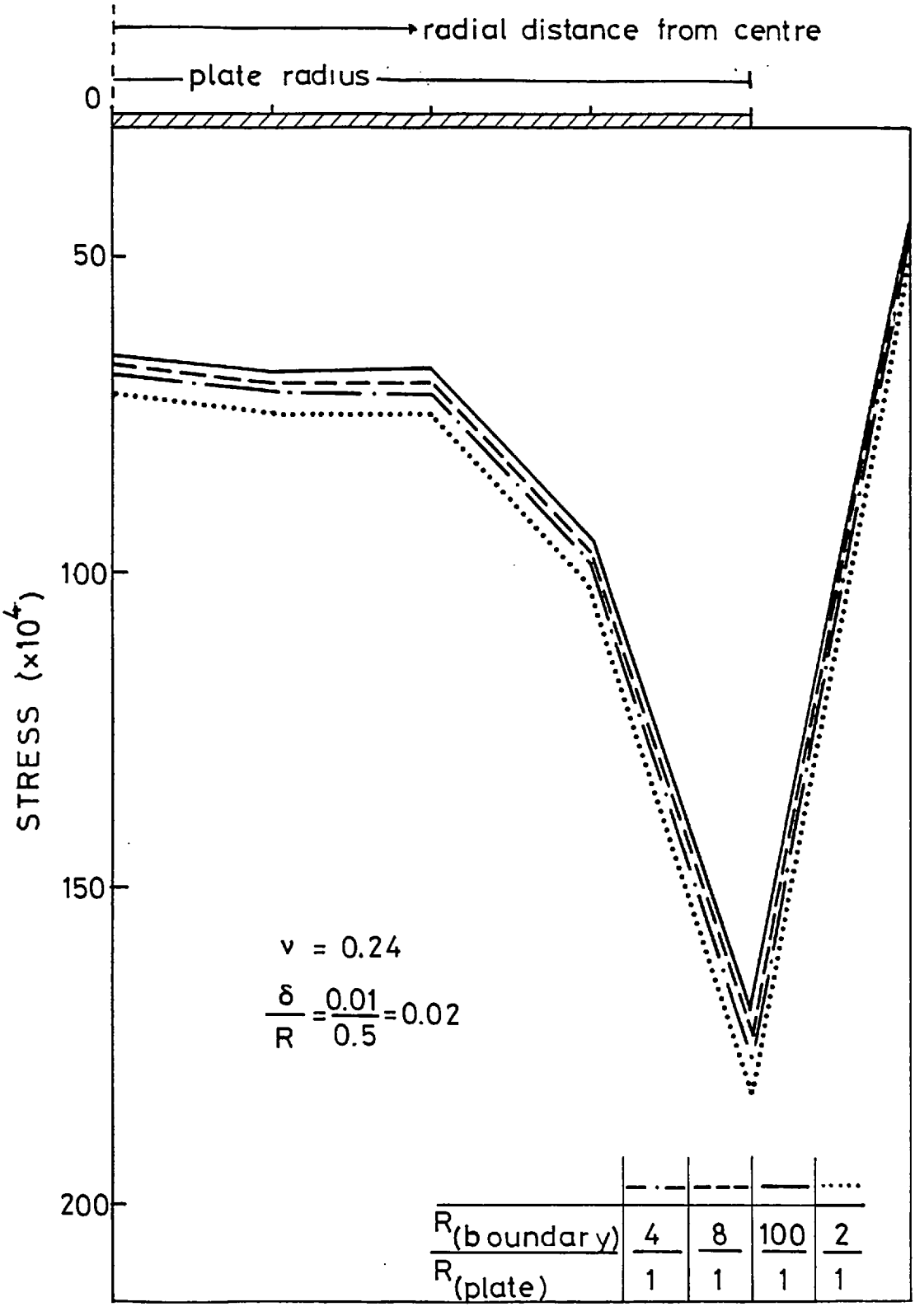
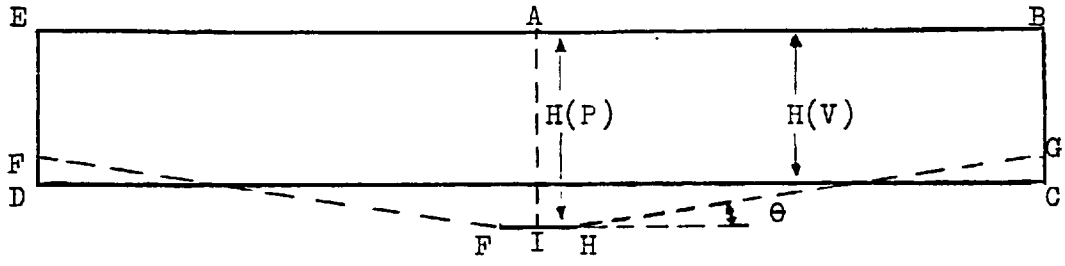


FIGURE A.3 - INFLUENCE OF WALL CONFINEMENT ON PLATE DEFORMATION MODULUS



EB = TESTING CHAMBER DIAMETER

FH = REFERENCE PLATE DIAMETER

H(P) = VERTICAL MOVEMENT OF REFERENCE PLATE

H(V) = VARIATION IN SAMPLE HEIGHT CORRESPONDING TO THE TOTAL VOLUME OF WATER EXPELLED FROM THE SAMPLE

θ = DEFLECTION ANGLE

$$\tan\theta = \frac{H(P) - BG}{AB - IH}$$

FIGURE A.4 - DEFLECTION ON THE TOP OF THE SAMPLE

APPENDIX B

PRELIMINARY TESTS

Some preliminary tests were carried out in samples which were prepared almost in the same manner as described in Section 7.1. In short, dry samples were built up inside the testing chamber and saturation was then proceeded using the vacuum technique. For compacting the sample, a bentonite layer was placed on the top of the sample and a hydraulic pressure was applied on the top of the bentonite layer. During the pressuresation, the drainage system at the bottom of the testing chamber was kept open.

Details of the central gland located on the testing chamber top plate is indicated in Fig. B.1.

The penetrometer pore pressure device consisted of a pressure transducer placed outside the penetrometer and connected to the porous tip through a double wall piezometer type tube. This system was found inadequate mainly due to the difficulties involved in achieving full saturation, see Fig. B.2. Trapped air inside the connexion gives a high compressibility to the system, resulting in a slow response time. Owing to the relatively long connexion between the porous tip and the pressure transducer, the compressibility of the tube can be considered a potencial source of errors during pore pressure measurements.

Figures B.3 to B.7 present the results obtained for this series of tests.

In addition to measurements of cone and sleeve resistances and pore pressure, the influence of the excess pore pressure dissipation upon the cone measurements was also investigated. For this purpose, some tests were carried out by stages and allowing full dissipation of the excess pore pressure during the interval between successive penetrations. The penetrometer was unloaded before being subjected to additional penetration. For test CPTB 2 (Fig. B.4) the excess pore pressure dissipation was followed by a higher cone resistance than the previous value corresponding to before the dissipation. This fact was not observed in the other tests.

These results were not considered in the analysis due to errors or inexactness involved during the measurements. The erroneous or inexact measurements were obtained as a consequence of:

1) Part load transfer from the conical point to the sleeve, See Section 5.5.3, Fig. 5.10. As a result the friction ratio (f_s/q_c) indicated very high values (compare to the values indicated in Fig. 8.30).

2) Slow response time of the pore pressure device, due to improper saturation. For the tests indicated in Figures B.5, B.6 and B.7, the pressure units did not indicate any excess pore pressure.

Excepting test CPTB 6 (Fig. B.8), all the other tests were carried out under atmospheric pressure. For test CPTB 6 the initial water pressure inside the testing chamber was equal to 7 Kg/cm^2. For this test the point and the sleeve resistances indicated values exceeding the range of the recording system.

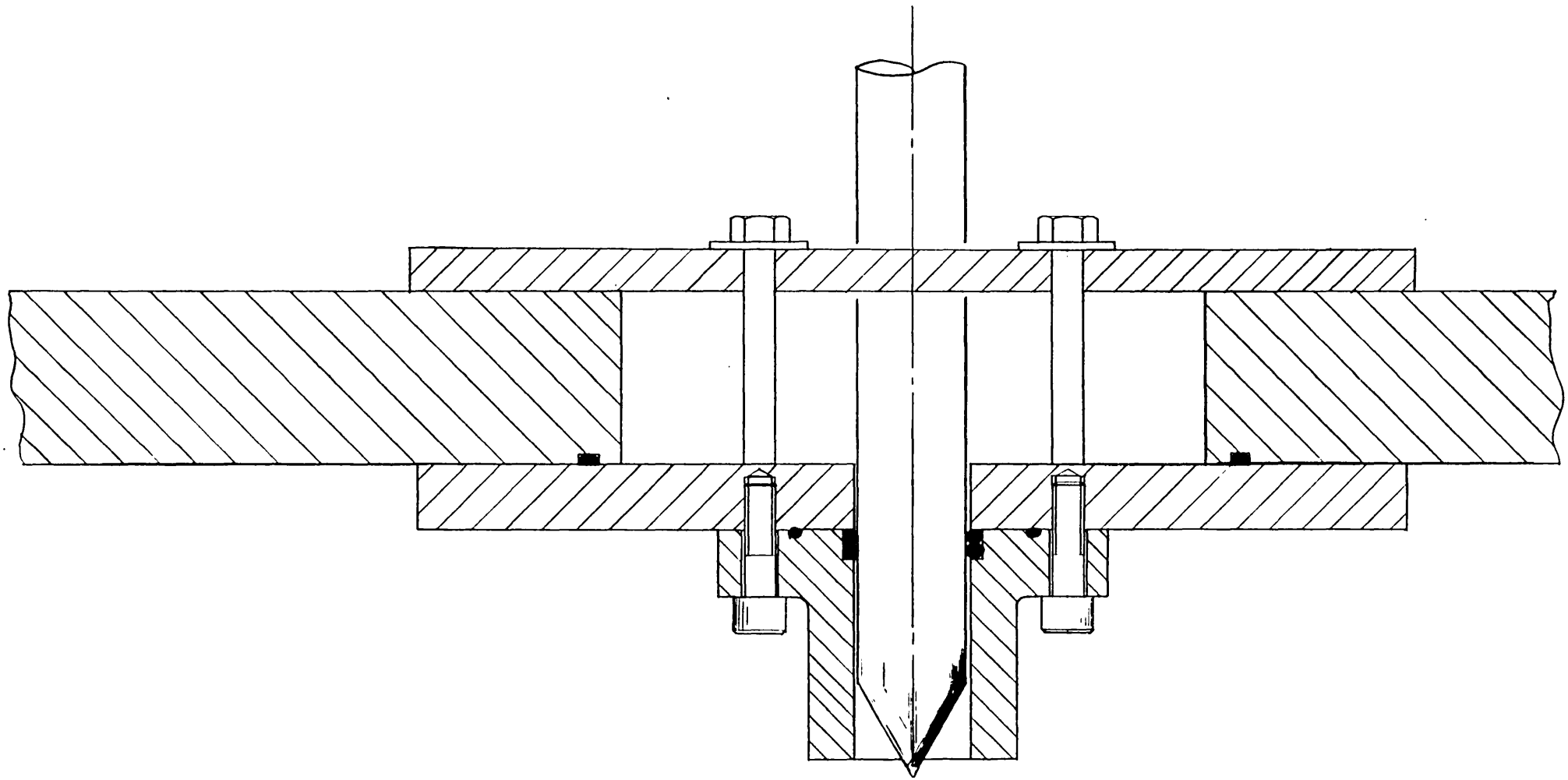


FIGURE B.1 - DETAILS OF THE CENTRAL GLAND

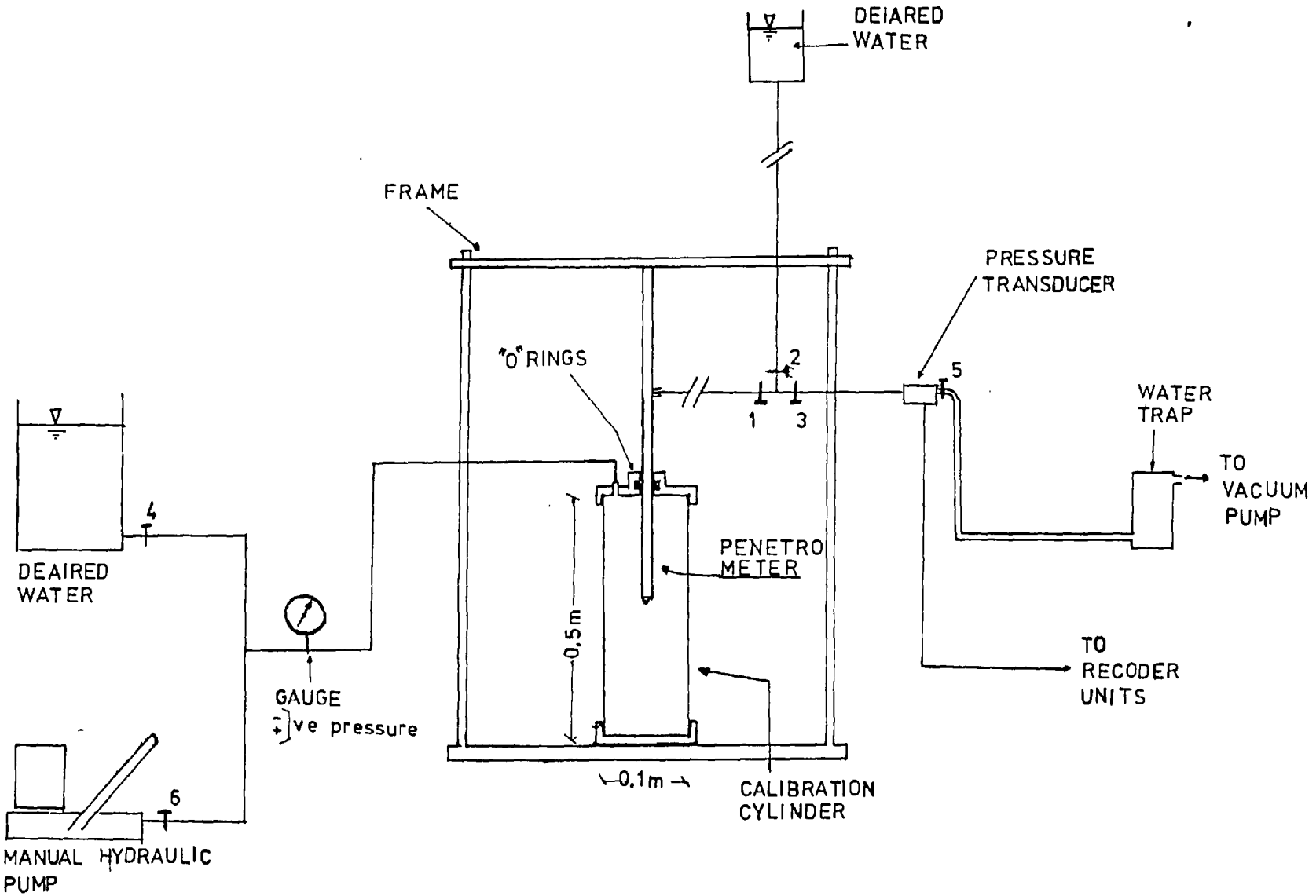


FIGURE B.2 -PORE PRESSURE SATURATION – CALIBRATION DEVICE

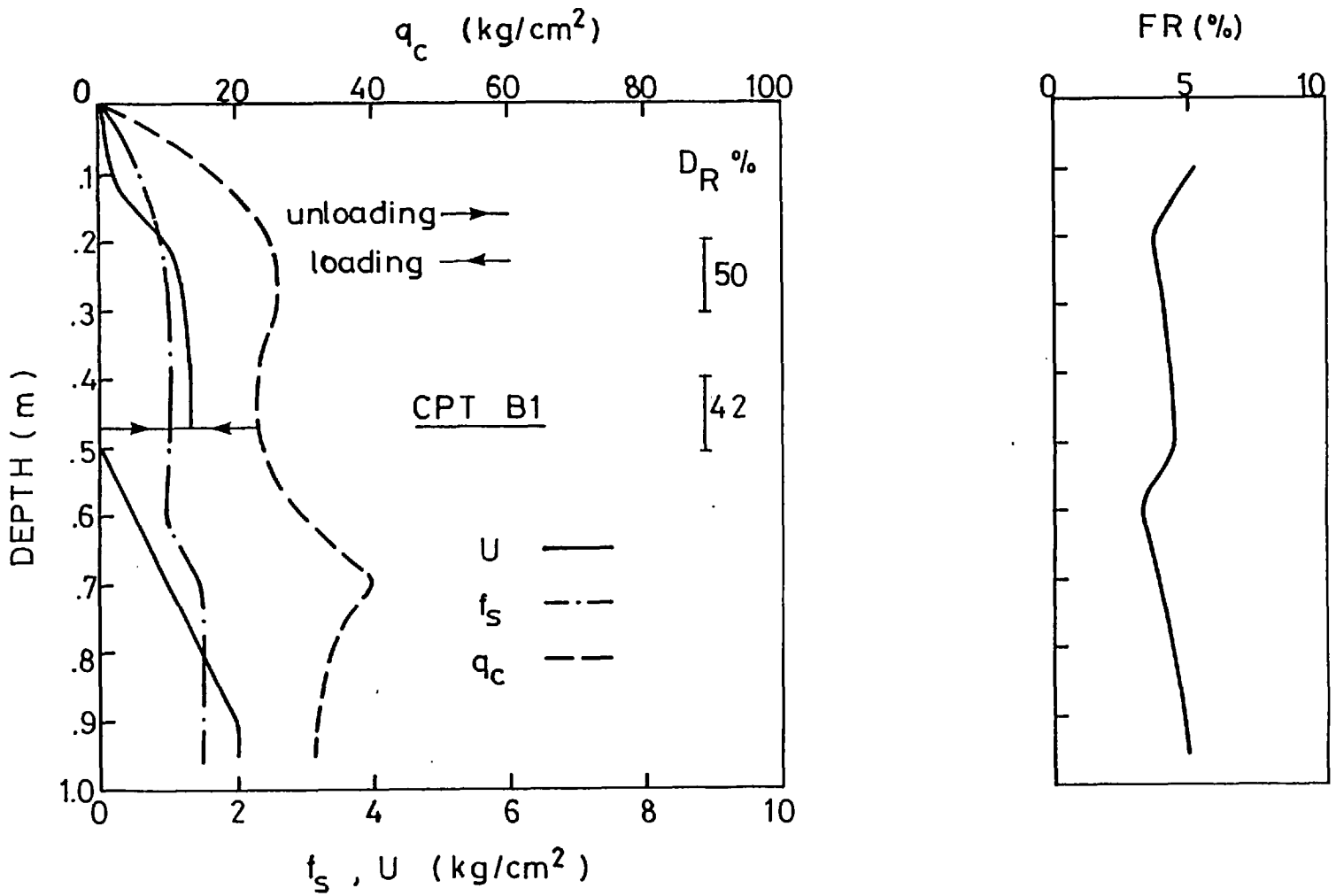
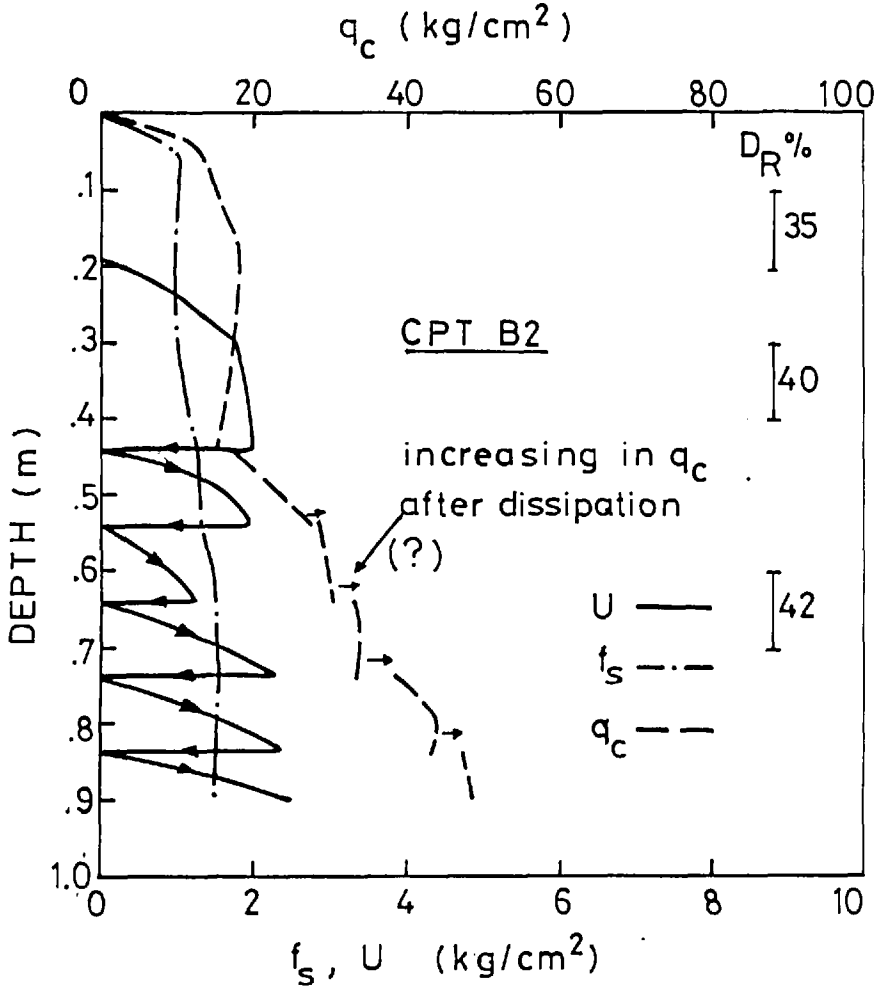


FIGURE B.3 - CONE PENETRATION TEST



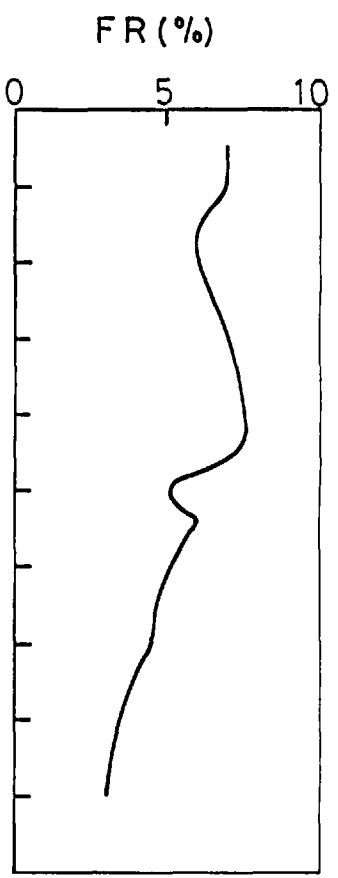


FIGURE B.4 - CONE PENETRATION TEST

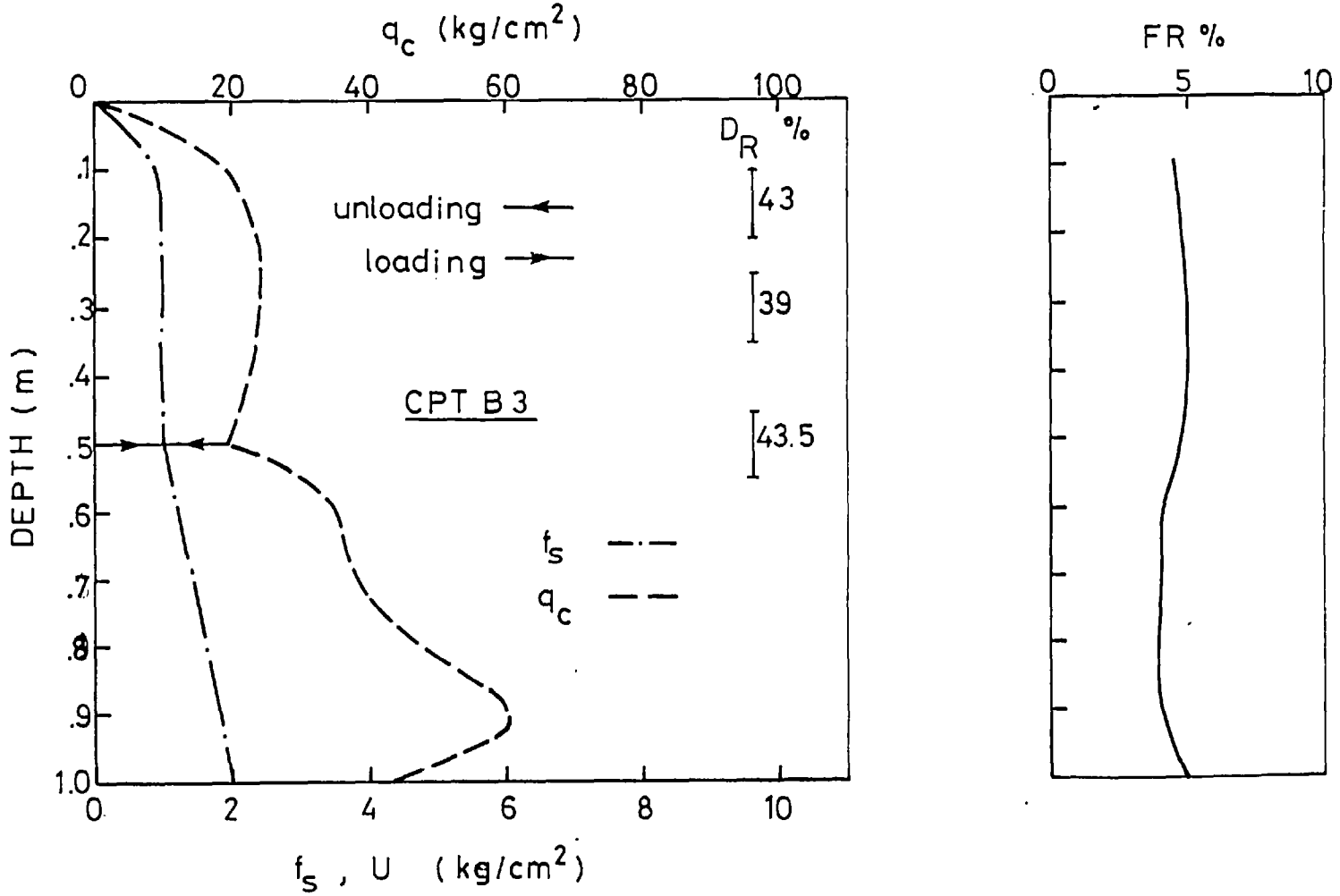


FIGURE B.5 - CONE PENETRATION TEST

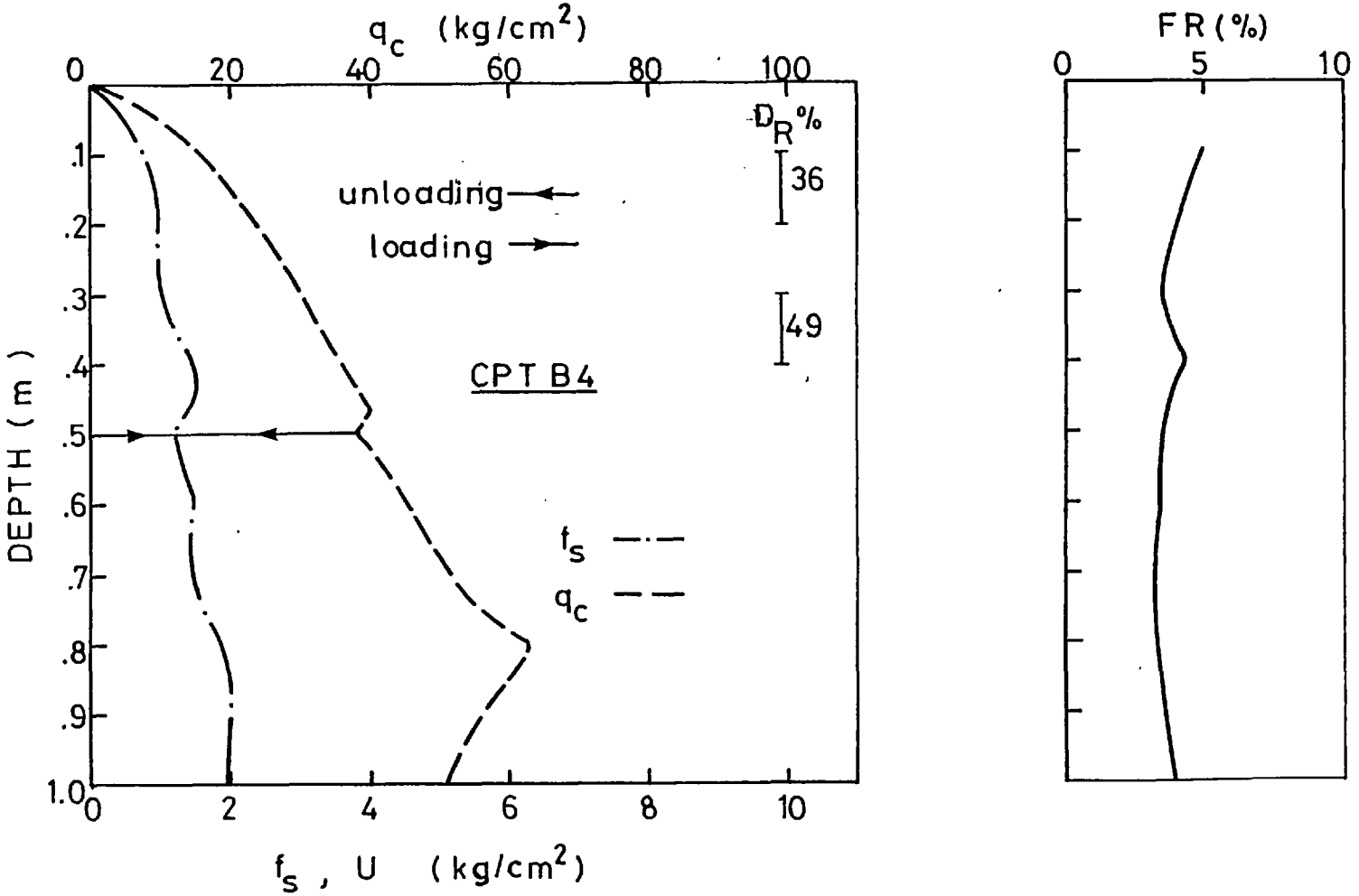


FIGURE B.6 - CONE PENETRATION TEST

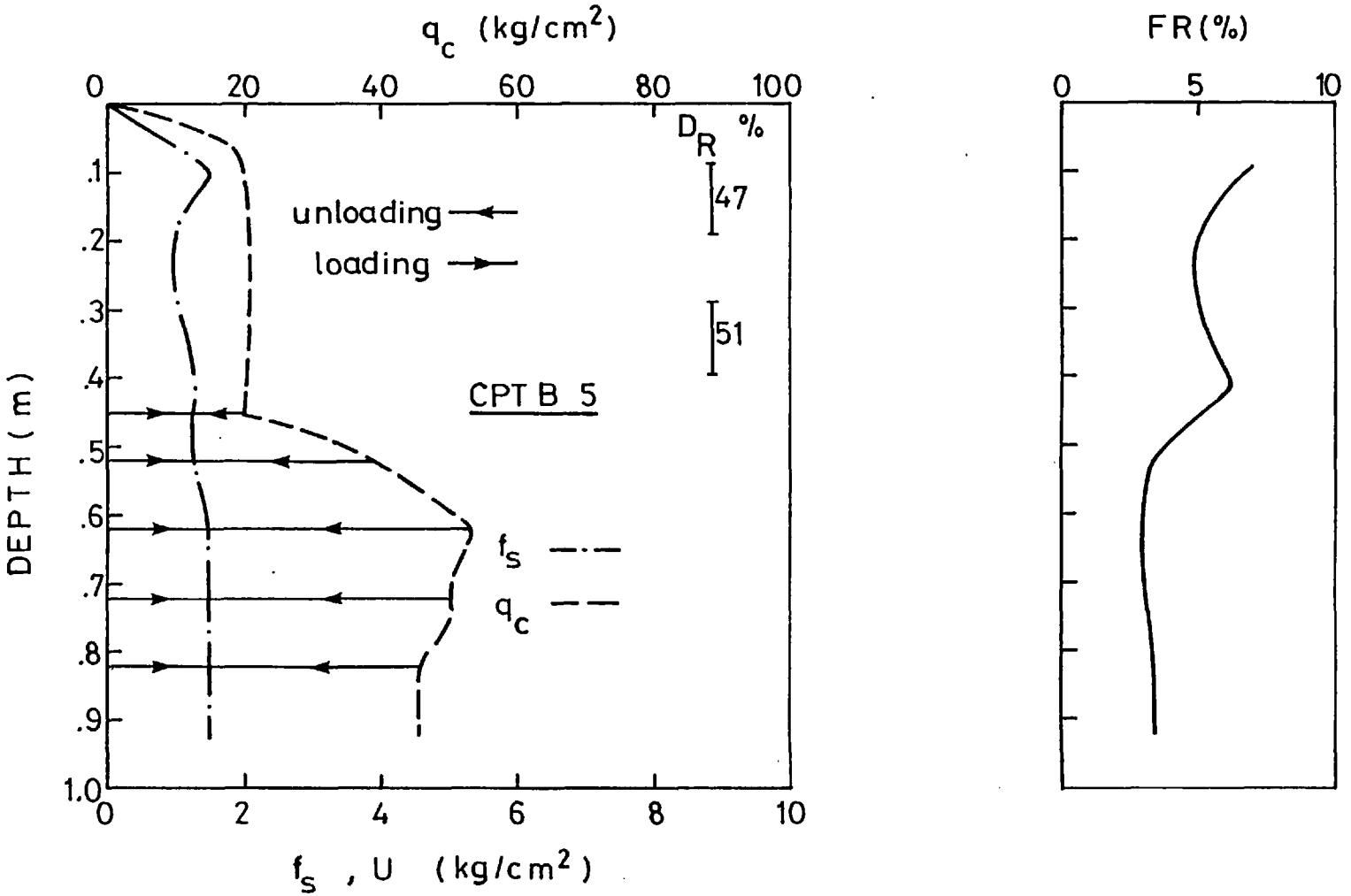


FIGURE B.7 - CONE PENETRATION TEST

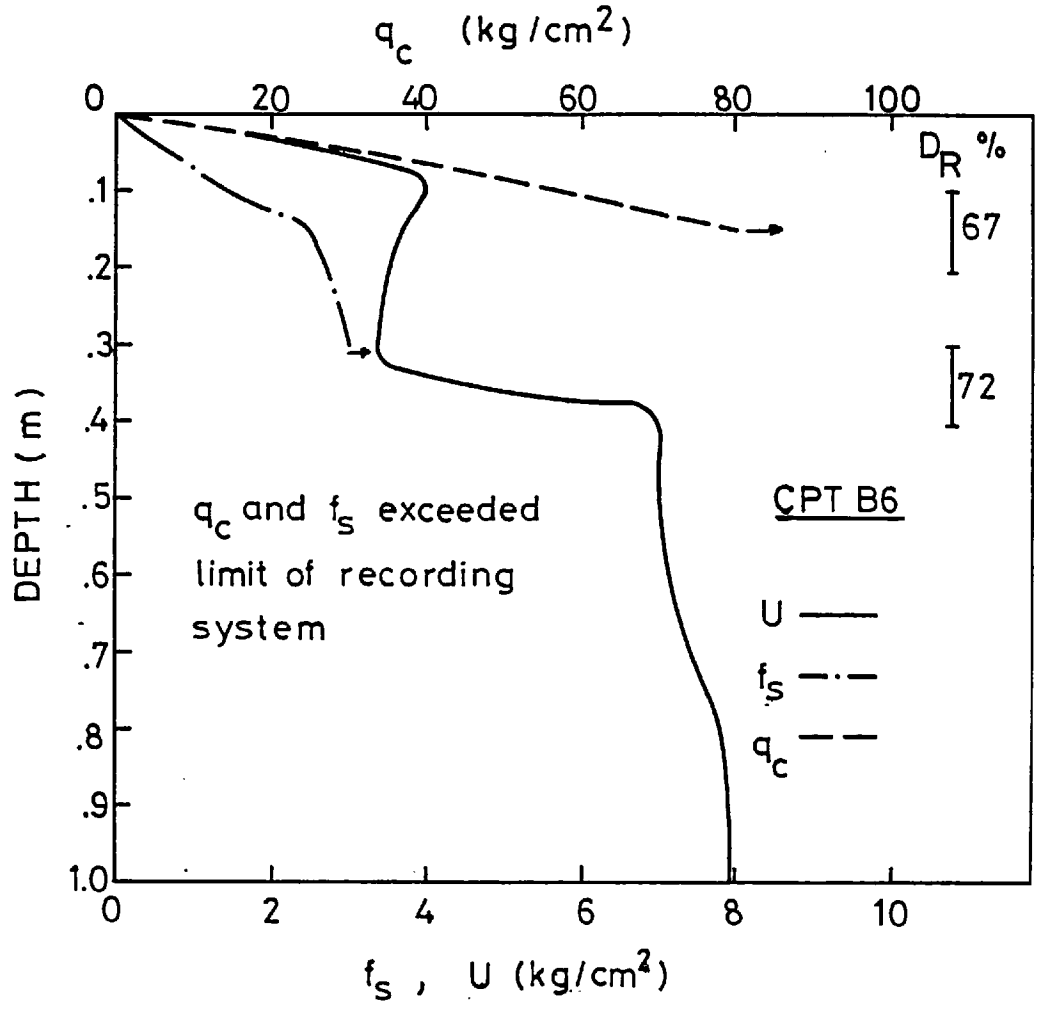


FIGURE B.8- CONE PENETRATION TEST

REFERENCES

Al-Awkati, Z., (1975)
On problems of soil bearing capacity at depth.
Ph.D. Thesis, Duke University, Durham, North Carolina.

Bachelier, M. and Parez, L. (1965)
Contribution a l'etude de la Compressibilite des sols a l'aide du penetrometre a cone.
Proc. 6th Int. Conf. SMFE, Montreal, September, Vol. II, pp. 3 - 7.

Baligh, M. M. (1976)
Cavity Expansion in sands with curved envelopes.
Journal, Geotechnical Engineering Division, A.S.C.E., Nov. GT11 pp. 1131 - 1146.

Baligh, M. M. (1975)
Theory of Deep Site Static Cone Penetration Resistance.
Massachusetts Institute of Technology, Publication No. R75 - 56.

Baligh, M. M.; Ladd, C. C. and Vivatrat, V. (1977)
Exploration and Evaluation of Engineering Properties of Marine Soils for Foundation Design of Offshore Structures.
Massachusetts Institute of Technology, Report No. MITSG 77-18.

Barenstsen, P. (1936)
Short Description of a Field-Testing Method with Cone-Shaped Sounding Apparatus.
Proc. 1st Conf. Soil Mech., Cambridge, Mass. Vol. I, pp. 7 - 10.

Begemann, H. K. (1953)
Improved Method of Determining Resistance to Adhesion Through a Loose Sleeve Placed Behind the Cone.
Proc. 3rd Int. Conf. Soil Mech. Found. Eng., Zurich, Vol. I, pp. 213 - 217.

Begemann, H. K. (1969)
The Dutch Static Penetration Test with the Adhesion Jacket Cone.
L. G. M. Mededeligen Publications, Delft Laboratory, Vol. XII, No. 4, April.

Begemann, H. K. (1965)

The Friction Jacket Cone as an Aid in Determining the Soil Profile.

Proc. 6th Int. Conf. Soil Mech. Found. Eng., Vol. I, pp. 17 - 20.

Bemben, S. M. and Myers, D. A. (1974)

The Influence of Rate of Penetration on Static Cone Resistance Values in Connecticut River Valley Varved Clay.

Proc. European Symposium on Penetration Testing, Stockholm, Vol. 2.2, pp. 33 - 34.

Bishop, A. W. and Henkel, D. J. (1972)

The Measurement of Soil Properties in the Triaxial Test.

Edward Arnold Ltd., London.

Bishop, R. F.; Hill, R. and Mott, N. F. (1945)

The Theory of Identation and Hardness Tests.

Proc. Physical Society, London, Vol. 57, no. 3, pp. 147 - 159.

Bjerrum, L. (1973)

Geotechnical Problems Involved in Foundations of Structures in the North Sea.

Geotechnique, Vol. 23, No. 3, pp. 319 - 358.

Bjerrum, L. and Johannessen, I. (1961)

Pore Pressure Resulting from Driving Piles in Soft Clay.

Proc. Conf. on Pore Pressure and Suction in Soils, Butterworths, London.

Bogdanovic, L. (1973)

Settlement of Stiff Structures (Silos) Founded on Soft Soil with Low Penetration Resistance.

Transactions of the SR Institute for Testing Materials, Pub. No. 34, Belgrade.

B.S. 1377 : (1975)

Methods of Test for Soils for Civil Engineering Purposes.

British Standards Institution.

Buisman, A. S. K., (1940)

Groundmechania, Waltmann, Delft.

Burmister, D. M. (1954)

Principles of Permeability Testing of Soils.

Symposium on Permeability of Soils, ASTM STP, pp. 3 - 20.

Chadwick, P. (1959)

The Quasi-Static Expansion of a Spherical Cavity in Metals and Ideal Soils.

Quarterly Journal of Mechanics and Applied Mathematics, Vol. 12, Part 1, pp. 349 - 376.

Chapman, G. A. (1974)

A Calibration Chamber for Field Test Equipment.

Proc. European Symposium on Penetration Testing, Stockholm, Vol. 2.2, pp. 59 - 65.

Clark, J. I. and Meyerhof, G. G. (1972)

The Behavior of Piles Driven in Clay. 1. An Investigation of Soil Stress and Pore Water Pressure as Related to Soil Properties.

Canadian Geotechnical Journal, Vol. 9, pp. 351 - 373.

Dahlberg, R. (1974)

Penetrometer Pressuremeter and Screw Plate Tests in a Preloaded Natural Sand Deposit.

Proc. European Symposium on Penetration Testing, Stockholm, Vol. 2.2, pp. 69 - 87.

Daramola, O. (1978)

The Influence of Stress - History on the Deformation of a Sand.

Ph. D. Thesis, University of London.

Dayal, U. and Allen, J. H. (1975)

The Effect of Penetration Rate on the Strength of Remolded Clay and Sand Samples.

Canadian Geotechnical Journal, Vol. 12, No. 3, pp. 336 - 348.

De Beer, E. E. (1967)

Bearing Capacity and Settlement of Shallow Foundations on Sand.

Proc. of Symposium on Bearing Capacity and Settlement of Foundations, Duke University, Durham, N. C., April 1965 pp. 15 - 33.

De Beer, E. E. (1945)

Études des Fondations sur Pilotis et des Fondations Directes.

L'Appareil de Pénétration en Profondeur.

Annales des Travaux Publics de Belgique, April, June, August.

De Beer, E. E. (1974b)

General Discussion on the Interpretation of Static Cone Resistance.

ESOPT, Stockholm, Vol. 2.1, pp. 119 - 124.

De Beer, E. E. (1974a)

Interpretation of the Results of Static Penetration Tests. Group IV Report, ESOPT, Stockholm, Vol. 2.1, p. 67.

De Ruiter, J. (1971)

Electric Penetrometer for Site Investigations.

Journal Soil Mech. and Found. Division, ASCE, Vol. 97, SM 2, pp. 457 - 472.

Domaschuk, L. (1968)

An Analysis of Pore Water Stress through a Separation of the Mean Normal and Deviatoric Components of Stress.

Proc. 21st. Canadian Soil Mech. Conf., Winnipeg, Manitoba.

Drozd, K. (1974)

The Influence of Moisture Content on Penetration Results. Discussion to European Symposium on Penetration Testing, Group 5, Vol. 2.1, pp. 162 - 164.

Drozd, K. (1965)

The Influence of Variable Moisture Content in Sand on the Results of Dynamic Penetration Tests.

Proc. 6th Int. Conf. Soil Mech. Found. Eng., written discussion to Section 2, Vol. III, pp. 335 - 336.

Drozd, K. and Svasta, M. (1974)

Penetration Testing in Czechoslovakia.

State-of-the-art Report presented to European Symposium on Penetration Testing, Vol. 1, pp. 27 - 32.

Eggestad, Å. (1974)

A New Method for Compaction Control of Sand.

Norwegian Geotechnical Institute, Publication No. 104, pp. 1 - 13.

Egorov, K. E. (1965)

Calculation of Bed for Foundations with Ring Footing.

Proc. 6th Int. Conf. Soil Mech. Found. Eng., Montreal, Vol. 2, pp. 41 - 45.

Eide, O. (1974)

Marine Soil Mechanics.

Preprint of Lecture presented at "Offshore North Sea" Technology Conference, Stavanger, p. 14.

Fellenius, W.; Blidberg, F.; Post, L. and Olsson, J. (1922)

State Railways Geotechnical Committee, 1914- 22, Final Report. Stockholm.

Folque, J. (1974)

Compressibility of Sands Determined by Means of Penetration Tests.

Proc. European Symposium on Penetration Testing, Stockholm, pp. 141 - 145.

Gibson, R. E. (1950)

Discussion, Journal of the Institution of Civil Engineers, Vol. 34, p. 82.

Gibson, R. E. and Anderson, W. F. (1961)

In Situ Measurements of Soil Properties with the Pressuremeter.

Civil Engineering and Public Works Review, Vol. 56, pp. 615 - 618.

Hansbo, S. (1974)

Discussion to Group 3, Future Developments, European Symposium on Penetration Testing, Stockholm, Vol. 2.1, pp. 109 - 110.

Hassib, M. H. (1951)

Consolidation Characteristics of Granular Soils.

Columbia University, New York.

Henkel, D. J. (1959)

The Relationships between the Strength, Pore Water Pressure and Volume Change Characteristics of Saturated Clays.

Geotechnique, Vol. 9, No. 3, pp. 119 - 135.

Holden, J. C. (1974)

General Discussion, Standardization and Future Cooperation.

ESOPT, Stockholm, Vol. 2.1, pp. 100 - 107.

Holden, J. C. (1971)

Research on Performance of Soil Penetrometers (at University of Florida).

Churchill Fellowship Final Report (C.R.B.)

Hough, B. K. (1957)

Basic Soils Engineering

Ronald Press, New York.

Huizinga, T. K. (1942)

Grondmechanica (Soil Mechanics)

N. V. Wed. J. Ahrend & Zoon, Amsterdam.

Janbu, N. (1974a)

General Discussion on the Interpretation of Static Cone Resistance.

ESOPT, Stockholm, Vol. 2.1, pp. 132 - 133.

Janbu, N. (1963)

Soil Compressibility as Determined by Oedometer and Triaxial Tests.

Proc. European Conf. Soil Mech. and Found. Eng., Wiesbaden.

Janbu, N. and Senneset, K. (1974)

Effective Stress Interpretation of In Situ Static Penetration Tests.

Proc. European Symposium on Penetration Testing, Stockholm, Vol. 2.2, pp. 181 - 193.

Ko, H. Y. and Scott, R. (1967)

Deformation of a Sand in Hydrostatic Compression.

Journal, SMFD, ASCE, May,SM 3.

Koizumi, Y. and Ito, K. (1967)

Field Tests with Regard to Pile Driving and Bearing Capacity of Piled Foundations.

Soils and Foundations. Vol. 7, No. 3.

Kok, L. (1974)

The Effect of the Penetration Speed and the Cone Shape on the Dutch Static Cone Penetration Test Results.

Proc. of ESOPT, Stockholm, Vol. 2.2, pp. 215 - 220.

Kolbuszewski, J. J. (1948)

An Experimental Study of the Maximum and Minimum Porosities of Sands.

Proc. 2nd Int. Conf. Soil Mech. Found. Eng., Rotterdam, Vol. 1, pp. 158 - 165.

Konrad, J. M. (1977)

Contribution au Calcul du Frottement Lateral des Pieux Flottants Fonces dans des Argiles Molles et Sensibles.

M. Sc. Thesis, Laval University, Quebec.

Krawczyk, J. V. (1969)

An Examination of Methods of Determining the Specific Gravity of Soils.

Road Research Laboratory Report No. LR 272.

Ladanyi, B. (1961)

Étude Théorique et Expérimentale de L'Expansion dans un Sol Pulvérulent d'une Cavité Presentant une Symetrie Sphérique ou Cylindrique.

Annales de Travaux Publics de Belgique, Vol. 62, pp. 105 - 148, 365 - 406.

Ladanyi, B. (1963)

Expansion of a Cavity in Saturated Clay Medium.

Journal of Soil. Mech. Found. Division, ASCE, Vol. 90, SM 4, pp. 127 - 161.

Laier, J. E.; Schmertmann, J. H. and Schaub, J. H. (1975)

Effect of Finite Pressuremeter Length in Dry Sand.

Proc. of Specialty Conference In Situ Measurements of Soil Properties, ASCE, Raleigh.

Lane, K. S. and Washburn, D. E. (1946)

Capillarity Tests by Capillarimeter and by Soil Filled Tubes.

Proc. Highway Research Board.

Lo. K. Y. and Stermac, A. F. (1965)

Induced Pore Pressure During Pile-Driving Operations.

Proc. 6th Int. Conf. Soil Mech. and Found.Eng., Montreal, Vol. II, pp. 285 - 289.

Massarch, K. R. (1976)

Soil Movement Caused by Pile Driving in Clay.

Inst. For Jord-Och Bergmekanik, Stockholm.

Massarch, K. R. and Broms, B. B. (1977)

Fracturing of Soil Caused by Pile Driving in Clay.

Proc. 9th Int. Conf. Soil Mech. Found. Eng., Tokio Vol. 1, pp. 197 - 200.

Massarch, K. R.; Broms, B. B. and Sundquist, O. (1975)

Pore Pressure Determination with Multiple Piezometer.

Proc. Conf. In Situ Measurement Soil Properties.

Raleigh, Vol. 1, pp. 260 - 265.

Meyerhoff, G. G. (1955)

Influence of Roughness of Base and Ground Water Conditions on the Ultimate Bearing Capacity of Foundations.

Geotechnique, Vol. 5, pp. 227 - 242.

Meyerhoff, G. G. (1965)

Shallow Foundations

Journal, Soil Mech. and Found. Division, ASCE, Vol. 91, SM 2, March, pp. 21 - 31.

Meyerhoff, G. G. (1951)

The Ultimate Bearing Capacity of Foundations.

Geotechnique, Vol. 2, No. 4, pp. 301 - 332.

Milligan, V. (1975)

Field Measurement of Permeability in Soil and Rock.

State-of-the-art Report to Section 1, Specialty Conference of the Geotechnical Engineering Division, ASCE, Raleigh, June.

Mindlin, R. D. (1936)

Force at a Point in the Interior of a Semi-Infinite Solid.

Journal Appl. Phys., Vol. 7, No. 5, pp. 195 - 202.

Mitchell, J. K. and Gardner, W. S. (1975)

In Situ Measurements of Volume Change Characteristics.

State-of-the-art Report Prepared for Section 5. Specialty Conference of the Geotechnical Engineering Division, ASCE, Raleigh, June.

Mitchell, J. K. and Lunne, A. T. (1978)

Cone Resistance as Measure of Sand Strength.

Journal of the Geotechnical Engineering Division, ASCE, GT 7, July, pp. 995 - 1012.

Nottingham, L. C. (1975)

Use of Quasi-Static Friction Cone Penetrometer Data to Predict Load Capacity of Displacement Piles.

Ph. D. Thesis Presented to the University of Florida, June.

Ostenfeld, C. (1942)

Forsög Med Päle (Pile Tests)

Ingeniorvidenskabelige Skrifter, C. E. Gad, Copenhagen, No. 3.

Plantema, G. (1953)

A Soil Pressure Cell and Calibration Equipment.

Proc. 3rd. Int. Conf. Soil Mech. Found. Eng., Zurich, Vol. 1.

Plantema, G. (1957)

Influence of Density on Sounding Results in Dry, Moist and Saturated Sands.

Proc. 4th. Int. Conf. Soil Mech. Found. Eng., London, pp. 237 - 240.

Poulos, H. G. and Davis, E. H. (1973)

Elastic Solutions for Soil and Rock Mechanics.

John Wiley & Sons, New York, p. 179.

Prandtl, L. (1921)

On the Penetration Strengths (Hardness) of Plastic Construction Materials and the Strength of Cutting Edges.

Zeit. Angew.Math. Mech., Vol. 1, No. 1, pp. 15 - 20.

Randolph, M. F. (1977)

A Theoretical Study of the Performance of Piles.

Ph. D. Thesis, University of Cambridge.

Reissner, H. (1924)

Zum Erddruckproblem (Concerning the earth-pressure problem).

Proc. 1st Int. Congress of Applied Mechanics, Delft, pp. 295 - 311.

Rocha-Filho, P. (1976)

Review on Cone Penetration Tests.

M.Sc. Thesis, University of London.

Roy, M. (1979)

Lecture Presented at the Civil Engineering Dept., Imperial College, University of London, February.

Sanglerat, G. (1972)

The Penetrometer and Soil Exploration.

Elsevier, Amsterdam.

Senneset, K. (1974)

Penetration Testing in Norway.

State-of-the-art Report to European Symposium on Penetration Testing. Stockholm, June, Vol. 1, pp. 85 - 95.

Schmertmann, J. H. (1971)

Consulting Report J. H. S., No. 87 to McClelland Engineers, Inc.

Schmertmann, J. H. (1969)

Dutch Friction-Cone Penetrometer Exploration of Research Area at Field 5, Eglin Air Force Base, Florida.

Contract Report S-69-4, US Army Engineer, Waterways Experiment Station, Vicksburg, Mississippi.

Schmertmann, J. H. (1974a)

Penetration Pore Pressure Effects on Quasi-Static Cone Bearing, q_c.

Proc. European Symposium on Penetration Testing, Stockholm, Vol. 2.2, pp. 345 - 351.

Schmertmann, J. H. (1974b)

Pore Pressure that Produce Nonconservative q_c Data.

Discussion to European Symposium on Penetration Testing, Group 4, Vol. 2.1, pp. 146 - 149.

Schmertmann, J. H. (1970)

Static Cone to Compute Static Settlement over Sand.

Journal, SMFD, ASCE, Vol. 96, SM 3, pp. 1011 - 1043.

Schmertmann, J. H. (1975)

The Measurement of In Situ Shear Strength.

State-of-the-art Presentation to Section 3, Specialty Conference of the Geotechnical Engineering Division, ASCE, Raleigh, June.

Schmertmann, J. H.; Hartman, J. P.; Brown, P. R. (1978)

Improved Strain Influence Factor Diagrams.

Journal, Geotechnical Engineering Division, ASCE, Vol. 104, No. GT8, August, pp. 1131 - 1135.

Schultze, E. and Melzer, K. J. (1965)

The Determination of the Modulus of Compressibility of Non - Cohesive Soils by Soundings.

6th Int. Conf. SMFE, Montreal, Vol. 1, pp. 354 - 358.

Schultze, E. and Moussa, A. (1961)

Factors Affecting the Compressibility of Sand.

Proc. 5th Int. Conf. on Soil Mech. and Found. Eng.,

Paris, Vol. 1, p. 335.

Sherwood, P. T. (1970)

The Reproducibility of the Results of Soil Classification and Compaction Tests.

Road Research Laboratory Report No. LR 339.

Skempton, A. W. (1951)

The Bearing Capacity of Clays.

Proc. British Building Research Congress, Vol. 1, pp. 180 - 189.

Skempton, A. W. (1954)

The Pore Pressure Coefficient A and B.

Geotechnique, Vol. 4, pp. 143 - 147.

Skempton, A. W.; Yassin, A. A. and Gibson, R. E. (1953)

Theorie de la Force Portante des Pieux.

Journées de Mechanique des Sols, Annales du Bâtiment et des Travaux Publics, Vol. 6, No. 63, pp. 285 - 290.

Soderberg, L. O. (1962)

Consolidation Theory Applied to Foundation Pile Time Effects.

Geotechnique, Vol. 12, pp. 217 - 232.

Sutherland, H. B. (1974)

Granular Materials

State-of-the-art Report, Proc. Conf. Settlement of Structures,

Cambridge, Pentech Press, London, pp. 473 - 499.

Taylor, D. W. (1948)

Fundamentals of Soil Mechanics.

John Wiley and Sons, New York.

Terzaghi, K. (1943)

Theoretical Soil Mechanics.

John Wiley and Sons, New York.

Terzaghi, K. (1930)

Die Trägfahigkeit von Phahlgründungen. (The Bearing Capacity of Pile Foundations).

Bautechnik, 8, Nos. 31, 34, pp. 475 - 478, 517 - 521.

Terzaghi, K. and Peck, R. B. (1967)

Soil Mechanics in Engineering Practice.

John Wiley and Sons, New York.

Thomas, D. (1968)

Deepsounding Test Results and the Settlement of Spread Footings on Normally Consolidated Sands.

Geotechnique, Vol. 18, pp. 472 - 488.

Torstensson, B. A. (1975)

Pore Pressure Soundings Instrument.

Proc. Conf. In Situ Measurement Soil Properties.

Raleigh, Vol. II, pp. 48 - 54.

Trofimenkov, J. G. (1964)

Field Methods for Testing the Structural Properties of Soils.

Moscow: Building Literature Publishing House.

Trofimenkov, J. G. (1974)

Penetration Testing in USSR.

State-of-the-art Report. ESOPT, Stockholm, Vol. 1, pp. 147 - 154.

Turnbull, W. J.; Shockley, W. G. and Cunny, R. W. (1960)

Summary of Rotary Cone Penetrometer Investigations.

Highway Research Board Special Report, No. 60, pp. 167 - 171.

Veismanis, A. (1974)

Laboratory Investigation of Electrical Friction-Cone Penetrometers in Sand.

Proc. of European Symposium on Penetration Testing, Stockholm, Vol. 2.2, pp. 407 - 419.

Vermeiden, J. (1948)

Improved Soundings Apparatus as Developed in Holland since 1936.

Proc. 2nd Int. Conf. Soil Mech. Found. Eng., Rotterdam, Vol. 1, pp. 280 - 287.

Vesic, A. S. (1967)

A Study of Bearing Capacity of Deep Foundations.

Georgia Institute of Technology, Final Report, Project B - 189.

Vesic, A. S. (1963)

Bearing Capacity of Deep Foundations in Sand.

National Research Council, Highway Research Board Record, No. 39, pp. 112 - 153.

Vesic, A. S. (1972)

Expansion of Cavities in Infinite Soil Mass.

Journal, SMFD, ASCE, March, SM 3, pp. 265 - 290.

Vesic, A. S. (1970)

Tests on Instrumented Piles, Ogeechee River Site.

Journal, SMFD, ASCE, Vol. 96, No. SM 2, pp. 561 - 584.

Webb, D. L. (1970)

Settlement of Structures on Deep Alluvial Sandy Sediments in Durban, South Africa.

Proc. Conf. on In Situ Behaviour of Soil and Rock, Inst. of Civil Engineers, London, pp. 181 - 188.

Wissa, A. E. Z.; Martin, R. T. and Garlanger, J. E. (1975)

The Piezometer Probe.

Proc. Conf. In Situ Measurement of Soil Properties.

Raleigh, Vol. I, pp. 536 - 545.

Wroth, P. C. (1975)

In Situ Measurement of Initial Stresses and Deformations Characteristics.

State-of-the-art Report to Session IV, Specialty Conference on In Situ Measurement of Soil Properties.

Releigh, North Carolina, June.